Drug Metabolism and Pharmacokinetics in the Lead Optimisation of Novel Positive Allosteric Modulators of α1 Strychnine Sensitive Glycine Receptors

Thesis submitted in accordance with the requirements of the University of Liverpool for the degree of Doctor of Philosophy by

Elinor Wylde

October 2015

Declaration

This thesis is the result of my own work. The material contained in the thesis has not been presented, nor is currently being presented, either wholly or in part for any other degree or other qualification.

Elinor Wylde

This research was carried out in the Liverpool School of Tropical Medicine and in the Department of Pharmacology at the University of Liverpool

Acknowledgments

I would like to thank my supervisors Prof. Martin Leuwer and Prof. Paul O'Neill for the opportunity to take part in this research and for all the help and guidance they have given over the course of my PhD. I would like to thank the members of the research group and our collaborators. A special thanks to Dr Chandra Pidathala and Dr Lee Taylor of the Liverpool University, Chemistry Department for sharing their research with me.

Thank you to the staff and students at the Liverpool School of Tropical Medicine and in the Department of Pharmacology, who helped me set up my research and provided me with an excellent working environment. Particularly to Dr Ally Shone, who kindly offered to take me under her wing and to whom I am extremely grateful.

Big thanks to my family, especially my parents, Kate and John for supporting me over throughout my undergraduate and postgraduate study. Thank you to my Aunt, Lynda who has offered me a place to stay during my studies.

Finally, I would like to express gratitude all my friends who have provided me with a great deal of emotional support. To my best friend Laura, who has always been with me from primary school to postgraduate study. Lastly to Emma, Sammy, Tom and Jamie, who have been there to encourage me and have given me some of my favourite moments over the last four years.

Dedication

This thesis is dedicated to my friends and family

Thank you for your support

Abstract

Chronic pain is a condition that is thought to affect roughly 8 million people in the UK. It is classified as pain that persists for more than 6 months. Chronic pain is commonly associated with depression, insomnia, anxiety and poor quality of life. Many treatments for chronic pain are accompanied by numerous debilitating side-effects, this in combination with insufficient pain relief means that approximately 50% of patients will discontinue their treatment. Most sufferers choose to live with the pain rather than deal with numerous adverse-effects. There is a great need for new therapeutics that are specifically designed to target the underlying mechanisms of chronic pain, therefore providing safer and more effective treatments.

One such mechanism is the down-regulation of strychnine-sensitive glycine receptors (SSGRs) localised in the dorsal horn. Glycinergic activity is known to be inhibitory and artificial stimulation can produce analgesia. Positive allosteric modulators acting on α1 SSGRs may able to compensate for the inhibitory glycinergic activity that is reduced in chronic pain. Previous work within the group lead into the identification of propofol analogues designed to be novel positive allosteric modulators of α1 SSGRs.

Work presented in this thesis describes the generation and optimisation of these analogues with a focus of drug metabolism and pharmacokinetics. The hit to lead process has resulted in the development of a lead compound that is highly potent at the target, has excellent pharmacokinetic and safety profiles and is able to produce high levels of analgesia in an animal model of neuropathic pain.

Abbreviations

°C	Degrees Celsius
Å	Angstrom(s)
AC	Adenylyl cyclase
ACN	Acrylonitrile
Ala	Alanine
aM	Attomolar
AUC	Area under the curve
cAMP	Cyclic adenosine monophosphate
Cl_{CYP}	Cytochrome P450 clearance
Cl_{int}	Intrinsic clearance
ClogD	Calculated distribution coefficient
ClogP	Calculated partition coefficient
cm	Centimetre(s)
d. H_20	Distilled water
Da	Daltons
DMPK	Drug metabolism and pharmacokinetics
DMSO	Dimethyl sulfoxide
EC_{50}	Half maximal effective concentration
EtOAc	Ethyl acetate
FA	Formic acid
FDA	Food and Drug Administration
g	Gram(s)
G	G-force
GABA	Gamma aminobutyric acid
$GABA_AR$	Gamma aminobutyric acid (subtype A) receptor
GlyR	Glycine receptor
HCN	Hyperpolarization-activated cyclic nucleotide-gated channel
HEPES	4-(2-hydroxyethyl)-1-piperazineethanesulfonic acid buffer
HLM	Human liver microsomes
hr(s)	Hour(s)
IC_{50}	Half maximal inhibitory concentration
KD	Knock-down animal model
Kg	Kilogram(s)
L	Litre(s)
LC	Liquid Chromatography

m/z	Mass-to-charge ratio
M+/M-	Molecular ion
MeOH	Methanol
mg	Milligram(s)
$MgCl_2$	Magnesium chloride
min(s)	Minute(s)
mL	Millilitre(s)
mM	Millimolar
mm	Millimetre(s)
MS	Mass spectrometer
mV	Millivolt(s)
n	Sample size
$NADP^+$	Nicotinamide adenine dinucleotide phosphate
NADPH	Reduced nicotinamide adenine dinucleotide phosphate
NaOH	Sodium hydroxide
NET	Norepinephrine transporter
ng	Nanogram(s)
nM	Nanomolar
nm	Nanometre(s)
NMDA	N-methyl-D-aspartate
OR	Opioid Receptor
P	p-value
PB	Phosphate Buffer
PBS	Phosphate Buffer Saline
PK/PD	Pharmacokinetic and pharmacodynamic
pKa	Negative logarithm of the acid dissociation constant
pM	Picomolar
RLM	Rat liver microsomes
rpm	Revolutions per minute
s	Second(s)
SEM	Standard error of the mean
SERT	Serotonin transporter
$T_{1/2}$	Half-life
V	Voltage/Volt(s)
α	Alpha
β	Beta
δ	Delta
κ	Kappa

µ	Mu
µg	Microgram(s)
µL	Microliter(s)
µM	Micromolar

Contents

Chapter 1

Chronic Pain

Table of Contents

1.1 Pain

1.1.1 Nociception

Pain is an unpleasant sensation that occurs when contact is made with noxious stimuli or when tissues, nerves or organs are damaged. Although uncomfortable, pain serves a protective purpose; it warns us of potential dangers and encourages us to guard injuries whilst they heal. Throughout history opium, in varying forms, has been used as a go-to for analgesia (pain relief)[1]. From the 1800s onwards, analgesic drugs such as morphine and aspirin have become more widely used. Improved understanding of how pain is processed has led to creation of therapies that target the inflammatory and neurological aspects of pain, as well as the varying degrees of pain severity[1]. Recently, chronic dysfunctional pain has emerged as legitimate disease and traditional therapies no longer provide sufficient relief. There is a serious need for new analgesics that are designed to specifically target the underlying mechanisms of chronic pain.

Nociception is the processing of sensory information stemming from contact with painful stimuli. In the early-1900s, specialised sensory neurons (nociceptors) transmitting noxious signals from the periphery into the spinal cord, where they synapse with projection neurons that feed into the central nervous system (CNS), were identified[2]. Nociceptive neurons are categorised into two groups, Aδ and C-fibres[3]. The cell bodies of these fibres originate in the dorsal root ganglion (DRG) of the spinal cord. Aδ-fibres are thin and lightly myelinated, a structure that allows for swift conduction of sensory transmissions[2]. They are commonly believed to be responsible for ‘first’ pain; the sharp, spike of pain that accompanies a quick

retreat of the injured appendage. 'Second' pain is a throbbing or burning ache that often arises from tissue damage. The conduction for this type of pain is much slower and perfectly suited to smaller, unmyelinated C-fibres[2; 3]. Both nociceptive neurons can be further differentiated by the types of stimuli they react to; some Aδ-fibres are exclusively activated by mechanical (i.e. touch) and others by thermal (i.e. heat), whilst C-fibres may be activate by mechanical, thermal and additional chemical (i.e. spice) stimuli[3]. Nociceptors all have much higher activation thresholds than their normal sensory counterparts and contain highly specialised transducers.

Many of nociceptive ion channels belong to the large, diverse transient receptor potential (TRP) non-specific cation channel family[2]. Vanilloid receptors (TRPV1-4), responding to heat and chemical stimuli were the first nociceptive transducers to be identified[2; 4]. Channel opening is temperature dependant, similar to what is seen in normal heat sensory neurons only with a higher temperature threshold (43°C)[5]. Vanilloid receptor-like channels (VRL) are another type of transducer that responds to heat. These channels have a higher temperature threshold than standard vanilloid channels (52°C) and are not responsive to vanilloids; vanilloids, such as capsaicin, are compounds that primarily activate TRPV channels. It is believed VRLs are most commonly expressed on large type I Aδ nociceptors, usually responsible for detecting intense heat[3; 4].

Response to painful cold is not as well defined as noxious heat. Only in the last decade have two transducers, TRPM8 and TRPA1, been identified. The role these channels play in the sensation of noxious cold is still not conclusive[6; 7]. The receptors that respond to painful touch, such as pressure and tissue distortion, and noxious chemicals (e.g. toxins, irritants and

flavonoids) have yet to characterised but it is likely that TRPs involved in nociception of temperature (e.g. TRPA1) play a key role[2; 6]. Exposure to noxious stimuli is frequently accompanied by physical damage. In an attempt to heal damage, an inflammatory response is triggered, causing the nervous system to become sensitised to pain (algesia)[8; 9].

1.1.2 Inflammatory Pain

Activation and increased sensitivity of nociceptive cation channels is caused by natural chemical mediators released following injury of nerves and tissues. The role of inflammation in pain propagation is a vast, complex process, that largely involves the production and release inflammatory mediators from immune cells that sensitise surrounding nerves to pain and promote regeneration [10].

Following trauma there is an influx of calcium ions (Ca^{2+}) into the neuron. Increased Ca^{2+} concentration initiates a series of intracellular events, including the release of nociceptive neurotransmitters, glutamate and substance P, and the activation of m-calpain and UPS (ubiquitin-proteasome system)[8; 10]. M-calpain promotes the release of more inflammatory mediators and, along with UPS, assists in the breakdown of the cytoskeleton, causing further damage and prompting additional inflammation[11; 12]. Sensory neurons also release adenosine triphosphate (ATP) that triggers Schwann cells to release free radicals and inflammatory proteins, for instance chemokines, cytokines and neurotrophins[9; 10]. The release of chemical mediators leads to the recruitment of more immune cells (e.g. Mast cells, neutrophils and macrophages) that also contribute to inflammation and alter permeability of the blood-nerve

barrier, allowing easier access of the injured site[8; 9]. As a result the excitability of injured neurons and surrounding uninjured neighbouring nerves is increased, often by changes in ion channel expression and function. For example, the activation of mast cells prompts the release tryptase and bradykinin, which induce pain hypersensitivity via protease-activated receptors (PARs). Activation of PARs sets off an intracellular cascade that cumulates in the increased activity and expression of cation channels, such as TRPV1[13]. Thus lowering the activation threshold of the neuron, as well as reducing the cool-down time for subsequent impulses. With less intense stimuli needed to trigger action potentials at a greater frequency, the nerve becomes hyperexcitable. In another example, potassium-channels are the down-regulated by RE1-silencing transcription factor (REST), which has been shown to be increased during inflammatory pain[14]. Potassium-channels are responsible for generating an inhibitory M-current that counteracts firing of action potentials. Decreasing the availability of functional potassium channels will lessen the effect of the M-current and increase neuronal excitability[15]. The role of inflammation in pain hypersensitivity is summarised in Figure 1.1.

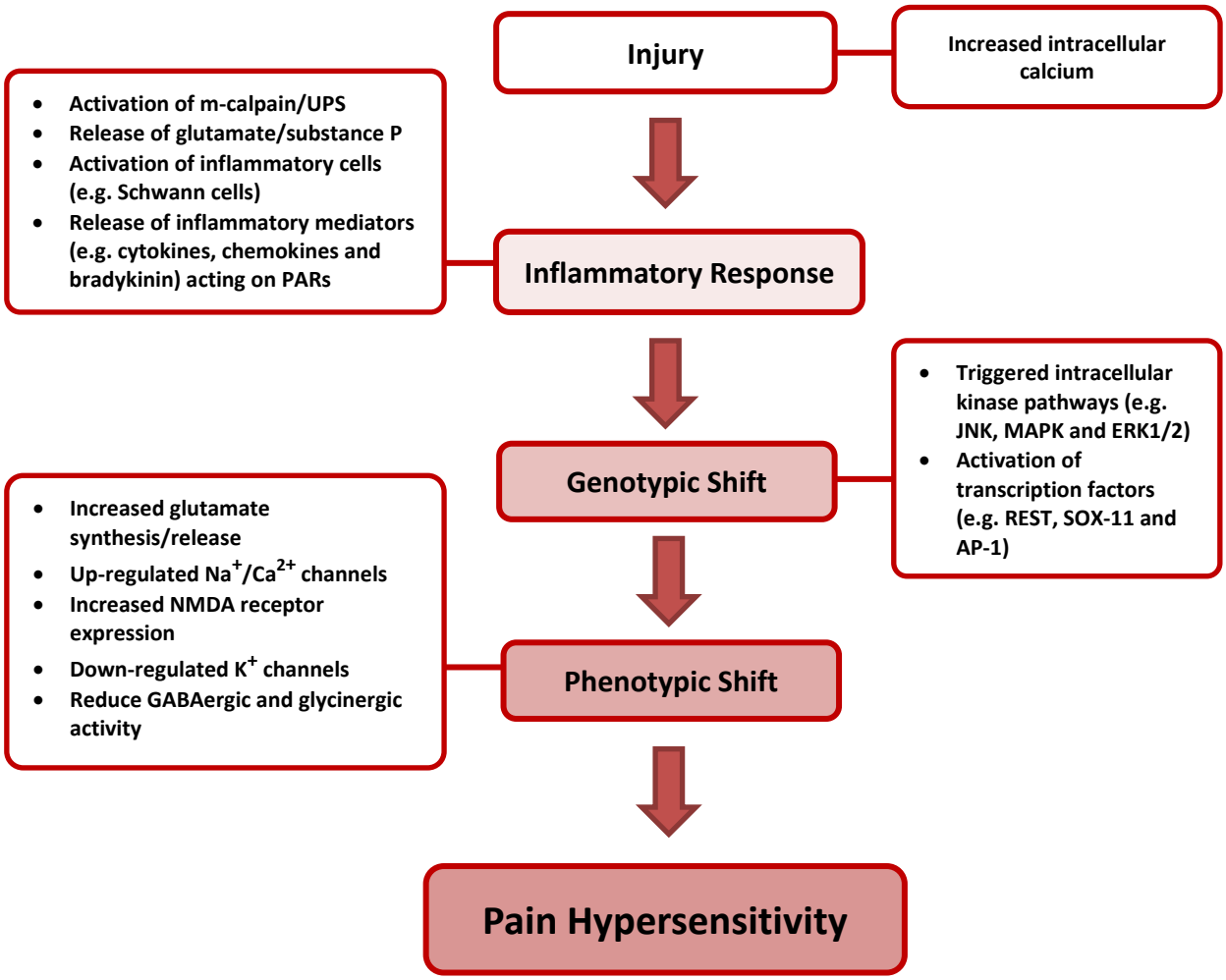

Figure 1.1. Inflammatory response, after injury, leads to pain hypersensitivity: Following injury, increased intracellular Ca^{2+} leads to the activation of m-calpain and UPS, initiating cellular breakdown. M-calpain also causes the release of algesic agents, ATP, glutamate and substance P and activates nearby immune cells. Inflammatory proteins, such as chemokines and bradykinin act on protease-activated receptors (PARs). This sets off a series of intracellular kinase pathways, including JNK, MAPK and ERK1/2 that trigger regulatory transcription factors, REST, SOX-11, AP-1, etc. The end result is up-regulation of Ca^{2+}/Na^{+} channels and NDMA receptors, as well as the down-regulation K^{+} channels and GABA/glycine receptors. Changes in expression of ion channels lower the activation threshold of neurons, making them more excitable. While altered expression of neurotransmitter receptors allow for easier communication between nociceptors. Adapted from Üçeyler *et al. 2006*[10].

1.1.3 Neuropathic Pain

Neuropathic pain (NP) describes hypersensitivity that follows injury within the somatosensory system[16]. Neuronal trauma in the peripheral nervous system (PNS) may occur as the result of physical trauma (e.g. surgical, poisoning, sports injury) or as a by-product of underlying disease (e.g. tumours, diabetes, degenerative disorders); trauma in the PNS drives maladaptive changes in the CNS[17]. If the trauma occurs in the CNS, commonly in the spinal cord, a permanent dysfunction of the somatosensory system is likely to develop. Damage in the CNS can be also caused by direct injury, stroke and degenerative diseases (e.g. multiple sclerosis)[17; 18].

The nature of the nerve that experiences damage has a profound effect on the development of neuropathic pain. As expected, damage to larger nerves, such as the sciatic nerve is 6x times more likely to cause NP than the damage to a smaller nerve[19]. Due to the nature of neuronal injury, particularly in the CNS, the restorative aspects of inflammation commonly aggravate the damaged nerve (i.e. formation of a glial scar), resulting in the maladaptive plasticity of the nervous system and often the development of chronic pain[20; 21].

Although increased sensitivity to pain is not ideal, it encourages us to 'protect' the effected site and many aspects of the immune response play a vital restorative role. Schwann cells promote the removal any debris that may disrupt tissue or nerve regeneration and the release of growth factors, vital for repair[8]. In the later stages of inflammation, leukocytes release anti-inflammatory proteins that supress production of inflammatory mediators[22]. It is important to note that regeneration only occurs when damage happens in the periphery;

injury in CNS results in glial scar around the site. The scar, formed through astrogliosis, prevents the restorative aspects of the immune response from reaching the site, simultaneously, trapping the destructive aspect[21]. As result the entire nociceptive pathway begins to destructively adapt, causing malfunction of the nervous system (neuropathic pain)[19; 20].

1.1.4 Chronic Pain

Chronic pain can be described as pain persisting for more than half a year or as pain that lasts past the point of projected healing. As with functional pain, chronic pain can be nociceptive, inflammatory or neuropathic however it serves no practical or restorative purpose[19]. As a disorder, chronic pain is often used to describe numerous pain related conditions including complex regional pain syndrome and common back pain[23]. Chronic pain can arise due to previous injury (e.g. nerve lesions during surgery), degenerative diseases (e.g. multiple sclerosis), functional disorders (e.g. Inflammatory Bowel Disease, IBD) or even as a side effect of long term treatments such as chemotherapy[17; 23; 24].

Roughly about 16% of the world's adult population suffer from chronic pain, with almost 8 million of them living in the United Kingdom[25; 26]. Unfortunately, despite its prevalence, chronic pain is severely mismanaged; one third of sufferers either refuse or discontinue treatment, due to misinformation, adverse-effects and insufficient pain relief[24]. Numerous genetic and environmental factors can contribute to the development of chronic pain, making it difficult to produce a 'one size fits all' treatment. Living with chronic pain seriously

decreases an individual's quality of life[27]. For people suffering from chronic pain, even getting dressed can be an excruciating experience and many cannot lead a normal healthy lifestyle; this in turn causes problems with weight gain and substance abuse[28; 29]. Not surprisingly chronic pain is part of a neurotic triad that encompasses depression and insomnia[27].

Patients suffering from chronic pain are often prescribed a combination of drugs, including existing analgesics and non-traditional analgesics. The main of aim treatment is to compensate the maladaptive changes in the nervous system by reducing functional nociception. Targeting aspects of the nervous system that are functioning normally often leads to dose-dependent adverse effects[23]. Meaning that as analgesic effect lessens over time; the dose cannot simply be increased. In an attempt minimise the side-effects without comprising on analgesia drugs are given in combination at lower doses[30]. For many patients, taking multiple drugs for chronic pain, in addition to any other medication is disheartening and a common reason behind withdrawing from treatment[24].

1.2 Managing Chronic Pain

1.2.1 Antidepressants and Anticonvulsants

Antidepressants are drugs initially used to treat major depression but have become popular treatments for various neurological disorders including addiction, anxiety, insomnia and pain. The use of antidepressants in the management of chronic pain is effective, not only because of the analgesic effect but also positive impact on mood and sleep behaviours; both of which are key grievances of chronic pain sufferers[27; 31]. There are numerous closely related drug classes that fall under the umbrella of antidepressants. In chronic pain management the most commonly prescribed class are tricyclic antidepressants (TCAs) (e.g. amitriptyline). These are non-specific re-uptake inhibitors of neurotransmitters, serotonin (5-HT) and noradrenaline (NA)[23; 32].

In the CNS, 5-HT and NA play an inhibitory role in the descending pain pathway; the pathway that feeds information from the brain to the periphery. TCAs, along with other antidepressants, increase the levels of 5-HT and NA in the synaptic space by preventing up-take by presynaptic neurons and glial cells[32; 33; 34]. Higher levels of inhibitory neurotransmitters will lead to greater inhibition of descending pain signals. It has been demonstrated however, that the onset of analgesia is much quicker than that of mood improvement, suggesting that TCAs produce analgesia through an assisted mechanism[33]. Although the exact mechanism is not known, it has been suggested that TCAs may act as antagonists at Na^+ and Ca^{2+} channels, thereby reducing neuronal excitability[35]. In addition, they may block the glutamate receptor NMDA (N-methyl-D-aspartate)[33; 36]. Serotonin–noradrenaline re-uptake inhibitors (SNRIs)

and selective serotonin re-uptake inhibitors (SSRIs) specifically target serotonin (SERT) and noradrenalin (NET) transporters and may also be prescribed to treat chronic pain; although the adverse effects associated with SNRIs and SSRIs are not as severe, they are not as effective as TCAs[37]. SNRIs have been known to be slightly more effective than SSRIs, suggesting that sufficient analgesia is not entirely dependent on serotoninergic activity[38]. Even though antidepressants are capable of producing a substantial amount of pain relief, some patients (approximately 10%) will discontinue taking them due to unpleasant side-effects[37]. The mechanism of action of antidepressants used to treat chronic pain is shown in Figure 1.2.

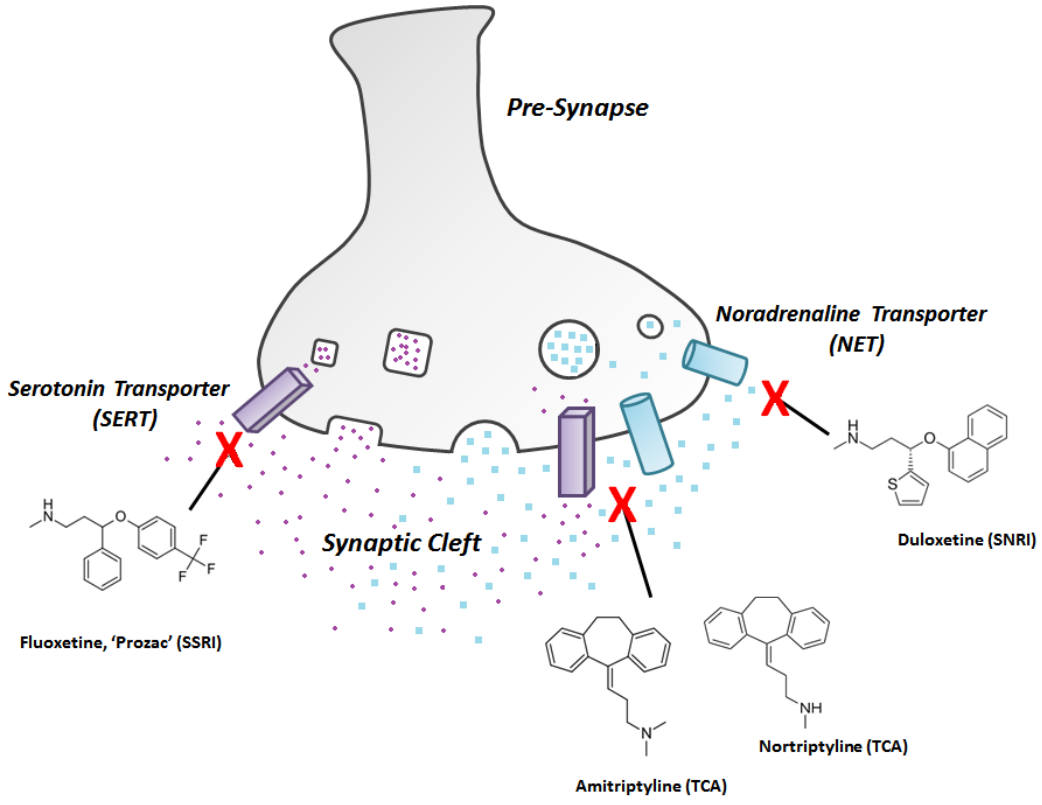

Figure 1.2. Structures and action of antidepressants: Serotonin (represented as purple circles) and noradrenaline (blue squares) are released into the synaptic cleft, where they act on post-synaptic receptors (not shown). Transporters up-take excess neurotransmitter back into the pre-synaptic neuron. TCAs (e.g. amitriptyline and nortriptyline) and SNRIs (e.g. Duloxetine) block both serotonin (SERT) and noradrenaline (NET) transporters. While SSRIs (e.g. Fluoxetine) are selective for SERT[37].

The second major drug class used to manage chronic pain are anticonvulsants. Originally intended to treat epilepsy, they are able to attenuate the neuropathic aspect of chronic pain, much like antidepressants. Anticonvulsants are typically cation channel blockers and are considered 'second-line' treatments due to an increased rate of patient withdrawal[39]. The most commonly prescribed anticonvulsant is carbamazepine, as it is better tolerated than its counterparts[37]. Carbamazepine (Figure 1.3) is sodium channel blocker that causes voltage-gated Na^+ channels (e.g. Nav1.7) to become 'locked' in their inactive state. Decreasing the abundance of functional Nav channels will make depolarisation harder to achieve and reduce the excitability of the nerve[40]. This is a useful countermeasure for increased Nav channel expression seen during chronic pain. While most anticonvulsants target Nav channels, some do have activity at voltage-gated Ca^{2+} channels, such as gabapentin and pregabalin (Figure 1.6)[39]; it is not unusual to prescribe two anticonvulsants, acting on different channels, together for maximum efficacy[41].

Figure 1.3. Chemical structures of anticonvulsants: Carbamazepine (*left*), a sodium channel blocker, is a common treatment for chronic pain. Clonazepam (*right*) is a member of the benzodiazepine family. Benzodiazepines are not as effective in treating pain as other anticonvulsants[39].

In addition to cation channel blockers, another type of anticonvulsant that has been used to treat pain is benzodiazepines (e.g. Clonazepam, Figure 1.3). Benzodiazepines enhance GABAergic activity in the nervous system[42]. GABA (γ-aminobutyric acid) is one of two neurotransmitters that modulate the body's natural inhibitory mechanism in the ascending pain pathway[43]. $GABA_A$ receptors are ligand-gated chlorine channels (Cl^-), which upon opening allow an influx of Cl^- and cause hyperpolarisation of a neuron. Clonazepam and other drugs of its class allosterically modulate GABA receptors, resulting in improved effectiveness of GABA[42]. The major pit fall of benzodiazepines is there powerful effect on the CNS, often leading to the development of psychosis. Heavy sedation and cognitive impairment are also common side-effects and are considered to outweigh the analgesic effect of benzodiazepines[37; 44]. As a result these drugs become extremely unpopular therapeutic options for chronic pain, as move effective alternatives have become available.

1.2.2 Non-Steroidal Anti-inflammatory Drugs and Opioids

Non-steroidal anti-inflammatory drugs (NSAIDs) are the world's most common treatment of functional pain. Over-the-counter NSAIDs, such as aspirin and ibuprofen, are effective pain relievers, whilst more potent prescription NSAIDs, e.g. Naproxen, are welcomed alternatives to opioids [38]. NSAIDs inhibit the synthesis of prostaglandins (PGs) by targeting the catalytic enzyme, cyclooxygenase (COX, Figure 1.4). PGs are released, typically by mast cells, during inflammatory. Not only do they increase the inflammatory response, but they also act directly on neurons to alter ion channel expression[45]. There are two types of COX enzymes; the first is

COX-1, a widely expressed enzyme involved in maintaining good gastrointestinal (GI) function. COX-2 is less commonly expressed than COX-1 and is up-regulated during inflammation. It has also been known to play a role in cardiovascular function[38; 46]. In addition to inhibiting COX enzymes, there is some evidence to suggest NSAIDs may have some antagonistic activity at NMDA receptors[45].

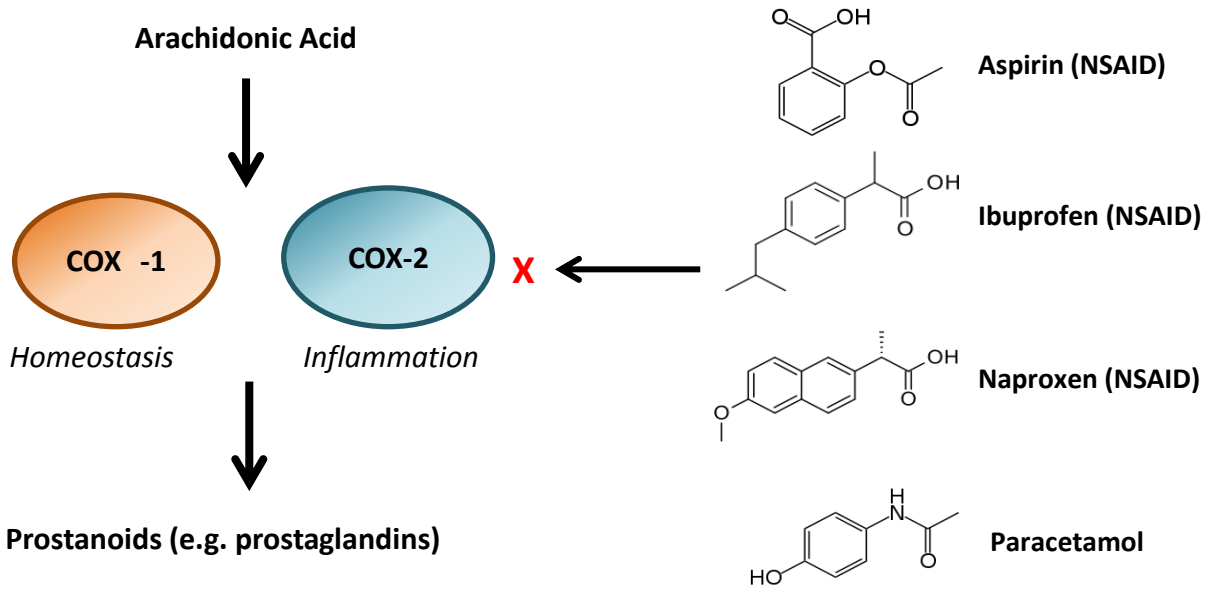

Figure 1.4. Mechanism of action of NSAIDs and paracetamol: COX-1 and COX-2 catalyse the conversion of arachidonic acid into prostanoids. Prostanoids are a family of inflammatory signalling chemicals that include prostaglandins, thromboxanes and the prostacyclins. Prostaglandins, in particular, play a key role in inflammatory pain[45].

As reducing inflammation in the peripheral nervous system is the main mechanism of NSAIDs, they are usually used to treat musculoskeletal disorders that have a large inflammatory pain competent (e.g. rheumatoid arthritis). Although they are not as useful in treating non-inflammatory degenerative diseases like osteoarthritis[47]. Acetaminophen or paracetamol (Figure 1.4) is often used to treat pain arising from osteoarthritis. While

paracetamol does inhibit COX-2 it is not considered a NSAID due to its minor anti-inflammatory effect. This is because paracetamol acts in the CNS, reducing pain sensitisation rather than in PNS, reducing over-all inflammation[46]. By acting in the CNS, paracetamol also has far less side effects and is a more favourable overall. In comparison, inhibition of COX in the periphery by NSAIDs, leads to a great number of side-effects that vastly decrease the practical use of these drugs in chronic pain management[38; 46].

Another traditional analgesic used to treat chronic pain are opioids acting on inhibitory receptors within the descending pain pathway[48]. Endogenous opioids, such as endorphins, are considered the body's natural morphine and not only alleviate pain but are also associated with positive feelings[49]. Synthetic opioid-like drugs can activate opioid receptors with greater efficacy than their natural occurring counterparts. Opioid receptors are G-protein couple receptors (GPCRs) and can be categorised into four types; μ- (MOR), δ- (DOR), κ- (KOR) and nociceptive- (NOR)[50]. They are all widely expressed throughout the nervous, gastrointestinal and immune systems. MOR, targeted by morphine, is the most common opioid receptor and is responsible for the greatest analgesic effect; however it is also the most associated with dependence and respiratory disorders. KOR is closely linked with sedation, whilst DOR and NOR have less analgesic activity they do not cause dependence and sedation to the same extent[38]. Activation of these receptors triggers multiple mechanisms by which analgesia is produced.

Opioids promote analgesia through various mechanisms; the first is inhibition of inflammatory mediator production (e.g. bradykinin). Activation of opioid receptors triggers a conformational change[49]. The receptor disbands and the G-protein component inhibits

activity of adenylyl cyclase (AC); an enzyme responsible for conversion of ATP to cAMP (cyclic adenosine monophosphate). Normally cAMP triggers a protein kinase cascade that ends in increased transcription of inflammatory proteins. Inhibition of this process by opioids leads to an anti-inflammatory effect[51]. Secondly, opioids raise activation thresholds and prevent frequent neuronal firing. Opioid binding increases the activity of Na^+/K^+ pumps [48]. This enhances the inhibitory M-current and causes the neuron to become hyperpolarised more easily. Finally, opioids can indirectly block Ca^{2+} channels, reducing the release of substance P and glutamate[50]. This is prevents stimulation of surrounding nerves. Some opioids, such as methadone, have additional activity, acting as NMDA antagonists and 5-HT/NA re-uptake inhibitors[49]. Despite powerful analgesic effects, opioids are one of the least favourable chronic pain treatments due to adverse effects. Three common opioids, used in pain management, are morphine, methadone and tramadol (Figure 1.5)

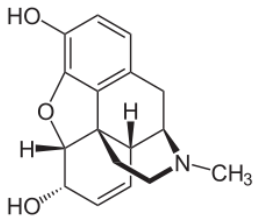

Morphine

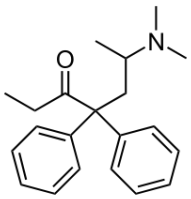

Methadone

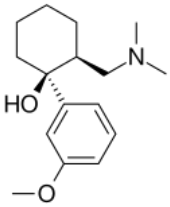

Tramadol

Figure 1.5: Structures of three opioids used to treat chronic pain[49].

1.2.3 Adverse-effects

Adverse effects that develop during treatment of chronic pain through antidepressants and anticonvulsants can be attributed to the effect of the drugs on the nervous system. Drugs acting on the parasympathetic system result in a wide range of side-effects such as dizziness, nausea, dry mouth and cardiac arrhythmias[23; 34; 37]. Anticonvulsants, in particular, have an affect the cardiovascular system, something that will can complications in patients with additional heart problems[44]. Although there is no apparent evidence that suggests anticonvulsants have a worse benefit risk relationship than antidepressants, it has still been reported that more than twice as many patients will stop using anticonvulsants[37].

Most antidepressants increase the presences of neurotransmitters (e.g. 5-HT and NA) in the nervous system, however in the most cases of chronic pain; the normal activity of these neurotransmitters is not hindered. Over-saturation of the CNS, predominantly by 5-HT, will result in adverse neurological effects such as sedation, nightmares and dysphoria[33]. 5-HT, along with opioid receptors, also plays a part in the reward pathway, so repeated use of antidepressants and opioids may cause addiction and dependence. Prolonged use of such drugs may lead to the development of withdrawal-like symptoms, e.g. headaches and agitation[52]. Many of these side-effects are dose-dependent; while a lower dose will results in less side-effects, it will also mean a reduction in analgesia. In order to maintain a sufficient level of pain relief, many drugs are given in combination with other analgesic drugs acting via different mechanisms.

The adverse effects of NSAIDs are linked directly to their mechanism of action. Both COX-1 and COX-2 play roles in vital homoeostasis. COX-1 is required for correct functioning of the GI system. Inhibition of COX-1 may result in renal impairment, ulceration and GI bleeding. Not only may these side-effects contribute to chronic pain but they can be fatal; in the past it has been reported that 12% of patients that develop NSAID driven GI diseases will die as a result[38]. Chronic pain is common amongst the elderly, who will be at greater risk of developing adverse effects in the GI tract. In an effort to prevent this, NSAIDs were re-designed to be selective for COX-2. Unfortunately COX-2 plays an important regulatory role in the cardiovascular system, therefore they are not suitable for patients with existing heart problems[44]. Painful indigestion (dyspepsia) is the most common reason for treatment withdrawal and is seen with both selective and non-selective NSAIDs[38; 53]. Changing the formulation of NSAIDs and combining them with protein pump inhibitors (PPIs) poses a possible solution. Napratec combines naproxen and a PPI (for its GI protective function) in an attempt to maintain efficacy while reducing risk[53; 54]. However, at present NSAIDs, along with opioids, are not considering for long term management of chronic pain. Instead they are used for brief symptomatic relief when needed[53].

As seen with other pain treatments, opioid use is usually accompanied by headaches, sedation, dizziness, and problems relating to GI tract (e.g. nausea and constipation)[46]. There is also a danger of hypoventilation if dosing is not corrected to be proportional to pain severity. Many of these side effects will lessen as treatment goes on or they can be counteracted with other drugs[44]. The most harmful side effects, tolerance and dependence, arise from prolonged use. The mechanism underlying these adverse effects is not clear although there are a number

of theories[55]. Firstly, it has been shown that upon receptor binding naturally occurring opioids will promote the expression of more receptors. This does not occur with opioid drugs, so quicker saturation of available receptors occurs[38]. Secondly, reduction in cAMP will cause the body to re-compensate by increasing ATP, AC and cAMP so receptor activation has less of an effect. In both cases, higher doses will be required to reach the same analgesic level and ultimately prolonged use of opioids will be needed for normal function[55]. It is also possible that taking high doses, long-term will contribute to chronic pain itself. Hyperalgesia may occur as NMDA receptors become sensitised due to increase opioid activity[38; 55]. If this occurs and opioid us is discontinued, patients can develop withdrawal symptoms. This is common with powerful opioids like morphine and methadone[44]. Some weaker opioids (e.g. Tramadol) are less likely to cause tolerance or dependence and can be used to prop up other drugs[46]. Despite this, the addictive nature of opioids often leads to substance abuse, making them a last resort for managing chronic pain.

1.2.4 Gabapentin and Pregabalin

Gabapentin and pregabalin are a distinctive type of anticonvulsants used in the management of chronic pain. Not only is gabapentin effective but it is also has less serious adverse effects; however common side-effects do include dizziness and sedation[56]. As Cav antagonists they are the only drug type in their class and are prescribed for a number of neurological related illnesses. Whilst their ability to alleviate pain falls just short of other psychoactive drugs, they do produce the least harmful side-effects[44; 56]. As adverse effects is

the main reason for switching or stopping a drug course, slight loss of efficacy is sometimes considered a minor sacrifice. Both drugs are often prescribed in combination with a lower dose of other treatments to counteract the loss of analgesia.

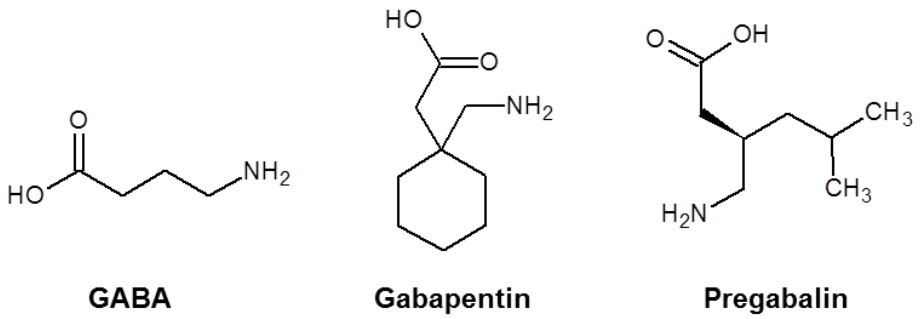

Figure 1.6. The structures of GABA, gabapentin and pregabalin[56].

Gabapentin and pregabalin are both analogues of the neurotransmitter γ-aminobutyric acid (GABA, Figure1.6). Initially these drugs were used as anticonvulsants but they have become a common treatment for chronic pain. Initially designed to cross the blood brain barrier (BBB) and mimic GABA, neither gabapentin nor pregabalin actually acts via directly on the GABAergic system[56]. Gabapentin acts on the α2-δ-1 subunit of voltage-gated Ca^{2+} channels. The purpose of α2-δ subunit is to assist the integration of the channel into the membrane. Binding of gabapentin impairs incorporation into the membrane and causes destabilisation of the pore[57]. There is some evidence to suggest that gabapentin may act on an additional auxiliary subunit, β4a, which also helps translocation to the membrane and compete with thrombospondin, a protein associated with synapse formation, although neither is believed to been the main mechanism of action[56; 58].

In chronic pain there is known to be an up-regulation of calcium channels. Gabapentin appears to have no effect on the normal expression of calcium channels but rather prevents the integration of the up-regulated channels. As a result there is a reduction in excess levels of intracellular calcium. As mentioned earlier, a rise in intracellular calcium is the trigger for numerous events that lead to increased transmission of nociceptive signals[10]. Decreasing the number of active Cav channels will interrupt some of the mechanisms that are responsible for pain hypersensitivity. There is some evidence that gabapentin also inhibits the synthesis of NF-κB, which is required for cytokine production[59]. It is likely that gabapentin reduces pain through a number of mechanisms working alongside one another. Pregabalin acts via the same major mechanism of action as gabapentin and has been shown to have greater potency and a quicker on-set of action[57].

The side-effects of both drugs include swelling, fatigue, and dizziness. Gabapentin has also been associated with depression and increase in suicidal thoughts. As with all therapies for chronic pain, lower doses are given in combination to diminish adverse-effects without comprising on analgesia. Non-steroidal anti-inflammatories (NSAIDs) and opiates are often used as initial treatments for acute pain; as pain becomes chronic, these traditional analgesics become unsuitable and patients are prescribed antidepressants and anticonvulsants[60; 61]. The most common drugs used to manage chronic pain are summarised in Table 1.1

Treatments currently prescribed may be effective for specific aspects of pain (i.e. NSAIDs for inflammatory pain and psychoactives for neuropathic) however, chronic pain is a complex condition with many contributing factors and mechanisms. Therefore, managing pain is difficult. Maximising analgesia and reducing adverse effects, takes effort and careful planning

on behalf of the clinician and the patient. Treatments usually work short-term but they are not suitable for long-term use. For many patients the neurological and physical side-effects, in addition to the requirement of take numerous drugs daily become too much, with roughly about 10% of patients[24] giving up on treatment and choosing to live with chronic pain. As such there is a serious need for more effective means of treating and managing chronic pain. The key to creating an effective treatment for chronic pain is to focus on what specifically causes dysfunctional pain. A greater understanding and utilisation the mechanisms that cause malfunction of the nervous system and contribute to chronic pain, present an opportunity for novel, more efficient treatments.

Table 1.1. Most common drugs used to treat chronic pain: Adapted from Jay *et al. 2014*[17].

Drug Class	Primary Mechanism of Action	Adverse Effects
Antidepressants		
Amitriptyline (TCA)	Inhibits re-uptake of 5-HT/ NA	Sedation, dry mouth, tinnitus, constipation, impaired vision, dizziness, discontinuation syndrome (anxiety, nausea, headaches).
Nortriptyline (TCA)	Inhibits re-uptake of NA/5-HT	
Desipramine (TCA)	Inhibits re-uptake of NA/5-HT	
Fluoxetine (SSRI)	SERT antagonist	
Duloxetine (SNRI)	SERT and NET antagonist	
Venlafaxine (SNRI)	SERT and NET antagonist	
Anticonvulsants		
Carbamazepine	Sodium channel blocker	Arrhythmias, migraines, dizziness, drowsiness, nausea, fatigue, depression, diarrhoea.
Oxcarbazepine	Sodium channel blocker	
Topiramate	Sodium/calcium channel blocker	
Gabapentin	Calcium channel binding antagonist	
Pregabalin	Calcium channel binding antagonist	
NSAIDs		
Aspirin	COX1/2 inhibitor	Gastric ulceration/bleeding, indigestion, increased blood pressure, diarrhoea, nausea.
Ibuprofen	COX1/2 inhibitor	
Naproxen	COX1/2 inhibitor	
Diclofenac	COX1/2 inhibitor	
Opioids		
Tramadol	μ-opioid receptor agonist	Dependence, tolerance, nausea, drowsiness, dry mouth, constipation.
Morphine	μ-opioid receptor agonist	
Methadone	μ-opioid receptor agonist	
Oxycodone	κ-opioid receptor agonist	
Miscellaneous		
Lidocaine (topical anaesthetic)	Sodium channel blocker	Rash
Paracetamol	COX2 inhibitor	Overdose hepatoxicity

1.3 Mechanisms of Chronic Pain

1.3.1 *Peripheral and Central Sensitisation*

Chronic pain has three unique symptoms, painful response to innocuous stimuli (allodynia) that may manifest as burning or itching sensation, increased sensitivity to noxious stimuli (hyperalgesia) and the pain in the absence of stimuli (spontaneous activity)[62]. These behaviours come about as a result of a complex series of interconnecting events that cause sensitisation of the nervous system[21]. In most cases, these changes are driven by the compensatory immune response that is triggered by neuronal injury. After healing, inflammation usually dissipates and the sensory circuitry involved to returns to normal, however in chronic pain the peripheral and central nervous system become permanently sensitised[19].

Sensitisation is caused by changes in ion channel expression and activity. Of particular interest is the up-regulation of Nav1 channel family. Several attempts have been made to pin-point the major Nav1 subtype involved in hyperexcitability. Through the use of channel blockers and knock-down (KD) mouse models, Nav1.3, Nav1.7 and Nav1.8, have all been implicated in neuron hypersensitivity; KD models involve a reduction in the expression of a vital genes [19,63]. Another cation channel, that has been attributed to sensitisation, is the HCN (hyperpolarisation-activated cyclic nucleotide-gated) channel. HCN channels are non-specific cation channels that are activated close to the threshold and help achieve depolarisation required for action potentials. These are known to be up-regulated during chronic pain and HCN antagonists are able to reduce spontaneous activity [64]. Down-regulation of K^+ channels

and up-regulation of Ca^{2+}, also play central roles in membrane hyperexcitability. In the case of temperature dependant channels (e.g. TRPV1-4), the activation threshold can be lowered so significantly that nociceptors are triggered by normal body temperature, thus giving the illusion of pain without a stimulus[3].

Altered expression and function of ion channels is the end-point of transcriptional events that are driven by restorative inflammation[22]. Pro-inflammatory mediators (e.g. ATP, bradykinin, PGE_2, etc.) trigger a series of calcium-dependant intracellular events, usually involving protein kinases, that lead to the activation of transcription factors[65].

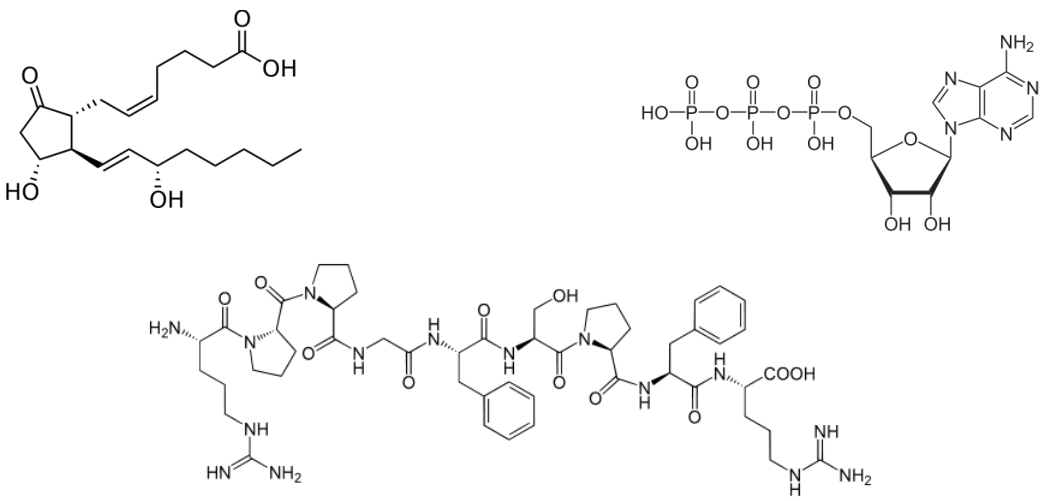

Figure 1.7. Structures of prostaglandin E2 (PGE_2) (*top left*), adenosine triphosphate (ATP) (*top right*) and bradykinin (*bottom*).

These events are complex and not well understood however a number key transcription factors have been identified, including SOX-11 (**S**ry-related HMG b**ox)**, AP-1 (activator protein 1) and ATF_3 (Activating transcription factor 3)[19]. Inflammatory mediated up-regulation is not just limited to activation of transcriptional pathways. Inflammatory proteins can aid the

trafficking and integration of ion channels, as well as direct or indirect agonism. For example, TRPV1 opening is mediated by inhibitory PIP_2 (phosphatidylinositol 4, 5-bisphosphate). Bradykinin acting on bradykinin receptor (B_2) receptors triggers the breakdown of PIP_2 by PLC (phospholipase C) into DAG (diacyl glycerol) and IP_3 (inositol 1, 4, 5-trisphosphate). IP_3 increases intracellular Ca^{2+}, while DAG activates protein kinase C (PKC) which can down-regulate potassium channels (Figure 1.8)[66]. Bradykinin, may also trigger the conversion of arachidonic acid into 12-HPETE (hydroperoxyeicosatetraenoic acid). 12 HPETE mimics the effect of vanilloids on TRPV channels[67; 68]. While, NF-κB acts on PAR2, triggering a kinase cascade, that involves ERK1/2 (extracellular-signal-regulated kinases) and JNK (c-Jun N-terminal kinases). This ultimately leads to activation of the previously mentioned PIP_2-PLC pathway[33].

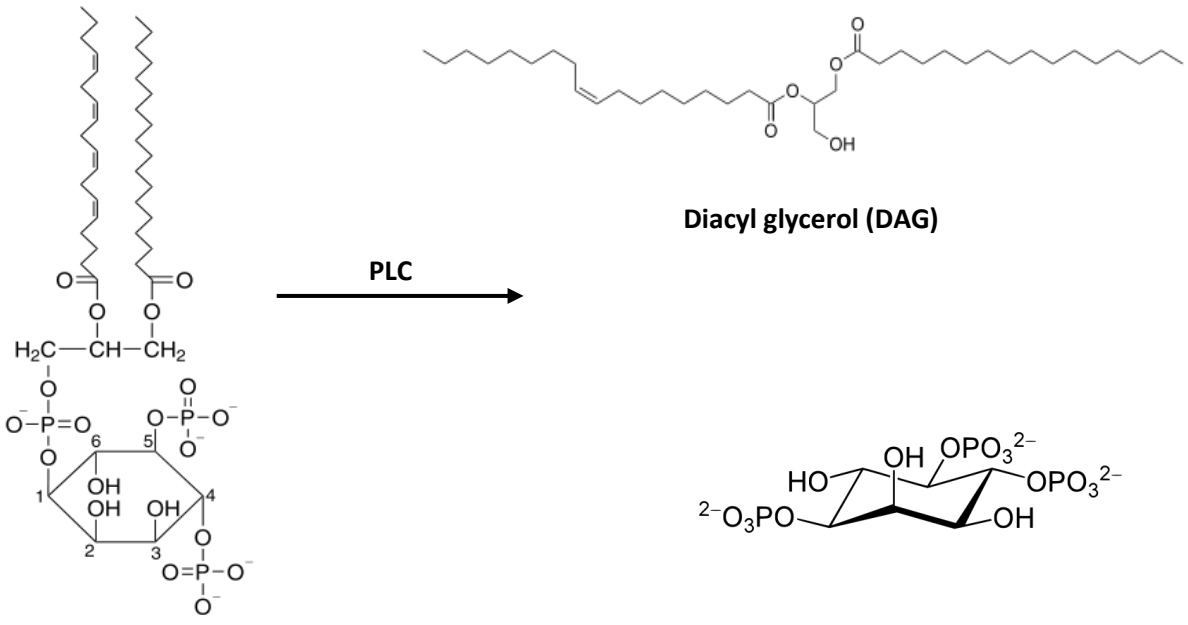

Figure 1.8. Breakdown of PIP_2 into IP_3 and DAG via the enzyme PLC: This pathway is triggered by bradykinin acting on B_2 receptors. PIP_2 regulates the opening of TRPV1, while IP_3 increases intracellular Ca^{2+} and DAG down-regulate potassium channels[66].

Another prominent inflammatory mediator in sensitisation is brain-derived neurotrophic factor (BDNF). This neurotrophin is released from affected neurons and immune cells during inflammatory pain and is heavily involved in the sensitisation of the nervous system[65]. BDNF increases glutamate activity via phosphorylation of NMDA subunits, NR1; more activate subunits means more functional receptors. Blocking BDNF production has been shown to reduce both hyperalgesia and allodynia[69].

Spontaneous activity is likely to be caused by the activation thresholds of nociceptive neurons lowering to that of normal body temperature[70]. Allodynia is the perception of pain following an innocuous stimulus (i.e. light touch). Malfunction of non-nociceptive neurons usually occurs at the site of injury (e.g. sensitisation) or in the dorsal horn (e.g. disinhibition), where sensory neurons from the PNS and CNS synapse. In most cases this type of pain occurs following mechanical stimuli (e.g. pressure, contraction, distension and sound), so allodynia is often referred to as mechanical allodynia[71].

Normally, neurons specialising mechanoreception are large, fast conducting myelinated Aβ-fibres[3]. Intracellular kinase cascades, such as the MAPK/ERK (mitogen-activated protein kinase/ extracellular signal-regulated kinases) pathway that is normally seen in noxious signalling has be revealed to occur in Aβ-fibres after neuronal injury[72]. Pro-inflammatory proteins (e.g. BDNF) are known to upregulate mechanosensory ion channels, PIEZO and TRPC. PIEZO2 (Piezo-type mechanosensitive ion channel component 2) is the pore forming subunit of cation channels found in sensory neurons and has been implicated in the development of allodynia[73; 74]. It is probable that increased sensitivity of both primary nociceptive and sensory fibres may influence projection neurons across the dorsal horn, i.e. activation of peripheral

mechanosensory neurons creates nociceptive inputs in the CNS. In addition, the activation threshold of, mechanically insensitive, TRPV channels may become so low that they respond to mechanical stimulus[73]. As well as neuronal sensitisation, it was a suggested that growth factors, released during inflammation, act on uninjured Aβ-fibres causing them to sprout new axons that grow into laminae II[75]. Recently it has been shown that these 'sprouts' may be an undiscovered sub-class of nociceptive neurons that become far more pronounced following nerve injury, the precise nature of these neurones remains a mystery[76].

Hyperexcitability of the nervous system is just one of the two major contributors to dysfunctional pain. The other is a malfunction of natural pain regulation between the PNS and CNS. Loss of inhibitory activity in the dorsal horn of the spinal cord is different from the descending pathways that involve 5-HT, NA and opioids[77]. Inhibition of the ascending pain pathway is heavily involved in regulation of signals from the PNS to the CNS and the interactions between nociceptive and non-nociceptive neurons.

1.3.2 Disinhibition

The dorsal horn is sub-divided into laminae I-V, where primary mechanosensory neurons terminate in the nucleus proprius (laminae III-V), while nociceptive neurons input into the marginal nucleus (laminae I) and substantia gelatinosa (laminae II)(Figure 1.9)[77; 78]. Small inhibitory interneurons synapse with neurons from the periphery and projection neurons than transmit signals to the brain (Figure 1.9). They regulate input between sensory neurons through GABAergic and glycinergic activity[79]. GABA/glycine, released from inhibitory

interneurons, acts post-synaptically on projection neurons[43]. These interneurons can be activated via inputs from descending nociceptive and non-nociceptive neurons, as well as inhibitory NA and 5-HT neurons[80]. Introduction of antagonists into this system are able to create an effect similar to allodynia and hyperalgesia[19]. This emphasises the importance of GABA and glycine in correct pain processing and role of disinhibition in chronic pain progression. GABA receptor type A ($GABA_AR$) and glycine receptors (GlyR) are both ligand-gated ion channels that allow chloride ions (Cl^-) to cross the membrane and cause hyperpolarisation[43]. Loss of functional GABAergic and glycinergic has been directly linked to the development of spontaneous activity, hyperalgesia and allodynia[81].

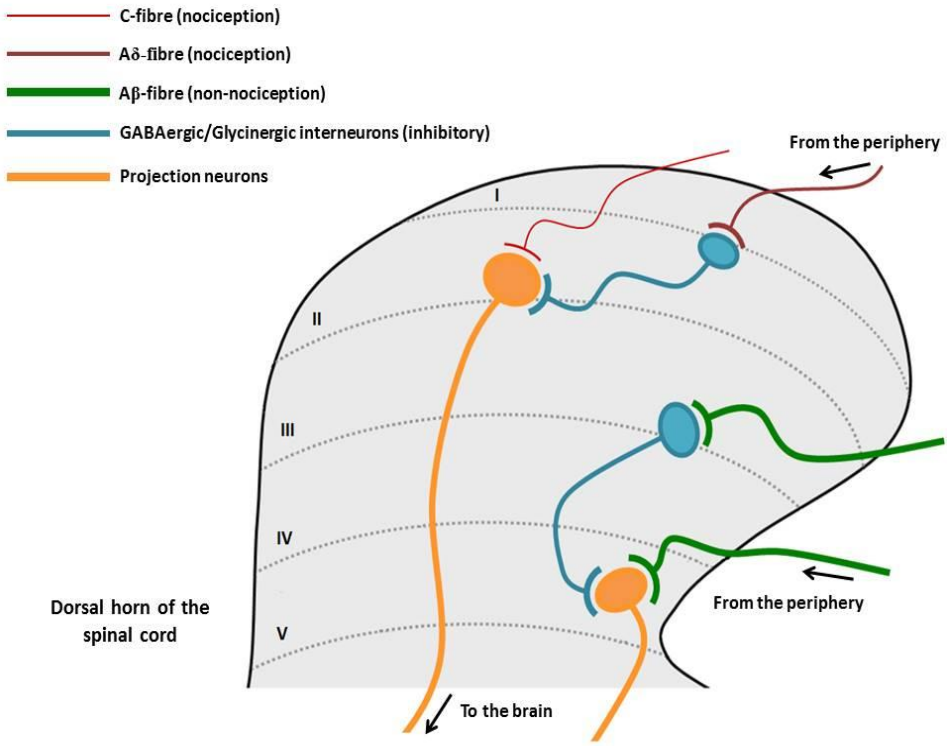

Figure 1.9. Simplified schematic of synapsing neurons in the dorsal horn: The dorsal horn is divided into laminae I-V. Nociceptive, C-fibres and Aδ-fibres synapse in laminae I and II. They interact with projection neurons, leading up to the thalamus and with inhibitory interneurons. Inhibitory interneurons regulate input into projection neurons through GABAergic or glycinergic activity. During chronic pain states, this mechanism is reduced[87,93].

One potential mechanism of disinhibition is a chlorine gradient shift from hyperpolarisation to depolarisation. The chlorine gradient relies on correct function of the potassium-chloride transporter 2 (KCC2). BDNF stimulates the down-regulation of KCC2[82]. In addition KCC2 relies on the Na^+/K^+ pump for homeostasis of potassium. Increased expression of Na^+ channels will alter the potassium gradient, which in turn impacts the chlorine gradient[82]. Another source of disinhibition is the down-regulation of post-synaptic GlyR. The prostaglandin, PGE_2 released during inflammation, acts on the EP_2 (prostaglandin E2 receptor). PGE_2 increases intracellular cAMP and triggers a protein kinase A (PKA) cascade[80]. PKA phosphorylates GlyRs and prevents successful ligand binding. EP_2 agonists can directly inhibit glycine activity and cause allodynia but they have no effect GABA, suggesting that glycine activity alone is an important part of ascending pain inhibition[81]. Apoptosis of inhibitory interneurons has also been reported, however the reasoning behind this remains unknown[19]. Although disinhibition plays a major role in chronic pain, many of the contributing mechanisms remain unclear. It certain that disinhibition is important to the development of allodynia and hyperalgesia, as one of the major features of inhibitory interneurons in the DRG is to prevent miscommunication between sensory and nociceptive neurons and the CNS. Rescuing inhibition offers an excellent therapeutic opportunity for chronic pain. $GABA_AR$ receptor already exists as a target for various anaesthetics and analgesics (i.e. Benzodiazepines) however due to a strong hypnotic side-effects, it is would not make a suitable therapeutic target[46]. In comparison GlyRs have largely been over-looked by the pharmaceutical industry.

Understanding the some of the process underlay chronic pain has led to the development of new drug targets. Drugs acting to mitigate the changes that lead to malfunction of pain

pathways, offer potentially more effective and safer treatments than those available currently. Many drug targets, that in the past have been overlooked, are now known to play vital roles in the development of both inflammatory and neuropathic chronic pain. Validation of these targets has inspired a new wave of potential treatments and the discovery of new analgesic properties of existing drugs (Table 1.2)[83]

Table 1.2. Novel compounds for the treatment of chronic pain in Phase II/III development: Taken from Gilron *et al. 2014*[83].

Compound	Company	Mechanism of Action	Stage of Development
DS-5565	Daiichi Sankyo	Calcium channel blocker	Phase II
CNV-2197944	Convergence Pharmaceuticals	T-type calcium channel blocker	Phase II
Z-160	Zalicus	N-type calcium channel blocker	Phase II
ABT-639	AbbVie	T-type calcium channel blocker	Phase II
GRC-17536	Glenmark	TRPA1 antagonist	Phase II
DWP-05195	Daewoong	TRPV1 antagonist	Phase II
GRC-15300	Glenmark	TRPV3 antagonist	Phase II
ICA-105665 (Icagen)	Pfizer	Potassium channel agonist	Phase II
CNSB-015 (Flupirtine)	Relevare Pharmaceuticals	Potassium channel agonist	Phase III
REL-10 xx (d-Methadone)	Relmada Therapeutics	Opioid receptor agonist	Phase II
CNV-1014802	Convergence Pharmaceuticals	Voltage-gated sodium channel blocker	Phase II
TD-9855	Theravance	5-HT/NA re-uptake inhibitor	Phase II
BND-11624	Brane Discovery	NMDA antagonist	Phase II
NXN-462	NeurAxon	Cannabinoid CB2 receptor agonist	Phase II

1.4 Novel Therapeutic Targets

1.4.1 M-Current

Pharmacological enhancers of the M-current are growing increasingly popular as analgesics. The I_m is an inhibitory current controlled by the opening of voltage-dependant K^+ channels (Kv) and can be described as a voltage-dependant non-inactivating K^+ current[15]. For most neurons, resting potential lies at -70mV and when the membrane potential surpasses -55mV, an action potential occurs. The Kv channels that are responsible for the M-current open at approximately -60mV [84]. During depolarisation, M-current is generated and acts as an opposing force to prevent the activation threshold from being achieved. In addition, it generates the refractory period, a period of hyperpolarisation following successful firing of an action potential that prevents successive stimulation of a neuron[85].

The Kv channels that produce M-current belong to the Kv7.1-5 family. Kv7.3 is the only type that is able exist in combination with the other subtypes, however only Kv7.2 has been known to generate M-current [15]. Many established mechanisms of dysfunctional pain, lend themselves to the reduction of the M-current. For example, bradykinin is able to close Kv7 channels via PKC, while PIP_2 is a vital co-factor for Kv7.2 function. A number of pain transmitters, such as glutamate, have also been shown to inhibit the M-current[85; 86]. Loss of M-current will mean that the activation threshold is reached much quicker and a reduction in the refractory period allows for repetitive firing of action potentials. The overall result is intense pain response following a weak stimulus; a key component in the development of

spontaneous activity and hyperalgesia. Drugs acting on Kv7.2/3 channels may be able to rescue normal M-current function and attenuate chronic pain.

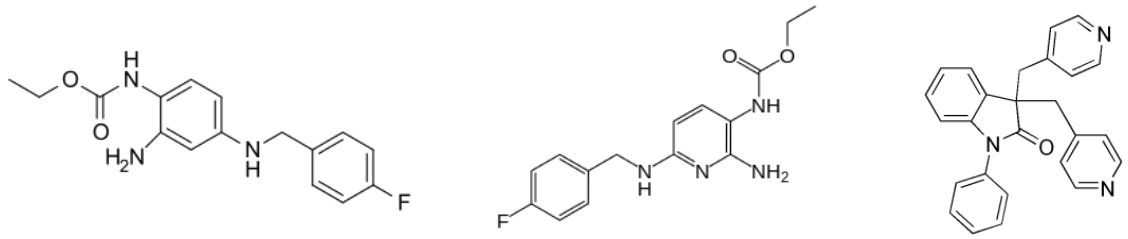

Figure 1.10: Anticonvulsants, retigabine (*left*) and flupiritine (*middle*) are being considered as new treatments for chronic pain. Linopirdine (*right*) is a Kv7.2/3 blocker used to reverse the effect of retigabine[87].

Many emerging treatments are based on existing drugs such as the anticonvulsants, retigabine and flupiritine (Figure 1.10)[87]. In an artificial hyperexcitability model, made to mimic sensitisation seen during chronic pain, both retigabine and flupiritine were able to diminish neuronal excitation[88]. Retigabine, like many anticonvulsants, was originally designed as modulator of $GABA_A$Rs; however it has shown to have a much higher affinity for Kv7 channels[89]. Administration of a Kv7.2/3 blocker, linopirdine, is able to reverse the analgesic effect of retigabine suggesting that Kv7.2/3 and the potentiation of M-currents is indeed the mechanism of action[15]. Retigabine can attenuate pain in neuropathic and inflammatory pain models. Intact nociceptive fibres do not response to retigabine, indicating that normal nociceptive processing will not be altered by retigabine, a positive attribute for an analgesic[89]. Flupiritine is the parent compound on which retigabine was based. For a long time, flupiritine was classified as a non-opioid analgesic and its mechanism of action was unknown[87]. It was believed that flupiritine may act on NMDA or $GABA_A$Rs; it is now known that Kv7.2/3 is the

major target[90]. Both flupiritine and retigabine are slowly becoming popular treatments for chronic pain, particularly pain arising from chemotherapy and fibromyalgia[15; 90]. As more research is carried out on Kv7.2/3 and the M-current, it is likely that flupiritine and retigabine, as well as new drugs of the same class will become prominent players in the management of chronic pain.

1.4.2 Sodium and Calcium Channels

Up-regulated Na^+ and Ca^{2+} channels are the crux of neuronal hyperexcitability. Not only does increased function of these channels result in greater frequency of action potentials but they also act as a trigger of numerous cellular events that affect other aspects of nociception. Decreasing the activity of these ion channels will inevitably lead to a reduction in pain, making them an obvious drug target. Unfortunately, many Na^+ and Ca^{2+} channels are vital for normal nociception so there is a danger that blocking these channels will negatively impact functional pain processing[91]. Regardless, investigating the effect of cation channel blockers on pain may pave the way for a new class of analgesics.

Non-selective cation ion channels involved in nociceptive present a good starting point. Novel antagonists acting on TRP channels, for example TRPV1, TRPA1 and TRPM8, are able to reduce varying pain behaviours in different pain models[92]. However, the results of the these studies are reliant on the pain model and the nature of analgesia achieved, due to direct role some channels play in development of pain[92; 93]. Thereby the usefulness of non-selective TRP antagonists does not translate well into patients, whom have numerous factors contributing

to their pain. Optimistically, the analgesic properties of TRP antagonist present a basis for the development of more viable treatments.

Recently research into the potential for Nav1 specific antagonists has been carried out[63]. Of particular interest is Nav1.7, where loss of function mutations effect normal nociception and KD mice models exhibit reduced pain behaviours[19; 63]. Lidocaine, a topical analgesic, and some anticonvulsants act as weak antagonists at Nav1 channels[91]. Most of the research of Nav1.7 antagonists is in its infancy, but the results are promising.

The use of Ca^{2+} channels blockers as analgesics is also being explored. N-type calcium channels (Cav2) are known to play role in the development of neuropathic and inflammatory pain through the use of KD mice models[94]. Ziconotide is an atypical drug used to treat severe pain. It is Cav2.2 channel antagonist that can only be administered via CSF infusion (cerebrospinal fluid) and causes crippling motor neuron effects[95]. While it is not suitable for the management of chronic pain, ziconotide has inspired the production of leconotide, a novel drug that has shown to be effective in pain models with little side effects[96]. Studies into novel blockers of Cav3.2 channels have also shown a reduction in allodynia in animal pain models[97].

1.4.3 Glutamate

As the major neurotransmitter involved in nociception, glutamate and its receptors have much potential as novel treatment targets. Many of the phenotypic changes that occur in neuropathic and inflammatory pain will increase glutamatergic activity, either through increased levels of glutamate itself or the expression and efficacy of its receptors. Glutamate plays an important role in sensory processing including functional nociception, therefore targeting the synthesis and release of glutamate does carry risk[98]. The alternative is to target the receptors that interact with glutamate and are up-regulated during chronic pain.

The most obvious target is NMDA receptors; NMDA receptors are an inotropic cation channel that opens upon binding of glutamate and various co-factors[99]. It has been well documented that NMDA receptors are up-regulated during chronic pain[25]. The concept of NMDA antagonists has existed for a number of decades, although very little research has been carried out in regards to creating a clinically approved analgesic[100]. Most current NMDA antagonists are used as anaesthetics and for veterinary purposes. Not only are they highly sedative but they cause a number of psychoactive side effects[101]. They provide some use in the treatment of motor neuron degenerative diseases and hyperalgesia stemming from opioid withdrawal, although this is a rare occurrence[102]. Like opioids, many NMDA antagonists are commonly used as drugs of substance abuse. The most well-known NMDA antagonist is ketamine (Figure 1.11).

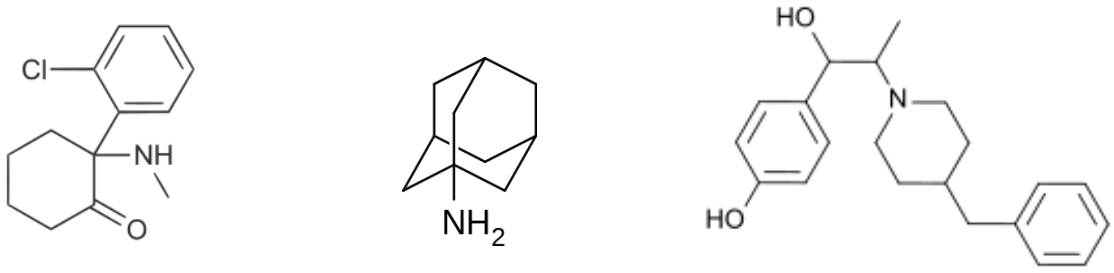

Figure 1.11. Structures of NMDA antagonists, ketamine (*left*), amantadine (*middle*) and ifenprodil (*right*)[102-104].

Ketamine is a NMDA antagonist that binds to NMDA receptor subunits and prevents proper formation of the receptor[101]. While ketamine is considered non-selective it is believed that it favours binding to the NR2A/D subunits (i.e. binding site of glutamate)[100; 101]. The antiviral, amantadine (Figure 1.11) is also a weak NMDA antagonist. While less potent than ketamine; amantadine is useful in treating a number of neurological conditions, although this is likely due to its dual dopaminergic effects[102]. Recently novel NR2 selective antagonists have shown to reduce analgesia without effecting cognitive or motor function[103]. This suggests that any analgesic effect of ketamine or amantadine is the result of preventing glutamate binding to NMDA. Ifenprodil (Figure 1.11) is a novel analgesic that directly targets N2B subunits and reduces pain without side-effects[104].

NMDA receptors are not the only potential drug target that may reduce glutamatergic activity. Glutamate also acts on its other receptor, mGluR (metabotropic glutamate receptor)[105]. These receptors are different from inotropic GluRs, which include NMDA amongst their ranks[106]. mGluRs are GPCRs that have 8 subtypes, one of which, mGluR1 has been implicated in neuropathic pain via KD mice models. Interest in these receptors is

mounting and in the past five years a series of studies have been carried out measuring the effect of novel allosteric antagonists in various pain models[105; 106; 107]. So far, these compounds have shown promise and may lead the way for new class of drugs that can be used to manage chronic pain.

1.4.4 *Glycine*

Glycine plays important excitatory and inhibitory roles in how the nervous system processes pain[43; 99]. In the past, little research into role of SSGRs as an analgesic target has been carried out. Now as more information comes to light about the importance of glycine, it is becoming an increasingly attractive drug target. Glycine has duel functions in nociception and both offer potential treatment targets.

While glycine plays a vital inhibitory role in nociception, it is also has a mild excitatory function. Glycine, along with D-serine, is a vital co-factor of NMDA receptors. Binding of glycine to the NR1 subunit allows glutamate to bind to the NR2 subunit, which opens the channel pore[48]. The NR1 binding site can be easily oversaturated, so the levels of glycine need to be carefully regulated. Glycine transporters, GlyT1 and GlyT2, harvest excess glycine from synaptic spaces to prevent oversaturation. GlyT1 and GlyT2 are members of the SLC6 family (sodium dependant solute carrier family 6) that are expressed both pre-synaptically and on glial cells[108]. GlyT1 is localised predominantly close to NMDA receptors, while both types are found near inhibitory interneurons. Inhibition of GlyT1 has been shown to attenuate allodynia. This is most likely due to increased levels of glycine at inhibitory synapses, as co-

administration of GlyR antagonist, strychnine can reverse the effect[99]. It is also possible that increased glycine levels cause saturation of the NMDA binding site. Oversaturation of the binding site may trigger endocytosis of the receptor, thus decreasing the number of functional NMDA receptors and neuronal excitability. However such an effect would need prolonged exposure at high concentrations[55; 99]. In addition, GlyT1 inhibition does not affect normal nociceptive, so the effect on NMDA is likely to play a very minor role in analgesia[99]. Increasing the levels of glycine acting on GlyRs is able to relieve pain to a greater extent than gabapentin, the 'gold standard' of analgesic agents. So it is highly probable that targeting the receptor itself will also produce an analgesic effect[109].

Drugs acting on GlyRs have the potential to produce a superior analgesic than those that exist currently. It is known that simply increasing glycine levels can attenuate pain and there is evidence to show that agents acting allosterically on GlyRs are more effective at increasing glycinergic activity than direct agonists[110]. This provides further basis for the GlyR as drug target. Some research has been conducted using cannabinoids as analgesics. Cannabidiol (CBD) and its analogue DH-CBD (dehydroxyl-CBD) are non-psychoactive cannabinoids that are able to increase inhibitory currents mediated by glycine (Figure 1.12). DH-CBD was also seen to restore function to GlyRs that had been affected by PGE_2. The reduction of inflammatory and neuropathic pain by CBD and DH-CBD through glycinergic activity was confirmed using strychnine and GlyR KD models; in both cases the analgesic effect as reversed[111]. The role of GlyRs as a drug target will be discussed further in Chapter 2.

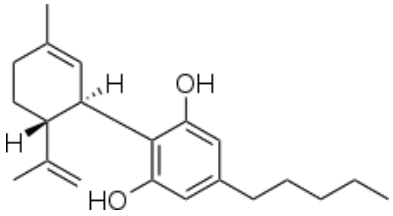

Figure 1.12. Structure of cannabidiol[111].

Allosteric modulators of GlyRs are promising analgesic agents. In comparison to other novel analgesics, such as retigabine, NMDA antagonists and cation ion channels, GlyR agonists have a more favourable pharmacologic response/side-effect relationship. As a bonus, the unique role that α1 SSGRs play in the spinal cord means that it is unlikely that they cause major on-target toxicity. Positive allosteric modulators (PAMs) of SSGRs have been shown to alleviate pain better gabapentin, a drug commonly used to treat chronic pain (see Chapter 3). As such PAMs of GlyRs, have the potential to become innovative, safe and effective analgesics.

1.5 Project Aims

The goal of this project is to carry out lead optimisation of positive allosteric modulators of glycine receptors expressing the α1 subunit, with the ultimate aim of generating a new treatment for chronic pain; glycine receptors containing the α3 subunit are known to be downregulated during the development of pain hypersensitivity. Restoring inhibitory glycinergic activity in nociceptive signalling presents a novel approach to treating chronic pain. The desired target profile for these compounds is shown in Table 1.3.

This thesis will be focussed on the optimisation on pharmacokinetics, particularly microsomal stability, *in vivo* rat metabolism and cytochrome P450 enzyme inhibition of propofol analogues. The ideal drug candidate should meet all criteria in outlined in Table 1.3.

Table 1.3. Lead optimisation target profile for this project.

Parameter	Target
Physiochemical	
Aq. Sol (mg/mL)	0.01- 0.5mg/mL (pH7.4)
LogP	≤4
LogD	1-3
MW (Da)	≤450
TPSA (Å)	40-90
HBD	≤3
pKa	3-9
MPO	4≥
Selectivity	
GlyRα1 EC_{50}	≤1μM
$GABA_AR$ EC_{50}	≥ 100x GlyRα1 EC_{50}
Pharmacokinetics	
Oral Bioavailability (%)	≥20
$T_{1/2}$ (Rat Liver Microsomes)	≥60 min
$T_{1/2}$ (Human Hepatocytes)	≥30 min
Brain CSF	3x GlyRα1 EC_{50} (at 2/3 hrs, 1-3mg/Kg)
Protein Binding	≤99.5%
Toxicity	
hERG toxicity	IC_{50} ≥ 10μM
HepG2 toxicity	No tox at 50x GlyRα1 EC_{50}
AMES genotoxicity	negative
CYP Inhibition	IC_{50} ≥ 10μM

1.6 References

1. Meldrum, M. L. (2003). A Capsule History of Pain Management. *Journal of the American Medical Association* **290**, 2470-2475.
2. Woolf, C. J. & Ma, Q. (2007). Nociceptors-Noxious Stimulus Detectors. *Neuron* **55**, 353-364.
3. Julius, D. & Basbaum, A. I. (2001). Molecular mechanisms of nociception. *Nature* **413**, 203-210.
4. Caterina, M. J., Rosen, T. A., Tominaga, M., Brake, A. J. & Julius, D. (1999). A capsaicin-receptor homologue with a high threshold for noxious heat. *Nature* **398**, 436-441.
5. Caterina, M. J. & Julius, D. (2001). The vanilloid receptor: A molecular gateway to the pain pathway. In *Annual Review of Neuroscience*, Vol. 24, pp. 487-517.
6. Bandell, M., Story, G. M., Hwang, S. W., Viswanath, V., Eid, S. R., Petrus, M. J., Earley, T. J. & Patapoutian, A. (2004). Noxious cold ion channel TRPA1 is activated by pungent compounds and bradykinin. *Neuron* **41**, 849-857.
7. Bautista, D. M., Siemens, J., Glazer, J. M., Tsuruda, P. R., Basbaum, A. I., Stucky, C. L., Jordt, S. E. & Julius, D. (2007). The menthol receptor TRPM8 is the principal detector of environmental cold. *Nature* **448**, 204-208.
8. Gaudet, A. D., Popovich, P. G. & Ramer, M. S. (2011). Wallerian degeneration: Gaining perspective on inflammatory events after peripheral nerve injury. *Journal of Neuroinflammation* **8**.
9. Hughes, P. M., Wells, G. M. A., Perry, V. H., Brown, M. C. & Miller, K. M. (2002). Comparison of matrix metalloproteinase expression during Wallerian degeneration in the central and peripheral nervous systems. *Neuroscience* **113**, 273-287.
10. Üçeyler, N. & Sommer, C. (2006). Wallerian degeneration and neuropathic pain. *Drug Discovery Today: Disease Mechanisms* **3**, 351-356.
11. Ehlers, M. D. (2004). Deconstructing the axon: Wallerian degeneration and the ubiquitin–proteasome system. *Trends in Neurosciences* **27**, 3-6.
12. Glass, J. D., Culver, D. G., Levey, A. I. & Nash, N. R. (2002). Very early activation of m-calpain in peripheral nerve during Wallerian degeneration. *Journal of the Neurological Sciences* **196**, 9-20.
13. Chen, Y., Yang, C. & Wang, Z. J. (2011). Proteinase-activated receptor 2 sensitizes transient receptor potential vanilloid 1, transient receptor potential vanilloid 4, and transient receptor potential ankyrin 1 in paclitaxel-induced neuropathic pain. *Neuroscience* **193**, 440-451.
14. Mucha, M., Ooi, L., Linley, J. E., Mordaka, P., Dalle, C., Robertson, B., Gamper, N. & Wood, I. C. (2010). Transcriptional control of KCNQ channel genes and the regulation of neuronal excitability. *Journal of Neuroscience* **30**, 13235-13245.
15. Rivera-Arconada, I., Roza, C. & Lopez-Garcia, J. A. (2009). Enhancing m currents: a way out for neuropathic pain? *Front Mol Neurosci* **2**, 4.
16. Costigan, M., Scholz, J. & Woolf, C. J. (2009). Neuropathic pain: A maladaptive response of the nervous system to damage, Vol. 32, pp. 1-32.

17. Jay, G. W. & Barkin, R. L. (2014). Neuropathic pain: Etiology, pathophysiology, mechanisms, and evaluations. *Disease-a-Month* **60**, 6-47.
18. Seroussi, R. (2015). Chronic Pain Assessment. *Physical Medicine and Rehabilitation Clinics of North America* **26**, 185-199.
19. Costigan, M., Scholz, J. & Woolf, C. J. (2009). Neuropathic pain: A maladaptive response of the nervous system to damage. In *Annual Review of Neuroscience*, Vol. 32, pp. 1-32.
20. Dubový, P. (2011). Wallerian degeneration and peripheral nerve conditions for both axonal regeneration and neuropathic pain induction. *Annals of Anatomy* **193**, 267-275.
21. Stemkowski, P. L., Biggs, J. E., Chen, Y., Bukhanova, N., Kumar, N. & Smith, P. A. (2013). Understanding and treating neuropathic pain. *Neurophysiology* **45**, 67-78.
22. Rotshenker, S. (2011). Wallerian degeneration: The innate-immune response to traumatic nerve injury. *Journal of Neuroinflammation* **8**.
23. Barkin, R. L. & Fawcett, J. (2000). The management challenges of chronic pain: The role of antidepressants. *American Journal of Therapeutics* **7**, 31-47.
24. Breivik, H., Collett, B., Ventafridda, V., Cohen, R. & Gallacher, D. (2006). Survey of chronic pain in Europe: Prevalence, impact on daily life, and treatment. *European Journal of Pain* **10**, 287-333.
25. Campbell, J. N. & Meyer, R. A. (2006). Mechanisms of Neuropathic Pain. *Neuron* **52**, 77-92.
26. Bridges, S. (2012). Chronic pain. *Health, social care and lifestyles*, 291.
27. Senba, E. (2015). A key to dissect the triad of insomnia, chronic pain, and depression. *Neuroscience Letters* **589**, 197-199.
28. Jamison, R. N., Stetson, B., Sbrocco, T. & Parris, W. C. (1990). Effects of significant weight gain on chronic pain patients. *Clin J Pain* **6**, 47-50.
29. Compton, P. & Athanasos, P. (2003). Chronic pain, substance abuse and addiction. *Nurs Clin North Am* **38**, 525-37.
30. Mao, J., Gold, M. S. & Backonja, M. M. (2011). Combination Drug Therapy for Chronic Pain: A Call for More Clinical Studies. *The Journal of Pain* **12**, 157-166.
31. McQuay, H. J. & Moore, R. A. (1997). Antidepressants and chronic pain. *British Medical Journal* **314**, 763-764.
32. Chan, H. N., Fam, J. & Ng, B. Y. (2009). Use of antidepressants in the treatment of chronic pain. *Annals of the Academy of Medicine Singapore* **38**, 974-979.
33. Ryder, S. A. & Stannard, C. F. (2005). Treatment of chronic pain: Antidepressant, antiepileptic and antiarrhythmic drugs. *Continuing Education in Anaesthesia, Critical Care and Pain* **5**, 18-21.
34. Verdu, B., Decosterd, I., Buclin, T., Stiefel, F. & Berney, A. (2008). Antidepressants for the treatment of chronic pain. *Drugs* **68**, 2611-2632.
35. Dick, I. E., Brochu, R. M., Purohit, Y., Kaczorowski, G. J., Martin, W. J. & Priest, B. T. (2007). Sodium channel blockade may contribute to the analgesic efficacy of antidepressants. *J Pain* **8**, 315-24.
36. Watanabe, Y., Saito, H. & Abe, K. (1993). Tricyclic antidepressants block NMDA receptor-mediated synaptic responses and induction of long-term potentiation in rat hippocampal slices. *Neuropharmacology* **32**, 479-86.

37. Fitzgerald, J. F., Romero, R. & Saberski, L. R. (1998). Complications of antidepressants, anticonvulsants, and antiarrhythmics for chronic pain management. *Techniques in Regional Anesthesia and Pain Management* **2**, 119-129.
38. Slater, D., Kunnathil, S., McBride, J. & Koppala, R. (2010). Pharmacology of nonsteroidal antiinflammatory drugs and opioids. *Seminars in Interventional Radiology* **27**, 400-411.
39. Maizels, M. & McCarberg, B. (2005). Antidepressants and antiepileptic drugs for chronic non-cancer pain. *Am Fam Physician* **71**, 483-90.
40. Jo, S. & Bean, B. P. (2014). Sidedness of carbamazepine accessibility to voltage-gated sodium channels. *Molecular Pharmacology* **85**, 381-387.
41. Finnerup, N. B., Baastrup, C. & Jensen, T. S. (2010). Anticonvulsants in the Management of Chronic Pain. In *Clinical Pain Management*, pp. 121-127. Wiley-Blackwell.
42. Nardi, A. E., Machado, S., Almada, L. F., Paes, F., Silva, A. C., Marques, R. J., Amrein, R., Freire, R. C., Martin-Santos, R., Cosci, F., Hallak, J. E., Crippa, J. A. & Arias-Carrión, O. (2013). Clonazepam for the treatment of panic disorder. *Current Drug Targets* **14**, 353-364.
43. Sivilotti, L. & Woolf, C. J. (1994). The contribution of GABA(A) and glycine receptors to central sensitization: Disinhibition and touch-evoked allodynia in the spinal cord. *Journal of Neurophysiology* **72**, 169-179.
44. Kapur, B. M., Lala, P. K. & Shaw, J. L. V. (2014). Pharmacogenetics of chronic pain management. *Clinical Biochemistry* **47**, 1169-1187.
45. Meves, H. (2006). The Action of Prostaglandins on Ion Channels. *Current Neuropharmacology* **4**, 41-57.
46. Schnitzer, T. J. (1998). Non-NSAID pharmacologic treatment options for the management of chronic pain. *American Journal of Medicine* **105**, 45S-52S.
47. Bonnet, C. S. & Walsh, D. A. (2005). Osteoarthritis, angiogenesis and inflammation. *Rheumatology* **44**, 7-16.
48. Wolosker, H. (2007). NMDA Receptor Regulation by D-serine: New Findings and Perspectives. *Molecular Neurobiology* **36**, 152-164.
49. Przewlocki, R. & Przewlocka, B. (2005). Opioids in neuropathic pain. *Current Pharmaceutical Design* **11**, 3013-3025.
50. Dietis, N., Rowbotham, D. J. & Lambert, D. G. (2011). Opioid receptor subtypes: Fact or artifact? *British Journal of Anaesthesia* **107**, 8-18.
51. Moore, A. R. & Willoughby, D. A. (1995). The role of cAMP regulation in controlling inflammation. *Clinical and Experimental Immunology* **101**, 387-389.
52. Bou Khalil, R. (2012). Addictive potentials of antidepressant drugs. In *Antidepressants: Pharmacology, Health Effects and Controversy*, pp. 27-48.
53. Shah, S. & Mehta, V. (2012). Controversies and advances in non-steroidal anti-inflammatory drug (NSAID) analgesia in chronic pain management. *Postgraduate Medical Journal* **88**, 73-78.
54. Sostek, M. B., Fort, J. G., Estborn, L. & Vikman, K. (2011). Long-term safety of naproxen and esomeprazole magnesium fixed-dose combination: phase III study in patients at risk for NSAID-associated gastric ulcers. *Curr Med Res Opin* **27**, 847-54.

55. Nong, Y., Huang, Y.-Q., Ju, W., Kalia, L. V., Ahmadian, G., Wang, Y. T. & Salter, M. W. (2003). Glycine binding primes NMDA receptor internalization. *Nature* **422**, 302-307.
56. Kukkar, A., Bali, A., Singh, N. & Jaggi, A. S. (2013). Implications and mechanism of action of gabapentin in neuropathic pain. *Archives of Pharmacal Research* **36**, 237-251.
57. Bockbrader, H. N., Wesche, D., Miller, R., Chapel, S., Janiczek, N. & Burger, P. (2010). A comparison of the pharmacokinetics and pharmacodynamics of pregabalin and gabapentin. *Clinical Pharmacokinetics* **49**, 661-669.
58. Eroglu, C., Allen, N. J., Susman, M. W., O'Rourke, N. A., Park, C. Y., Özkan, E., Chakraborty, C., Mulinyawe, S. B., Annis, D. S., Huberman, A. D., Green, E. M., Lawler, J., Dolmetsch, R., Garcia, K. C., Smith, S. J., Luo, Z. D., Rosenthal, A., Mosher, D. F. & Barres, B. A. (2009). Gabapentin Receptor α2δ-1 Is a Neuronal Thrombospondin Receptor Responsible for Excitatory CNS Synaptogenesis. *Cell* **139**, 380-392.
59. Park, S., Ahn, E. S., Han, D. W., Lee, J. H., Min, K. T., Kim, H. & Hong, Y. W. (2008). Pregabalin and gabapentin inhibit substance P-induced NF-kappaB activation in neuroblastoma and glioma cells. *J Cell Biochem* **105**, 414-23.
60. Park, H. J. & Moon, D. E. (2010). Pharmacologic Management of Chronic Pain. *The Korean Journal of Pain* **23**, 99-108.
61. Tavakoli, M. & Malik, R. A. (2008). Management of painful diabetic neuropathy. *Expert Opinion on Pharmacotherapy* **9**, 2969-2978.
62. Dong, Z. & Yu, S. Y. (2013). Neuropathic pain and headache. *Chinese Journal of Contemporary Neurology and Neurosurgery* **13**, 752-754.
63. Lynch, S. M., Tafesse, L., Carlin, K., Ghatak, P. & Kyle, D. J. (2015). Dibenzazepines and dibenzoxazepines as sodium channel blockers. *Bioorganic and Medicinal Chemistry Letters* **25**, 43-47.
64. Pardridge, W. M. (2012). Drug transport across the blood-brain barrier. *J Cereb Blood Flow Metab* **32**, 1959-1972.
65. Pardridge, W. M. (2005). The Blood-Brain Barrier: Bottleneck in Brain Drug Development. *NeuroRx* **2**, 3-14.
66. Pangalos, M. N., Schechter, L. E. & Hurko, O. (2007). Drug development for CNS disorders: strategies for balancing risk and reducing attrition. *Nat Rev Drug Discov* **6**, 521-32.
67. Abbott, N. J., Patabendige, A. A. K., Dolman, D. E. M., Yusof, S. R. & Begley, D. J. (2010). Structure and function of the blood–brain barrier. *Neurobiology of Disease* **37**, 13-25.
68. Wang, H., Ehnert, C., Brenner, G. J. & Woolf, C. J. (2006). Bradykinin and peripheral sensitization. *Biological Chemistry* **387**, 11-14.
69. Cheng, H. T., Suzuki, M., Hegarty, D. M., Xu, Q., Weyerbacher, A. R., South, S. M., Ohata, M. & Inturrisi, C. E. (2008). Inflammatory pain-induced signaling events following a conditional deletion of the N-methyl-d-aspartate receptor in spinal cord dorsal horn. *Neuroscience* **155**, 948-958.
70. Foster, E., Wildner, H., Tudeau, L., Haueter, S., Ralvenius, W. T., Jegen, M., Johannssen, H., Hösli, L., Haenraets, K., Ghanem, A., Conzelmann, K. K., Bösl, M. & Zeilhofer, H. U. (2015). Targeted ablation, silencing, and activation establish glycinergic dorsal horn neurons as key components of a spinal gate for pain and itch. *Neuron* **85**, 1289-1304.

71. Rice, J. E. (2014). Chapter 7 - Drug Metabolism. In *Organic Chemistry Concepts and Applications for Medicinal Chemistry* (Rice, J. E., ed.), pp. 145-201. Academic Press, Boston.
72. Cox, P. J. (2001). Essentials of pharmaceutical chemistry. *TALANTA -OXFORD THEN AMSTERDAM-* **54**, 419.
73. Lolignier, S., Eijkelkamp, N. & Wood, J. N. (2014). Mechanical allodynia. *Pflügers Archiv - European Journal of Physiology*.
74. Takakusa, H., Masumoto, H., Mitsuru, A., Okazaki, O. & Sudo, K. (2008). Markers of electrophilic stress caused by chemically reactive metabolites in human hepatocytes. *Drug Metab Dispos* **36**, 816-23.
75. Bolden Jr, S., Zhu, X. Y., Etukala, J. R., Boateng, C., Mazu, T., Flores-Rozas, H., Jacob, M. R., Khan, S. I., Walker, L. A. & Ablordeppey, S. Y. (2013). Structure-activity relationship (SAR) and preliminary mode of action studies of 3-substituted benzylthioquinolinium iodide as anti-opportunistic infection agents. *European Journal of Medicinal Chemistry* **70**, 130-142.
76. Woodbury, C. J., Kullmann, F. A., McIlwrath, S. L. & Koerber, H. R. (2008). Identity of myelinated cutaneous sensory neurons projecting to nocireceptive laminae following nerve injury in adult mice. *Journal of Comparative Neurology* **508**, 500-509.
77. Wager, T. T., Chandrasekaran, R. Y., Hou, X., Troutman, M. D., Verhoest, P. R., Villalobos, A. & Will, Y. (2010). Defining Desirable Central Nervous System Drug Space through the Alignment of Molecular Properties, in Vitro ADME, and Safety Attributes. *ACS Chemical Neuroscience* **1**, 420-434.
78. Meyer, T., Aarbakke, J. & Scheline, R. R. (1976). The Metabolism of Biphenyl. I. Metabolic Disposition of 14C–Biphenyl in the Rat. *Acta Pharmacologica et Toxicologica* **39**, 412-418.
79. Dutertre, S., Becker, C. M. & Betz, H. (2012). Inhibitory glycine receptors: An update. *Journal of Biological Chemistry* **287**, 40216-40223.
80. Wang, J. & Urban, L. (2004). The impact of early ADME profiling on drug discovery and development strategy. *DDW DRUG DISCOVERY WORLD* **5**, 73-86.
81. Ahmadi, S., Lippross, S., Neuhuber, W. L. & Zeilhofer, H. U. (2002). PGE2 selectively blocks inhibitory glycinergic neurotransmission onto rat superficial dorsal horn neurons. *Nature Neuroscience* **5**, 34-40.
82. Gallo, J. M. (2010). Pharmacokinetic/Pharmacodynamic-Driven Drug Development. *Mount Sinai Journal of Medicine: A Journal of Translational and Personalized Medicine* **77**, 381-388.
83. Gilron, I. & Dickenson, A. H. (2014). Emerging drugs for neuropathic pain. *Expert Opinion on Emerging Drugs* **19**, 329-341.
84. Öz, P., Huang, M. & Wolf, F. (2015). Action potential initiation in a multi-compartmental model with cooperatively gating Na channels in the axon initial segment. *Journal of Computational Neuroscience*.
85. Passmore, G. M., Selyanko, A. A., Mistry, M., Al-Qatari, M., Marsh, S. J., Matthews, E. A., Dickenson, A. H., Brown, T. A., Burbidge, S. A., Main, M. & Brown, D. A. (2003). KCNQ/M currents in sensory neurons: Significance for pain therapy. *Journal of Neuroscience* **23**, 7227-7236.

86. Suh, B. C. & Hille, B. (2005). Regulation of ion channels by phosphatidylinositol 4,5-bisphosphate. *Current Opinion in Neurobiology* **15**, 370-378.
87. Maljevic, S. & Lerche, H. (2013). Potassium channels: A review of broadening therapeutic possibilities for neurological diseases. *Journal of Neurology* **260**, 2201-2211.
88. Visockis, V. & King, A. E. (2013). M-channels modulate network excitatory activity induced by 4-aminopyridine in immature rat substantia gelatinosa in vitro. *Brain Research* **1513**, 9-16.
89. Blackburn-Munro, G. & Jensen, B. S. (2003). The anticonvulsant retigabine attenuates nociceptive behaviours in rat models of persistent and neuropathic pain. *European Journal of Pharmacology* **460**, 109-116.
90. Szelenyi, I. (2013). Flupirtine, a re-discovered drug, revisited. *Inflammation Research* **62**, 251-258.
91. Hoyt, S. B., London, C., Abbadie, C., Felix, J. P., Garcia, M. L., Jochnowitz, N., Karanam, B. V., Li, X., Lyons, K. A., McGowan, E., Priest, B. T., Smith, M. M., Warren, V. A., Thomas-Fowlkes, B. S., Kaczorowski, G. J. & Duffy, J. L. (2013). A novel benzazepinone sodium channel blocker with oral efficacy in a rat model of neuropathic pain. *Bioorganic and Medicinal Chemistry Letters* **23**, 3640-3645.
92. Sałat, K. & Filipek, B. (2015). Antinociceptive activity of transient receptor potential channel TRPV1, TRPA1, and TRPM8 antagonists in neurogenic and neuropathic pain models in mice. *Journal of Zhejiang University: Science B* **16**, 167-178.
93. Rahman, W. & Dickenson, A. H. (2013). Voltage gated sodium and calcium channel blockers for the treatment of chronic inflammatory pain. *Neuroscience Letters* **557**, 19-26.
94. Belardetti, F. (2010). Evolving therapeutic indications for N-type calcium channel blockers: From chronic pain to alcohol abuse. *Future Medicinal Chemistry* **2**, 791-802.
95. Yamamoto, T. & Takahara, A. (2009). Recent updates of N-type calcium channel blockers with therapeutic potential for neuropathic pain and stroke. *Current Topics in Medicinal Chemistry* **9**, 377-395.
96. Kolosov, A., Goodchild, C. S. & Cooke, I. (2010). CNSB004 (leconotide) causes antihyperalgesia without side effects when given intravenously: A comparison with ziconotide in a rat model of diabetic neuropathic pain. *Pain Medicine* **11**, 262-273.
97. Jarvis, M. F., Scott, V. E., McGaraughty, S., Chu, K. L., Xu, J., Niforatos, W., Milicic, I., Joshi, S., Zhang, Q. & Xia, Z. (2014). A peripherally acting, selective T-type calcium channel blocker, ABT-639, effectively reduces nociceptive and neuropathic pain in rats. *Biochemical Pharmacology* **89**, 536-544.
98. Kidd, B. L. & Urban, L. A. (2001). Mechanisms of inflammatory pain. *British Journal of Anaesthesia* **87**, 3-11.
99. Harvey, R. J. & Yee, B. K. (2013). Glycine transporters as novel therapeutic targets in schizophrenia, alcohol dependence and pain. *Nature Reviews Drug Discovery* **12**, 866-885.
100. Niesters, M. & Dahan, A. (2012). Pharmacokinetic and pharmacodynamic considerations for NMDA receptor antagonists in the treatment of chronic neuropathic pain. *Expert Opinion on Drug Metabolism and Toxicology* **8**, 1409-1417.

101. Collins, S., Sigtermans, M. J., Dahan, A., Zuurmond, W. W. A. & Perez, R. S. G. M. (2010). NMDA Receptor Antagonists for the Treatment of Neuropathic Pain. *Pain Medicine* **11**, 1726-1742.
102. Meintjes, R. A. (2012). An overview of the physiology of pain for the veterinarian. *Veterinary Journal* **193**, 344-348.
103. Chen, S. R., Samoriski, G. & Pan, H. L. (2009). Antinociceptive effects of chronic administration of uncompetitive NMDA receptor antagonists in a rat model of diabetic neuropathic pain. *Neuropharmacology* **57**, 121-126.
104. Park, M. K., Lee, J. H., Yang, G. Y., Won, K. A., Kim, M. J., Park, Y. Y., Bae, Y. C. & Ahn, D. K. (2011). Peripheral administration of NR2 antagonists attenuates orofacial formalin-induced nociceptive behavior in rats. *Progress in Neuro-Psychopharmacology and Biological Psychiatry* **35**, 982-986.
105. Yang, Y. L., Sun, W., Peng, C., Zhang, X. Y. & Yang, X. H. (2011). Research progress of selective mGluR1 antagonists. *Yaoxue Xuebao* **46**, 1167-1172.
106. Kim, Y., Kim, J., Kim, S., Ki, Y., Seo, S. H., Tae, J., Ko, M. K., Jang, H. S., Lim, E. J., Song, C., Cho, Y., Koh, H. Y., Chong, Y., Choo, I. H., Keum, G., Min, S. J. & Choo, H. (2014). Novel thienopyrimidinones as mGluR1 antagonists. *European Journal of Medicinal Chemistry* **85**, 629-637.
107. Brumfield, S., Korakas, P., Silverman, L. S., Tulshian, D., Matasi, J. J., Qiang, L., Bennett, C. E., Burnett, D. A., Greenlee, W. J., Knutson, C. E., Wu, W. L., Sasikumar, T. K., Domalski, M., Bertorelli, R., Grilli, M., Lozza, G., Reggiani, A. & Li, C. (2012). Synthesis and SAR development of novel mGluR1 antagonists for the treatment of chronic pain. *Bioorganic and Medicinal Chemistry Letters* **22**, 7223-7226.
108. Supplisson, S. & Roux, M. J. (2002). Why glycine transporters have different stoichiometries. *FEBS Letters* **529**, 93-101.
109. Morita, K., Motoyama, N., Kitayama, T., Morioka, N., Kifune, K. & Dohi, T. (2008). Spinal antiallodynia action of glycine transporter inhibitors in neuropathic pain models in mice. *Journal of Pharmacology and Experimental Therapeutics* **326**, 633-645.
110. Maksay, G. & Bíró, T. (2002). Dual cooperative allosteric modulation of binding to ionotropic glycine receptors. *Neuropharmacology* **43**, 1087-1098.
111. Xiong, W., Cui, T., Cheng, K., Yang, F., Chen, S. R., Willenbring, D., Guan, Y., Pan, H. L., Ren, K., Xu, Y. & Zhang, L. (2012). Cannabinoids suppress inflammatory and neuropathic pain by targeting α3 glycine receptors. *Journal of Experimental Medicine* **209**, 1121-1134.

Chapter 2

The Glycine Receptor as a Drug Target

Table of Contents

2.1 Targeting the Glycine Receptor

2.1.1 Strychnine-Sensitive Glycine Receptors

Chronic pain is currently treated using a combination of traditional painkillers and psychoactives. Many of these therapeutic strategies result in numerous adverse-effects and patients often experience a decline in pain relief over time. There is an urgent need for new analgesics that target the underlying mechanisms of dysfunctional pain. One prospective approach is restoring the glycinergic activity, reduced in chronic pain, through modulation of GlyRs.

These receptors are inotropic chloride channels expressed post-synaptically on nerves in the dorsal horn[1]. They respond to glycine released by inhibitory interneurons and when activated trigger hyperpolarisation. When glycine binds to the receptor a conformational change is triggered and the ion channel becomes permeable to Cl^- ions[1].

It is thought that GlyRs mediate a much faster inhibitory current than $GABA_A$Rs. Many nociceptors, particularly in laminae I, appear to predominantly interact with glycinergic interneurons[2]. Typically, neurons that express GlyRs are found in the spinal cord, most abundantly in the cervical and lumbar regions, and the brain stem[3]. A number of GlyRs also appear in the brain, however they are small in number and their exact role in pain processing is uncertain[4]. GlyRs were originally differentiated from $GABA_A$Rs by the relationship with the toxic alkaloid, strychnine. Strychnine allosterically binds to a site near the ion channel pore and is able to antagonise the receptor, although it is readily displaced by the binding of glycine[3]. Administration of strychnine is able to induce allodynia, signifying that GlyRs are

contribute to dysfunctional pain behaviours[5]. Strychnine is often used to determine if a compound is interacting with GlyRs[3].

GlyRs belong to the cysteine-loop (Cys-loop) ligand-gated ion channel (LGIC) receptor family. LGICs are a common receptor type for many neurotransmitters including GABA and 5-HT[2]. All LGICs subunits share similar structural features, notably a long extracellular N-terminal binding domain (ECD) containing the highly conserved Cys-loop, four transmembrane segments (TM1-4) with an intracellular loop between TM3-4 and a small extracellular C-terminal[6; 7; 8]. Based on structurally similar LGICs, it is believed that TM2 domains form the channel pore and upon ligand binding rotate, opening the channel. There is evidence to suggest that the arginine residues in the TM2 domains become charged in such a way that repels cations but allows the flow of anions[6].

The SSGR itself has five subunits, α1-4 and β1, that can form homomeric and heteromeric pentamers[9]. All homomeric pentamers are can be formed by small α-subunits, while heteromeric pentamers must contain the larger β-subunit at a ratio of 2α:3β[4]. The β-subunit is a supportive subunit, vital for trafficking, agonist binding and receptor clustering at the synapse. The subunit contains a cytoplasmic loop that binds to the scaffolding protein, gephyrin and interacts with transporter proteins, Vps35 and neurobeachin to help integration into the membrane[10; 11; 12]. The α-subunits are usually categorised into α1-3, with α4 being a pseudo-gene. Out of all the subunits, α1 is the most abundant and is a major component of many heteromers. In the embryo, α2 is the dominant subunit, however during early postnatal development many GlyRα2s are replaced with the α1β heteromers[9]. The α3 subunit was once considered to the least abundant, however it is now know that heteromers containing α3 are

densely localised in the laminae I-II and have been directly implicated in sensitisation of the PNS during inflammatory pain[4].

2.1.2 Role of GlyRα3 in Chronic Pain

Once considered a minor subunit of adult GlyRs, GlyRα3 are now known to play a substantial part in the development of peripheral sensitisation and allodynia[13; 14]. GlyRα3, along with GlyRα1, are believed to regulate signalling between first-order nociceptors and projection neurons in dorsal horn[15]. While both subunits are found in the laminae I-II only α3 has been implicated in disinhibition. As mentioned earlier, in a study by Xiong *et al.*, two cannabinoids CBD and DH-CBD were able to attenuate analgesia via GlyRs, more specifically through modulation of GlyRα3[14]. The properties of CBD and DH-CBD were not as prominent in mice lacking GlyRα3 ($Glra3^{-/-}$)[14], further verifying that α3 is the major contributor to glycine disinhibition. In addition, normal nociception is not changed in $Glra3^{-/-}$ mice, suggesting that the α3 subunit only plays a role in dysfunction pain behaviours[13]. Application of PGE_2 was shown to reduce glycine mediated currents and trigger pain sensitisation in wild type mice but not in $Glra3^{-/-}$ mice[13]. In the same study, administration of PKA inhibitor peptides was able to reverse the effect on glycine currents by PGE_2, whilst strychnine reversed the effect of DH-CBD

While the structure of the two subunits is highly conserved (80-90%)[6], there is a difference in the conformational change that occurs following glycine binding. This difference is thought to be the result of the serine residue within the intracellular loop between TM3-4 that can be

phosphorylated by PKA[16]. A mutation in this sequence (Ser^{346}→Ala^{346}) is able to obstruct the effect of PGE_2 on GlyRα3[13]. It is likely that PGE_2, causes a distortion of the glycine binding site in α3 subunits through PKA phosphorylation[16]. A loss in functional GlyRα3 has a major impact on the normal glycinergic activity in the dorsal horn. To compensate, the activity of GlyR containing the α1 subunit would need to be increased by pharmacological intervention.

2.1.3 Allosteric Modulation of Glycine Receptors

From a pharmaceutical perspective, little research has been conducted into utilising GlyRs as a drug target. A great deal compounds including Zn^{2+}, anaesthetics, alcohols and 5-HT antagonists have been known to potentiate glycine response[17; 18]. Mutations at Ser^{267} residue in the TM2 domain can significantly reduce the effect of abuse solvents, such as toluene, and anaesthetics, suggesting that major allosteric sites lie within the membrane, close to the channel pore[19; 20]. Extracellular allosteric sites close to the ligand-binding site have also been identified for Zn^{2+}[21].

PAMs have a number of advantages over direct agonist. Unlike direct agonists, PAMs do not have to compete for a binding site, as many receptors have multiple, highly conserved allosteric sites[22]. They also rely on natural release of the neurotransmitter, meaning that normal physiological signalling is not disrupted; PAMs may even be able to reset biological functions that have become hindered, something that would be advantageous in restoring lost glycinergic activity. Furthermore if pharmacological intervention is dependent on the availability of the biological ligand and receptor, the likelihood of target-based toxicity will be

lessened[23]. Finally, receptors can become oversaturated if exposed to a potent agonist, leading to internalisation or inac**ti**vation[24; 25].

In the case of LGICs, repeated exposure to a highly concentrated agonists can lead to desensitisation of the receptor[26]. Many compounds that antagonise GlyRs only do so at high glycine concentrations, whereas at low concentrations they increase affinity for glycine. In the prolonged presence of a ligand, many GlyRs shift between open and desensitised states[18; 27]. This implies that the GlyR is vulnerable to desensitisation. It has been proposed that many positive modulators increase the rate of state transition and the duration of ligand effect rather than boost glycine affinity[27]. While some allosteric modulators do allow for greater strychnine displacement by glycine[28]. Allosteric modulators are more effective at potentiating glycine currents than direct agonists through a various mechanisms[29].

Unlike $GABA_AR$ agonists, anaesthetics acting via GlyRs are able attenuate pain without any hypnotic side effects. This provides further evidence that positive allosteric modulators of GlyRs have the potential to become novel analgesics. One of most potent allosteric modulators of GlyR is the anaesthetic propofol[30].

2.1.4 Propofol and Glycine Receptors

Over a century after the introduction of surgical anaesthetics, propofol (Diprivan) has become one of the most extensively used anaesthetics during short surgical procedures[31]. Administered intravenously, due to its poor solubility, propofol (2,6-di-isoprophylphenol) is a

highly lipophilic phenol whose alky groups at the 2 and 6 positions are vital for its hypnotic effect (Figure 2.1)[32]. Propofol is popular because of its rapid on-set of activity (less than minute) and the smooth transition between anaesthesia and wakefulness (i.e. no nausea or respiratory issues)[31].

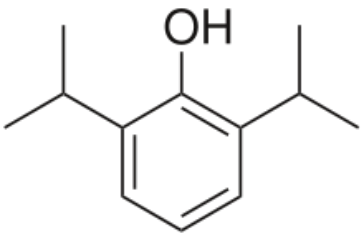

Figure 2.1. The structure of 2, 6-di-isoprophylphenol (Propofol)[31].

The ease of surfacing from sedation is largely related to the quick distribution and rapid metabolism of propofol. Propofol also has few serious side-effects making it a standard choice for commonplace procedures[31; 33]. The foremost grievance of patients treated with propofol is pain upon injection; with a high incidence (80%) of patients report a burning sensation following administration[34]. At therapeutic levels propofol is able to activate peripheral nociceptors through TRPV1 and TRPA1, leading to pain after initial dosing[34; 35]. Certain formulations of propofol, such as fospropofol (a pro-drug), does not elicit pain and are becoming common means of inducing anaesthesia[36].

Propofol produces anaesthesia by activating $GABA_A$ receptors. The binding site is found in β subunits of $GABA_A$Rs and lies between the extracellular and transmembrane domains, close to sites in TM1-2 that determine sedation[37]. Specific mutations in the subunit β3 are able to block the sedative effect of propofol[38; 39]. As well as enhancing inhibitory chloride currents,

propofol is able to block the release of acetylcholine (ACh) in the hippocampus and frontal cortex; this is thought to be independent to sedation by means of an alternative binding site[40]. Propofol is purely used as a sedative and has no intrinsic analgesic properties; however reports show patients treated with propofol have been shown to experience less intense post-operative pain when compared to isoflurane and some minor analgesia is experienced during propofol infusion[41; 42]. It is possible that propofol may inhibit the phosphorylation of NR1, however this effect only occurs at higher than therapeutic concentrations[42]. Another effect of high propofol concentrations is the amplification of glycine facilitated currents[39].

2.1.5 GlyRα1 as a Drug Target

As with many anaesthetics, propofol is a non-selective low-affinity modulator of GlyRs[30]. Propofol, despite having specificity for $GABA_{A,}$ has established dose-dependent activity at GlyRα1, both in the presence and absence of glycine[30; 39]. At low glycine concentrations, propofol is thought to slow the transition of open receptors to their deactivated states[43]. In the presence of partial agonists, taurine and β-alanine, propofol is able to increase affinity and response to exceed that of a full agonist, glycine[17]. Propofol also has a negative modulatory effect at very high glycine concentrations, possibly due to inhibitory receptor-receptor interactions[43]. It has been reported that propofol has mild activity at GlyRα2, although the modulation is much stronger in GlyRα1[44].

Mutations in the α1 subunit have varying effects on propofol modulation. For instance changes in the large intracellular will decrease propofol enhancement, while mutations in

transmembrane domains have the opposite effect[45; 46]. Water-filled cavities within TM2-3 domains of α1 subunits are thought to be a major binding site for propofol[45]. Structural changes triggered by agonist binding have no influence on the activity of propofol, suggesting that effects of propofol and glycine binding within the receptor are unrelated[47]. Hyperekplexia (startle disease) is a rare hereditary condition that is associated with mutations in the α1 subunit of GlyRs[46]. It has been directly linked to an arginine residue (Arg^{271}) in the TM2 domain. This mutation effects agonist binding and channel opening[48]. Surprisingly, propofol emits a greater response on mutated α1 subunits in comparison to wild type. Propofol is also able to increase agonist affinity to normal levels in mutated subunits[46]. It is likely propofol mediates sedation through $GABA_A$ and analgesia through the GlyR. As such propofol presents a good starting point for the development of a novel analgesic.

A number of studies have demonstrated that propofol analogues are able to potentiate glycine currents to a greater extent than propofol itself[30]. Particularly, halogen substitutions at the 4-position have a much higher efficacy at GlyRs in comparison to propofol[49; 50]. In addition, these analogues show little to no activity for $GABA_ARs$[51]. A series of novel analgesics based around the core structure of propofol may prove to an effective way to target the GlyR.

2.2 Propofol Analogues

2.2.1 Substituted Phenols

Propofol and its halogenated analogues have been shown to produce analgesia without sedation through the activation of GlyRs. This same phenomenon is also seen with other commonly used anaesthetics, most of which are halogens themselves[52]. In order to focus the direction of structural modification, it must be determined what structural aspects have the largest impact on specificity for GlyRs over $GABA_A$Rs. Many halogenated anaesthetics do not show significant specificity for either receptor, so it is possible that the phenolic core of propofol is responsible for greater selectivity towards $GABA_A$Rs.

A series of phenol derivatives have previously been tested at GlyRα1s to investigate the influence of propofols phenolic group on glycine modulation. Testing was carried out in the presence of glycine (10μM) and modulation was determined as changes in the chloride current[53]. The structures and EC_{50} values of the compounds is presented in Table 2.1. The results show that the basic phenolic structure is not sufficient to potentiate glycine mediated currents. All of the compounds failed to achieve a lower EC_{50} than propofol. It is already known that the alky groups at the 2 and 6 positions in propofol are needed for activity at $GABA_A$Rs[32], and the data suggest that this is also true of GlyRs. Therefore when designing propofol analogues, the core structure should be maintained. As seen in previous literature, halogenation at the *para*-position appeared to boost efficacy glycine receptors. It is likely that *para*-halogenation propofol analogues would prove to be more effective than the parent compound.

Table 2.1. The EC_{50} values of phenol derivatives acting at GlyRα1: Phenol derivatives were tested in the presence of glycine (10μM) at recombinant GlyRα1s. The effect on chloride currents was recorded and the EC_{50} values were determined as 50% of the maximal potentiation of the current[52].

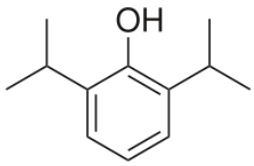	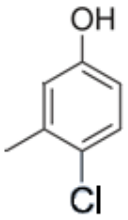	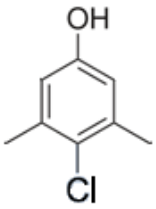	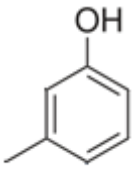
EC_{50} = 4.8μM	**EC_{50}= 8μM**	**EC_{50} = 13μM**	**EC_{50} = 59μM**
	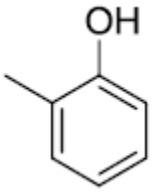	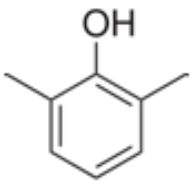	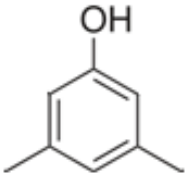
	EC_{50}= 70μM	**EC_{50} = 226μM**	**EC_{50} = 254μM**

2.2.2 Testing at GlyRα1

Propofol analogues acting on GlyRs to produce analgesia has been thoroughly investigated. From this point a series of compounds or 'hits' can be synthesised with the intention of increasing efficacy at the tar. The activity at GlyRα1 of potential hits as tested in an efficient but 'low-throughput' electrophysiology assay[54]. Whole cell voltage-clamp electrophysiology was used to measure the activity of hit compounds at GlyRα1. Cells were transfected with cDNA to express recombinant GlyRα1β1 on the cell surface. Cells were treated with 10μM glycine and the test compound at varying concentrations, and the voltage

response was recorded (Figure 2.2). Compounds that showed no activity at 1µM were not investigated further due limitations of unstable cell lines. These studies were carried out under the supervision of Prof. Bodo Laube at the University of Tübingen, Germany. To ensure selectivity for the target, compounds were also tested against $GABA_ARs$ at BioFocus DPI Limited (Saffron Walden, UK). The experimental methods for these assays are presented in Appendix II and IV.

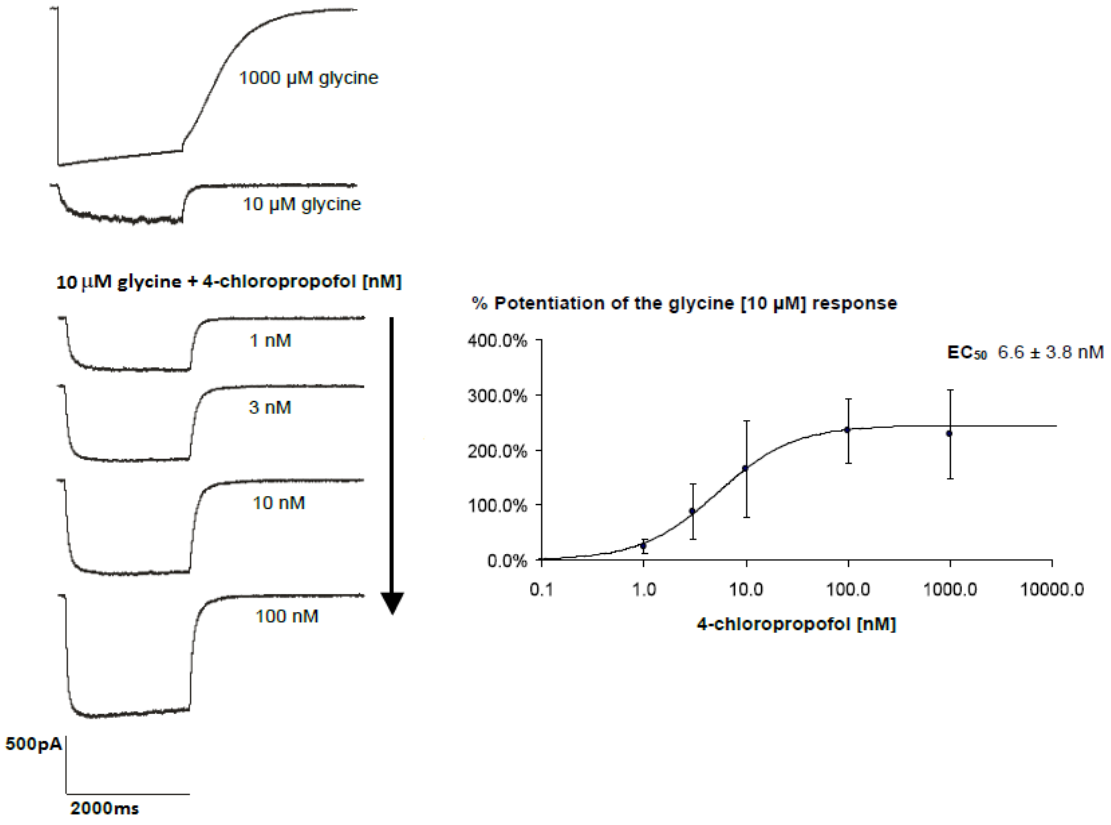

Figure 2.2. Potentiation of glycine response by 4-chloropropofol.
Left, Top: Representative current traces produced by a glycine at 1000µM (maximal concentration) and 10µM (sub-maxima concentration).
Left, Bottom: Current traces demonstrating the effect of glycine (10µM) with an increasing concentration (1-100nM) of 4-chloropropofol.
Right: Dose-response curve of 4-chloropropofol acting on glycine receptors in the presence of glycine (10µM). EC50 values were determined as 50% of the maximal potentiation of glycine current.
**GlyRα1 EC50 experiments were carried out under the supervision of Prof. Bodo Laube at the University of Tübingen, Germany.*

2.2.3 Halogenated Propofol Analogues

The EC_{50} values for phenols derivatives at GlyRα1 suggests that the core structure of propofol must be maintained for functionality, but the addition of a halogen at the *para*-position may increase affinity. A number of halogenated propofol analogues have previously demonstrated selectivity for GlyRs over $GABA_ARs$[40; 49; 50]. One halogenated analogue, 4-iodopropofol acts on $GABA_ARs$ and is able to inhibit ACh release but is not hypnotic [40]. This suggests that incorporation of halogens can have a drastic effect on which binding site is targeted by a compound. 4-bromopropofol can prevent the firing of action potentials, an effect that is reversed by strychnine[50]. Finally, 4-chloropropofol is able to augment glycine mediated chloride currents in an artificial model of hyperekplexia[49].

Based on previous literature, three halogenated propofol analogues were tested against GlyRα1 at the University of Tübingen. The physiochemical properties of each compound were also generated *in silico,* as an indicator for good absorption and solubility (Table 2.2). Compounds with low molecular weight (MW), ClogP and ClogD are more likely to cross the BBB and have adequate exposure at the target; consequently it is advantageous to estimate the physiochemical properties as early as possible.

The halogenated analogues were able to increase glycine response at low concentrations (nM) and were approximately 1000 fold more potent than propofol at GlyRα1. This data validates *para*-substitution of propofol as an approach for increasing affinity for GlyRs over $GABA_AR$, as it is unlikely that such low concentrations will be sufficient for activation of $GABA_ARs$[55]. All the compounds had ClogP (<5) and MW (<450Da) within an acceptable range

for a drug. ClogD for each compound was higher than desired and the estimated aqueous solubility (Aq. Sol.) was poor[56]. It is recommended that drugs have solubility close to 50µM to ensure good absorption and permeability, which will contribute to bioavailability and CNS penetration[56]. As a result of its high efficacy at the target, as well as having the most 'drug-like' physiochemical properties (i.e. lowest ClogP, ClogD, MW and highest Aq. Sol.), 4-chloroprofol was chosen for testing in an animal model of chronic pain.

Table 2.2. GlyRα1 EC_{50} data and *in silico* physiochemical properties of halogenated propofol analogues.

**GlyRα1 EC50 data provided by the University of Tübingen.*

Compound	EC_{50} (µM)	ClogP	ClogD	Aq. Sol. (µM)	MW
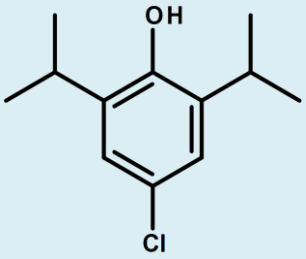 **4-chloropropofol**	0.00066 ± 0.0038	4.49	4.4	18.37	212
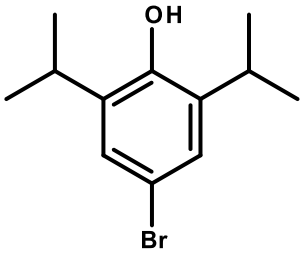 **4-bromopropofol**	0.00062 ± 0.0018	4.63	4.67	10.81	257
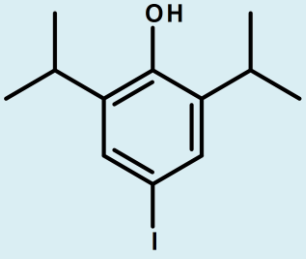 **4-iodopropofol**	0.00067 ± 0.0033	4.82	4.82	14.85	304

2.3 Biological Testing of 4-Chloropropofol

2.3.1 Metabolism of 4-Chloropropofol

Before 4-Chloropropofol could be validated in a neuropathic pain model, a pharmacokinetic (PK) profile had to be determined. Studying the *in vivo* metabolism of a compound not only ensures satisfactory levels of free drug are available at the target site but also provides brief insight into potential toxicities. Early metabolic testing can reduce number of animals used in proof of concept studies and acts as an indicator for success at later stages of development; it is estimated that roughly half drug candidates will fail to enter pre-clinical testing as a result of poor absorption, distribution, metabolism and excretion (ADME)[57].

Pharmacokinetics of 4-chloropropfol (Table 2.3) was investigated via *in vivo* rat metabolism. Rats were dosed orally (p.o) at 8 mg/kg and intravenously (i.v) at 1 mg/kg. Blood samples were taken from the tail vein at time points 0 min, 30 min, 1 hr, 2 hrs, 4hrs and 6hrs (p.o) and 0 min, 15 min, 30 min, 1 hr, 2 hrs and 6hrs (i.v). The final time point (6hrs) was taken by cardiac puncture following termination. The experiments were carried out in triplicate by the DMPK Group at ChemPartners Ltd, Shanghai, China.

Table 2.3: Pharmacokinetic parameters of 4-chloropropfol.
**Data provided by ChemPartners Ltd, China.*

Parameters	I.V	P.O	Bioavailability F (%)
	1mg/Kg	8mg/Kg	
AUC (min*µg/mL)	7.39	42.8	72.4
C_{max} (µg/mL)	0.11	0.1	
T_{max} (min)	15	30	
$t_{1/2}$ (min)	48.8	398	
Cl (mL/min/Kg)	14.8	146	
V_d (L/Kg)	11.8	79.6	

The clearance rate (146 mL/min/kg) and volume of distribution (80.6 L/kg) for 4-chloropropofol, following oral dosing was much higher than the desired value in rats (Cl=10-45 mL/min/kg, V_d=0.5-10 L/kg)[58]. However, the half-life (398min) of the compound was also quite long, with a short T_{max} (30mins) and a reasonable C_{max} (100ng/mL). This indicates that 4-chloroporpofol is rapidly absorbed although it appears to be widely distributed within tissue. The oral bioavailability (72.4%) exceeded the recommended value of 30% in rats[58]. Although the overall PK profile is not ideal, the data suggest that 4-chloropropofol is quickly absorbed with relativity high plasma concentrations, meaning drug exposure at the target should be sufficient to elicit a response.

2.3.2 4-Chloropropofol in a Neuropathic Pain Model

Testing 4-chloropropofol in a neuropathic pain model not only endorses modification of the *para*-position but also provides proof that the GlyR is a viable analgesic target. The effect of 4-chloropropofol in the Chung Lesion model of neuropathic pain was carried out by Dr Laiche Djouhri in the Department of Pharmacology, University of Liverpool[59].

As with the parent drug, 4-chloropropofol also had poor solubility and was formulated as a pro-drug, similar to fospropofol. Both 4-chloropropofol and the formulated pro-drug were tested to observe the effect of solubility. Neuropathic pain was induced following spinal nerve ligation (SNL). A period of 7 days was left between surgery and dosing in order for neuropathic pain to develop. Animals were dosed orally at 8mg/kg. Heat hyperalgesia was tested as paw withdrawal latency from a hot plate and mechanical allodynia (MA) was

measured as paw withdrawal threshold (PWT) in response to gradually increasing pressure. The results are shown in Figure 2.3.

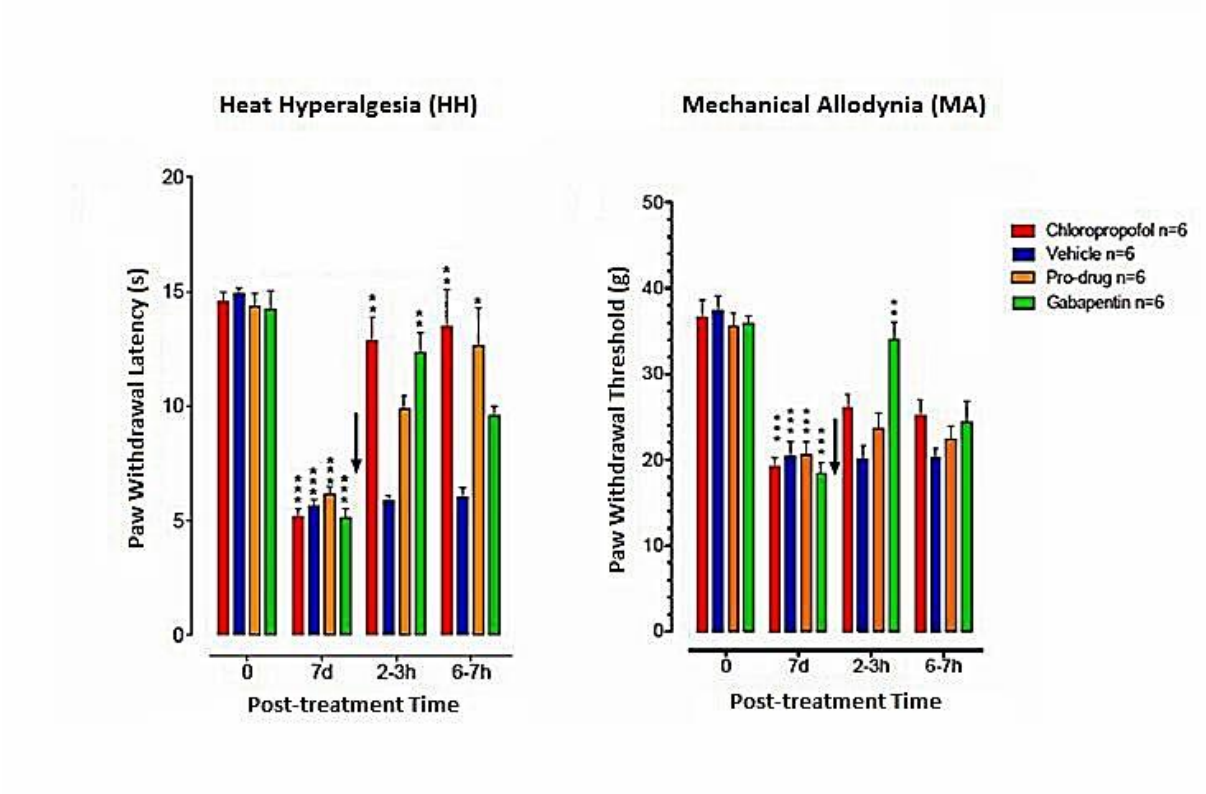

Figure 2.3. Effects of oral administrations of 4-chloropropofol and pro-drug in Chung lesion model of neuropathic pain: Rats were habituated for one week prior to experiment. A comparison was made between the pre-SNA base-line (t=0) and 7 days post-surgery using one way ANOVA with Dunnets multiple comparison to ensure neuropathic pain had developed. The rats were dosed orally at 8mg/Kg with 4-chloropropofol (n=6) or pro-drug (n=6). A vehicle control and positive control (gabapentin, 30mg/Kg, i.p.) included. The data is expressed as mean (± SEM). Comparisons between post drug values and vehicle values were made using two way ANOVA followed by Bonferroni corrections (* = P ≤ 0.05, ** = P ≤ 0.01, *** = P 0.001)

**Data provided by Dr Laiche Djouhri, University of Liverpool.*

At both post-dose time points (2-3hrs and 6-7hrs), 4-chloropofol was more effective than gabapentin in attenuating hyperalgesia. As expected the prodrug had a slower on-set of action due to its dependence on metabolic activation. At 6-7hrs post-dose, the pro-drug was more effective than gabapentin but not as effective as 4-chloropropofol. No sedation was observed following administration of 4-chloropropofol, suggesting that the analgesic effect is mediated through GlyRs rather than $GABA_A$ [31].

While 4-chloropropofol was able to attenuate hyperalgesia, the same effect was not seen for mechanical allodynia; 4-chloropropofol and its pro-drug had very little impact on PWT. At 2-3hrs, gabapentin was able to significantly reduce allodynia but this effect was not seen with 4-chloropropofol. Attenuation of hyperalgesia but not allodynia has been noted before in this particular pain model, with retigabine[60; 61]. This suggested that heat hyperalgesia and mechanical allodynia are developed through different mechanisms and that GlyRs are predominately involved in the development of hyperalgesia.

To summarise, analogues of propofol acting at GlyRs rather than the traditional target $GABA_A$Rs, possibly present a new class of analgesics. Halogenation at the *para*-position is thought to have an effect on target selectivity of propofol. A halogen analogue, 4-chloropropofol underwent various biological tests that that ended with validation in an animal neuropathic pain model. 4-chloroprofol has shown to have greater affinity for GlyRs compared to propofol. In addition, it is able to attenuate hyperalgesia to a greater extent than the 'gold-standard' gabapentin in a neuropathic animal pain model. Unfortunately the physiochemical properties and pharmacokinetic profiling of 4-chloroprofol were not acceptable for a potential

drug candidate. To improve the physiochemical properties of the analogue, it was decided that further modification at the *para*-position would be investigated.

2.4 Bi-Phenyl Analogue Series

2.4.1 Bi-Phenyl Analogues

It has previously been established that substitution at the *para*-position can increase selectivity of GlyR over $GABA_A$ and that 'large' compounds with a high molecular volume, such as 4-iodopropofol, can be accommodated at the binding site. On this basis, it was decided that the limitations of side chain complexity and size would be explored through the addition of a phenyl ring. There is a vast list of possible substitutions that can be incorporated to the second ring. In order to narrow down the possibilities, a Craig plot was used.

The Craig plot is a tool, commonly used by medicinal chemists, that categorises substitutions by their electronic and hydrophobic effects in comparison to hydrogen[62]. Electron donating structures with high hydrophobic values are usually metabolically unstable, while highly electrophilic structures may form toxic metabolites[63; 64]; as such these side-chains are often dismissed. Electron withdrawing substitutions, such as halogen, carbonyl and trifluoromethyl, are stabilising and are frequently used to improve the physiochemical properties of a compound[65]. The use of the Craig plot, analogue synthesis and *in silico* physiochemical predication was all carried out in the Department of Chemistry at the University of Liverpool.

A series of bi-phenyl analogues, constructed around a common scaffold were synthesised (Figure 2.4). Many of the compounds included chlorine and fluorine at the *ortho*, *meta* and *para*-positions. Each compound demonstrated improved potency at GlyRα1 (EC_{50} at low picomolar concentrations) and as seen with halogenated phenols the compounds with chlorine at the *para*-position were the most effective. Although all compounds showed excellent activity at the desired target, the physiochemical properties in particular ClogP was higher that desired (≥6).

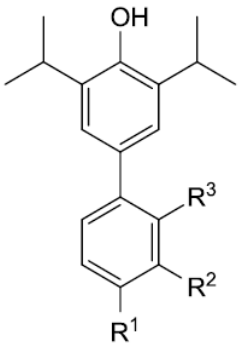

Figure 2.4. Bi-phenyl propofol analogue scaffold.

2.4.2 Physiochemical Properties

The early generation of hit compounds is a time-consuming process. With unlimited chemical possibilities, it is difficult to identify a compound that has ideal drug-like properties. Generally a series of guidelines are followed to single out compounds with the highest chance of being developed into an approved drug[66]. Built upon Lipinski's 'rule of five', drugs especially those acting in the CNS must meet certain criteria; i) ClogP below 5, ii) ClogD below 3, iii) MW below 450Da, iv) no more than 3 hydrogen bond donors (HBD), v) topological polar surface

area (TPSA) between 40-90 Å, vi) pKa below 8-10[67; 68]. These parameters can be used as an indicator of predict solubility, absorption and distribution. Compounds with physiochemical properties outside of these recommended ranges are unlikely to transition well into a therapeutic agent that can be used by patients. These guidelines are often used as measures of 'drug-likeness' and it is essential that analogues in this project fall within these ranges.

2.4.3 Bi-phenyl Amide Analogues

The addition of larger sider-chains at the *para*-position increased potency at the target receptor, unfortunately at the cost of other drug-like attributes. In an attempt to improve the physiochemical properties of the analogues while maintaining efficacy at GlyRα1, it was decided that heterocyclic amides would be incorporated into the bi-phenyl analogue structure. Heterocyclic amides are often used to improved TPSA and solubility of a structure[69].

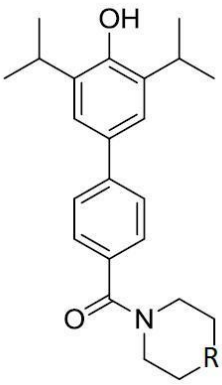

Figure 2.5. The bi-phenyl amide scaffold.

The bi-phenyl amide analogues all showed a marked improvement in ClogP and ClogD, however the values were still outside of optimal values. The other physiochemical properties,

TPSA, MW, HBD and pKa were closer to acceptable levels. While the drug-like properties of the analogues has improved, the efficacy at the target receptor was considerably poorer. Most of these analogues were unable to activate GlyRα1 below the cut-off concentration (1μM).

The only compound in the series that was able to successfully activate (EC_{50}<1μM) glycine receptors was LT-01-45 (2, 6-diisopropyl-4-(6-(trifluoromethyl) pyridin-3-yl) phenol). Unfortunately some activity was also seen at $GABA_AR$ (EC_{50}=0.12μM) but this was higher than what was seen at GlyRα1, signifying specificity for the drug target (Table 2.4).

Table 2.4: GlyRα1 EC_{50} data, CNS MPO score and *in silico* physiochemical properties of LT-01-45.
**Compounds synthesis and in silico testing were carried out in the Department of Chemistry, University of Liverpool (UK) and GlyRα1 EC50 data provided by the University of Tübingen.*

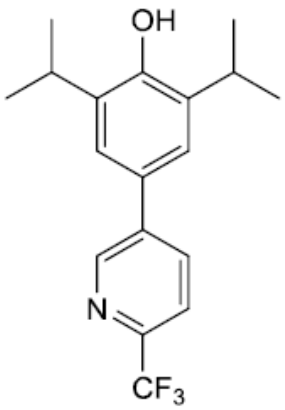 **LT-01-45**	**GlyRα1 EC_{50} =** 0.0001μM
	$GABA_AR$ EC_{50} = 0.12μM
	ClogP = 5.55
	ClogD = 3.70
	TPSA = 33.12Å
	MW = 322.35Da
	HBD = 1
	pKa = 9.22

Due to poor physiochemical parameters and lack of constant activity at the target, the bi-phenyl series was terminated. However before dismissal, the effect of a large *para* side-chain on metabolic stability was considered. As the most successful analogue in the series, LT-01-45 was selected to be tested for metabolic resistance against cytochrome P450 enzymes (CYPs).

2.5 Metabolic Stability of LT-01-45

2.5.1 Microsomal Stability

Determination of a good metabolic profile is an essential aspect of early drug discovery. In addition to being active at the target, having drug-like properties and a favourable PK/PD profiles, a candidate compound must also be metabolically stable. In particular, candidates must be resistant to phase I metabolism by CYPs. These enzymes are responsible for the metabolism of more than 70% of drugs currently on the market, including, propofol[70; 71].

Understanding how a compound is metabolised by CYPs is useful for a number of reasons. CYP mediated metabolism is often considered the 'modification' stage, in which a functional group is introduce to allow further metabolism. Drugs that undergo excessive CYP metabolism are usually excreted quickly and have reduced exposure at the target site[72]. In addition the induction or inhibition of CYPs by other drugs, supplements or food can increase the levels of toxic drugs or their metabolites[73]. While these analogues are not designed to form non-toxic metabolites, it is important to recognise the extant by which a candidate will be metabolised by CYPs, as this can offers insight into future drug-drug interactions.

Microsomal stability testing in lead generation and optimisation is common practice. The use of microsomes for measuring CYP mediated metabolism allows for a high-throughput screening, which is useful at early stages of development where there is a high number of test compounds[74]. Accessible and inexpensive, microsomes are ideal for determining which lead candidates are likely to have favourable drug-like ADME properties[75]. They also give greater control over the testing environment, in that specific co-factors can be used to single out metabolising enzymes, like CYPs or UGTs (uridine 5'-diphospho-glucuronosyltransferases). In this project, microsomes were used to investigate CYPs; phase II metabolism was carried out by ChemPartners using whole hepatocytes. It is expected that the propofol analogues will show increase microsomal stability over the parent drug.

2.5.2 Metabolism of Propofol

Propofol undergoes rapid hepatic metabolism with almost all (80%-90%) of the administered dose excreted in the urine as conjugated metabolites[76]. As a phenolic compound, propofol does not require the introduction of a polar functional group for conjugation, however some phase I metabolism does occur. The two major routes of metabolism for propofol are glucuronide conjugation of the phenol and hydroxylation at the *para*-position. Just less than half of the dose is thought to undergo CYP metabolism[71; 76]. CYP mediated metabolism results in the formation of 4-hydroxypropofol (Figure 2.6). This intermediate can be further oxidised or conjugated through glucuronidation and to some extent, sulfation[77]. Many CYP isoforms may take part in the hydroxylation of propofol but

members of CYP2B, and to a lesser extent CYP2C, sub-families appear to have the greatest impact on propofol biotransformation[71; 77; 78].

Propofol exhibits a substantial amount of pharmacokinetic and pharmacodynamic variation between individuals. Inter patient variation usually manifests as recovery time from sedation. Patients that gain consciousness quicker are likely to metabolise propofol by the quickest route, direct glucuronidation[79]. It is thought that 4-hydroxypropofol formed during CYP metabolism may have some hypnotic activity, which can also prolong the sedative effect[80]. Metabolic efficiency is probably caused by the high incidence of polymorphisms with metabolising enzymes (e.g. CYPs are highly polymorphic) or differences in expression, relating to gender and race[79;81]. Polymorphic CYPs appear to contribute greatly to inter-patient variability, despite being lesser metabolisers of propofol[81].

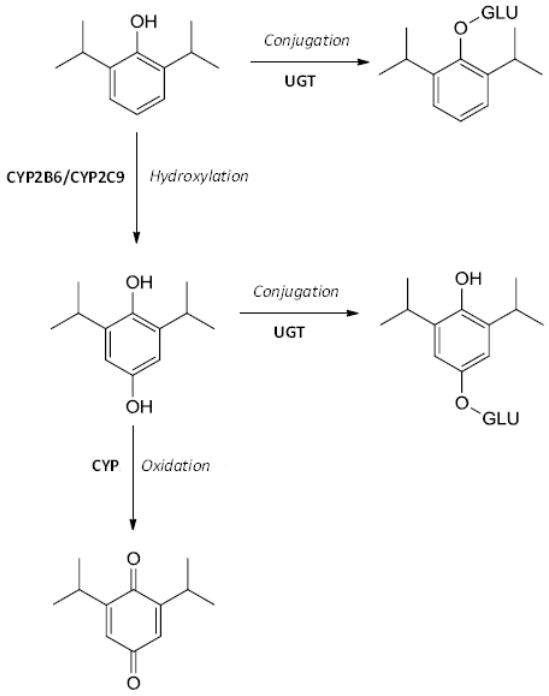

Figure 2.6. Metabolism of propofol: Propofol undergoes CYP mediated phase I metabolism into 4-hydroxyprofol, which can be further oxidised or conjugated via glucuronidation. CYP (Cytochrome P450), UGT (uridinediphosphate glucuronosyl transferase), GLU (Glucuronic acid)[21].

Phase I metabolism of propofol predominately occurs at the *para*-position. The addition of a large side-chain should block hydroxylation, while the introduction of a trifluoromethyl group is a popular means of increasing resistance to CYP oxidation[82] (Figure 2.7). This should reflect in a prolonged half-life and reduced clearance.

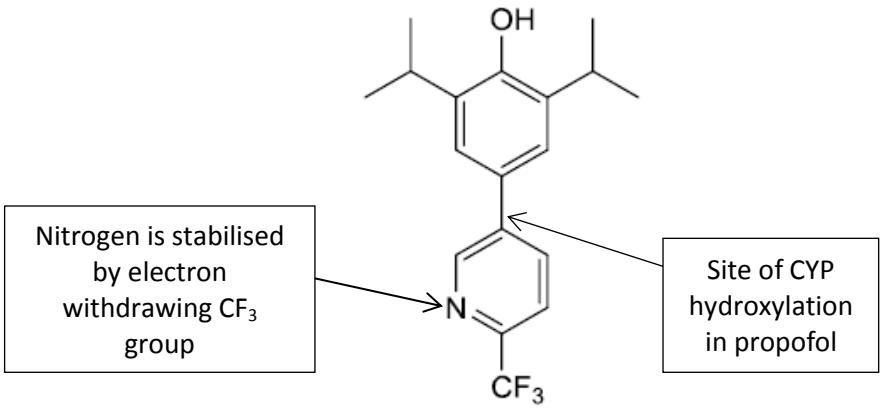

Figure 2.7. The site of CYP mediated metabolism is blocked by the side-chain in LT-01-45.

2.5.3 Microsomal Stability Assay

Microsomal stability assay was carried using rat and human liver microsomes. The assay was incubated at 37°C for 60 min (n=6). Samples were taken at time points 0, 10, 30 and 60 min. The drug samples were extracted from the microsomal fractions and prepared for analysis by liquid-chromatography mass-spectrometry (LC-MS). Microsomal stability was determined as a percentage remaining of 0 min. PK parameters, half-life and intrinsic clearance were calculated using microsomal stability-time plots.

2.5.4 Results and Discussion

A series of bi-phenyl propofol analogues were created with the intention to produce a new analgesic acting through GlyR modulation. Within this series, only one compound, LT-01-45, showed satisfactory activity at GlyRα1. LT-01-45 also exhibited some activity at $GABA_AR$ making it an unsuitable choice for further development. In addition the compound also demonstrated poor drug-like properties. Before the bi-phenyl amide scaffold was rejected outright, it was decided that the impact on metabolism of a side-chain at the *para*-position would be tested. CYP mediated metabolism of propofol usually occurs at this position, therefore blocking the site should increase metabolic stability.

Metabolism of LT-01-45 by CYPs was tested using rat and human liver microsomes (RLM and HLM). LT-01-45 (1μM) was incubated with the microsomes for 60 minutes. Samples were taken at appropriate time points and analysed using LC-MS. The data is represented as time plots in Figure 2.8. Statistical analysis was performed using one-tailed T-Test in Microsoft Excel.

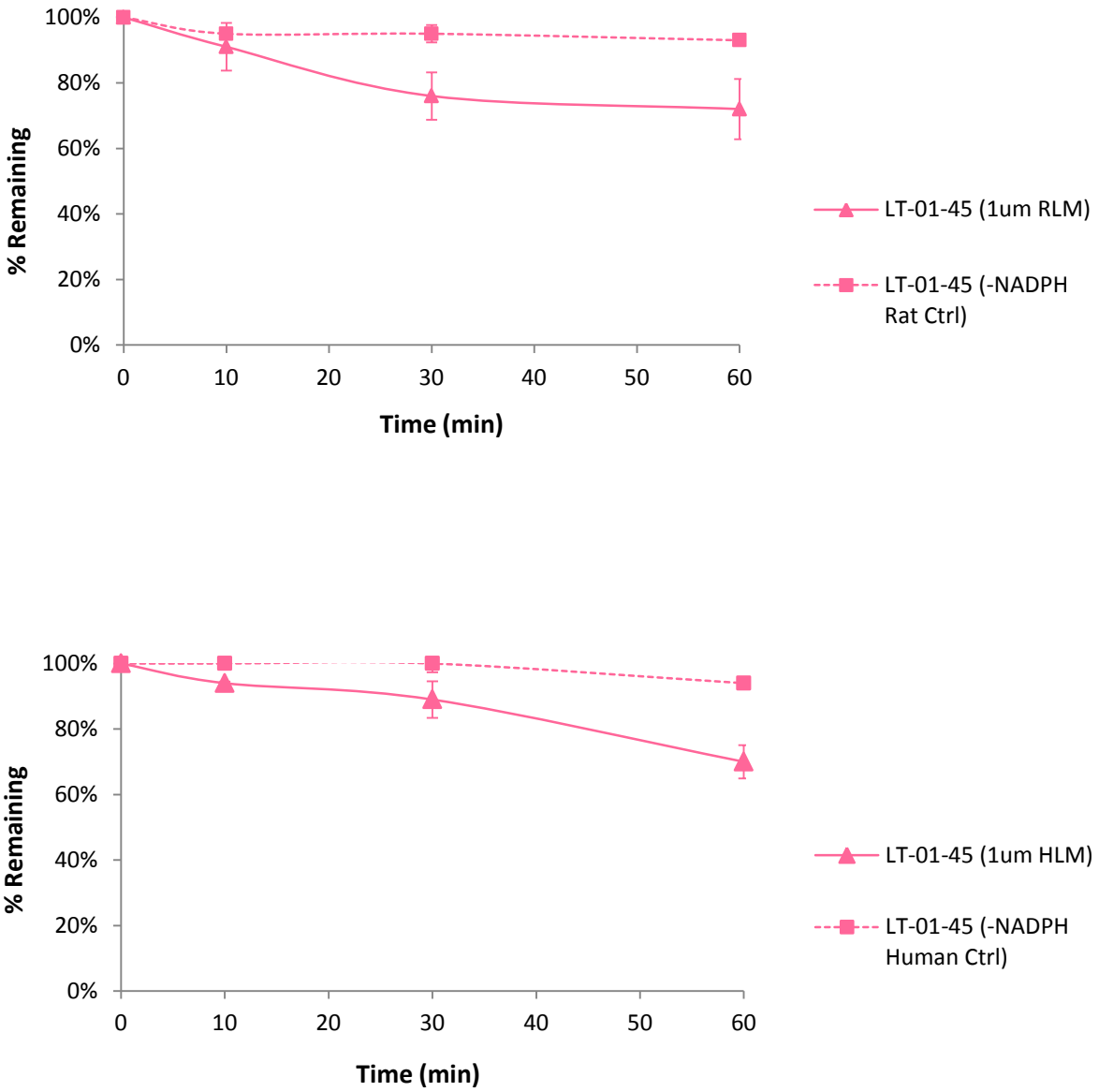

Figure 2.8.Microsomal stability data for LT-01-45 in rat (*above*) and human (*below*) liver microsomes: LT-01-45 (1µM) was incubated for 60 minutes in rat and human liver microsomes (1mg/mL protein). Each individual experiment was carried out in duplicate. A control without essential co-factor, NADPH was also carried out. The data is expressed as mean (± SEM) (n=6). Data comparison between drug and control incubation was carried out using one tailed T-Test (RLM *P*=0.06 and HLM *P*=0.07).

The data shows that LT-01-45 undergoes approximately 20% (±0.16) turnover in rat microsomes. The turnover in humans was slightly higher at roughly 25% (±0.09) metabolism in comparison to the control. Following statistical analysis, there was no significant difference seen between the test incubations and the control lacking co-factor NADPH in both rat (*P*=0.06) and human (*P*=0.07) liver microsomes. The data was used to calculate microsomal PK parameters, $T_{1/2}$, Cl_{CYP} and Cl_{int}. In the following equations the rate constant K, was the gradient of microsomal stability-time plots. It was converted to half-life ($T_{1/2}$) using the correction factor, 0.693. $T_{1/2}$ was then used to calculate the clearance by CYPs (Cl_{CYP}). A scaling factor, taken from a protocol provided by ChemPartners[83], was used to calculate the intrinsic clearance per Kg (Cl_{int}):

$$T_{1/2} = 0.693/K$$

$$Cl_{CYP} = (volume/microsomal\ protein\ concentration) * (0.693/T_{1/2})$$

$$Clint = Cl_{CYP} * Scaling\ Factor\ ^{83}$$

The PK parameters for LT-01-45 are shown in Table 2.5. LT-01-45 had a long half-life in both rat (150 minutes) and human (144 minutes) microsomes. The microsomal clearance was low (RLM = 4.6µL/min/mg and HLM=4.8µL/min/mg). These values are within the desirable range for metabolically stable drugs (RLM ≤ 13.32mL/min/mg and HLM ≤8.6 mL/min/mg)[84]. After scaling up the intrinsic clearance was also favourable (RLM = 8.3mL/min/Kg and HLM = 6mL/min/Kg). In human microsomes the intrinsic clearance of propofol has been estimated to be around 11-15mL/min/Kg[85; 86]. This value is significantly higher compared to LT-01-45. This

provides evidence that the major site of CYP hydroxylation of propofol occurs at the *para*-position and blocking of this site can greatly improve the metabolic stability of the compound.

Table 2.5. Microsomal pharmacokinetic parameters of LT-01-45: Parameters were calculated using microsomal stability-time plots and equations taken from ChemPartners protocol.

	RLM	HLM
$T_{1/2}$ (min)	150	144
Cl_{CYP}(µL/min/mg)	4.6	4.8
Cl_{int}(mL/min/kg)	8.3	6

The introduction of side-chains into propofol not only increases potency at the target receptor but also improves metabolic stability. Although these are clear advantages over the parent structure, there is still the pressing issue of poor physiochemical properties.

Maintaining good physiochemical properties of the analogues is a vital part of the candidate selection process. Using these parameters as a stringent measure of success is restrictive and wasteful. For example while ClogP is an important gauge for absorption and metabolism, all the analogues generated at this point were rejected based on high Clog. However, many of these compounds showed excellent efficacy at the target and LT-01-45 (ClogP=5.5) had a good metabolic profile. Rejection of these compounds based on ClogP value is wasteful, as helpful information about structure in relation to favourable attributes is dismissed.

In addition It has been reported that 44% of approved CNS drugs have ClogP above 5[87]. If the guidelines utilised here had been followed, these drugs would have never been developed. This shows that judging potential candidates on their individual properties and strictly following the ranges outlined in the 'rule of five' is not the most efficient way to determine potential leads.

Fortunately, a new method of high-throughput *in silico* screening has recently been introduced by Pfizer. This method is referred to as multi-parameter optimisation (MPO). MPO is designed to rate compounds on their overall drug-likeness and has been specifically geared towards drugs that penetrate the CNS. It was decided that MPO would be used to determine which analogues would be developed further.

2.6 References

1. Dutertre, S., Becker, C. M. & Betz, H. (2012). Inhibitory glycine receptors: An update. *Journal of Biological Chemistry* **287**, 40216-40223.
2. Chéry, N. & De Koninck, Y. (1999). Junctional versus extrajunctional glycine and GABA(A) receptor-mediated IPSCs in identified lamina I neurons of the adult rat spinal cord. *Journal of Neuroscience* **19**, 7342-7355.
3. Snyder, S. H. (1975). Fifth Gaddum Memorial Lecture, University of Bristol, September 1974, The glycine synaptic receptor in the mammalian central nervous system. *British Journal of Pharmacology* **53**, 473-484.
4. Lynch, J. W. & Callister, R. J. (2006). Glycine receptors: A new therapeutic target in pain pathways. *Current Opinion in Investigational Drugs* **7**, 48-53.
5. Sivilotti, L. & Woolf, C. J. (1994). The contribution of GABA(A) and glycine receptors to central sensitization: Disinhibition and touch-evoked allodynia in the spinal cord. *Journal of Neurophysiology* **72**, 169-179.
6. Lynch, J. W. (2004). Molecular structure and function of the glycine receptor chloride channel. *Physiological Reviews* **84**, 1051-1095.

7. Hogg, R. C., Buisson, B. & Bertrand, D. (2005). Allosteric modulation of ligand-gated ion channels. *Biochemical Pharmacology* **70**, 1267-1276.
8. Moss, S. J. & Smart, T. G. (2001). Constructing inhibitory synapses. *Nature Reviews Neuroscience* **2**, 240-250.
9. Becker, C. M., Hoch, W. & Betz, H. (1988). Glycine receptor heterogeneity in rat spinal cord during postnatal development. *EMBO Journal* **7**, 3717-3726.
10. del Pino, I., Paarmann, I., Karas, M., Kilimann, M. W. & Betz, H. (2011). The trafficking proteins Vacuolar Protein Sorting 35 and Neurobeachin interact with the glycine receptor β-subunit. *Biochemical and Biophysical Research Communications* **412**, 435-440.
11. Tretter, V., Mukherjee, J., Maric, H. M., Schindelin, H., Sieghart, W. & Moss, S. J. (2012). Gephyrin, the enigmatic organizer at GABAergic synapses. *Frontiers in Cellular Neuroscience*.
12. Tyagarajan, S. K. & Fritschy, J.-M. (2014). Gephyrin: a master regulator of neuronal function? *Nat Rev Neurosci* **15**, 141-156.
13. Harvey, R. J., Depner, U. B., Wässle, H., Ahmadi, S., Heindl, C., Reinold, H., Smart, T. G., Harvey, K., Schütz, B., Abo-Salem, O. M., Zimmer, A., Poisbeau, P., Welzl, H., Wolfer, D. P., Betz, H., Zeilhofer, H. U. & Müller, U. (2004). GlyR α3: An Essential Target for Spinal PGE2-Mediated Inflammatory Pain Sensitization. *Science* **304**, 884-887.
14. Xiong, W., Cui, T., Cheng, K., Yang, F., Chen, S. R., Willenbring, D., Guan, Y., Pan, H. L., Ren, K., Xu, Y. & Zhang, L. (2012). Cannabinoids suppress inflammatory and neuropathic pain by targeting α3 glycine receptors. *Journal of Experimental Medicine* **209**, 1121-1134.
15. Ahmadi, S., Lippross, S., Neuhuber, W. L. & Zeilhofer, H. U. (2002). PGE2 selectively blocks inhibitory glycinergic neurotransmission onto rat superficial dorsal horn neurons. *Nature Neuroscience* **5**, 34-40.
16. Stemkowski, P. L., Biggs, J. E., Chen, Y., Bukhanova, N., Kumar, N. & Smith, P. A. (2013). Understanding and treating neuropathic pain. *Neurophysiology* **45**, 67-78.
17. Bíró, T. & Maksay, G. (2004). Allosteric modulation of glycine receptors is more efficacious for partial rather than full agonists. *Neurochemistry International* **44**, 521-527.
18. Chesnoy-Marchais, D. (2003). Potentiation of glycine responses by dideoxyforskolin and tamoxifen in rat spinal neurons. *European Journal of Neuroscience* **17**, 681-691.
19. Beckstead, M. J., Weiner, J. L., Eger Ii, E. I., Gong, D. H. & Mihic, S. J. (2000). Glycine and γ-aminobutyric acid(A) receptor function is enhanced by inhaled drugs of abuse. *Molecular Pharmacology* **57**, 1199-1205.
20. Mascia, M. P., Gong, D. H., Eger Ii, E. I. & Harris, R. A. (2000). The anesthetic potency of propanol and butanol versus propanethiol and butanethiol in α1 wild type and α1(S267Q) glycine receptors. *Anesthesia and Analgesia* **91**, 1289-1293.
21. Hirzel, K., Müller, U., Latal, A. T., Hülsmann, S., Grudzinska, J., Seeliger, M. W., Betz, H. & Laube, B. (2006). Hyperekplexia Phenotype of Glycine Receptor α1 Subunit Mutant Mice Identifies Zn2+ as an Essential Endogenous Modulator of Glycinergic Neurotransmission. *Neuron* **52**, 679-690.

22. Conn, P. J., Lindsley, C. W., Meiler, J. & Niswender, C. M. (2014). Opportunities and challenges in the discovery of allosteric modulators of GPCRs for treating CNS disorders. *Nat Rev Drug Discov* **13**, 692-708.
23. Conn, P. J., Christopoulos, A. & Lindsley, C. W. (2009). Allosteric modulators of GPCRs: a novel approach for the treatment of CNS disorders. *Nature reviews. Drug discovery* **8**, 41-54.
24. Chesnoy-Marchais, D. & Cathala, L. (2001). Modulation of glycine responses by dihydropyridines and verapamil in rat spinal neurons. *European Journal of Neuroscience* **13**, 2195-2204.
25. Wang, J. & Urban, L. (2004). The impact of early ADME profiling on drug discovery and development strategy. *DDW DRUG DISCOVERY WORLD* **5**, 73-86.
26. Devillers-Thiéry, A., Galzi, J. L., Eiselé, J. L., Bertrand, S., Bertrand, D. & Changeux, J. P. (1993). Functional architecture of the nicotinic acetylcholine receptor: A prototype of ligand-gated ion channels. *The Journal of Membrane Biology* **136**, 97-112.
27. Kirson, D., Todorovic, J. & Mihic, S. J. (2012). Positive allosteric modulators differentially affect full versus partial agonist activation of the glycine receptor. *Journal of Pharmacology and Experimental Therapeutics* **342**, 61-70.
28. Chesnoy-Marchais, D., Lévi, S. & Acher, F. (2000). Glycinergic potentiation by some 5-HT3 receptor antagonists: Insight into selectivity. *European Journal of Pharmacology* **402**, 205-213.
29. Maksay, G., Laube, B. & Betz, H. (1999). Selective blocking effects of tropisetron and atropine on recombinant glycine receptors. *Journal of Neurochemistry* **73**, 802-806.
30. Ahrens, J., Haeseler, G., Leuwer, M., Mohammadi, B., Krampfl, K., Dengler, R. & Bufler, J. (2004). 2,6 Di-tert-butylphenol, a nonanesthetic propofol analog, modulates α1β glycine receptor function in a manner distinct from propofol. *Anesthesia and Analgesia* **99**, 91-96.
31. Pecaro, B. C. & Houting, T. (1985). Diprivan (ICI 35868, 2, 6, di-isoprophylphenol), a new intravenous anesthetic. *Oral Surgery, Oral Medicine, Oral Pathology* **60**, 586-588.
32. Skues, M. A. & Prys-Roberts, C. (1989). The pharmacology of propofol. *Journal of Clinical Anesthesia* **1**, 387-400.
33. Aronson, J. K. (2014). Management of pain during injection of propofol. *Adverse Drug Reaction Bulletin* **287**, 1107-1110.
34. Fischer, M. J. M., Leffler, A., Niedermirtl, F., Kistner, K., Eberhardt, M., Reeh, P. W. & Nau, C. (2010). The general anesthetic propofol excites nociceptors by activating TRPV1 and TRPA1 rather than GABAA receptors. *Journal of Biological Chemistry* **285**, 34781-34792.
35. Matta, J. A., Cornett, P. M., Miyares, R. L., Abe, K., Sahibzada, N. & Ahern, G. P. (2008). General anesthetics activate a nociceptive ion channel to enhance pain and inflammation. *Proceedings of the National Academy of Sciences of the United States of America* **105**, 8784-8789.
36. Zou, S. T. (2015). Clinical application of fospropofol: Research advances. *Journal of International Pharmaceutical Research* **42**, 165-169.
37. Yip, G. M. S., Chen, Z. W., Edge, C. J., Smith, E. H., Dickinson, R., Hohenester, E., Townsend, R. R., Fuchs, K., Sieghart, W., Evers, A. S. & Franks, N. P. (2013). A propofol

binding site on mammalian GABA A receptors identified by photolabeling. *Nature Chemical Biology* **9**, 715-720.

38. Jurd, R., Arras, M., Lambert, S., Drexler, B., Siegwart, R., Crestani, F., Zaugg, M., Vogt, K. E., Ledermann, B., Antkowiak, B. & Rudolph, U. (2003). General anesthetic actions in vivo strongly attenuated by a point mutation in the GABA(A) receptor beta3 subunit. *The FASEB journal : official publication of the Federation of American Societies for Experimental Biology* **17**, 250-252.
39. Belelli, D., Pistis, M., Peters, J. A. & Lambert, J. J. (1999). The interaction of general anaesthetics and neurosteroids with GABA(A) and glycine receptors. *Neurochemistry International* **34**, 447-452.
40. Sanna, E., Motzo, C., Usala, M., Serra, M., Dazzi, L., Maciocco, E., Trapani, G., Latrofa, A., Liso, G. & Biggio, G. (1999). Characterization of the electrophysiological and pharmacological effects of 4-iodo-2,6-diisopropylphenol, a propofol analogue devoid of sedative-anaesthetic properties. *British Journal of Pharmacology* **126**, 1444-1454.
41. Bandschapp, O., Filitz, J., Ihmsen, H., Berset, A., Urwyler, A., Koppert, W. & Ruppen, W. (2010). Analgesic and antihyperalgesic properties of propofol in a human pain model. *Anesthesiology* **113**, 421-8.
42. Fassoulaki, A. (2011). Is propofol an analgesic? *European Journal of Anaesthesiology (EJA)* **28**, 481-482.
43. Dong, X. P. & Xu, T. L. (2002). The actions of propofol on γ-aminobutyric acid-A and glycine receptors in acutely dissociated spinal dorsal horn neurons of the rat. *Anesthesia and Analgesia* **95**, 907-914.
44. Davies, D. L., Crawford, D. K., Trudell, J. R. & Alkana, R. L. (2005). Propofol acts on different sites than ethanol and butanol in recombinant glycine receptors: Evidence from pressure studies. In *International Congress Series*, Vol. 1283, pp. 312-314.
45. Moraga-Cid, G., Yevenes, G. E., Schmalzing, G., Peoples, R. W. & Aguayo, L. G. (2011). A single phenylalanine residue in the main intracellular loop of α1 γ-aminobutyric acid type a and glycine receptors influences their sensitivity to propofol. *Anesthesiology* **115**, 464-473.
46. O'Shea, S. M., Becker, L., Weiher, H., Betz, H. & Laube, B. (2004). Propofol Restores the Function of "Hyperekplexic" Mutant Glycine Receptors in Xenopus Oocytes and Mice. *Journal of Neuroscience* **24**, 2322-2327.
47. Lynagh, T., Kunz, A. & Laube, B. (2013). Propofol modulation of α1 glycine receptors does not require a structural transition at adjacent subunits that is crucial to agonist-induced activation. *ACS Chemical Neuroscience* **4**, 1469-1478.
48. Maksay, G., Bíró, T., Laube, B. & Nemes, P. (2008). Hyperekplexia mutation R271L of α1 glycine receptors potentiates allosteric interactions of nortropeines, propofol and glycine with [3H]strychnine binding. *Neurochemistry International* **52**, 235-240.
49. de la Roche, J., Leuwer, M., Krampfl, K., Haeseler, G., Dengler, R., Buchholz, V. & Ahrens, J. (2012). 4-Chloropropofol enhances chloride currents in human hyperekplexic and artificial mutated glycine receptors. *BMC Neurology* **12**.
50. Eckle, V. S., Grasshoff, C., Mirakaj, V., O'Neill, P. M., Berry, N. G., Leuwer, M. & Antkowiak, B. (2014). 4-bromopropofol decreases action potential generation in spinal

neurons by inducing a glycine receptor-mediated tonic conductance. *British Journal of Pharmacology* **171**, 5790-5801.

51. Ahrens, J., Leuwer, M., De La Roche, J., Foadi, N., Krampfl, K. & Haeseler, G. (2009). The non-anaesthetic propofol analogue 2,6-di-tert-butylphenol fails to modulate GABAA receptor function. *Pharmacology* **83**, 95-98.
52. Chen, Y., Dai, T. J. & Zeng, Y. M. (2007). Strychnine-sensitive glycine receptors mediate the analgesic but not hypnotic effects of emulsified volatile anesthetics. *Pharmacology* **80**, 151-157.
53. Haeseler, G., Ahrens, J., Krampfl, K., Bufler, J., Dengler, R., Hecker, H., Aronson, J. K. & Leuwer, M. (2005). Structural features of phenol derivatives determining potency for activation of chloride currents via α(1) homomeric and α(1)β heteromeric glycine receptors. *British Journal of Pharmacology* **145**, 916-925.
54. Hughes, J. P., Rees, S. S., Kalindjian, S. B. & Philpott, K. L. (2011). Principles of early drug discovery. *British Journal of Pharmacology* **162**, 1239-1249.
55. Trapani, G., Latrofa, A., Franco, M., Altomare, C., Sanna, E., Usala, M., Biggio, G. & Liso, G. (1998). Propofol analogues. Synthesis, relationships between structure and affinity at GABA(A) receptor in rat brain, and differential electrophysiological profile at recombinant human GABA(A) receptors. *Journal of Medicinal Chemistry* **41**, 1846-1854.
56. Lipinski, C. A., Lombardo, F., Dominy, B. W. & Feeney, P. J. (2012). Experimental and computational approaches to estimate solubility and permeability in drug discovery and development settings. *Advanced Drug Delivery Reviews* **64**, 4-17.
57. Kola, I. & Landis, J. (2004). Can the pharmaceutical industry reduce attrition rates? *Nature reviews Drug discovery* **3**, 711-716.
58. Kerns, E. & Di, L. (2008). *Drug-like Properties: Concepts, Structure Design and Methods: from ADME to Toxicity Optimization*, Elsevier Science.
59. Chung, J. M., Kim, H. K. & Chung, K. (2004). Segmental spinal nerve ligation model of neuropathic pain. *Methods in molecular medicine* **99**, 35-45.
60. Blackburn-Munro, G. & Erichsen, H. K. (2005). Antiepileptics and the treatment of neuropathic pain: Evidence from animal models. *Current Pharmaceutical Design* **11**, 2961-2976.
61. Kim, K. J., Yoon, Y. W. & Chung, J. M. (1997). Comparison of three rodent neuropathic pain models. *Experimental Brain Research* **113**, 200-206.
62. Farrar, V. A., Ciechanowicz-Rutkowska, M., Grochowski, J., Serda, P., Pilati, T., Filippini, G., Hinko, C. N., El-Assadi, A. & Moore, J. A. (1993). Synthesis and calculated log P correlation of imidooxy anticonvulsants. *Journal of Medicinal Chemistry* **36**, 3517-3525.
63. Rice, J. E. (2014). Chapter 7 - Drug Metabolism. In *Organic Chemistry Concepts and Applications for Medicinal Chemistry* (Rice, J. E., ed.), pp. 145-201. Academic Press, Boston.
64. Takakusa, H., Masumoto, H., Mitsuru, A., Okazaki, O. & Sudo, K. (2008). Markers of electrophilic stress caused by chemically reactive metabolites in human hepatocytes. *Drug Metab Dispos* **36**, 816-23.

65. Eberlein, T. H. (2008). Essentials of Organic Chemistry: For Students of Pharmacy, Medicinal Chemistry, and Biological Chemistry (Paul M. Dewick). *Journal of Chemical Education* **85**, 204.
66. Anthony, D. & Lockey, M. (2001). 'Hit'to 'lead'and 'lead'to 'candidate'optimisation using multi-parametric principles. *Drug Discovery* **2**, 11.
67. Manallack, D. T. (2007). The pK(a) Distribution of Drugs: Application to Drug Discovery. *Perspectives in Medicinal Chemistry* **1**, 25-38.
68. Pajouhesh, H. & Lenz, G. R. (2005). Medicinal Chemical Properties of Successful Central Nervous System Drugs. *NeuroRx* **2**, 541-553.
69. Cox, P. J. (2001). Essentials of pharmaceutical chemistry. *TALANTA -OXFORD THEN AMSTERDAM-* **54**, 419.
70. Cohen, L. H., Remley, M. J., Raunig, D. & Vaz, A. D. N. (2003). In vitro drug interactions of cytochrome p450: An evaluation of fluorogenic to conventional substrates. *Drug Metabolism and Disposition* **31**, 1005-1015.
71. Guitton, J., Buronfosse, T., Desage, M., Flinois, J. P., Perdrix, J. P., Brazier, J. L. & Beaune, P. (1998). Possible involvement of multiple human cytochrome P450 isoforms in the liver metabolism of propofol. *British Journal of Anaesthesia* **80**, 788-795.
72. Zanger, U. M. & Schwab, M. (2013). Cytochrome P450 enzymes in drug metabolism: Regulation of gene expression, enzyme activities, and impact of genetic variation. *Pharmacology & Therapeutics* **138**, 103-141.
73. Hardy, K. D., Wahlin, M. D., Papageorgiou, I., Unadkat, J. D., Rettie, A. E. & Nelson, S. D. (2014). Studies on the role of metabolic activation in tyrosine kinase inhibitor-dependent hepatotoxicity: Induction of CYP3A4 enhances the cytotoxicity of lapatinib in HepaRG cells. *Drug Metabolism and Disposition* **42**, 162-171.
74. Plant, N. (2004). Strategies for using in vitro screens in drug metabolism. *Drug Discovery Today* **9**, 328-336.
75. Zhang, D., Luo, G., Ding, X. & Lu, C. (2012). Preclinical experimental models of drug metabolism and disposition in drug discovery and development. *Acta Pharmaceutica Sinica B* **2**, 549-561.
76. Loryan, I., Lindqvist, M., Johansson, I., Hiratsuka, M., Van Der Heiden, I., Van Schaik, R. H., Jakobsson, J. & Ingelman-Sundberg, M. (2012). Influence of sex on propofol metabolism, a pilot study: Implications for propofol anesthesia. *European Journal of Clinical Pharmacology* **68**, 397-406.
77. Tai, Y. T., Lin, Y. L., Chang, C. C., Cherng, Y. G., Don, M. J. & Chen, R. M. (2015). Ring-oxidative biotransformation and drug interactions of propofol in the livers of rats. *BioMed Research International* **2015**.
78. Chan, W. H., Chen, T. L., Chen, R. M., Sun, W. Z. & Ueng, T. H. (2006). Propofol metabolism is enhanced after repetitive ketamine administration in rats: The role of cytochrome P-450 2B induction. *British Journal of Anaesthesia* **97**, 351-358.
79. Iohom, G., Ni Chonghaile, M., O'Brien, J. K., Cunningham, A. J., Fitzgerald, D. F. & Shields, D. C. (2007). An investigation of potential genetic determinants of propofol requirements and recovery from anaesthesia. *European Journal of Anaesthesiology* **24**, 912-919.

80. Lian, Q. Q., Pan, P. P., Li, J. W., Lin, H., Hu, G. X., Zuo, M. Z. & Cai, J. P. (2015). Impact of CYP2C9 polymorphism found in the Chinese population on the metabolism of propofol in vitro. *Biological and Pharmaceutical Bulletin* **38**, 531-535.
81. Court, M. H., Duan, S. X., Hesse, L. M., Venkatakrishnan, K. & Greenblatt, D. J. (2001). Cytochrome P-450 2B6 is responsible for interindividual variability of propofol hydroxylation by human liver microsomes. *Anesthesiology* **94**, 110-119.
82. Nagib, D. A. & MacMillan, D. W. C. (2011). Trifluoromethylation of arenes and heteroarenes by means of photoredox catalysis. *Nature* **480**, 224-228.
83. Lubei Mao, J. H., Changxia Li. (2013). To evaluate metabolic stability of test compound in incubation with rat liver microsomes. In *Metabolic stability* (Co, S. C., ed.).
84. Di, L., Kerns, E. H., Ma, X. J., Huang, Y. & Carter, G. T. (2008). Applications of high throughput microsomal stability assay in drug discovery. *Combinatorial Chemistry and High Throughput Screening* **11**, 469-476.
85. Gill, K. L., Gertz, M., Houston, J. B. & Galetin, A. (2013). Application of a Physiologically Based Pharmacokinetic Model to Assess Propofol Hepatic and Renal Glucuronidation in Isolation: Utility of In Vitro and In Vivo Data. *Drug Metabolism and Disposition* **41**, 744-753.
86. Al-Jahdari, W. S., Yamamoto, K., Hiraoka, H., Nakamura, K., Goto, F. & Horiuchi, R. (2006). Prediction of total propofol clearance based on enzyme activities in microsomes from human kidney and liver. *Eur J Clin Pharmacol* **62**, 527-33.
87. D. Segall, M. & D. Segall, M. (2012). Multi-Parameter Optimization: Identifying High Quality Compounds with a Balance of Properties. *Current Pharmaceutical Design* **18**, 1292.

Chapter 3

Lead Optimisation

Table of Contents

3.1 Early Drug Development

3.1.1 Multiparameter Optimisation

The early generation of hit compounds is a time-consuming process. With unlimited structural possibilities, it is difficult to identify which compounds will have ideal drug-like properties. In this project, Lipinski's rule of five was used to evaluate each hit. Many compounds were dismissed due to high ClogP, regardless of their activity at the target. This method was considered restrictive and slow; it was decided an alternate means of assessing new hits was greatly needed. Fortunately, a new system for evaluating novel drugs (Multiparameter optimisation), had just recently been introduced by Pfizer and others, and has quickly gaining in popularity[1].

MPO is an algorithm that predicts *in silico,* six main physiochemical properties featured in the 'rule of five'; ClogP, ClogD, MW, HBD, TPSA and pKa[2]. Each property is measured on a scale (T0-1) and the sum of these values is the MPO score (0-6)[1]. For CNS drugs, the recommended MPO is 4-6[2]. The key advantage of this system is that, an acceptable MPO can be reached in a variety of ways. For instance, a compound with a low ClogP score (e.g. LT-01-45) may have high scores in other categories, meaning that it can still be accepted based on its overall MPO score. Unfortunately, LT-01-45 achieved a MPO score of 3, too low for drugs capable of penetrating into the CNS. However two parameters, MW and HBD, were within the acceptable range (Table 3.1), illustrating that MPO can be used to identify the strengths and weaknesses of a hit. The inclusion of individual scores highlights areas that may be tweaked to improve drug-likeness.

Table 3.1. MPO score of LT-01-45: Breakdown of MPO score for LT-01-45. The analogue has poor ClogP and ClogD. The TSPA and pKa values were adequate, while MW and HBD were excellent. Overall the compound failed to achieve the recommended score of 4. Colour coded T0 scores: red = poor, orange = average, green = good.
**MPO data was provided by the Department of Chemistry.*

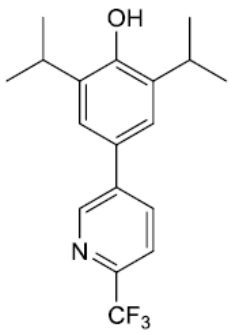

LT-01-45

Parameter	T0 Score
ClogP = 5.55	**0.00**
ClogD = 3.70	**0.15**
TPSA = 33.12 Å	**0.65**
MW = 322.35Da	**1.00**
HBD = 1	**0.83**
pKa = 9.22	**0.39**
CNS MPO = 3.0	

In a study by Segall *et al*. (2012), the MPO algorithm was applied to FDA approved drugs and Pfizer drug candidates. A high correlation (74%) of approved CNS drugs had a MPO score above 4. Analysis was also carried on drug candidates currently being developed by Pfizer, where it was found that 60% of these compound had a MPO above 4[2]. Many of these candidates had less than optimal individual scores and would have been dismissed based on traditional guidelines. High MPO scores can also be suggestive of good 'absorption, distribution, metabolism, excretion and toxicity' (ADME-T) properties. Drugs that work in the CNS must have high passive apparent permeability (P_{app}) and low glycoprotein (p-gp efflux) liability in order to pass through the BBB. They must also have low intrinsic clearance (Cl_{int}) and show little to no toxicity[3; 4; 5]. In MPO validity studies, favourable ADME-T traits correlated

with high MPO scores[2]. This suggests that MPO is not only able to measure the drug-likeness of a compound but may be used to predict ADME, safety and, more importantly the likelihood of CNS penetration.

3.1.2 CNS Penetration

The failure rate of neurotherapeutic candidates proceeding into pre-clinical development is almost twice as high as that of non-CNS drug candidates. Furthermore, drugs acting in the CNS are also far less likely to be approved for clinical and commercial use[6]. Difficulties in developing CNS drugs arise from the complex and high risk nature of treating neurological diseases. Aside from toxicity, distribution of a drug into the CNS is one of the most pressing challenges faced when developing a neurological therapeutic, with as little as 2% of small-molecule drugs successfully crossing the BBB[7].

The BBB is made up of three compartments that form a huge physical barrier between the brain and the rest of the body[8]. The first boundary is a layer of compact endothelial cells covering capillaries and microvessels that contact with brain tissue[6]. Tight intracellular junctions between the endothelial cells control the passage of large molecules, while astrocytes mediate correct transportation across the BBB. This first layer has the largest surface area for exchange and directly connects the blood and the brain[6]. It is often considered the true barrier and is the main consideration of CNS penetration. The two other layers are, an epithelial cell layer forming a barrier between blood and cerebrospinal fluid (BCSFB) and an aranoid epithelial barrier between CSF and subdural space[8].

The BBB exists to ensure the safety and homeostasis of the CNS. Specialised ion channels regulate ionic gradients needed for correct synaptic signalling[9]. Protein transporters, such as p-glycoprotein transporters (p-gp), are able to eject any molecules that could be harmful to the CNS, as well as excess levels of neurotransmitters[3]. The lipid bi-layer of the BBB is permeable to small lipophilic molecules, gases, and naturally occurring chemicals, such as hormones and neurotransmitters[8]. Small drugs (e.g. propofol) also may passively diffuse through the BBB. It is recommended that drug candidates have low MW and good lipophilicity in order to pass into the CNS[10]. Candidates with high P_{app} are able to diffuse across the BBB with greater ease, while those with low substrate affinity for p-gp transporters are much less likely to be transported out of the CNS[3].

The high correlation between MPO score and drugs with high P_{app} and low p-gp affinity, suggests that MPO may be used to predict CNS penetration. It was decided that MPO would be used to evaluate compounds in this project. The physiochemical properties were generated *in silico* and the MPO algorithm was applied. Hits with an acceptable score (MPO ≥ 4) and good selectivity for GlyRα1 (E_{50}=1μM) were selected for further development.

3.1.3 Drug Development Process

The research and development process of a new drug is generally divided into three phases; drug discovery, pre-clinical development and clinical trials[11]. The process is summarised in Figure 3.1, wherein the 'drug discovery' phase is detailed in blue. The whole process can take as long as 15-20 years and can end-up costing billions of dollars, with the

most time and money spent during the clinical testing stage[12]. In the last decade, it has been estimated that as few as 11% of drug candidates will move into pre-clinical development, while on average only 1% of drugs are approved for market per year[7;13].

Toxicity and poor ADME profiles account for more than half of drug candidates failing[14]. During pre-clinical development, failure is can be costly; however during clinical trials where time, money and reputation have been greatly invested, failure can be devastating. Therefore it is far more advantageous to thoroughly refine drug candidates during lead optimisation, where the stakes are much lower. The focus of early drug development is largely composed of generating candidates with high efficacy at the target and optimising good physiochemical properties. In recent years, the incorporation of pharmacokinetic and safety profiling alongside pharmacodynamic testing has become increasingly commonplace[15].

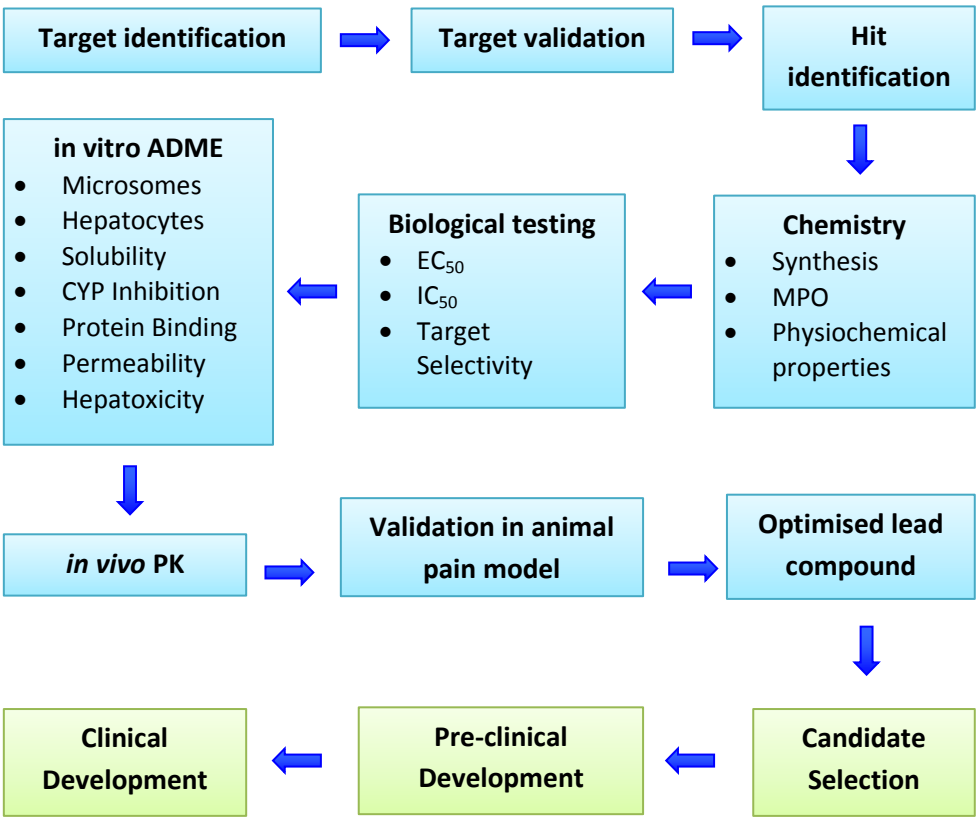

Figure 3.1. Outline of our drug development process: The drug development process often begins with the identification and validation of a biological target. A series of 'hit' compounds that may interact with the chosen target are synthesised. These compounds are assessed *in silico* for drug-likeness. Successful compounds will be tested for target efficacy. Lead compounds that demonstrate good target selectivity will then be optimised using data gathered from *in vitro* and *in vivo* metabolism and pharmacokinetics. A lead compound is then validated in an animal model of disease (i.e. neuropathic pain). Optimised drug candidates can then move into pre-clinical development.

3.1.4 ADME Testing

The study of pharmacokinetic alongside, pharmacodynamic testing helps build a better picture of how a drug will act in a living organism[16]. ADME and toxicity studies during lead optimisation are useful, not only in refining a drug candidate but foreshadowing any potential

pitfalls further down the development pipeline. Toxicity and pharmacokinetics can be integrated into lead optimisation in a number of ways. Absorption and distribution can be measured using cell permeability assays; Caco-2 permeability P_{app} (optimal value >1x10^{-6} cm^{-1})[17] is a good measure of absorption through intestinal epithelium. Metabolic stability can be interpreted as intrinsic clearance from sub-cellar microsomal fractions or whole hepatocyte studies (desired Cl_{int} <30µL/min/mg protein)[17]. Rat models of metabolism are extremely useful for measuring ADME in a working biological system. Pharmacokinetic parameters in rats include, clearance (Cl), volume of distribution (V_d), maximal plasma concentration (C_{max}), peak plasma concentration time (T_{max}), plasma half-life ($T_{1/2}$) and bioavailability (F%)[15]. However, animal models should be used sparingly due to economical and ethical reasons. Toxicity is often measured as viability in various cell lines (no effect at EC_{50})[17]. Most notability, Hep G2 cells are commonly used to investigate hepatoxicity, a major cause of toxicity–related failure[18]. Hepatoxicity can also be the result of negative drug-drug interactions (DDIs). Such interactions are usually a consequence of induction or inhibition of metabolising enzymes. Cytochrome P450 (CYP) inhibition (EC_{50} >10µM) is a popular way to identify adverse DDIs[17; 18].

These techniques can be used to further optimise compounds that have passed initial target validation screening with an acceptable MPO score. Candidates that show drug-like properties in various ADME and toxicity tests can then be further validated in an animal model of pain.

3.1.5 Pharmacodynamic Testing for Neuropathic Pain Drugs

A drug candidate may exhibit high potency at the target receptor, along with a favourable PK profile and good drug-like physiochemical properties but it is vital to validate effectiveness in an animal model of the target disease. There are numerous methods of inducing pain and measuring analgesia in animal models[19]. In this project, neuropathic pain behaviours, allodynia and hyperalgesia were induced using the Chung lesion model of neuropathic pain.

The Chung lesion was developed as a more controlled model of peripheral nerve injury[20]. Traditionally models of peripheral nerve injury involved the ligation or partial axotomy of the sciatic nerve. The sciatic nerve is one of the largest in body and is derived from many spinal nerves including those in the lumbar and sacral segments. Therefore direct injury to the sciatic nerve will have a large impact on the PNS and will result in a greater variability of developed neuropathic pain behaviours [19]. Chung *et al.* developed a pain that involved the ligation of a spinal nerve rather than axotomy[20]. Traditionally the Chung lesion model targets either the lumbar spinal nerve 5 or 6, in this project however, the left sciatic nerve was selected for ligation (see Appendix III)[19]. In order to reduce the number of animals used, only a select number of the most promising candidates were chosen to be tested in the Chung lesion model. Candidate efficacy was tested against the drugs currently used to treat chronic pain. The effect of the candidate on mechanical allodynia was measured by foot withdrawal threshold (g) in response to gradually increasing innocuous mechanical stimulus[21]. While hyperalgesia was measured the by paw withdrawal latency (s) from a constant source

noxious cold (10°C)[21]. All neuropathic pain model testing was carried out under the supervision of Prof. McMahon at King's College London, UK.

3.2 Lead Generation

3.2.1 *Amino-alkyl Analogues*

MPO evaluation of the bi-phenyl analogues indicates that these compounds are unlikely to cross the BBB. Breakdown of the MPO scores highlighted a major issue with high ClogP and ClogD. The addition of common solubilising substitutions, such as morpholine and other heterocyclic amines (Figure 3.2), should reduce the ClogP and ClogD whilst retaining good TSPA[22]. Some of the bi-phenyl analogues already featured a morpholine ring and still maintained poor solubility. It is probable that this was caused by the inclusion of the phenyl ring. Removal of the ring will reduce the steric hindrance of the structure and hopefully improve the physiochemical properties of the analogues.

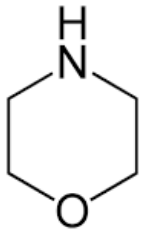

Figure 3.2. Structure of morpholine.[22]

Review of the literature lead to the discovery of an earlier study, wherein propofol analogues containing morpholine rings were tested for efficacy at $GABA_AR$. These amino-alkyl

propofol analogues were developed by Cooke *et al.*, with the intention of improving the solubility of propofol[23]. The analogues were able to cause sedation, but the effect was not reversed by the inclusion of a $GABA_AR$ antagonist, TBPS (t-butyl bicyclo-phosphorothionate)[23]. This suggests that the hypnotic activity of these analogues is not mediated through $GABA_AR$. In addition to having no activity at $GABA_AR$, the amino-alkyl analogues also demonstrated superior solubility. Moreover, these analogues were not tested for activity at GlyRs, so there is a possibility that heterocyclic amine analogues may be able to potentiate glycine currents without activing $GABA_AR$. On this basis it was decided that a series of amino alkyl analogues would be synthesised (Figure 3.3).

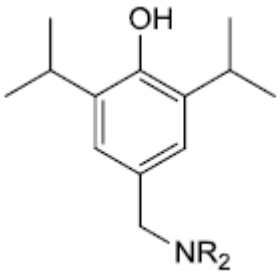

Figure 3.3. Amino-alkyl analogue scaffold.

These analogues exhibited slightly improved physiochemical properties over their predecessors. Unfortunately the aq. Solubility, pKa and ClogP were still too high, whilst the TPSA had fallen below an acceptable range. MPO evaluation predicted that none of the compounds would be capable of BBB penetration. As a final testing measure, the compounds were tested for target efficacy but none were able to activate glycine receptors under the cut-off concentration of 1μM.

As part of this rationale a series of analogues based on 2,6-di-tert-butylphenol were also synthesised. 2,6-di-tert-butylphenol is a non-sedative propofol analogue (Figure 3.4) that is able to potentiate glycine to a greater extent than propofol and is unable to activate $GABA_A$Rs [24,25].

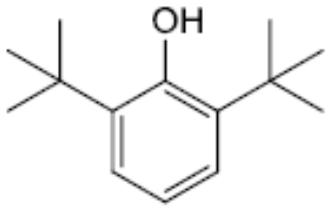

Figure 3.4. The structure of 2,6-Di-tert-butylphenol.

The 2,6-di-tert-butylphenol analogues were synthesised and analysed for their MPO scores. The physiochemical properties of these analogues were worse. In both analogue sets, the structures containing morpholine had the most favourable individual physiochemical properties. The MPO evaluation for the two morpholine analogues is detailed in Table 3.2.

In addition to poor *in vitro* activity the amino-alkyl compounds also carry the risk of forming toxic metabolites. Benzyl amines are able to form quinone methides, a reactive electrophilic metabolite that can interact with many biological nucleophiles (e.g. proteins). Blocking metabolism at the methylene position with a carbonyl group may prevent the formation of quinone methides. The introduction of a polar carbonyl could also improve pKa, TSPA and ClogP.

Table 3.2. MPO score of amino-alkyl analogues: Breakdown of MPO score for two best performing analogues of the amino-alkyl series. Both analogues contained a morpholine. The 2,6-Di-tert-butylphenol analogue had a lower MPO score and higher ClogP compared to the propofol analogues. While the propofol analogue did not have a ClogP value that would normally be considered acceptable, the T0 score contributed highly to its overall MPO score.
**MPO data was provided by the Department of Chemistry.*

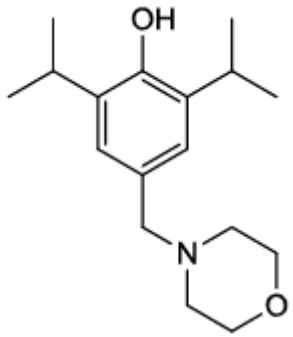		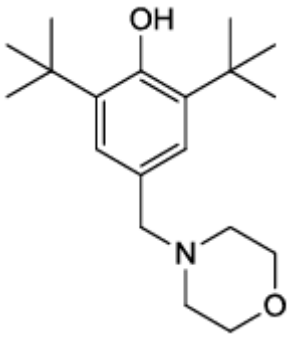	
Parameter	T0 Score	**Parameter**	**T0 Score**
ClogP = 3.60	**0.70**	**ClogP** = 4.67	**0.17**
ClogD = 2.70	**0.65**	**ClogD** = 3.50	**0.25**
TPSA = 32.70 Å	**0.63**	**TPSA** = 32.70 Å	**0.63**
MW = 277.4 Da	**1.00**	**MW** = 305.45 Da	**1.00**
HBD = 1	**0.83**	**HBD** = 1	**0.83**
pKa = 10.89	**0.00**	**pKa** = 12.01	**0.00**
CNS MPO = 3.8		**CNS MPO = 2.9**	

3.2.2 Amide Analogues

The replacement of the phenyl ring with a benzyl morpholine group did improve the physiochemical properties of the compounds, although it had little effect on receptor selectivity. The amino-alkyl analogues may also produce toxic metabolites in the form of quinones. The introduction of a carbonyl will result in the creation of an amide analogue. In this analogue series the vulnerable benzyl link is protected, potentially making the compounds more metabolically stable. Furthermore, the carbonyl group should influence the solubility and polarity of the compound (e.g. reduced ClogP and increase TPSA).

Table 3.3. MPO evaluation of amide analogues, LT-01-25 and LT-01-26
**Data from the Department of Chemistry.*

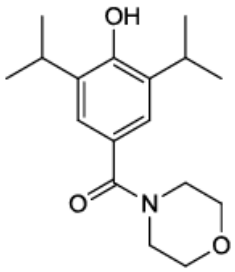 **LT-01-25**		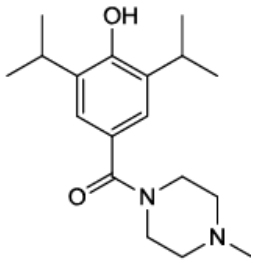 **LT-01-26**	
Parameter	**T0 Score**	**Parameter**	**T0 Score**
ClogP = 3.10	**0.95**	**ClogP** = 3.54	**0.73**
ClogD = 2.80	**0.60**	**ClogD** = 2.50	**0.85**
TPSA = 49.8 Å	**1.00**	**TPSA** = 43.78 Å	**1.00**
MW = 291.1 Da	**1.00**	**MW** = 304.43 Da	**1.00**
HBD = 1	**0.83**	**HBD** = 1	**0.83**
pKa = 10.10	**0.00**	**pKa** = 10.14	**0.00**
CNS MPO = 4.3		**CNS MPO = 4.4**	
Gly EC_{50} = 0.35 nM		**Gly EC_{50} = 1.2 pM**	

All the amide analogues showed a marked improvement in their physiochemical properties. Although, only two compounds, LT-01-25 and LT-01-26 were able achieved a MPO score above 4 (Table 3.3). While the MPO scores were extremely close, the individual scores show that LT-01-26 has a better ClogD value. ClogD is a very important parameter, as it is a measure of ClogP in relation to physiological pH changes[26]. Within this series only LT-01-25 and LT-01-26 were able to activate GlyR at a much lower concentration than propofol. As seen in Table 3.3, LT-01-26 had a lower EC_{50} value and it showed not activity at $GABA_AR$, unlike LT-01-25, which had a minor effect ($GABA_AR$ EC_{50}= 30μM). Following the success of MPO evaluation and high potency for the target receptor, LT-01-25 and LT-01-26 were chosen to undergo *in vitro* and *in vivo* PK/PD testing.

3.2.3 Tert-butyl Amide Analogues

Amide analogues of 2,6-di-tert-butylphenol were also synthesised. Based on the progress seen with the amide morpholine analogues, the addition of a carbonyl may decrease the ClogP, ClogD and pKa of the original *tert*-butyl analogues. The new amide analogues did show an improvement in regards to ClogP, TSPA and pKa, nevertheless the predicted parameters were still not within an acceptable range. Following MPO evaluation, none of the *tert*-butyl amide analogues were able to reach the desired score of ≥4. The highest scoring analogues, LT-01-88 and LT-01-89, are shown in Table 3.4.

The *tert*-butyl amide analogues were tested for GlyR efficacy. Due to unstable cell lines it was not feasible to test every compound. Based on poor MPO score LT-01-88 did not undergo

electrophysiological testing. LT-01-89, on the other hand, was one of the three compounds chosen to be tested at GlyRα1.

Table 3.4. MPO evaluation of tert-butyl amide analogues, LT-01-88 and LT-01-89.
**Information provided by the Department of Chemistry (Gly EC_{50} value for LT-01-88 not available).*

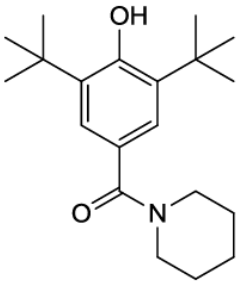 LT-01-88		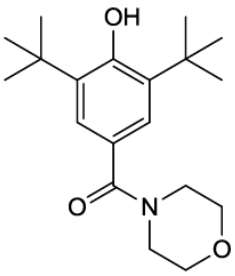 LT-01-89	
Parameter	**T0 Score**	**Parameter**	**T0 Score**
ClogP = 5.13	**0.0**	**ClogP** = 4.10	**0.45**
ClogD = 3.70	**0.15**	**ClogD** = 4.70	**0.00**
TPSA = 40.54 Å	**1.00**	**TPSA** = 49.77 Å	**1.00**
MW = 317.47 Da	**1.00**	**MW** = 319.44 Da	**1.00**
HBD = 1	**0.83**	**HBD** = 1	**0.83**
pKa = 10.70	**0.00**	**pKa** = 10.52	**0.00**
CNS MPO = 3.0		**CNS MPO = 3.3**	
-		**Gly EC_{50} = 0.46 nM**	

Table 3.4 shows that the predicted drug-likeness of the tert-butyl amide analogues is not as promising as the amide morpholine compounds. Even so, LT-01-89 did show a good level of selectivity, in keeping with that of the amide morpholine analogues, LT-01-25 and LT-01-26. It was determined that LT-01-89 would be investigated further. Although LT-01-88 was not

selected for GlyRα1 efficacy, the analogue was included in microsomal stability studies with LT-01-25, LT-01-26 and LT-01-89.

3.3 Pharmacological Testing of Amide Analogues

3.3.1 Metabolic Stability

In comparison to earlier propofol analogues in this project, the amide compounds have shown a huge improvement in their drug-like properties. Three of these analogues, LT-01-25, LT-01-26 and LT-01-88 were able to successfully modulate GlyRs. These compounds, as well as another analogue, LT-01-88, were selected to undergo the same microsomal stability testing as a previous analogue, LT-01-45. The major site of CYP metabolism has also been blocked by a *para*-substitution. The newly substituted carbonyl group will help protect the benzyl link, another possible site of metabolism (Figure 3.5).

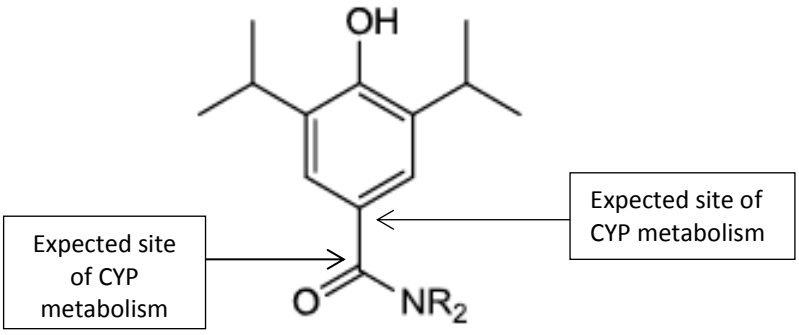

Figure 3.5. Potential sites of CYP mediated metabolism are blocked in amide morpholine analogues.

The analogues were tested with the same protocol used for LT-01-45 in rat and human liver microsomes (RLM and HLM). The compounds were incubated at 37°C for 60 minutes. Samples were taken at 0, 10, 30 and 60 min. The samples were analysed using LC-MS. Microsomal stability results are shown in Figure 3.6 (LT-01-25), Figure 3.7 (LT-01-26), Figure 3.8 (LT-01-88) and Figure 3.9 (LT-01-89). Microsomal parameters are shown in Table 3.5.

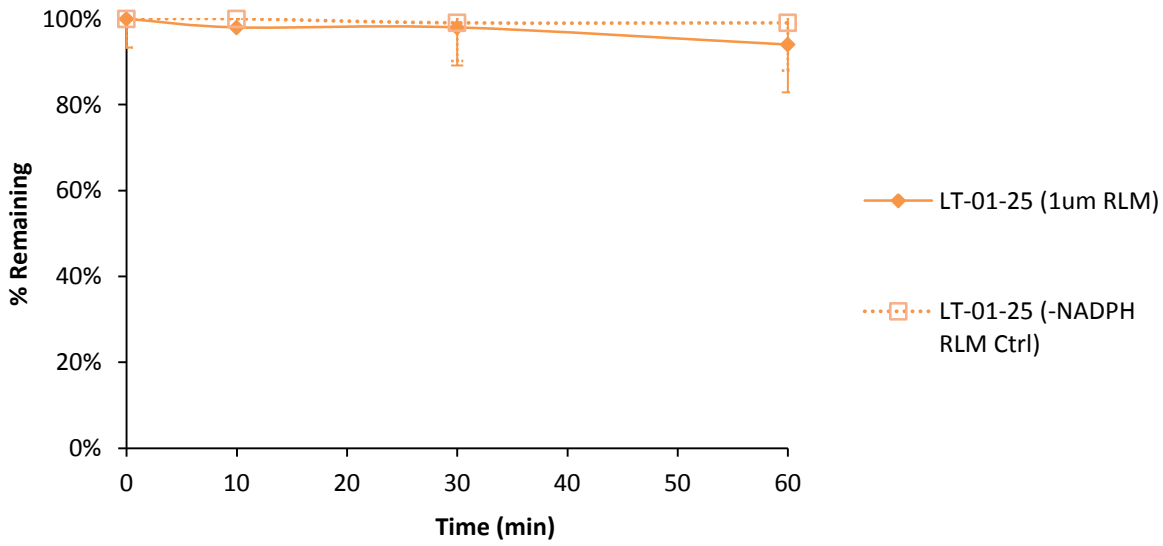

Figure 3.6a. Microsomal stability data for LT-01-25 in rat liver microsomes: LT-01-25 (1µM) was incubated for 60 minutes in rat liver microsomes (1mg/mL protein). Each individual experiment was carried out in duplicate. A control without essential co-factor, NADPH was also carried out. The data is expressed as mean (± SEM) (n=6). Data comparison between drug and control incubation was carried out using one tailed T-Test (*P*=0.08). Total turnover was 5% (±0.09).

The total turnover for LT-01-25 in rats was 5% (±0.09). For human microsomes the turnover was slightly higher in at 8% (±0.17). There was no statistical significance between the controls and the incubations at 60 minutes (RLM *P*=0.08, HLM *P*=0.06). The half-life in both species was exceptionally long, with the compound estimated to last over 8 hours. The microsomal clearance was well within an acceptable range (RLM = 0.9 µL/min/mg and HLM = 1.3 µL/min/mg). The predicted intrinsic clearance was nearly 10-fold lower than that of propofol. LT-01-25 was the most microsomal stable analogue tested at this point in the project. Its stability can be attributed to the carbonyl group, which prevents the hydroxylation by CYPs and helps maintain favourable drug-like properties.

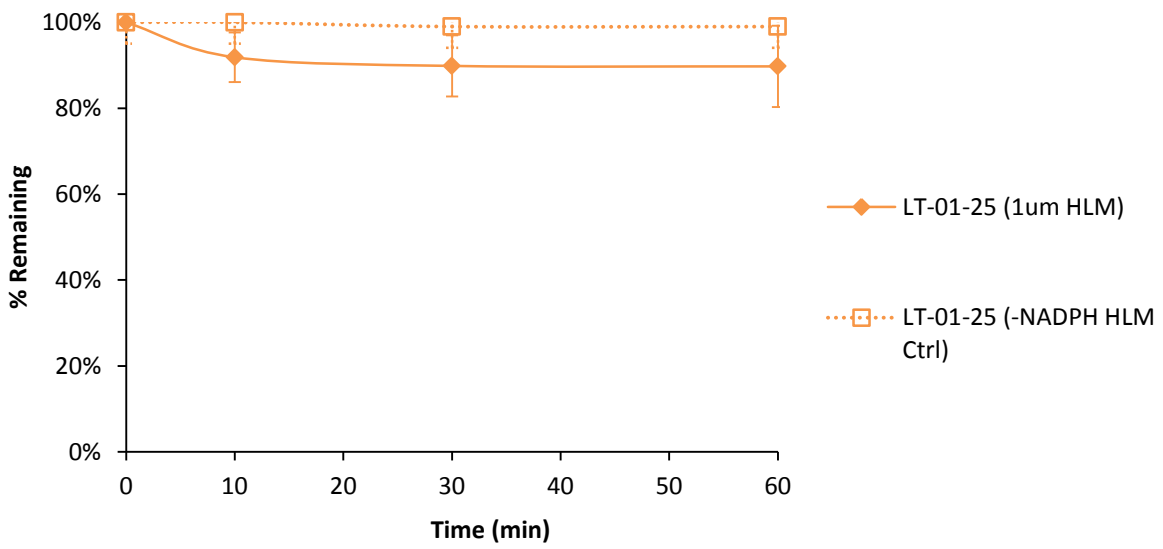

Figure 3.6b. Microsomal stability data for LT-01-25 in human liver microsomes: LT-01-25 (1µM) was incubated for 60 minutes human liver microsomes (1mg/mL protein). Each individual experiment was carried out in duplicate. A control without essential co-factor, NADPH was also carried out. The data is expressed as mean (± SEM) (n=6). Data comparison between drug and control incubation was carried out using one tailed T-Test (*P*=0.06) and the total turnover 8% (±0.17).

In contrast, the other amide analogue, LT-01-26 had a dramatically different microsomal profile. Despite the fact that LT-01-26 is more potent at the drug target, it is far less stable than LT-01-25. After 60 minute most of analogue had been broken-down by rat microsomes, leaving a mere 7% (±0.02) of the starting amount remaining. Following statistical analysis, the difference between the test incubation and control was significant (*P*=0.05). The intrinsic clearance was still lower that propofol, however the microsomal clearance was well above the margin for highly metabolised drugs (recommended Cl_{CYP} ≤ 26.88 mL/min/kg).

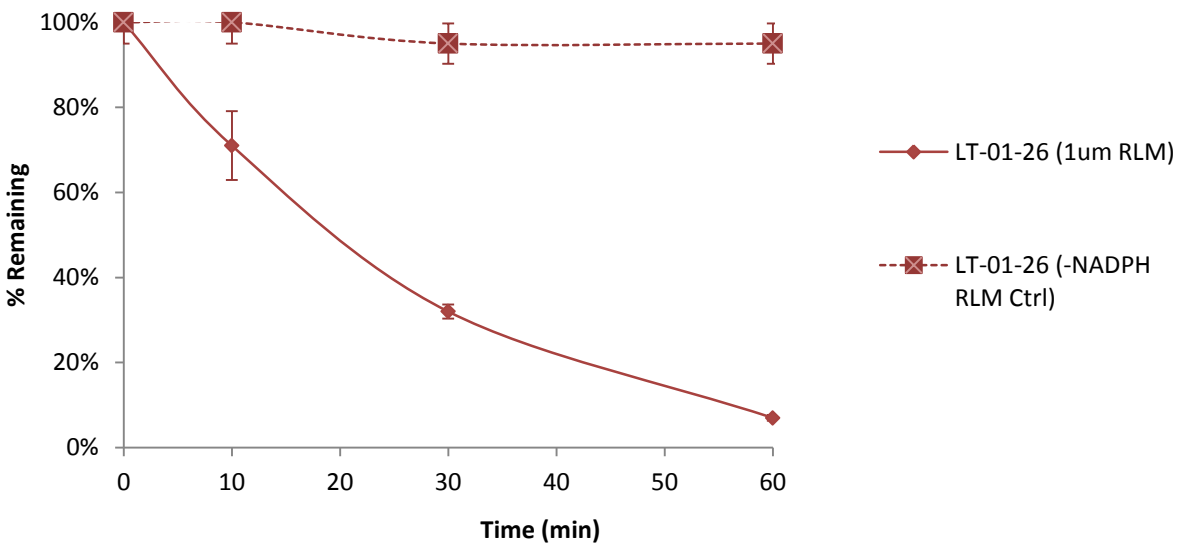

Figure 3.7a. Microsomal stability data for LT-01-26 in rat liver microsomes: The data is expressed as mean (± SEM) (n=6). Data comparison between drug and control incubation was carried out using one tailed T-Test (RLM *P*=0.05 and HLM *P*=0.09). The total turnover at 60 minutes was 88% (±0.01).

In human microsomes, LT-01-26 fared considerably better. The overall turnover was 32% (±0.09) and was not statistically different to the control (*P*=0.09). The half-life is estimated to be over 2 hours, although this was still the shortest of all the analogues tested so far. The microsomal and intrinsic clearance values were also the highest, but were still within a satisfactory range. The rapid metabolism of LT-01-26 is probably the result of the exposed *N*-methyl group that replaced the morpholine of LT-01-25. The data indicates that the morpholine should be maintained for good stability.

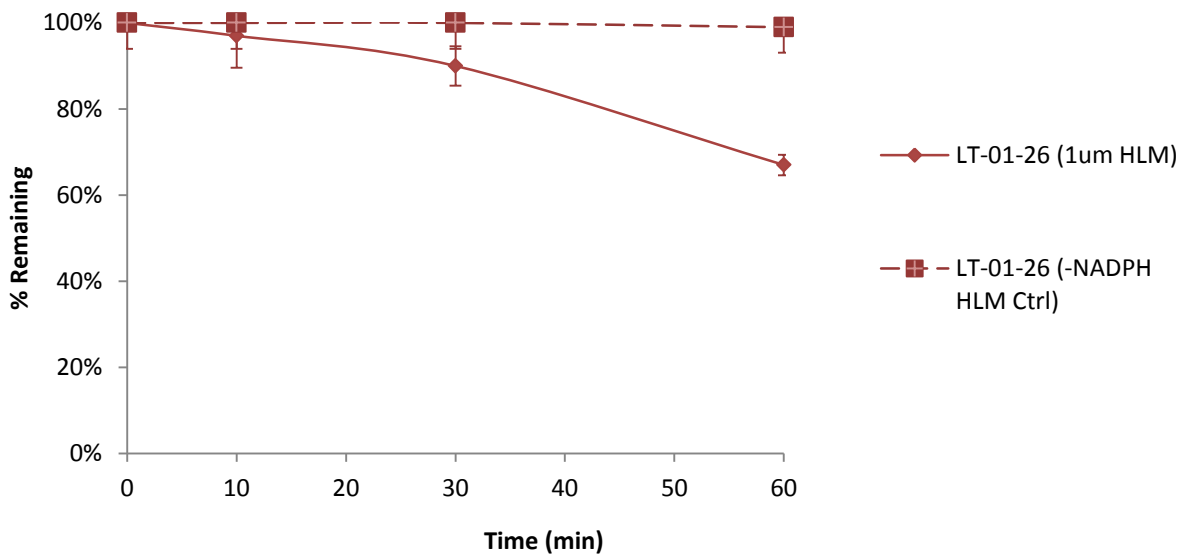

Figure 3.7*b*.Microsomal stability data for LT-01-26 in human liver microsomes: The data is expressed as mean (± SEM) (n=6). Data comparison between drug and control incubation was carried out using one tailed T-Test (*P*=0.09). After 60 minutes the turnover in comparison to the control was 32% (±0.09).

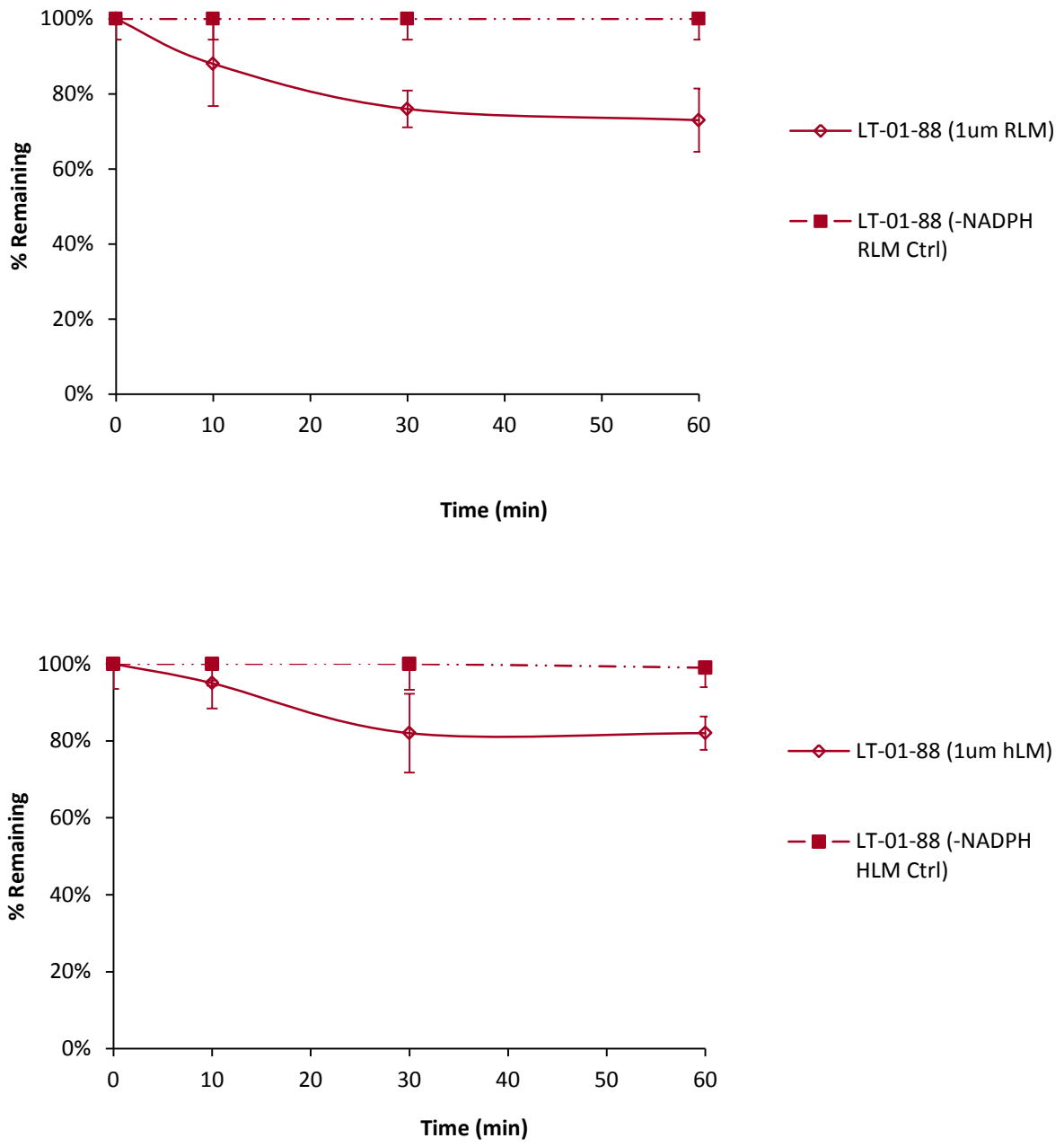

Figure 3.8. Microsomal stability data for LT-01-88 in rat (*above*) and human (*below*) liver microsomes: The data is expressed as mean (± SEM) (n=6). Data comparison between drug and control incubation was carried out using one tailed T-Test (RLM *P*=0.04 and HLM *P*=0.06). The turnover in RLM was 25% (±0.15) and 17% (±0.07) in HLM.

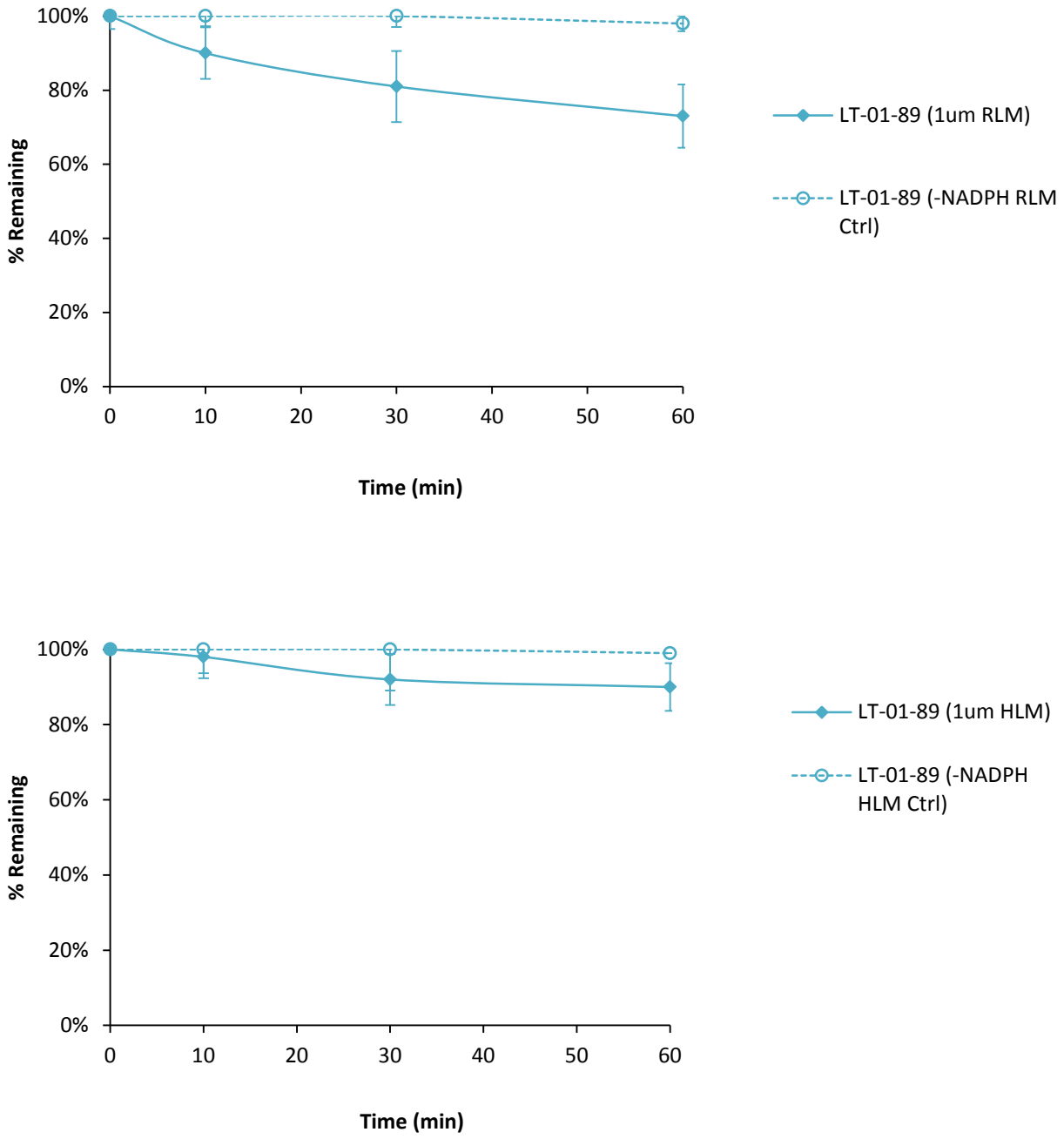

Figure 3.9. Microsomal stability data for LT-01-89 in rat (*above*) and human (*below*) liver microsomes: The data is expressed as mean (± SEM) (n=6). Data comparison between drug and control incubation was carried out using one tailed T-Test (RLM *P*=0.04 and HLM *P*=0.06). LT-01-89 had an overall turnover of 25% (±0.15) in RLM and 9% (±0.11) in HLM.

The *tert*-butyl analogues expressed similar microsomal profiles, though LT-01-89 showed marginally higher stability. This could parallel of the differences scene with LT-01-25 and LT-01-26, where the morpholine is contributing to greater stability. In rats, the maximum turnover for both compounds was 25% (±0.15). Statistical analysis showed a significant difference (P=0.04) between the control and test incubation, despite the overall turnover being lower than LT-01-26 in human microsomes, a value that was not statistically significant. This is most likely due to higher general stability of the *tert*-butyl analogues in the control incubation. LT-01-89 had a lower turnover in HLM (9% ±0.11) than LT-01-88 (17% ±0.07). The half-life for both compounds was high, LT-01-88 (RLM = 173 mins, HLM = 223 mins) and LT-01-89 (RLM = 165 mins, HLM = 407 mins). The microsomal clearance was within a metabolically stable range and the intrinsic clearance values were lower than propofol. As seen with the amide analogues, the compound containing morpholine, LT-01-89 had a more favourable microsomal profile.

There is a vast difference in the metabolic stability of the two amide analogues can be seen. LT-01-25 was the most stable analogues, whilst LT-01-26 was almost completely metabolised by rat CYPs. The *tert*-butyl analogues underwent some metabolic breakdown, with both compounds sharing similar microsomal turnover with the bi-phenyl analogue, LT-01-45. The microsomal parameters were calculated using the formulas used to calculate the parameters for LT-01-45. The values for the amide and *tert*-butyl analogues is summarised in Table 3.5

Table 3.5. Microsomal pharmacokinetic parameters of amide analogues: Microsomal stability-time plots were used to generate the parameters for LT-01-25, LT-01-26, LT-01-88 and LT-01-89.

	$T_{1/2}$ (min)		Cl_{CYP}(µL/min/mg)		Cl_{int} (mL/min/kg)	
	RLM	**HLM**	**RLM**	**HLM**	**RLM**	**HLM**
LT-01-25	770	533	0.9	1.3	1.6	1.75
LT-01-26	46	126	15	5.8	26.88	6.9
LT-01-88	173	223	4.0	3.1	7.2	3.9
LT-01-89	165	407	4.2	1.7	7.5	2.1

Based on the microsomal data above, it is clear that LT-01-25 has the most desirable metabolic stability, followed by LT-01-89. It was decided that these compounds would be tested in rat and human hepatocytes. With major sites of CYP metabolism blocked in these analogues, studying the metabolism in microsomes can only provide limited information. It is vital that other routes of metabolism are studied. The used of whole hepatocytes allows for simultaneous testing of multiple metabolic pathways, including the main route of propofol metabolism, glucuronidation.

Whole hepatocytes are extremely useful for in-depth metabolic studies without the use of animals. Unfortunately, difficulty securing large quantities of functional cells places a major restriction the practicality of hepatocytes. It was decided that only two analogues, LT-01-25 and LT-01-89 would be sent for testing. Hepatocyte testing was carried out by ChemPartners. The compounds (1µM) were incubated for 120 minutes. Samples were taken at 0, 15, 30, 60 and 120 min. The hepatocyte parameters are presented in Table 3.6.

Table 3.6. Metabolic stability of LT-01-25 and LT-01-89 in rat and human hepatocytes: The compounds were incubated in rat and human hepatocytes at a concentration of 1µM. Samples were collected at 0, 15, 30, 60 and 120 minutes (n=2) (See Appendix V).
**Data from ChemPartners.*

	$T_{1/2}$ (min)		Cl_{int} (mL/min/kg)	
	Rat	**Human**	**Rat**	**Human**
LT-01-25	429	59	7.55	28.69
LT-01-89	324	2387	9.99	0.72

The data provided by ChemPartners shows that LT-01-25 undergoes substantially more metabolism in human hepatocytes than microsomes. It is likely that glucuronidation of the phenol is responsible. In LT-01-89, the hydroxyl group is protected by additional methyl groups, so the compound is more resistant to conjugation. The values for rat hepatocytes are lower than the microsomal value, but remain better than LT-01-89. The *in vitro* metabolic profiles of both compounds are encouraging; however these analogues need to undergo more detailed testing to fully understand their pharmacokinetic properties.

3.3.2 In vivo Metabolism

Determining pharmacokinetic parameters through *in vivo* metabolic studies is an essential part of lead optimisation. Whilst microsomes are useful for high-throughput screening and hepatocytes involve multiple metabolic pathways, they are not sufficient replacements for a

living organism. Many internal and external factors (e.g. genetics and diet) may intersect and contribute to the absorption, distribution or metabolism of a compound. Studying the *in vivo* metabolism of a drug candidate, allows the pharmacokinetics to be viewed in context of living system. This will allow for a more accurate prediction of metabolism in man. When working with animals, it is important to maintain 'the 3Rs' (Replace, Reduce, Refine); as part of this philosophy only select number of compounds were chosen for the following studies.

The first analogue to be tested was LT-01-25. The selection was based on the strong metabolic profile generated through microsomal stability experiments. LT-01-25 was administrated orally at 10mg/Kg. The dose was based on information provided by ChemPartners in earlier metabolic studies. Rats were given free access to food and water. Blood was collected, under anaesthesia, from the tail vein at 0.25, 0.5, 1, 3, 5, 7 and 24 hrs post oral dosing. The analogue was formulated in 10% DMSO, 10% solutol, and 80% saline (0.9%). This vehicle was taken from the protocol used by ChemPartners in earlier pharmacokinetic studies. Another group of rats were dosed intravenously at 5mg/Kg and blood samples were collected at 0.08, 0.25, 0.5, 1, 3 and 6 hrs post dose from the tail vein. To improve fluidity of the vehicle for i.v administration, the formulation was modified to 10% DMSO, 20% solutol and 70% d.H_2O. The samples were analysed using LC-MS and the data presented as drug concentration in plasma against time (Figures 3.10 and 3.11).

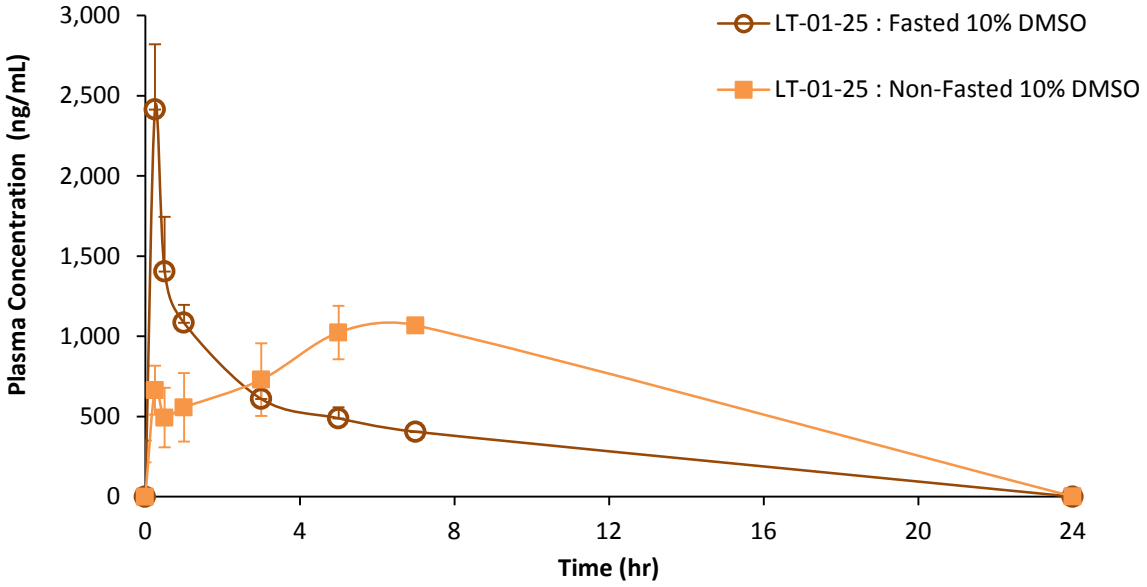

Figure 3.10. Metabolism of LT-01-25 in rats following 10mg/Kg dose (P.O): Rats were dosed orally at 10mg/kg. Fasted rats has restricted access to food 12 hours prior to dosing.LT-01-25 was formulated in 10% DMSO, 10% solutol, and 80% saline (0.9%). Blood was collected, under anaesthesia, from the tail vein at 0.25, 0.5, 1, 3, 5, 7 and 24 hrs post oral dosing. Plasma concentration (ng/mL) levels were calculated from AUC values and represented as mean values (±SEM) (n=4).

The pilot experiment showed initial absorption was poor and fell quickly before slowing rising over the course of a few hours (Figure 3.10). This indicates that enterohepatic circulation of LT-01-25 may be taking place. Enterohepatic circulation is a process wherein biliary excretions from the liver are re-absorbed through the intestine[27]. Re-circulation is commonly categorised by multiple concentration peaks. The cycling of a drug can lead to a prolonged pharmacological response and the build of toxic drugs/metabolites[27]. Enterohepatic circulation can be influenced by a number of factors including, physiochemical properties, diet, genetics, disease and interactions with other drugs[27]. In this case the most

likely causes are the properties of LT-01-25 itself, or food. To investigate the impact of food on metabolism a group of rats were denied access to food for 12 hours prior to oral dosing. Food access was returned immediately following administration of the drug.

Food appeared to have a significant impact on the absorption of the drug. In the fasted group the peak concentration was more than two-fold higher and achieved within the first hour. The plasma concentration fell quite rapidly after the peak. In contrast, the non-fasted group showed much slower absorption on average over the course of 8 hours. After 24 hours the concentration in both groups was too low to be accurately quantified.

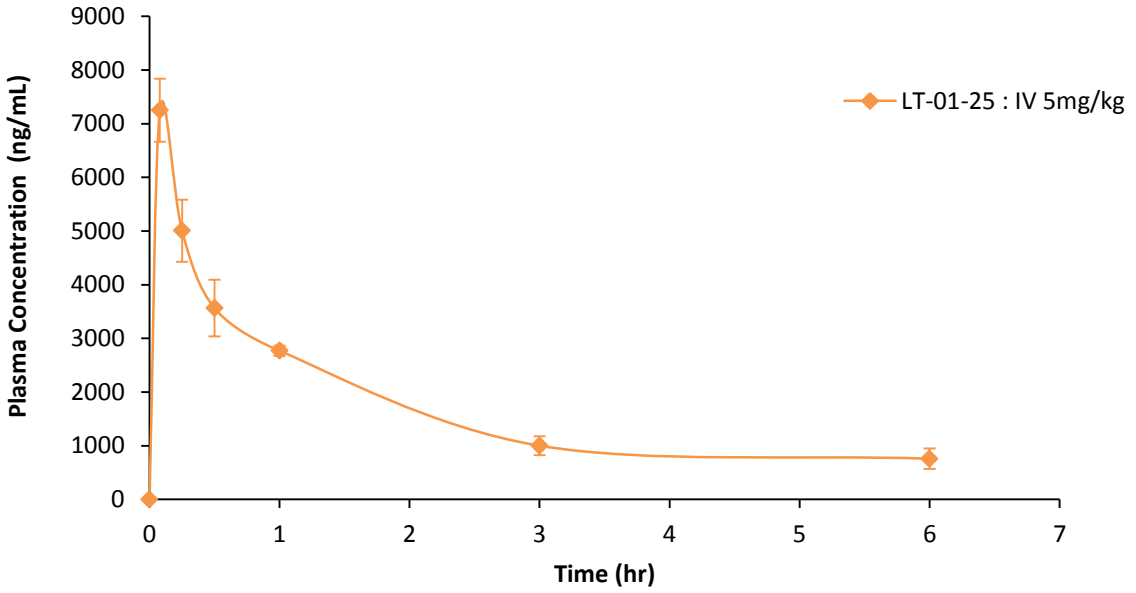

Figure 3.11. Metabolism of LT-01-25 in rats following 5mg/Kg dose (I.V): Rats were dosed intravenously at 5mg/kg. LT-01-25 was formulated in 10% DMSO, 20% solutol, and 70% H_2O. Blood was collected under anaesthetic from the tail vein at 0.08, 0.25, 0.5, 1, 3 and 6 hrs post dose. Plasma concentration (ng/mL) levels were calculated from AUC values and represented as mean values (±SEM) (n=4).

A much greater exposure in the plasma was seen following I.V dosing. The peak was reached instantly and the compound was quickly cleared until roughly 3 hours, where the plasma concentrated appeared to plateau.

As the initial pharmacokinetic profiles of LT-01-25 were promising, it was decided to test the analogue in an alternate vehicle. It is important to consider the use of different vehicles, as they can have an effect on absorption and thus metabolism[28]. DMSO, in particular, is useful for compounds with poor solubility but it can have an effect on the absorption and distribution of a drug [29]. In addition, DMSO has been associated with minor inflammation and local toxicity[30]. A standard suspension vehicle (SSV) made up of 0.5% sodium carboxymethylcellulose, 0.5% benzyl alcohol, 0.4 Tween 80 and 98.6% saline was selected. LT-01-25 was formulated in SSV and administrated to fasted and non-fasted rats. The sample protocol was used to collect, prepare and analyse the samples. The concentration-time plot is shown in Figure 3.12.

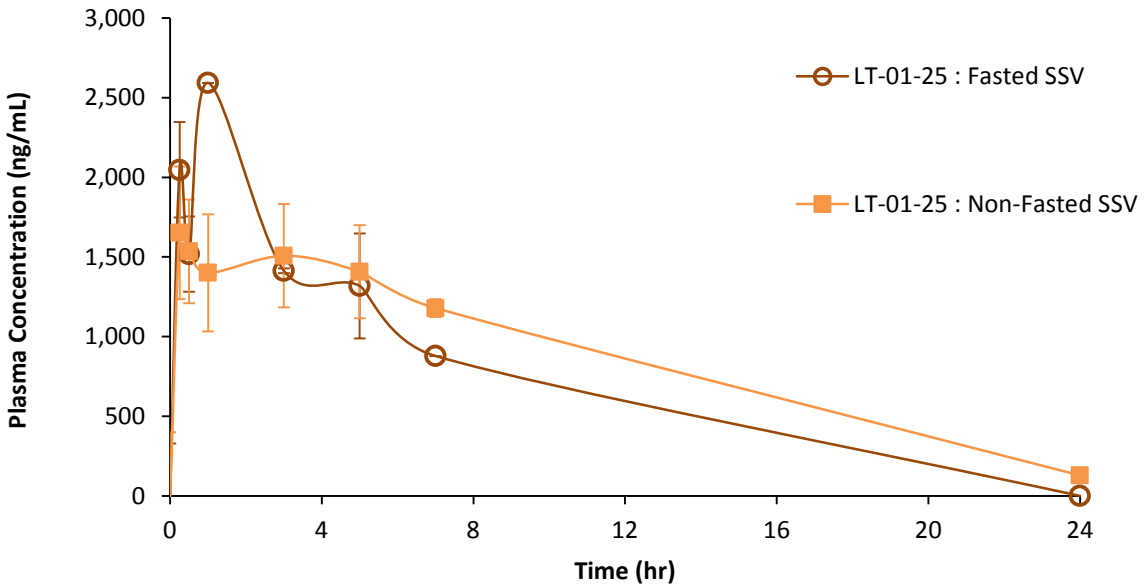

Figure 3.12. Metabolism of LT-01-25 in rats following 10mg/Kg dose (P.O) in an alternative vehicle: Rats were dosed orally at 10mg/kg. Fasted rats has restricted access to food 12 hours prior to dosing.LT-01-25 was formulated in SSV (0.5% sodium carboxymethylcellulose, 0.5% benzyl alcohol, 0.4 Tween 80 and 98.6% saline). Blood was collected under anaesthetic from the tail vein at 0.25, 0.5, 1, 3, 5, 7 and 24 hrs post oral dosing. Plasma concentration (ng/mL) levels were calculated from AUC values and represented as mean values (±SEM) (n=3).

Changing the vehicle from 10% DMSO to SSV appeared to have a positive effect on the exposure of the analogue in the plasma. Absorption in the fasted group was slightly slower, although the peak concentration was higher. Formulating LT-01-25 in SSV seems to have diminished the effect of food. The differences in plasma concentration between the two groups in not as distinct as with the original formulation. This suggests that DMSO may have been affecting intestinal re-absorption. Pharmacokinetic parameters were generated using PK Solutions software and the values for LT-01-25 have been collected in Table 3.7.

Table 3.7. Pharmacokinetic parameters of LT-01-25: Pharmacokinetic parameters were generated from the data presented in Figures 3.10-12. Parameters calculated using PK Solutions in a one-compartmental analysis.

Parameters	10% DMSO (P.O) – 10mg/Kg		SSV (P.O) – 10mg/Kg	
	FASTED	NON-FASTED	FASTED	NON-FASTED
AUC (hr*ng/mL)	8532.8	20421.4	18130	19032.8
C_{max} (µg/mL)	2.4	1.7	2.6	2.1
T_{max} (min)	18	240	60	15
$T_{1/2}$ (min)	84	84	84	217
CL (L/min/Kg)	1.9	0.5	0.5	0.5
V_d (L/Kg)	2.3	0.97	1.1	2.7

Parameters	I.V	P.O	Relative Bioavailability F (%)
	5mg/Kg	10mg/Kg	
AUC (hr*ng/mL)	1275.4	20421.4	81.6
C_{max} (µg/mL)	-	1.7	
T_{max} (min)	-	240	
$t_{1/2}$ (min)	90	84	
Cl (L/hr/Kg)	3.2	0.5	
V_d (L/Kg)	1.01	0.97	

The overall pharmacokinetic profile of LT-01-25 was encouraging. On average the C_{max} was high in all the test groups (>1500ng/mL). In most cases the peak plasma concentration was reached within an hour, with the exception of non-fasted rats dosed with the DMSO containing vehicle (T_{max} = 240mins). This is thought to be the result of re-absorption in the intestine. Interestingly non-fasted rats dosed with the SSV formulation exhibited the shortest T_{max} (15mins), suggesting that DMSO may aggravate enterohepatic circulation. The clearance

was almost with a recommended range of 10-40 mL/min/kg, while the distribution was well within an acceptable range. Based on good absorption it was decided that future PK experiments would be carried out using SSV. Food appeared to have less of an impact when SSV was used, so it was also decided that rats would no longer be fasted.

As the second most metabolically stable compound, LT-01-89 was also selected to undergo *in vivo* PK testing. LT-01-89 (10mg/Kg) was formulated in SSV and administrated orally in non-fasted rats. LT-01-89 was also given as an intravenous dose at 5mg/Kg in 10% DMSO, 20% solutol and 70% d.H_2O. Blood was collected at the same time points used for LT-01-25 and the samples were analysed using LC-MS. The data is expressed below in Figure 3.14 and Table 3.8

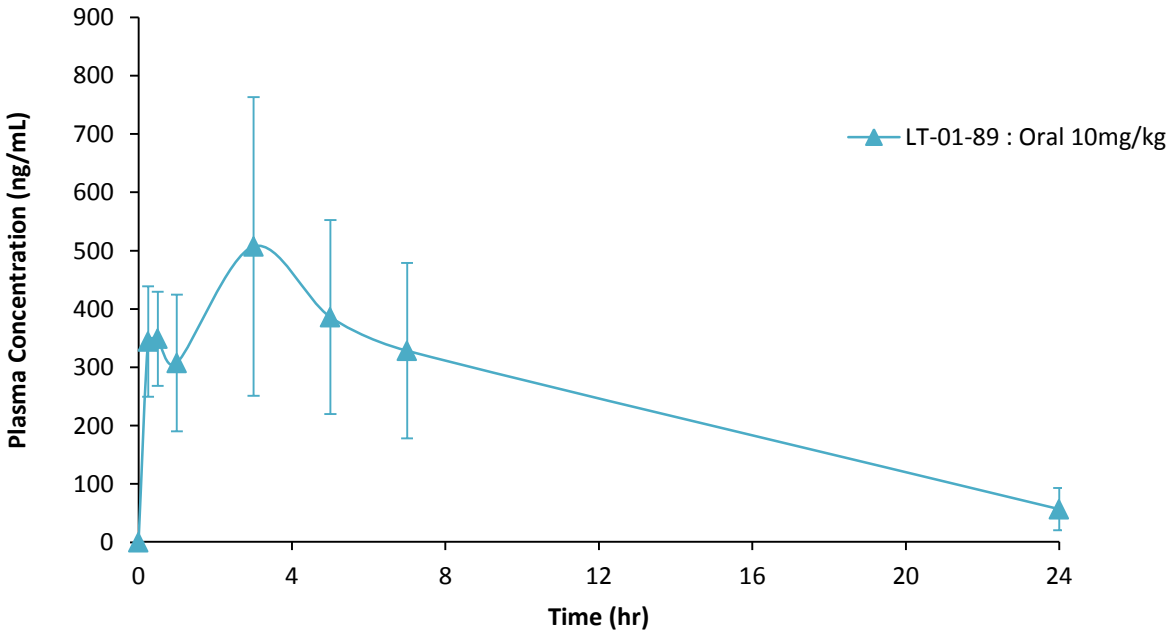

Figure 3.13a. Metabolism of LT-01-89 in rats: Rats were dosed orally at 10mg/Kg (SSV). Blood samples were taken at 0.25, 0.5, 1, 3, 5, 7 and 24 hrs post dose. Plasma concentration levels (ng/mL) were calculated from AUC values and represented as mean (±SEM) (n=3).

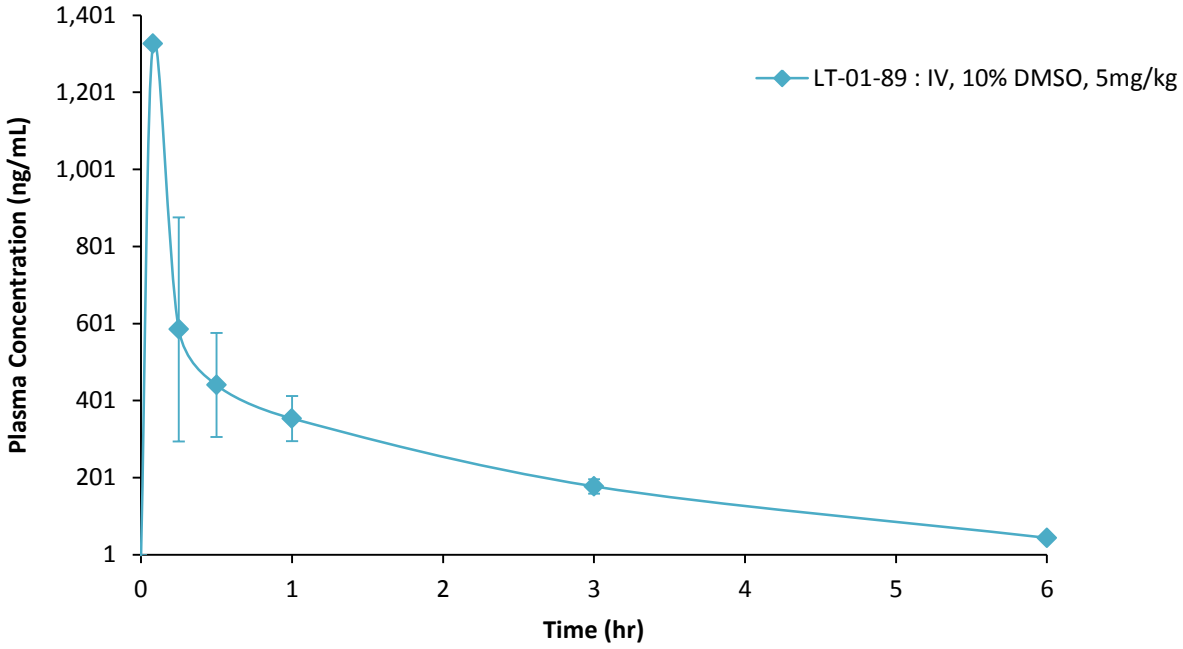

Figure 3.13b. Metabolism of LT-01-89 in rats: Rats were dosed intravenously at 5mg/Kg (10% DMSO, 10% solutol and 80% saline). Blood samples were taken at 0.08, 0.25, 0.5, 1, 3 and 6 hrs post dose. Plasma concentration levels (ng/mL) were calculated from AUC values and represented as mean (±SEM) (n=2).

LT-01-89 was absorbed fairly slowly (T_{max} = 180min) and the peak plasma concentration was much lower that LT-01-25 (Cmax = 720ng/mL). The clearance was much higher than LT-01-25 but still fell with an acceptable range, whereas the V_d was within a desire range (7.2L/Kg). The relative bioavailability was 49%, a passable value but not on par with LT-01-25, which had a relative bioavailability of 81.6%. Generally, LT-01-89 had an adequate pharmacokinetic profile, however the absorption and distribution was poor when compared to LT-01-25.

Table 3.8. Pharmacokinetic parameters of LT-01-89: Pharmacokinetic parameters were generated from the data presented in Figures 3.13. Parameters calculated using PK Solutions using a one-compartmental analysis.

Parameters	I.V	P.O	Relative Bioavailability F (%)
	5mg/Kg	10mg/Kg	
AUC (min*µg/mL)	92.2	455.3	49
C_{max} (µg/mL)	-	0.72	
T_{max} (min)	-	180	
$t_{1/2}$ (min)	90	216	
Cl (L/min/Kg)	0.3	0.5	
V_d (mL/Kg)	7.1	7.2	

LT-01-26 also underwent brief *in vivo* metabolic testing. Despite being readily broken-down in rat liver microsomes, LT-01-26 remains the most potent analogue. Following the same protocol as LT-01-25 and LT-01-89, this analogue was only tested in non-fasted rats at 10mg/Kg (P.O) in SSV. The results are shown in Figure 3.14. The pharmacokinetic parameters are shown in relation to LT-01-25 and LT-01-89 in Table 3.9.

The peak concentration for LT-01-26 was reached quickly (<30min), however the total exposure in the plasma was poor (500ng/mL). This suggests that while LT-01-26 is rapidly absorbed, the majority of the dose undergoes extensive first-pass metabolism. This is supported by the high turnover seen in rat liver microsomes and would account for the low pharmacokinetic values. Low plasma concentrations and high hepatic metabolism means that LT-01-26 is unlikely to achieve sufficient exposure at the drug target.

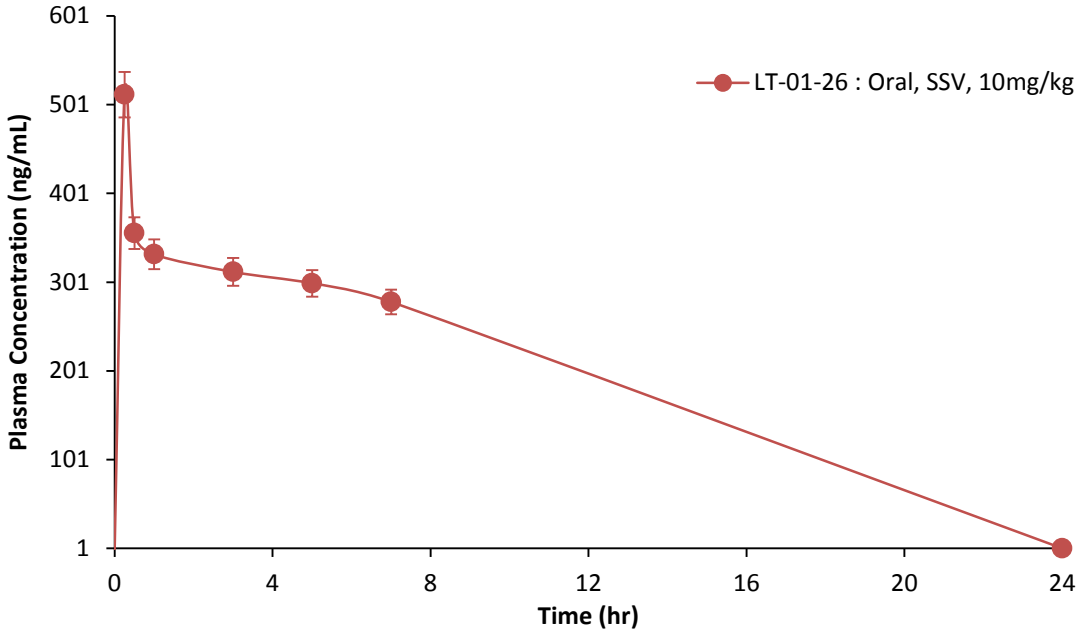

Figure 3.14. Metabolism of LT-01-26 in rats: Rats were dosed orally at 10mg/Kg in SSV. Blood samples were collected at 0.25, 0.5, 1, 3, 5, 7 and 24 hrs post dose. Plasma concentration (ng/mL) levels were calculated from AUC values and represented as mean values (±SEM) (n=2).

Table 3.9. Pharmacokinetic parameters of amide propofol analogues: LT-01-25, LT-01-26 and LT-01-89 were formulated in SSV and administered to rats at 10mg/Kg (P.O). Pharmacokinetic parameters calculated using PK Solutions in a one-compartmental analysis.

Parameters	LT-01-25	LT-01-26	LT-01-89
AUC(min*µg/mL)	1140	273	455.3
C_{max} (µg/mL)	2.1	0.5	0.72
T_{max} (min)	15	18	180
$t_{1/2}$ (min)	217	72	216
CL (L/hr/kg)	0.5	2.2	0.5
V_d (mL/Kg)	2.7	3.7	7.2

Out of the three analogues tested, LT-01-25 had the most promising PK profile. High drug exposure and bioavailability may compensate for LT-01-25 being less potent at GlyRα1 than LT-01-26. The only *tert*-butyl analogue tested, LT-01-89 had poor exposure in the plasma due to ineffectual absorption and was the least potent at GlyR, making it the least suitable as a drug candidate. Throughout the *in vivo* pharmacokinetic studies no obvious signs of toxicity were observed. Although this is encouraging, it is possible that the analogues could be interacting negatively with metabolising enzymes. It is thought that metabolism related toxicity is mostly caused by the inhibition of CYPs. As such, the inhibition of CYPs should be investigate as part of lead optimisation.

3.3.3 Cytochrome P450 and Toxicity

As few as 5% of drugs will successfully enter the market following clinical trials, with almost 50% of drugs failing due to a poor safety profile[31]. In many of these cases toxicity can be linked to drug metabolism[32]. As the majority of metabolism takes place in the liver, this type of toxicity usually manifests as drug-induced liver injury (DILI). DILI is complex disease with many contributing factors including genetic, pharmacological and environmental[33]. It is also a major cause of drug withdrawal[34]. Although the full mechanism underlying DILI is not understood in its entirety, metabolising enzymes, particularly CYPs are thought to play a significant role[35]. DILI is believed to occur in three phases, a drug-specific stage (e.g. formation of a reactive metabolite), cellular specific stage (e.g. oxidative stress, immune response) and finally the pro-death stage (e.g. activation of necrotic signalling)[33].

A common trigger of the immune response involved in DILI is believed to be the formation of metabolic adducts[36]. These adducts act as neo-antigens initiating an immune attack on healthy hepatocytes[37]. The liver has a high number of innate immune cells (e.g. Kupffer, natural killer cells) and adaptive cells (e.g. T-cells). These cells are responsible for the breakdown of red blood cells (Kupffer) and hepatocytes (natural killer cells) following extreme cellular stress[33]. The role of the immune system in DILI is supported by the long-onset (1-8 weeks) and symptoms (rash and fever) that are usually associated with DILI[36].

Certain drugs and their metabolites may form metabolic intermediate complexes or protein adducts with CYPs[18]. Conjugation with CYPs inhibits their activity and impacts the metabolism of other drugs. CYPs are responsible for metabolising more than 70% of approved drugs, preventing this action can have serious ramifications especially if build-up of a particular drug can lead to an overdose[38]. CYP adduct driven DILI occurs through oxidative stress and mitochondrial dysfunction[36]. The formation of adducts trigger the activation of MAP kinases. These kinase cascades converge into the P-JNK pathway which promotes oxidative stress and causes MPT[33]. MPT is the swelling and subsequent rupture of mitochondria. The ruptured mitochondria release Ca^{2+} and apoptotic factors into the cell, thus causing cell death[37].

The prevention of unforeseen CYP induced DILI is an extremely important consideration in choosing a drug candidate. One of the easiest methods for HTS of adverse drug-CYP interactions is to study enzyme inhibition. This can be done through various methods; the most accessible method is the use of fluorescent based screening kits[39].

3.3.4 Cytochrome P450 Inhibition Screening of Amide Analogues

Testing for CYP inhibition is something that can be done with relative ease at early developmental stages, saving time and resources at later stages. In this instance, inhibition of CYPs was measured using a fluorescence assay provide by Life Sciences, UK[40]. In this assay a substrate is tagged with fluorescent dye and incubated with the compound and a one of five CYP isoforms; CYP1A2, CYPC9, CYP2C19, CYP2D6 and CYP3A4. These five isoforms are believed to be responsible for 90% negative CYP interactions[39]. Upon metabolism the dye is released and emits fluorescence. The level of fluorescence is used as a direct measure of inhibition (Fig 3.15)[40].

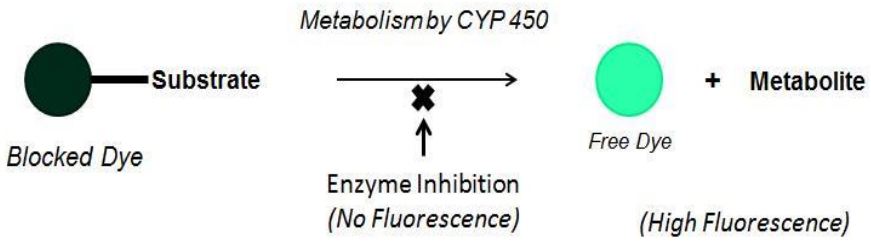

Figure 3.15. **Conversion of non-fluorescent substrate to highly fluorescent metabolite by CYP450**: CYP enzymes transform the tagged substrate into a free dye that emits fluorescence. Compounds that inhibit CYPs will inhibit this reaction, resulting in no fluorescence[39].

Using a 96-well plate, 40µL of test compound (0.1µM, 1µM and 10µM) was added to individual wells in triplicate. A master pre-mixed containing, reaction buffer, desired Baculosomes® and regeneration system was prepared and 50µL was added to each well. The plate was incubated at room temperature for 10 minutes. A mixture containing reaction buffer, NADP+ and Vivid™ Substrate was pre-made. The reaction was started by addition of

10µL of substrate mixture to each well, making a final volume of 100µL. The plate was incubated in a Varioskan™ flash multimode plate reader at 37.1°C for 60 minutes. Data was collected using SkanIt™ Software. The results at the highest testing concentration (µ10M) for each CYP isoform are presented in Figures 3.16a-e.

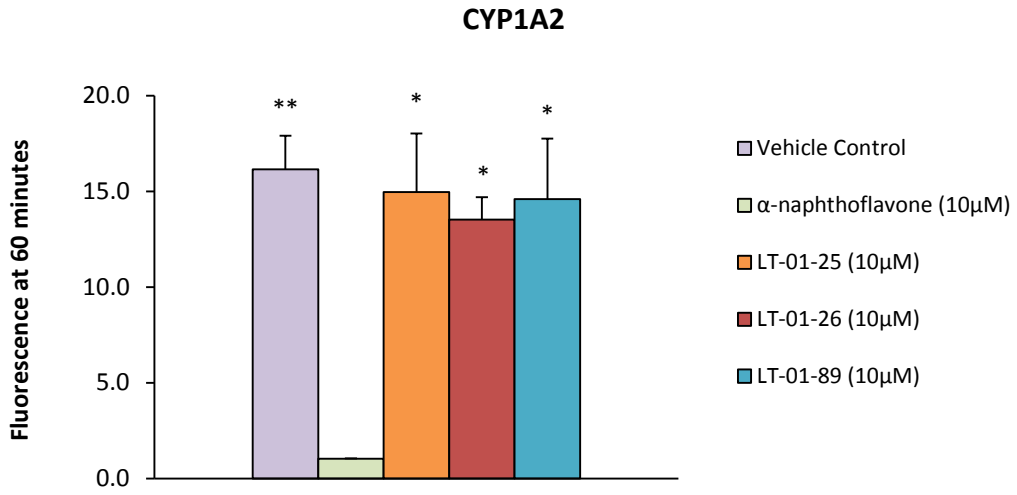

Figure 3.16*a*. Inhibition of CYP1A2 by LT-01-25, LT-01-26 and LT-01-89: CYP1A2 baculosomes incubated with test compounds (10µM) for 60 mins in a fluorescent plate reader (37.1°C). Inhibition was measured by the maximum fluorescence at 60 mins. A vehicle control (1.25% DMSO) and positive control (α-Naphthoflavone, 10µM) were also tested as a comparison for inhibition. Data is presented as mean ±SEM (n=3). Statistical analysis was carried out between the positive control and test compounds using one-tailed T-Test (* = P ≤ 0.05, ** = P ≤ 0.01, *** = P ≤ 0.001).

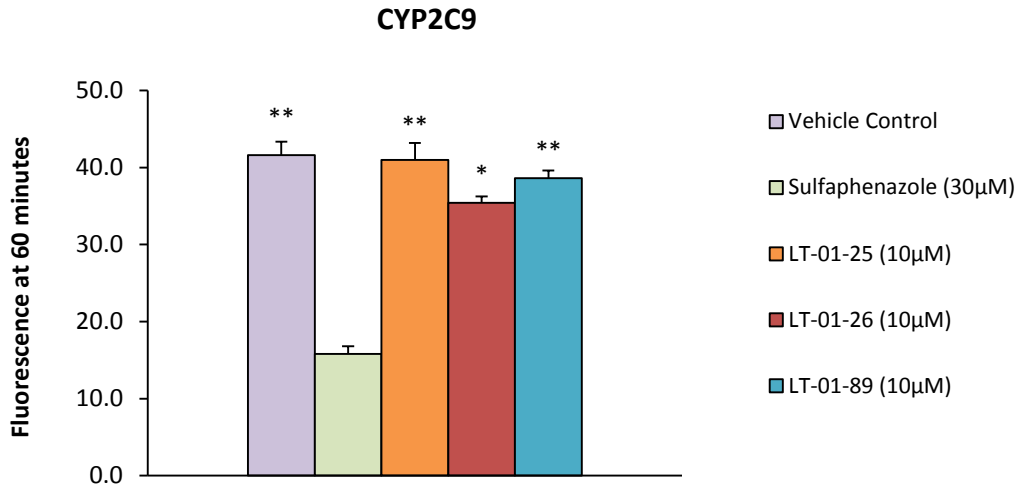

Figure 3.16*b*. Inhibition of CYP2C9 by LT-01-25, LT-01-26 and LT-01-89: CYP2C9 baculosomes incubated with test compounds (10µM) for 60 mins in a fluorescent plate reader (37.1°C). Inhibition was measured by the maximum fluorescence at 60 mins. A vehicle control (1.25% DMSO) and positive control (Sulfaphenazole, 30µM) were also tested as a comparison for inhibition. Data is presented as mean ±SEM (n=3). Statistical analysis was carried out between the positive control and test compounds using one-tailed T-Test (* = P ≤ 0.05, ** = P ≤ 0.01, *** = P ≤ 0.001).

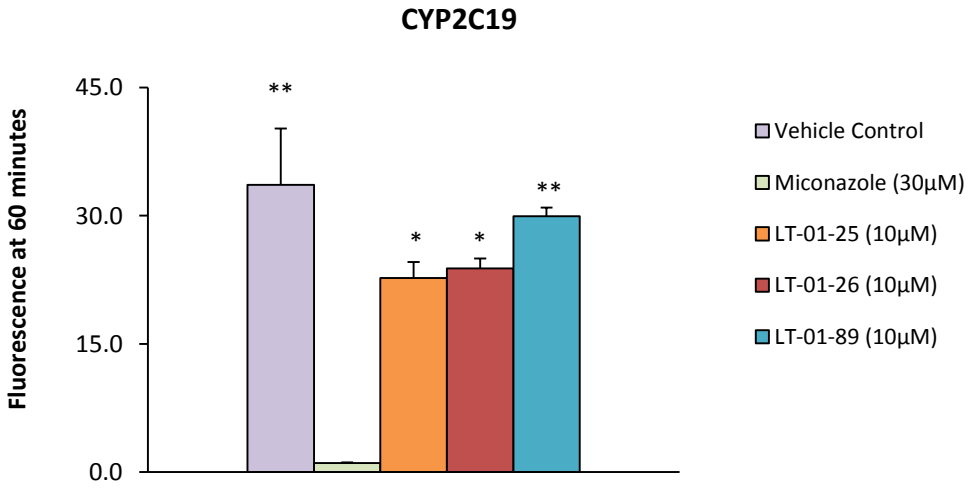

Figure 3.16*c*. Inhibition of CYP2C19 by LT-01-25, LT-01-26 and LT-01-89: CYP2C19 baculosomes incubated with test compounds (10µM) for 60 mins in a fluorescent plate reader (37.1°C). Inhibition was measured by the maximum fluorescence at 60 mins. A vehicle control (1.25% DMSO) and positive control (Miconazole, 30µM) were also tested as a comparison for inhibition. Data is presented as mean ±SEM (n=3). Statistical analysis was carried out between the positive control and test compounds using one-tailed T-Test (* = P ≤ 0.05, ** = P ≤ 0.01, *** = P ≤ 0.001).

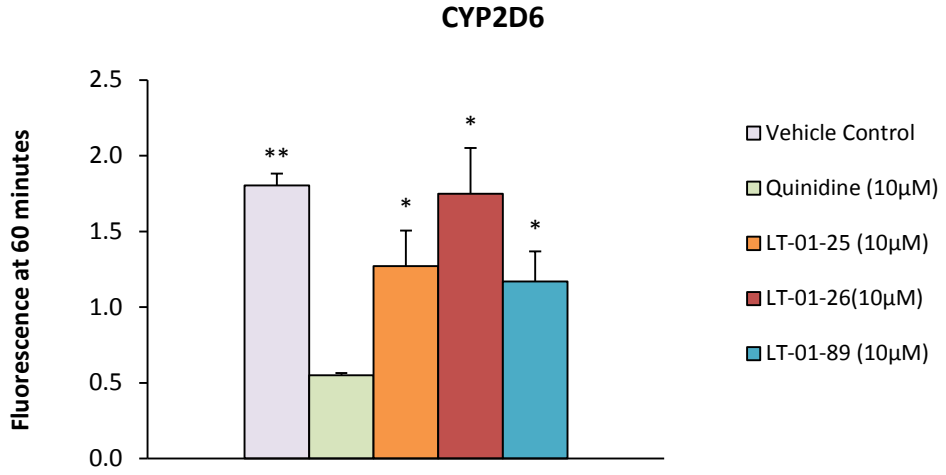

Figure 3.16*d*. Inhibition of CYP2D6 by LT-01-25, LT-01-26 and LT-01-89: CYP2D6 baculosomes incubated with test compounds (10µM) for 60 mins in a fluorescent plate reader (37.1°C). Inhibition was measured by the maximum fluorescence at 60 mins. A vehicle control (1.25% DMSO) and positive control (Quinidine, 10µM) were also tested as a comparison for inhibition. Data is presented as mean ±SEM (n=3). Statistical analysis was carried out between the positive control and test compounds using one-tailed T-Test (* = P ≤ 0.05, ** = P ≤ 0.01, *** = P ≤ 0.001).

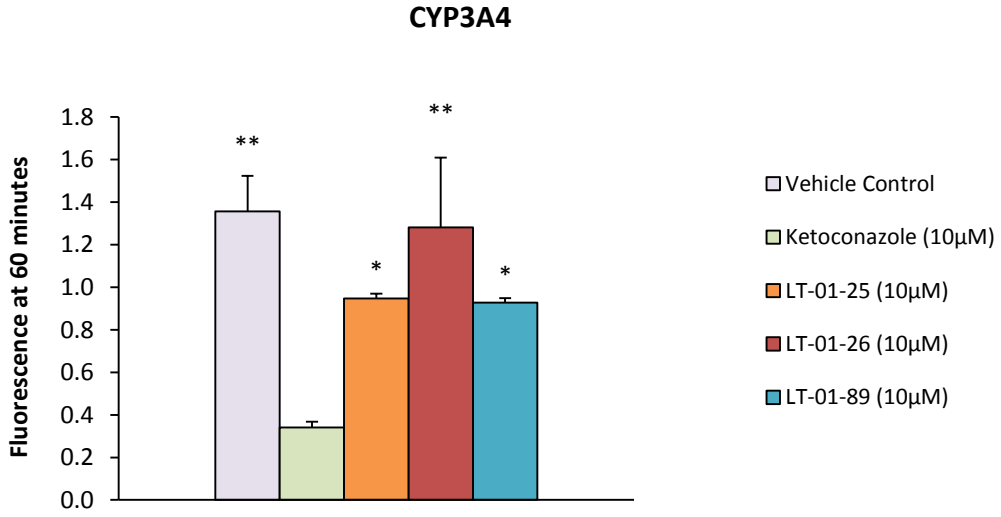

Figure 3.16*e*. Inhibition of CYP3A4 by LT-01-25, LT-01-26 and LT-01-89: CYP3A4 baculosomes incubated with test compounds (10µM) for 60 mins in a fluorescent plate reader (37.1°C). Inhibition was measured by the maximum fluorescence at 60 mins. A vehicle control (1.25% DMSO) and positive control (Ketoconazole, 10µM) were also tested as a comparison for inhibition. Data is presented as mean ±SEM (n=3). Statistical analysis was carried out between the positive control and test compounds using one-tailed T-Test (* = P ≤ 0.05, ** = P ≤ 0.01, *** = P ≤ 0.001).

The analogues, along with a vehicle and positive control, were incubated with selected CYP isoforms. Fluorescence was used to measure CYP activity following a successful reaction. The positive controls were chosen in accordance to the protocol provided in the CYP inhibition assay kit from Life Technologies and are FDA recommended controls[41]. These drugs are known to inhibit CYPs. The structures of the positive controls are shown in Figure 3.17.

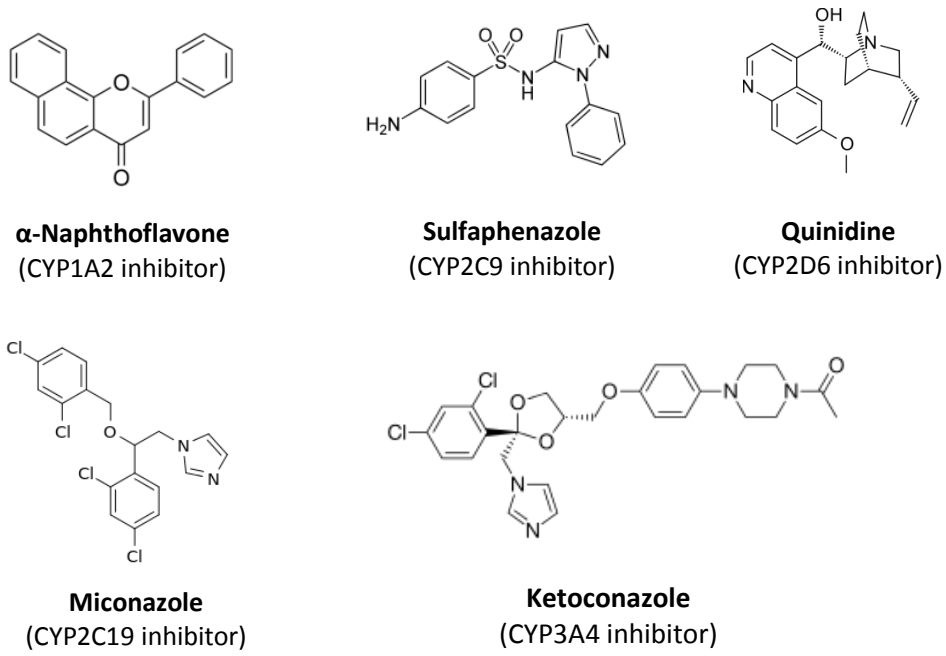

Figure 3.17. Positive controls used in CYP inhibition screening assay: These drugs are known inhibitors of CYP. They are recommended by the FDA for use as positive controls in CYP studies[40].

In these experiments, the vehicle control (1.25% DMSO) was taken as 0% inhibition. Inhibitory activity of the analogues was viewed as a percentage difference from the vehicle control. For statistical analysis the positive control was used as a comparison. The difference between the analogues and positive controls was statistically significant for all five CYP

isoforms tested. If the level of fluorescence generated in the positive controls is assumed to be maximum inhibition of the enzyme then each analogue demonstrated considerably less inhibition.

Overall the analogues did not have a great effect on CYP activity. The highest incidence of inhibition was seen with CYP2D6 treated with LT-01-89 (38% ±0.19 inhibition). LT-01-25 also caused some reduction in metabolic activity (33% ±0.23), whereas LT-01-26 was seen to have very little effect (5.5% ±0.30). CYP3A4 also showed some mild inhibition, again with LT-01-26 having the least effect (LT-01-25 = 30.7% ±0.02, LT-01-26 = 7.6% ±0.32 and LT-01-89 = 31% ±0.02). Similar inhibitory activity occurred with CYP2C19, although LT-01-89 was now the least potent compound (LT-01-25 = 32% ±1.87, LT-01-26 = 30% ±1.64 and LT-01-89 = 12% ±3.36). The analogues had little to no effect on CYP1A2 and CYP2C9. The levels of inhibition for both isoforms fell below 10%, with the exception of LT-01-26, which inhibited CYP1A2 by 16% (±1.18), in comparison to the vehicle control.

The FDA guidelines state that a weak CYP inhibitor has an $IC_{50} \geq 10\mu M$[42]. In these investigations the maximum inhibition caused by analogues over the course of an hour was did not fall below 50%, therefore accurate IC_{50} values could not be determined. However, none of the analogues were able to achieve more than 40% inhibition at 10µM, suggesting that these compounds are weak inhibitors of CYP[41].

The pharmacokinetic testing of the amide analogues has helped establish excellent metabolic profiles for each compound. Data from CYP inhibition screening suggests that these compounds are unlikely to form adducts with CYPs or prevent the metabolism of other drugs.

While each analogue shows promise, LT-01-25 has the best PK profile overall. The final major test to determine whether LT-01-25 is the most suitable drug candidate is validation in an animal model of chronic pain.

3.3.5 Validation in a Model of Neuropathic Pain

The amide analogues were testing in the Chung lesion of neuropathic pain model. These studies were carried out using fasted, male, Wistar rats at the King's College London (UK) under the supervision of Prof. Stephen McMahon. The protocol for these experiments can be seen in the appendix. Neuropathic pain developed over a week following surgery. The rats were then orally dosed at three concentrations; 3mg/Kg, 10mg/Kg and 30mg/Kg. Behavioural tests for mechanical allodynia and cold hyperalgesia, were conducted at 1, 3, 6 and 24 hours post-dose. Mechanical allodynia was tested using von Frey hairs and cold hyperalgesia using a cold plate (10°C). The positive control used was the sodium channel blocker, lamotrigine (30mg/Kg P.O.) and the vehicle control was 10% DMSO, 10% solutol and 80% Saline (0.9%). The formulated pro-drug of 4-chloropropofol (30mg/Kg) was also tested against LT-01-25 (Figure 3.18*a*-*b*). Analgesia was measured at percentage reversal from the baseline taken prior to dosing.

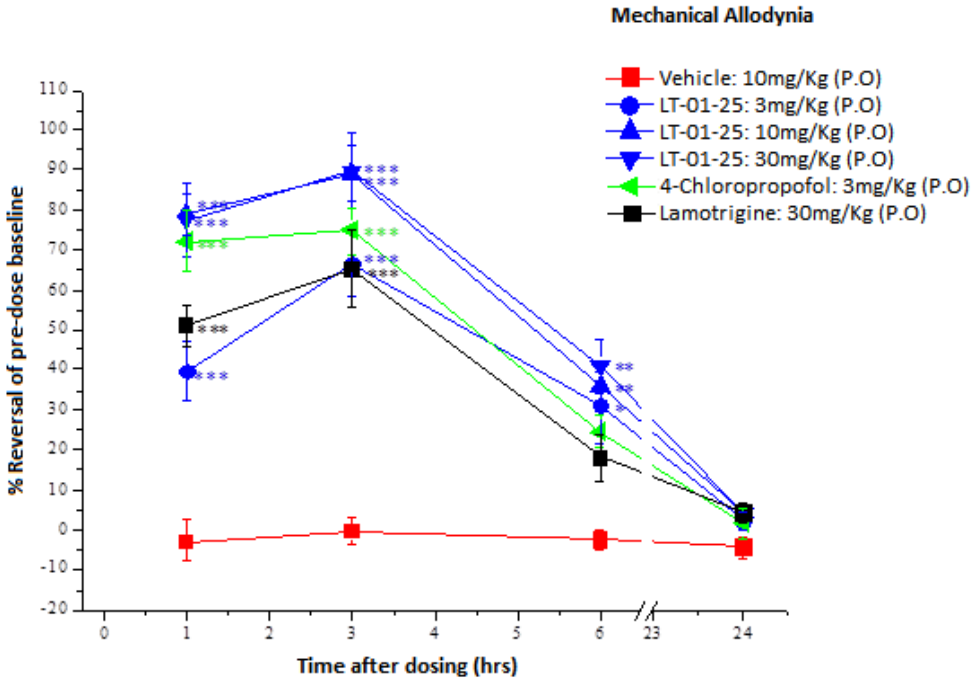

Figure 3.18*a*. The effect of LT-01-25 on mechanical allodynia in the Chung lesion neuropathic pain model: Fasted, male, Wistar rats were treated with LT-01-25 at 3, 10 and 30mg/Kg (Vehicle = 10% DMSO, 10% solutol, 80% saline). Lamotrigine and formulated pro-drug 4-chloropropofol (30mg/Kg) were used as comparisons. Mechanical allodynia was measured as paw withdrawal latency after pressure applied with von Frey hairs. The data is presented as mean ± SEM (n=6) percentage reversal of the pre-dose baseline. Statistical analysis between LT-01-25 and the lamotrigine control was carried using out one-way ANOVA, comparison and Tukey's HSD test for time-matched vehicle group (* = P ≤ 0.05, ** = P ≤ 0.01, *** = P 0.001).

LT-01-25 was able to attenuate mechanical allodynia to a greater degree than lamotrigine at the same dose (30mg/Kg). The maximum reversal (90%) was seen at 3 hours, this value was the same for both 10mg/Kg and 30mg/Kg. In contrast, lamotrigine was only to achieve at 60% reversal, this was the same for lowest dose of LT-01-25 (3mg/Kg). LT-01-25 also outperformed 4-chloropopofol, which produced a 70% reversal at 3 hours.

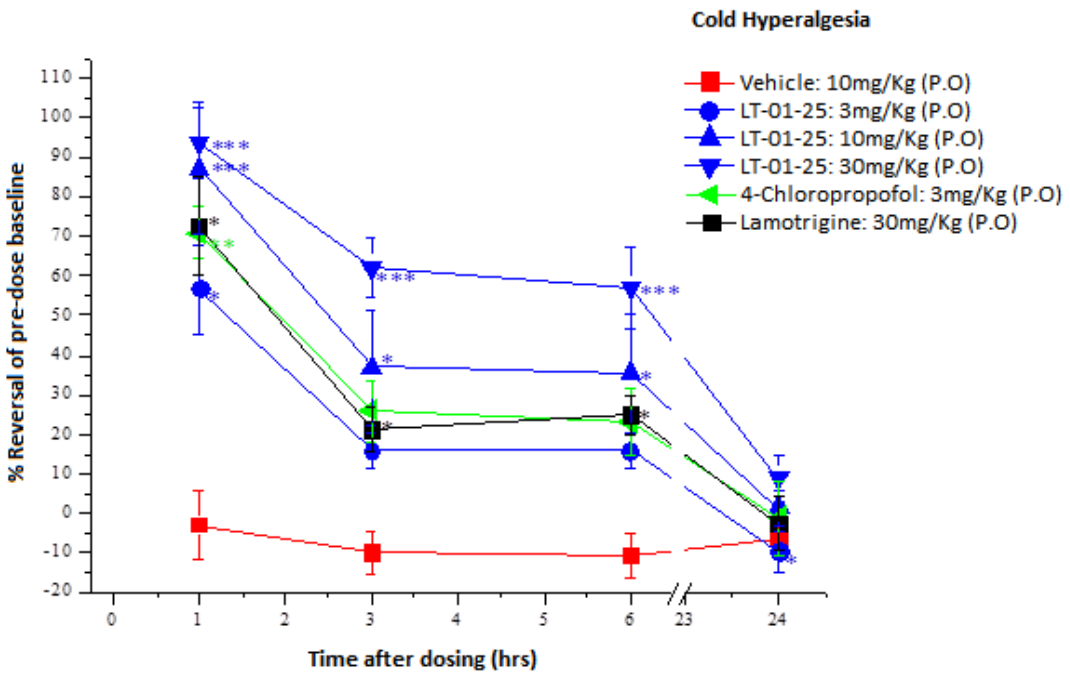

Figure 3.18b. The effect of LT-01-25 on cold hyperalgesia in the Chung lesion model of neuropathic pain: Fasted, male, Wistar rats were treated with LT-01-25 at 3, 10 and 30mg/Kg (Vehicle = 10% DMSO, 10% solutol, 80% saline). Lamotrigine and formulated pro-drug 4-chloropropofol (30mg/Kg) were used as controls. Cold hyperalgesia was measured as paw withdrawal latency from a source of noxious cold (10°C). The data is presented as mean ± SEM (n=6) percentage reversal of the pre-dose baseline. Statistical analysis between LT-01-25 and the lamotrigine control was carried using out one-way ANOVA, comparison and Tukey's HSD test for time-matched vehicle group (* = P ≤ 0.05, ** = P ≤ 0.01, *** = P 0.001).

At the highest dose, LT-01-25 had a more dramatic effect on cold hyperalgesia. The highest reversal (95%) was achieved at 1 hour by LT-01-25 (30mg/Kg). Lamotrigine and 4-chloropropofol produced approx. 70% reversal at the same time point. The analgesic effect persisted over the course of 6 hours. At the 6 hour point, LT-01-25 exhibited double the analgesic effect produced by lamotrigine and 4-chloropropofol. This is consistent will the long-half, low clearance and high metabolic stability of LT-01-25. LT-01-89 was tested under the

same conditions as LT-01-25, however the formulated 4-chrolopropopofol was removed as it was deemed unnecessary. The results are shown below in Figure 3.19*a*-*b*.

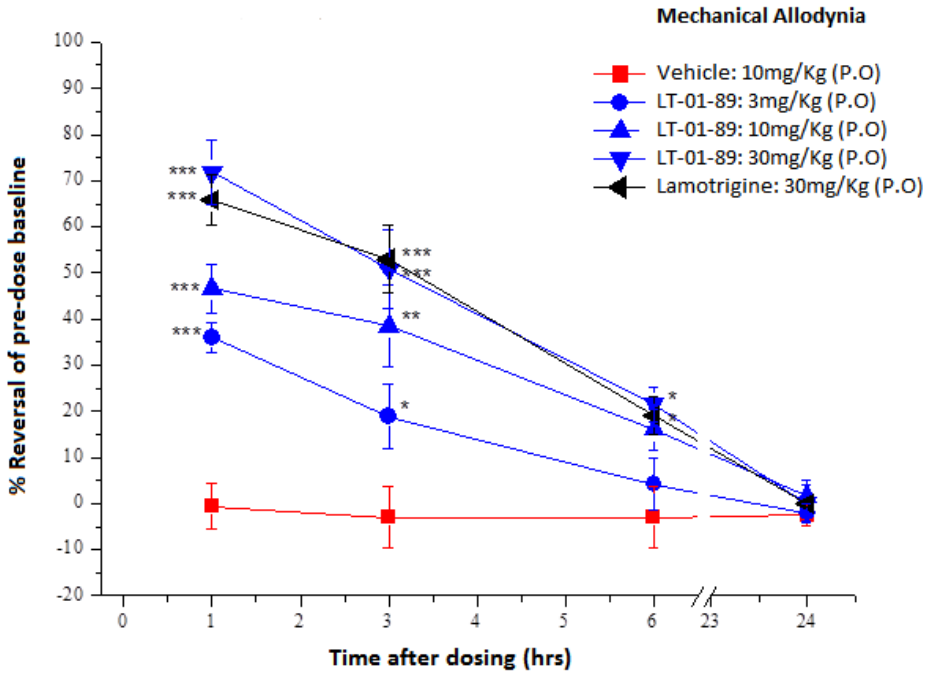

Figure 3.19*a*. The effect of LT-01-89 on mechanical allodynia in the Chung lesion model of neuropathic pain: Fasted, male, Wistar rats were treated with LT-01-89 at 3, 10 and 30mg/Kg (Vehicle = 10% DMSO, 10% solutol, 80% saline). Lamotrigine (30mg/Kg) was used as a positive control. Mechanical allodynia was measured as paw withdrawal threshold from application of von Frey hairs. The data is presented as mean ± SEM (n=6) percentage reversal of the pre-dose baseline. Statistical analysis between LT-01-89 and lamotrigine was performed using a one-way ANOVA, comparison and Tukey's HSD test was used for time-matched vehicle group (* = P ≤ 0.05, ** = P ≤ 0.01, *** = P 0.001). **Data provided by King's College London.*

LT-01-89 was able to achieve peak analgesia quicker than LT-01-25 (1 hour), this is surprising as LT-01-89 has much longer T_{max} (3 hours). The level of reversal was not as high (75%), which is in keeping with the much lower C_{max} of LT-01-89 (720ng/mL). LT-01-89 was able to produce greater reversal in comparison to lamotrigine (65%) at the same dose and

time point. The effect of LT-01-89 steadily falls after over the course of 6 hours, where the reversal was roughly 20%. This is likely due to the high clearance and low bioavailability of LT-01-89.

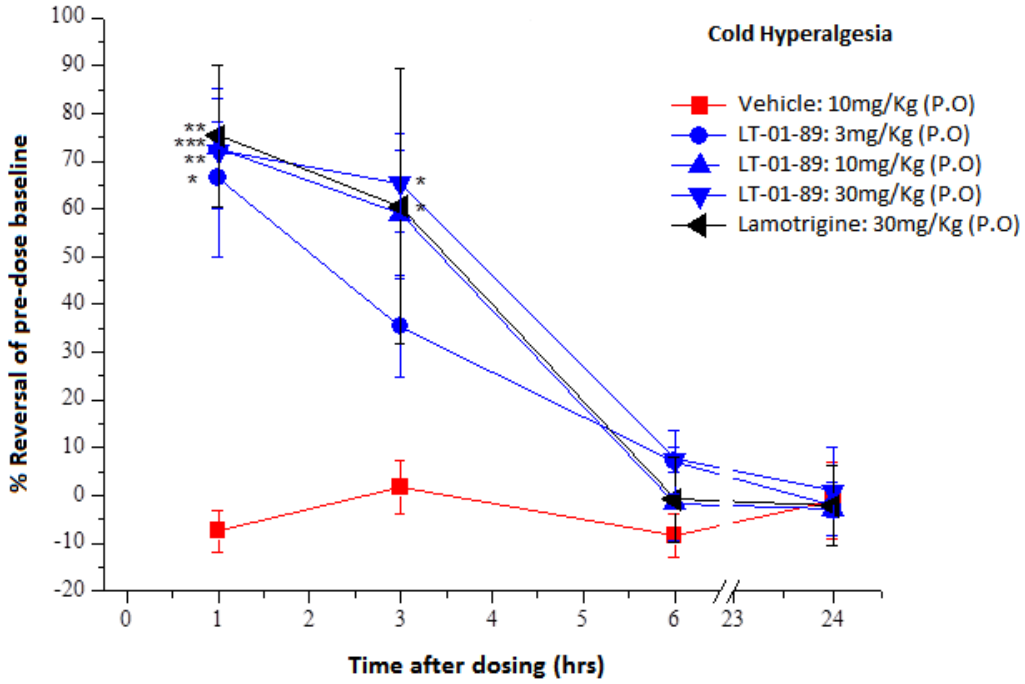

Figure 3.19b. The effect of LT-01-89 on cold hyperalgesia in the Chung lesion neuropathic pain model: Fasted, male, Wistar rats were treated with LT-01-89 at 3, 10 and 30mg/Kg (Vehicle = 10% DMSO, 10% solutol, 80% saline). The positive control was lamotrigine (30mg/Kg). Cold hyperalgesia was measured as paw withdrawal latency from a source of noxious cold (10°C). The data is presented as mean ± SEM (n=6) percentage reversal of the pre-dose baseline. Statistical analysis between LT-01-89 and the positive control was carried out using out one-way ANOVA, comparison and Tukey's HSD test for time-matched vehicle group (* = P ≤ 0.05, ** = P ≤ 0.01, *** = P 0.001).
**Data provided by King's College London.*

The effect of LT-01-89 on cold hyperalgesia was very similar to what as was seen for allodynia. The maximum reversal was 70% at 1 hour, this gradually diminished to 10% after 6 hours. The analogue was also able to match the reversal of the positive control. For LT-01-26,

the positive control was changed to gabapentin (30mg/Kg), as it is considered the 'gold standard' comparison for novel analgesics and has known side-effects than lamotrigine[43]. The data for LT-01-26 in presented above in Figure 3.20*a-b*.

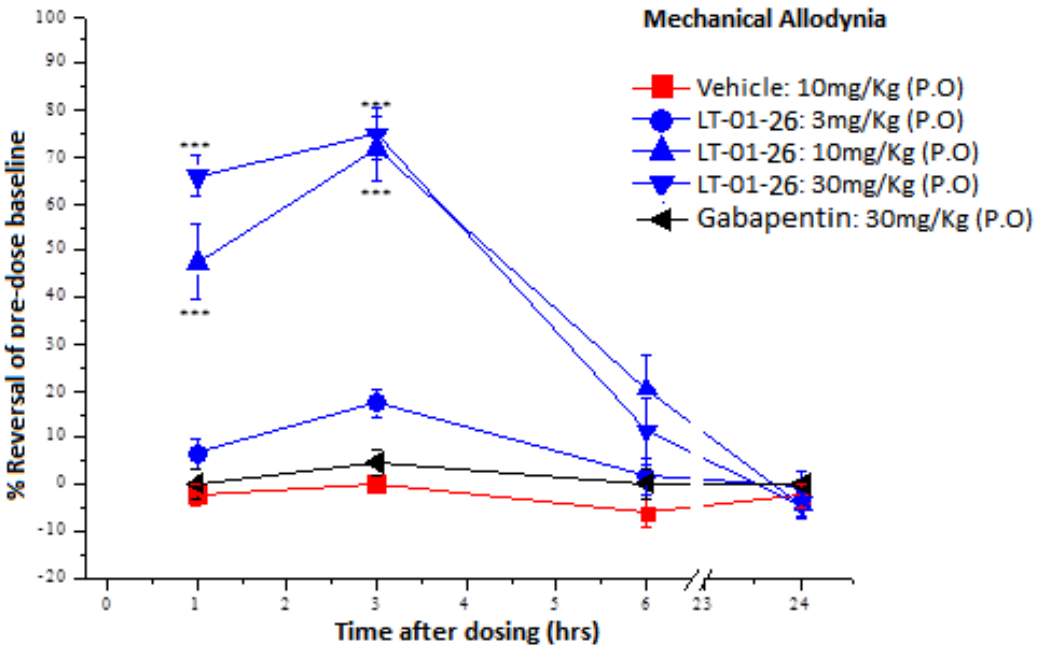

Figure 3.20*a*. The effect of LT-01-26 on mechanical allodynia in the neuropathic Chung lesion pain model: Fasted, male, Wistar rats were treated with LT-01-25 at 3, 10 and 30mg/Kg (Vehicle = 10% DMSO, 10% solutol, 80% saline). Gabapentin (30mg/Kg) was used as a positive control. Mechanical allodynia was measured as paw withdrawal threshold from application of von Frey hairs. The data is presented as mean ± SEM (n=6) percentage reversal of the pre-dose baseline. Statistical analysis between LT-01-89 and lamotrigine was performed using a one-way ANOVA, comparison and Tukey's HSD test was used for time-matched vehicle group (* = $P \leq 0.05$, ** = $P \leq 0.01$, *** = P 0.001).
**Data provided by King's College London.*

In the allodynia behavioural tests, the peak effect (75% reversal) for LT-01-26 was seen at 3 hours at both concentrations (10 and 30mg/Kg). Initial analgesia, at 1 hour, was greater in the higher dose (10mg/Kg = 55%, 30mg/Kg =65%). The analgesic effect quickly fell, resulting

in only 10%-20% reversal at 6 hours. The swift descent in reversal is most probably caused by the extensive metabolism of LT-01-26, indicated by its short half-life. LT-01-26 was able to attenuate mechanical allodynia better than gabapentin at ten-fold lower dose.

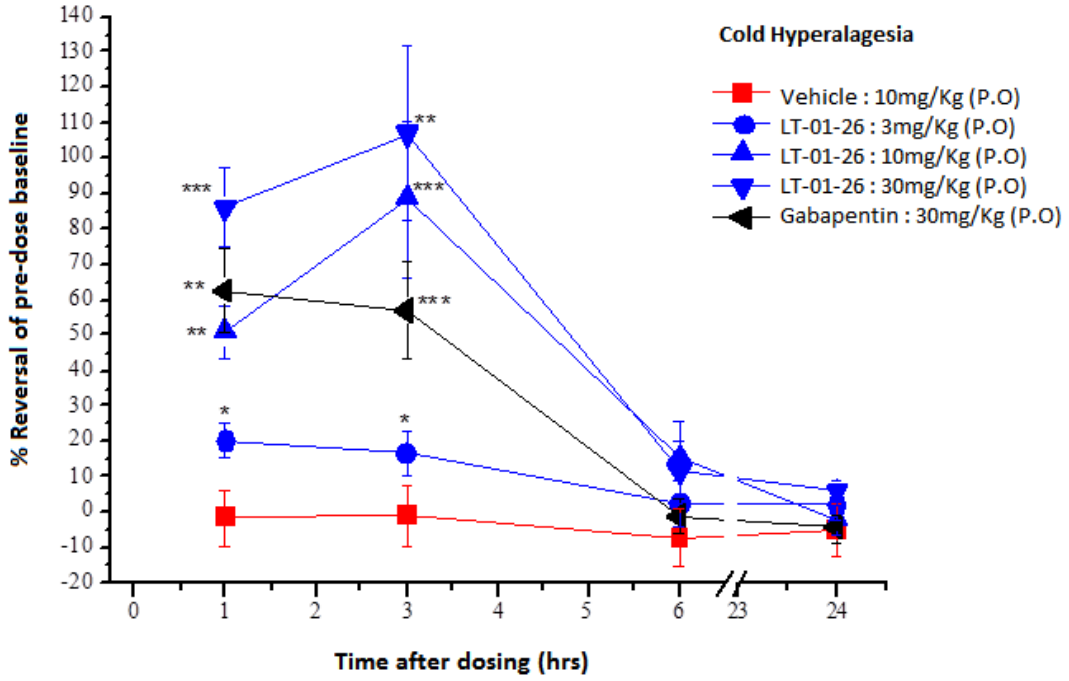

Figure 3.20b. The effect of LT-01-26 on cold hyperalgesia in the Chung lesion model of neuropathic pain: Fasted, male, Wistar rats were treated with LT-01-26 at 3, 10 and 30mg/Kg (Vehicle = 10% DMSO, 10% solutol, 80% saline).The positive control was gabapentin (30mg/Kg). Cold hyperalgesia was measured as paw withdrawal latency from a source of noxious cold (10°C). The data is presented as mean ± SEM (n=6) percentage reversal of the pre-dose baseline. Statistical analysis between LT-01-26 and the lamotrigine control was carried using out one-way ANOVA, comparison and Tukey's HSD test for time-matched vehicle group (* = P ≤ 0.05, ** = P ≤ 0.01, *** = P 0.001).
**Data provided by King's College London.*

The analgesic effect of LT-01-26 on hyperalgesia was similar to what was seen in mechanical allodynia. The initial reversal at 1 hour was high; this rose to a maximum reversal of 105% at 3 hours before rapidly falling to 15% at 6 hours. Even so, LT-01-26 was able to achieve greater reversal than gabapentin at a lower dose (10mg/Kg).

At 24 hours all compounds, regardless of dose or behavioural testing returned to the pre-dose baseline. This is consistent with the extremely low plasma concentrations seen at 24 hours in the PK studies. All three analogues were able to attenuate pain in neuropathic pain model; LT-01-25 and LT-01-26 were far more effective than currently prescribed analgesics, whilst LT-01-89 was able to match the analgesic effect. As LT-01-89 was not as effective as LT-01-25 and LT-01-26 in the Chung lesion model, so it was decided that it wouldn't undergo further pharmacological testing. The maximum percentage reversal for each compound can be seen in Table 3.10 and Table 3.11.

Table 3.10. Maximum percentage reversal of mechanical allodynia in the Chung lesion model of neuropathic pain: LT-01-25, LT-01-26 and LT-01-89 were tested at three concentrations in the Chung lesion pain model. Data is presented as a percentage reversal of the pre-dose baseline in mechanical allodynia behavioural tests. The highest reversal values are highlighted.

Compound/Dose (mg/Kg)	Max % Reversal	Time (hr)
LT-01-25 (3 mg/Kg)	65%	3 hrs
LT-01-25 (10 mg/Kg)	90%	3 hrs
LT-01-25 (30 mg/Kg)	**90%**	**3 hrs**
LT-01-26 (3 mg/Kg)	20%	3 hrs
LT-01-26 (10 mg/Kg)	70%	3 hrs
LT-01-26 (30 mg/Kg)	**75%**	**3 hrs**
LT-01-89 (3 mg/Kg)	35%	1 hrs
LT-01-89 (10 mg/Kg)	65%	1 hrs
LT-01-89 (30 mg/Kg)	**75%**	**1 hrs**

Table 3.11. Maximum percentage reversal of cold hyperalgesia in the Chung lesion model of neuropathic pain: LT-01-25, LT-01-26 and LT-01-89 were tested at three concentrations in the Chung lesion pain model. Data is presented as a percentage reversal of the pre-dose baseline in mechanical allodynia behavioural tests. The highest reversal values are highlighted.

Compound/Dose (mg/Kg)	Max % Reversal	Time (hr)
LT-01-25 (3 mg/Kg)	55%	1 hrs
LT-01-25 (10 mg/Kg)	88%	1 hrs
LT-01-25 (30 mg/Kg)	**95%**	**1 hrs**
LT-01-26 (3 mg/Kg)	20%	1 hrs
LT-01-26 (10 mg/Kg)	90%	3 hrs
LT-01-26 (30 mg/Kg)	**105%**	**3 hrs**
LT-01-89 (3 mg/Kg)	65%	1 hrs
LT-01-89 (10 mg/Kg)	70%	1 hrs
LT-01-89 (30 mg/Kg)	**70%**	**1 hrs**

3.3.6 Additional Pharmacology

Along with good drug-like properties and a strong metabolic profile, validation in an animal model of disease is one of the most important aspects in lead optimisation. There are a number of *in vitro* pharmacological tests frequently included in early drug development that have yet to be discussed. These assays can be carried out as part of lead optimisation and ensure a greater chance of success further down the development pipeline.

Many of these guidelines have already being tested as part of the optimisation process previously mentioned in this project. The remaining criteria are associated to ADME and safety. The first two recommendations are directly related to distribution. The first is protein

binding in the plasma. It is recommended that the total amount of drug bound to proteins does not exceed 99.5%, to guarantee a minimum exposure of free drug. The quantity of free drug within the CNS is measured by brain CSF levels. Protein binding and CSF experiments were carried out by ChemPartners using fasted, male, Wistar rats dosed orally with 3mg/Kg (10% DMSO, 10% solutol, 80% Saline). Establishing ADME of a drug candidate can be extremely useful in predicting toxicological risk, however metabolism does not account for all possible toxicities.

There are three commonplace assays that must be performed as part of drug safety profiling. The first is the use of hERG (human ether a-go-go related gene) to measure the risk of cardiotoxicity[44]. Cells can be transfected with hERG to express inward rectifying voltage-gated potassium channels, normally found in the heart[44]. Inhibition of these channels causes long QT intervals, which can lead to fatal tachyarrhythmias such as Torsade de Pointes; many TCAs, for example Amitriptyline, are associated with QT interval prolongation[45]. Drugs should not antagonise these channels below a concentration of 10µM. hERG toxicity was tested by ChemPartners using Chinese hamster ovary cells (CHO-K1) were transfected with hERG and incubated with the test compounds at a 10 point concentration range. This assay was carried out by ChemPartners.

Aside from cardiotoxicity, hepatoxicity also be established. Incubation with hepG2 liver cells is a common and efficient means of determining cellular toxicity. A drug must not exhibit cytotoxicity at a concentration that is lower than 50x EC_{50}[17]. The test compounds were incubated (37°C) with hepG2 cells across a concentration range (maximum concentration = 500µM).

The mutagenic properties of a drug candidate should also be assessed. A well-used method of testing drug-induced mutagenesis is the Ames assay. Within this assay, histidine dependant Salmonella strains containing a variety of mutations in the histidine. These mutations make the bacteria vulnerable to mutagenesis[46]. The strains are grown on an agar plate containing trace amounts of histidine[46]. Mutated bacteria will become histidine independent and flourish. If few colonies are seen, then the test compound is considered non-mutagenic[46]. In this project compounds (250μg/mL) were incubated (37°C) for 48 hours with TA98 and TA100 strains. The Ames assay and MTT cytotoxicity were conducted by Cyprotex. The protocols for each assay can be found in Appendix VIII, IX and X. The desired testing criteria used to drive lead optimisation is this project can be seen in Table 3.12.

Table 3.12. Target testing criteria for LT-01-25 and LT-01-26.

*•Data provided by Department of Chemistry ◊ $GABA_AR$ EC_{50} value from BioFocus *Data provided by ChemPartners + Data provided by Cyprotex*

Parameter	Recommendation	LT-01-25	LT-01-26
Physiochemical			
•Aq. Sol (mg/mL)	0.01 - 0.5mg/mL (pH7.4)	0.025mg/mL (pH7.4)	-
•LogP	≤4	3.10	3.54
•LogD	1-3	2.88	2.50
•MW (Da)	≤450	291	304
•TPSA (Å)	40-90	49.80	43.78
•HBD	≤3	1	1
•pKa	3-9	10.10	10.14
•MPO	4≥	4.3	4.4
Selectivity			
*GlyRα1 EC_{50}	≤1µM	0.35nM	1.2pM
◊$GABA_AR$ EC_{50}	≥ 100x GlyRα1 EC_{50}	≥30µM (1000x)	≥30µM (1000x)
Pharmacokinetics			
Oral Bioavailability (%)	≥20	81.6	-
$T_{1/2}$ (Rat Liver Microsomes)	≥60 min	770 min	46 min
*$T_{1/2}$ (Human Hepatocytes)	≥30 min	59 min	-
*Brain CSF	3x GlyRα1 EC_{50} (at 2/3 hrs, 1-3mg/Kg)	10x GlyRα1 EC_{50}	-
*Protein Binding	≤99.5%	62%	38%
Toxicity			
*hERG toxicity	IC_{50} ≥ 10µM	IC_{50} ≥ 10µM	-
+HepG2 toxicity	No tox at 50x GlyRα1 EC_{50}	No tox below 500µM	-
+AMES genotoxicity	negative	negative	-
CYP Inhibition	IC_{50} ≥ 10µM	IC_{50} ≥ 10µM	IC_{50} ≥ 10µM

From Table 3.12 it is clear that LT-01-25 meets every desired testing criteria with the exception of pKa, which is slightly too high; the sample problem applies to LT-01-26 as well. In addition, LT-01-26 also demonstrated poor metabolic stability in microsomes. LT-01-26 is still undergoing metabolic testing in human hepatocytes, as well as toxicity testing so it cannot be said with complete confidence that LT-01-25 is a more suitable lead; however results from microsomal studies and neuropathic pain testing show that LT-01-25 has better metabolic stability and thereby has a stronger analgesia effect in a model of neuropathic pain. The remaining problem with LT-01-25 is its high pKa; drugs acting in the CNS should have a pKa value below 9, whereas LT-01-25 has a value above 10[47]. Despite this, LT-01-25 was effective in the pain model, suggesting that the compound is able to penetrate the CNS. It was decided that further investigation into structural optimisation would be carried out.

3.4 Lead Optimisation

3.4.1 LT-01-25 Analogues

The introduction of electronegative substitutes, such as amines, methyl groups and various heterocycles, can not only reduce the pKa of a compound but may have a positive impact on efficacy, metabolism and bioavailability. The current lead compound, LT-01-25, has met every desired criteria with the exception of pKa. As part of the lead optimisation process, a series of analogues based around LT-01-25 were synthesised and tested for efficacy at the target.

Out of the new analogue series only a small number maintained activity at GlyRα1. The first attempt at structure optimisation involved the addition of a single methyl group at various

positions in the morpholine ring. Over 50% of drugs on the market contain at least one methyl group and numerous endogenous ligands also contain many methyl groups, making them a common building-block in drug design[48]. The inclusion of a methyl can improve the physiochemical properties of a compound, particularly solubility. Furthermore there is evidence to suggest that methyl groups may increase affinity for the desired target by reducing the energy required for binding, thus boosting potency and selectivity. Methyl groups should be used cautiously as they are vulnerable to metabolic attack[48].

Table 3.13. MPO evaluation of LT-02-39.
**Data was provided by the Department of Chemistry.*

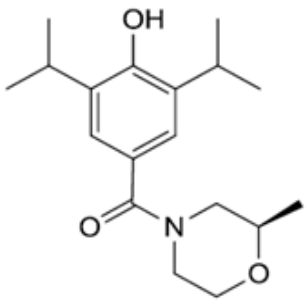

LT-02-39

Parameter	T0 Score
ClogP = 3.6	0.7
ClogD = 3.9	0.05
TPSA = 49.77 Å	1.00
MW = 305.41 Da	1.00
HBD = 1	0.83
pKa = 10.08	0.00
CNS MPO = 3.6	
GlyRα1 EC_{50} = 60pM	

The only monomethyl analogue to successful activate GlyRα1 below 1μM was LT-02-39 shown in Table 3.13. This analogue was far more potent than LT-01-25 (EC_{50} = 0.35 nM), with an EC_{50} value in the picomolar range. Some activity was seen at $GABA_AR$ (EC_{50}= 30μM), although the massive difference in EC_{50} concentration between GlyRα1 and $GABA_AR$, shows great level of selectivity for the target. There was a very minor decrease in pKa, unfortunately the value is still >10. The ClogD increased, which cause the overall MPO scored to fall below the optimal value of 4. This indicates that LT-02-39 may have difficulty crossing the BBB. As LT-02-39 shares many structural similarities with LT-01-25, it was decided that more dramatic modification would be tested.

The morpholine ring was removed and replaced with an azetidine ring. Azetidine rings are heavily influenced by surrounding functional groups[49]. In the case of LT-02-50 the ring is attached to fluorine (Table 3.14). As the most electronegative element, fluorine is often used as a means of reducing pKa. Fluorine may also stabilise surrounding functional groups and form extremely strong bonds with carbon due to its powerful electron withdrawing effect. The replacement of hydrogen with fluorine can also affect the pharmacology of a compound, improving absorption, distribution and metabolism[50].

Table 3.14. MPO evaluation of LT-02-50.
**MPO data provided by the Department of Chemistry.*

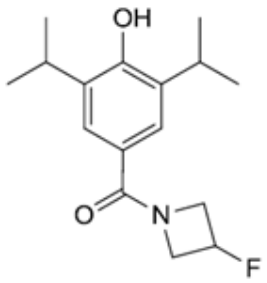

LT-02-50

Parameter	T0 Score
ClogP = 3.3	0.85
ClogD = 3.57	0.22
TPSA = 40.54 Å	1.00
MW = 279.35 Da	1.00
HBD = 1	0.83
pKa = 9.77	0.11
CNS MPO = 4.0	
GlyRα1 EC_{50} = 1.2pM	

The addition of fluorine brought the pKa down to 9.77, which is just within the desired range. The ClogD increased, meaning that the MPO score was lower than that of LT-01-25 (MPO=4.3) however the score does imply good CNS penetration (CNS MPO ≥4). LT-02-50 also demonstrated higher efficacy at GlyRα1. Unlike LT-01-25, this compound showed no affinity for $GABA_AR$ at the highest testing concentration 30µM, confirming excellent selectivity for the target. This may relate to the readiness of fluorine to form hydrophobic bonds within the binding pocket of receptors[50]

The third approach was to replace the morpholine ring with a spirocyclic group (Table3.15). While morpholines are useful for improving solubility they can often become metabolic hotspots. Spirocyclic compounds are considered to be highly metabolically stability and are an established alternative to morpholines[51]. In terms of solubility, lipophilicity and pKa, many spirocycles can emulate the properties of carbonyls[52].

Table 3.15. MPO evaluation of LT-02-53.
**MPO data was provided by the Department of Chemistry.*

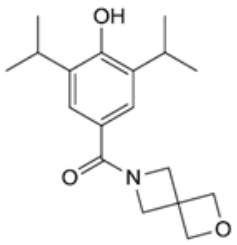

LT-02-53

Parameter	T0 Score
ClogP = 3.3	0.85
ClogD = 3.93	0.04
TPSA = 49.77 Å	1.00
MW = 303.34 Da	1.00
HBD = 1	0.83
pKa = 10.10	0.00
CNS MPO = 3.7	
GlyRα1 EC_{50} = 1.6pM	

The spirocyclic analogue did have a lower pKa that LT-01-25, but it was still above the recommended value for CNS penetration. As seen with LT-02-39 and LT-02-50, changes to the

morpholine ring increases the ClogD, which has effected on the overall MPO. LT-02-53, achieved a score of 3.7, which is just below the desired value of 4. On a positive note, this compound showed substantial improvement in efficacy at GlyRα1, and there was no activity seen at $GABA_AR$.

Piperazine, along with morpholines and spirocycles, is a structural motif that is frequently used in drug design. Similarly to spirocycles, compounds featuring piperazine, may have an advantage over morpholines in terms of physiochemical properties and metabolic stability[52]. The piperazine analogue, LT-02-86, can be seen in Table 3.16.

Table 3.16. MPO evaluation of LT-02-86.
**MPO data was provided by the Department of Chemistry.*

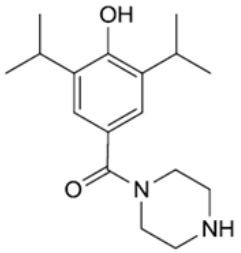

LT-02-86

Parameter	T0 Score
ClogP = 3.1	0.96
ClogD = 1.92	1.00
TPSA = 52.57 Å	1.00
MW = 290.40 Da	1.00
HBD = 1	0.83
pKa = 10.14	0.00
CNS MPO = 4.8	
GlyRα1 EC_{50} = 137aM	

Unfortunately no progress was seen in the pKa value of LT-02-86. Piperazine substitution resulted in a slight increase in pKa. On the other hand, the ClogP and ClogD were vastly improved, bringing the CNS MPO scored to 4.8, one of the highest values out of all the analogues. LT-02-86 also produced an exceptionally strong response at GlyRα1. The EC_{50} value was in the attomolar concentration range, potentially making extremely potent compared LT-01-25.

So far the optimisation of LT-01-25 has been focussed on alterations to the morpholine ring. It is already known that the basic phenolic structure of propofol must be maintained for GlyRα1 activity. Phenols are hugely common in pharmacological agents; meaning that any compound containing a phenol runs the risk of acting off-target and causing toxicity. Furthermore phenols provide a perfect platform for metabolic conjugation[53]. On this basis, the use of phenols in novel drug design is discouraged. For these analogues, it would be ideal to find a suitable replacement that retains the pharmacological effect but has a reduced risk of off-target toxicity and improved metabolic stability.

Bioisosteres are functional groups that have similar biological responses but different chemical structures. Numerous studies have shown that heterocyclic phenol bioisosteres, particularly containing amines can be used to recreate the properties of phenols. In a study by Wright *et al.* (2000), phenolic analogues were designed as NMDA antagonists. In order to improve the poor PK of these analogues, a series of phenol bioisosteres were produced, these compounds showed great bioavailability and potency[53]. In another study, phenolic oestrogen receptor ligands were replaced with phenol bioisosteres (Figure 3.21). Again these heterocyclic bioisosteres displayed improved potency, absorption and metabolic stability[54].

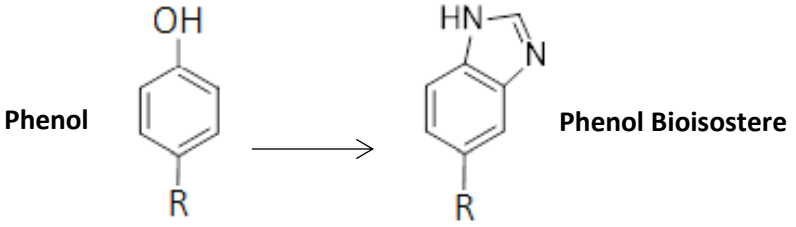

Figure 3.21. Structures of phenol and the phenol bioisostere scaffold from Wilkening *et al.* (2006).

Based on the rationale and evidence from these studies, it was decided the effect of phenol bioisostere substitution would be investigated in this project. A bioisostere of LT-01-25 was synthesised and tested (Table 3.17)

Table 3.17. MPO evaluation of RKA-018.
**MPO data was provided by the Department of Chemistry.*

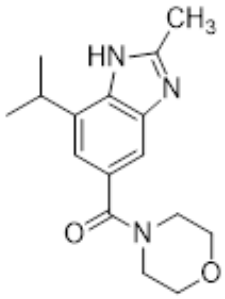

RKA-018

Parameter	T0 Score
ClogP = 2.21	**1.000**
ClogD = 2.50	**0.750**
TPSA = 53.93 **Å**	**1.000**
MW = 287.36 **Da**	**1.000**
HBD = 1.00	**0.833**
pKa = 13.10	**0.000**
CNS MPO = 4.6	
GlyRα1 EC_{50} = 4.2nM	

The EC_{50} concentration for RKA-018 was lower than that of LT-01-25; however the phenol bioisostere was not as potent as the other analogues discussed above. The pKa was significantly increased however the low ClogP and ClogD gave RKA-018 the second highest MPO score in the project.

The purpose of LT-01-25 optimisation was to improve the physiochemical properties, particularly pKa. For the most part, the substitutions provided molecules with good all-around properties. Many of the structural groups used also had a positive impact on efficacy at GlyRα1. Other well-known effects that have been reported are better absorption, higher bioavailability and less metabolic breakdown. To determine whether these substitutions have a positive impact on pharmacokinetics, they were tested using rat and human liver microsomes.

3.4.2 Metabolic Stability

As the metabolic profile of the lead compound, LT-01-25 is already desirable; it would be interesting to see whether in can be further enhanced. The new analogues that were successful able activate GlyRα1 below 1μM were selected to be incubated with rat and liver microsomes following the same protocol applied to LT-01-25. The data for LT-02-39 (Figure 3.22), LT-02-50 (Figure 3.23), LT-02-53 (Figure 3.24), LT-02-86 (Figure 3.25) and RKA-018 (Figure 3.26) is presented and discussed below.

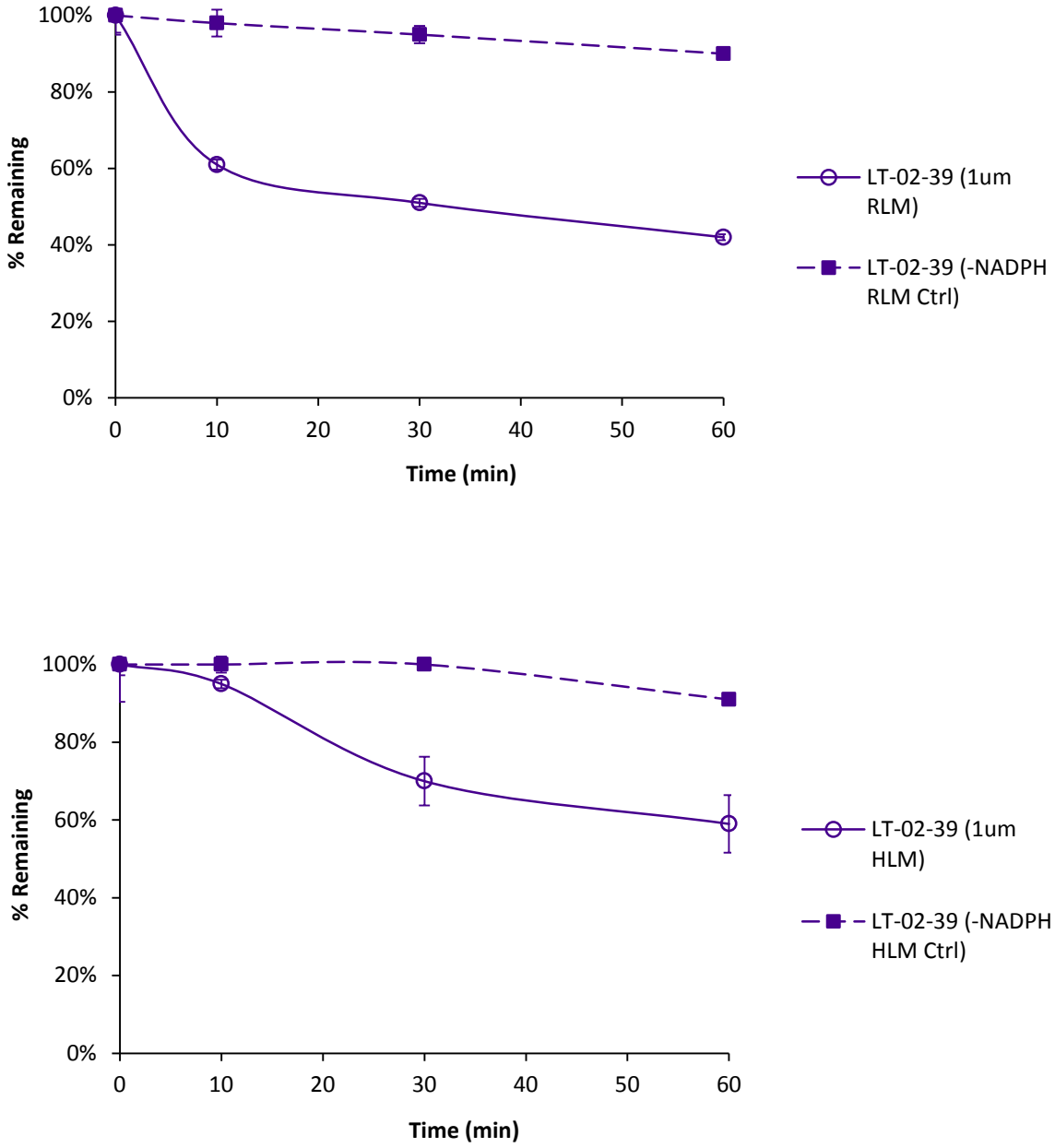

Figure 3.22. Microsomal stability data for LT-02-39 in rat (*above*) and human (*below*) liver microsomes: LT-02-39 (1µM) was incubated for 60 minutes in rat and human liver microsomes (1mg/mL protein). Each individual experiment was carried out in duplicate. A control without essential co-factor, NADPH was also carried out. The data is expressed as mean (± SEM) (n=6). Data comparison between drug and control incubation was carried out using one tailed T-Test (RLM *P*=0.03 and HLM *P*=0.06). Total turnover in RLM was 48% (±0.007) and 32% (±0.08) in HLM.

The monomethyl analogue, LT-02-39 was the only analogue of its set that showed potency at the target receptor. The EC_{50} value was in the picomolar range, making the compound far more potent that LT-01-25. However, LT-02-39 underwent a fair amount of metabolic breakdown, predominantly in rats with some metabolism occurring in human microsomes. The total turnover in rats was 48% (±0.007) in comparison to the control; in humans this value was a bit lower at 32% (±0.08). The half-life in both species was moderately low at 86 minutes (RLM) and 96 minutes (HLM).

In humans the microsomal clearance (Cl_{CYP}) was 7.2μL/min/mg protein, this is close the recommended cut off at 8.2 μL/min/mg protein. The intrinsic was calculated as 9 mL/min/Kg; this is similar to the estimated clearance of propofol in HLM (11-15 mL/min/Kg). The rat microsomal clearance was 8x higher compared to LT-01-25. Increase in metabolic breakdown is most probably due to the inclusion of the methyl group in the morpholine ring. While, LT-02-39 is more potent than LT-01-25, high rate of microsomal breakdown will probably result in poor exposure at GlyRα1. The pharmacological response is likely to be weaker and short-lived, similar to what is seen with LT-01-26; a compound that was more biological potent but less metabolically stable, therefor not as effective in the neuropathic pain model.

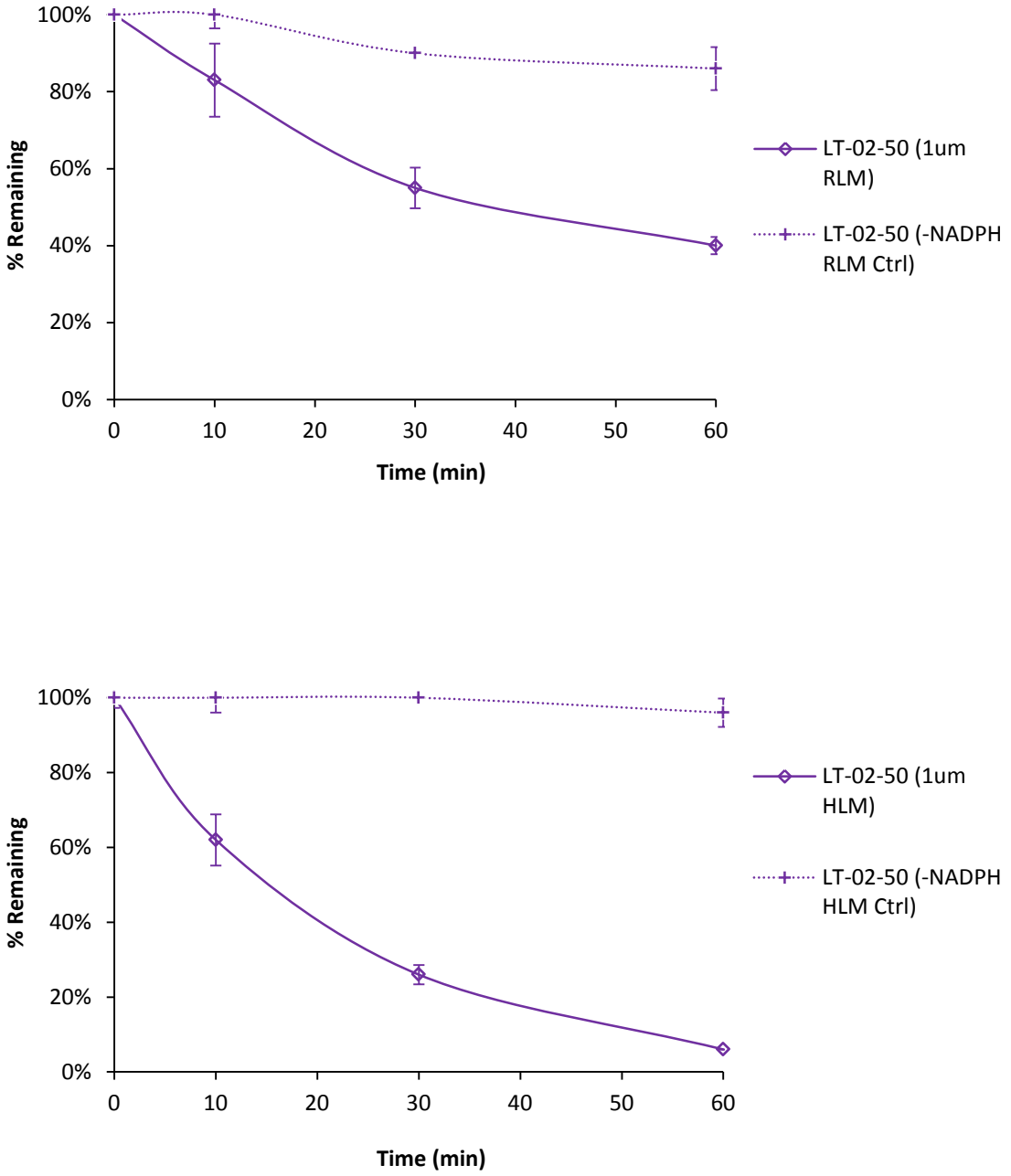

Figure 3.23. Microsomal stability data for LT-02-50 in rat (*above*) and human (*below*) liver microsomes: The data is expressed as mean (± SEM) (n=6). Data comparison between drug and control incubation was carried out using one tailed T-Test (RLM *P*=0.04 and HLM *P*=0.04). LT-02-50 had an overall turnover of 46% (±0.02) in RLM and 90% (±0.60) in HLM.

Fluorine is often used as a means of improving PK, so it would be expected that the fluorine azetidine analogue would be the most stable compound. However, LT-02-50 underwent nearly complete metabolism in human microsomes leaving only 10% (±0.6) of the original amount remaining after 60 minutes. The half-life was extremely low (47 minutes) and Cl_{CYP} was 14.7 µL/min/mg protein, this is almost double the maximum recommended value (8.2 µL/min/mg protein). The Cl_{int} (18.5 mL/min/Kg) exceeded the estimated value for propofol. LT-02-50 fared better in rats, with a total breakdown of 46% (±0.02). It should be noted that the compound showed much more degradation (approx.14%) in the control incubations, suggesting that the compound itself may not be stable. This could have contributed to the high levels of breakdown. Even with high efficacy at the target, poor stability and extensive metabolism will ultimately impact analgesic performance.

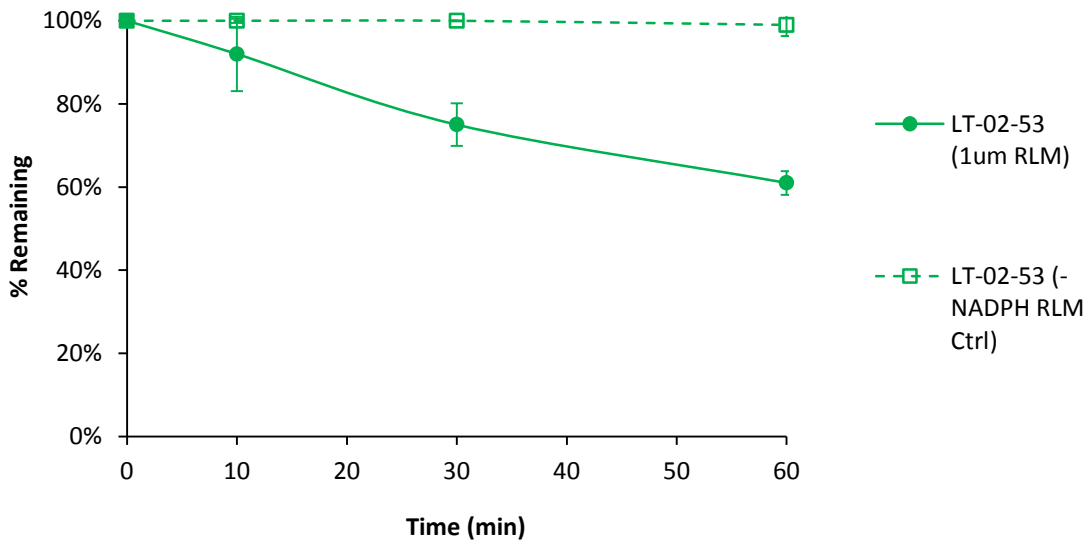

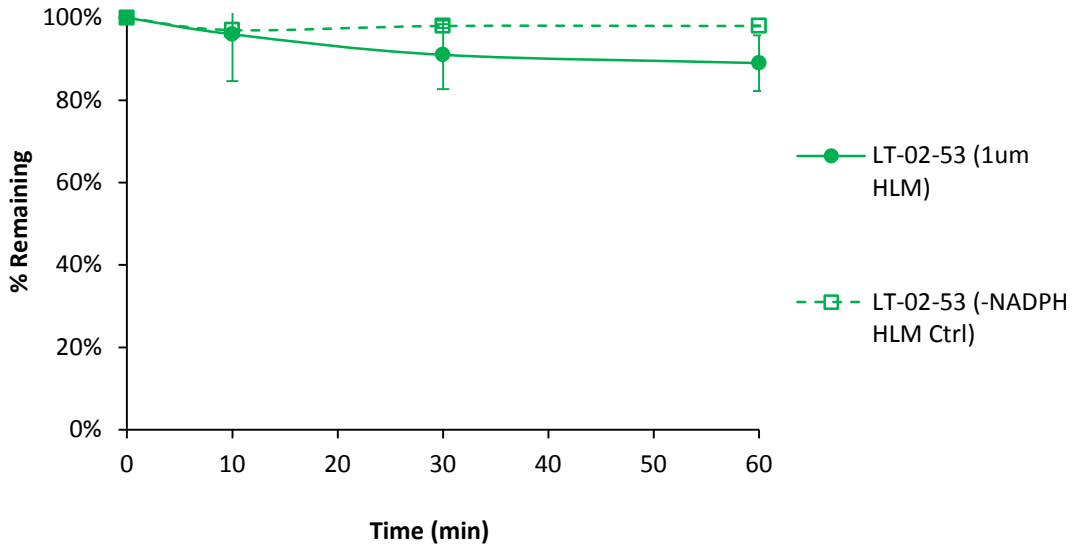

Figure 3.24. Microsomal stability data for LT-02-53 in rat (*above*) and human (*below*) liver microsomes: The data is expressed as mean (± SEM) (n=6). Data comparison between drug and control incubation was carried out using one tailed T-Test (RLM *P*=0.06 and HLM *P*=0.08). LT-02-53 had an overall turnover of 38% (±0.02) in RLM and 9% (±0.06) in HLM.

The spirocyclic compound, LT-02-53 was exceedingly stable in human microsomes, showing only 9% (±0.06) metabolism at 60 minutes in comparison to the control. The analogue has a long half-life (407 minutes) and clearance values (Cl_{CYP} = 7.7 µL/min/mg protein and Cl_{int} = 2.1 mL/min/Kg) were comparable to that of LT-01-25 and LT-01-89. Unfortunately, such stability was not sustained across species. In rat microsomes, a total turnover of 38% (±0.02) was seen. The half-life (106 minutes), Cl_{CYP} (6.5 µL/min/mg protein) and Cl_{int} (11.7 mL/min/Kg) were better than those of LT-02-39 and LT-02-50.

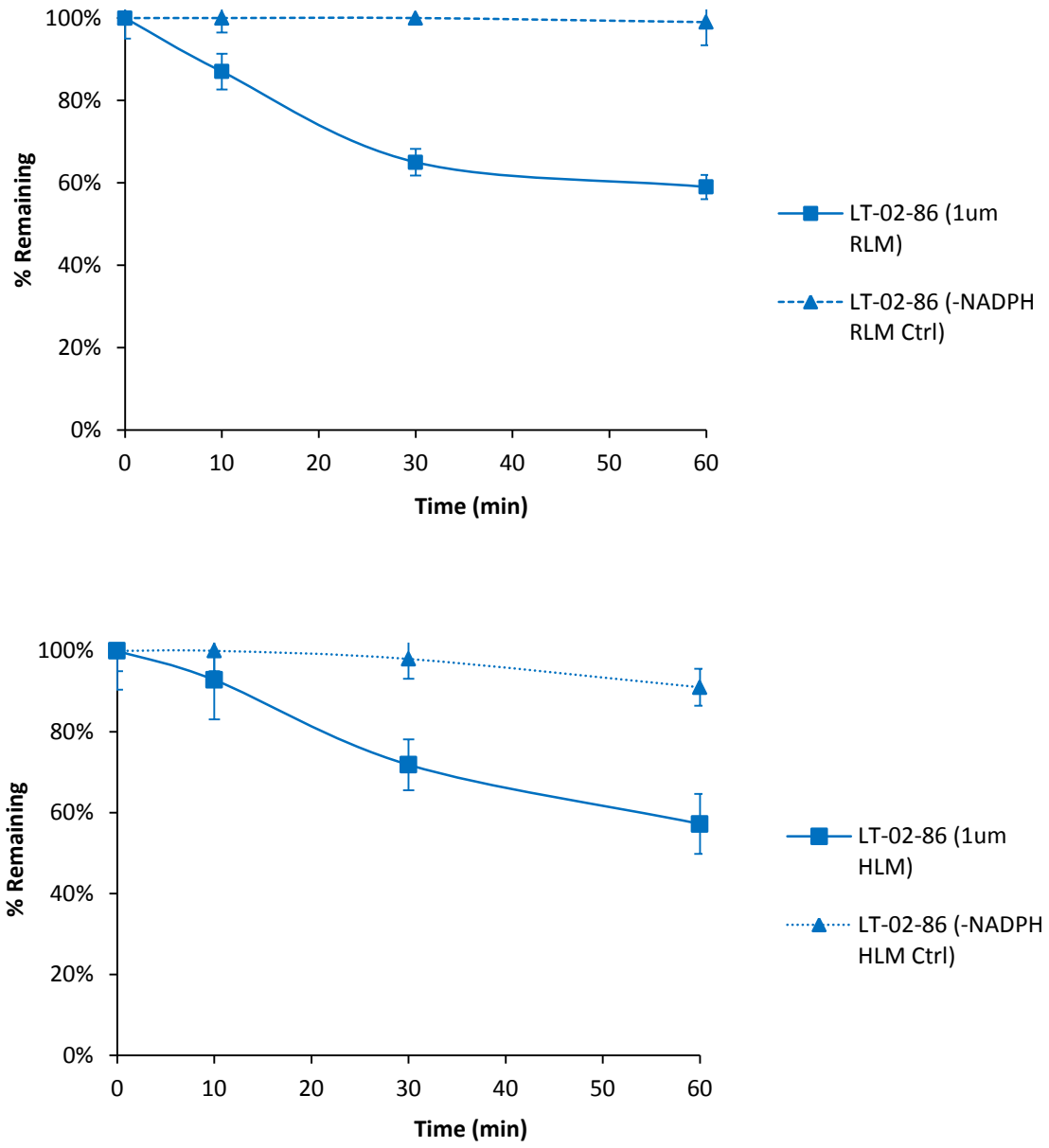

Figure 3.25. Microsomal stability data for LT-02-86 in rat (*above*) and human (*below*) liver microsomes: The data is expressed as mean (± SEM) (n=6). Data comparison between drug and control incubation was carried out using one tailed T-Test (RLM *P*=0.05 and HLM *P*=0.06). LT-02-86 had an overall turnover of 40% (±0.74) in RLM and 34% (±0.07) in HLM.

The metabolic profile of LT-02-86 is very similar to that of LT-02-39. The piperazine compound has a somewhat higher metabolic resistance in rat microsomes, perhaps due to the replacement of the *N*-methyl with an NH function with the piperazine ring system. The half-life in humans (95 minutes) was almost identical to that of LT-02-39, as was the Cl_{CYP} (7.3µL/min/mg protein) and Cl_{int} (9 mL/min/Kg). LT-02-86 was more stable in rats with an overall turnover of 40% (±0.74) and a half-life of 103 minutes. Both clearance values were within a desired range, although they were much higher than LT-01-25. Although LT-02-86 demonstrated extraordinary efficacy at GlyRα1, the high CYP metabolic rate is likely to lessen exposure and weaken the analgesic effect in an animal model of pain. However the compound is very stable in humans, suggesting that results from *in vivo* pharmacodynamic testing in rats might not be truly reflective of the pharmacological response in man.

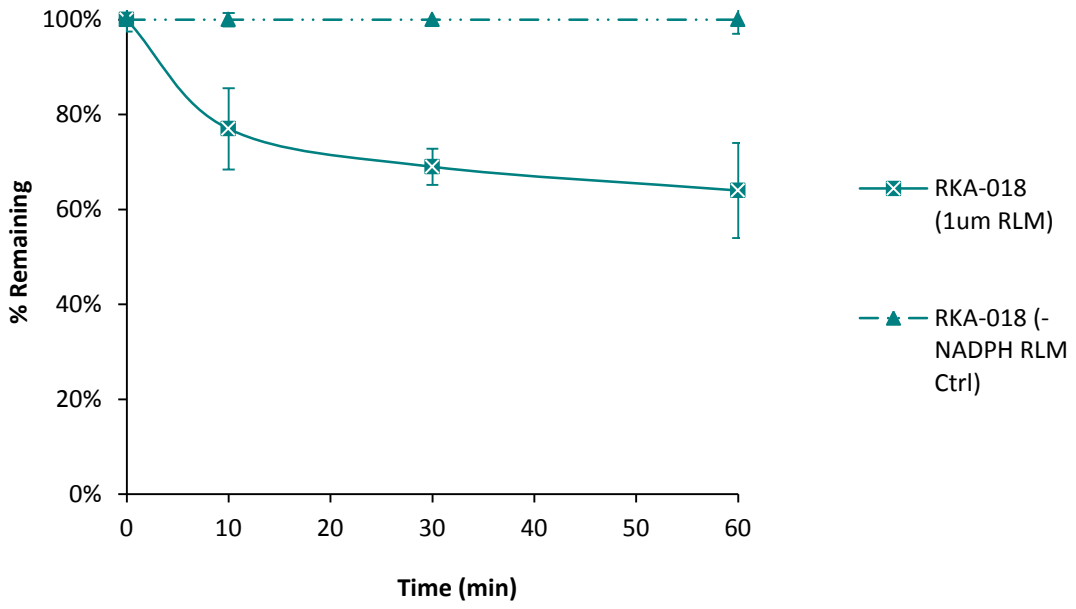

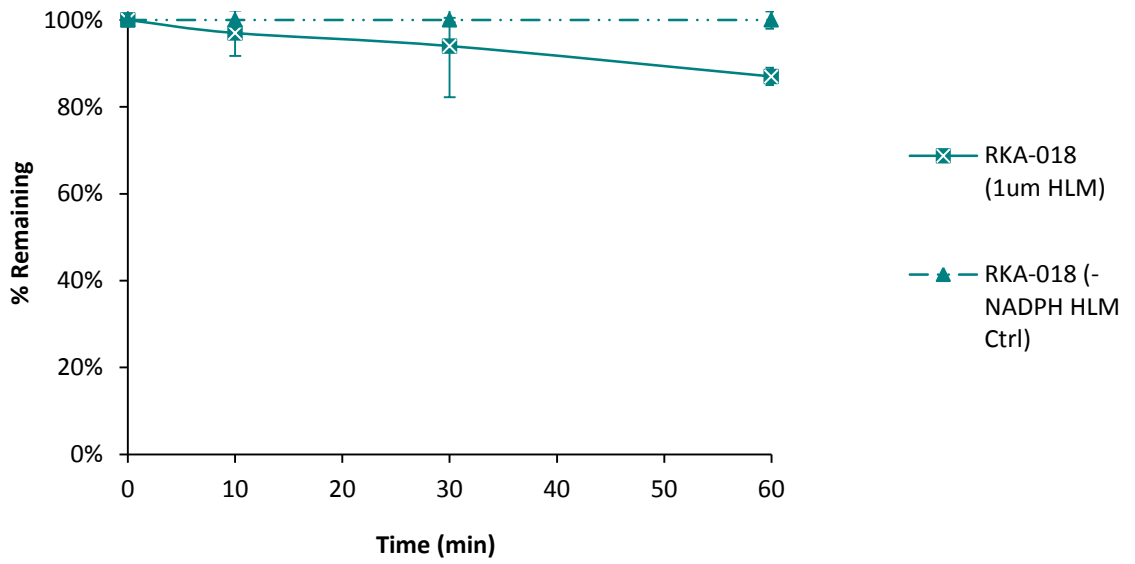

Figure 3.26. Microsomal stability data for RKA-018 in rat (*above*) and human (*below*) liver microsomes: The data is expressed as mean (± SEM) (n=6). Data comparison between drug and control incubation was carried out using one tailed T-Test (RLM *P*=0.03 and HLM *P*=0.07). RKA-018 had an overall turnover of 36% (±0.10) in RLM and 13% (±0.02) in HLM.

As with, LT-02-53, the phenol bioisostere, RKA-018 showed good metabolic resistance in humans and underwent some metabolism in rat microsomes. RKA-018 was not as stable as LT-02-53 but still demonstrated better stability than the other LT-01-25 analogues tested. The overall metabolism was 36% (±0.10) in rats and 13% (±0.02) in humans. As expected, the half-life was longer in humans (330 minutes) than rats (135 minutes). The clearance values were well within the desired ranges and lower than that of propofol. It is probable that CYP metabolism in taking place at the methyl group within the phenolic bioisostere. The microsomal parameters for each analogue are collected in Table 3.18.

Table 3.18. Microsomal pharmacokinetic parameters of LT-01-25 analogues

	$T_{1/2}$ (min)		Cl_{CYP}(µL/min/mg)		Cl_{int}(mL/min/Kg)	
	RLM	**HLM**	**RLM**	**HLM**	**RLM**	**HLM**
LT-02-39	86	96	8	7.2	14	9
LT-02-50	70	47	9.9	14.7	17.7	18.5
LT-02-53	106	407	6.5	1.7	11.7	2.1
LT-02-86	103	95	6.7	7.3	12	9
RKA-018	135	330	5.1	2.1	9.1	2.6

Surprisingly none of the LT-01-25 analogues, showed improved microsomal stability over the original lead compound, however all the compounds showed excellent metabolic stability. In accordance with microsomal clearance guidelines all the compounds, bar LT-02-50, fall into the low clearance category for both species. Although, LT-02-50 demonstrated moderate human microsomal clearance, the value was at the lower end of the classification bracket (Table 3.19).

Table 3.19. Microsomal clearance classification[55].

	Microsomal Clearance (µL/min/mg)		
	Low	**Moderate**	**High**
Human	< 8.6	8.6 - 47.0	> 47.0
Rat	< 13.2	13.2 – 71.9	> 71.9

While these compounds all showed increase potency, extensive metabolism may hinder their effectiveness at reducing pain in a living organism. However the microsomal data only

provides information about one metabolic pathway. The major route of metabolism in LT-01-25 is thought to be glucuronidation. There is a possibility that these analogues have better resistance to phase II metabolism. The analogues were sent to ChemPartners for testing. Fasted, male, Wistar rats were dosed orally at 10mg/Kg (10% DMSO, 10% solutol and 80% saline). The pharmacokinetic parameters were calculated based on concentration levels in the plasma. The parameters are shown in Table 3.20. LT-02-39 is currently undergoing testing, so a full data-set is not yet available and LT-02-53 and RKA-018 are waiting to be tested.

Table 3.20. Pharmacokinetic parameters of LT-01-25 analogues
**Parameters provided by ChemPartners*

	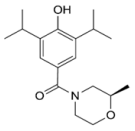 **LT-02-39**	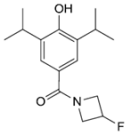 **LT-02-50**	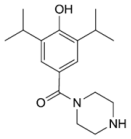 **LT-02-86**
T_{max} (min)	40	30	60
C_{max} (ng/mL)	3723	995	664
$T_{1/2}$ (min)	154.2	154.8	184.8
CL (mL/hr/kg)	--	1.64	2.11
F (%)	--	38.8	74

From the data of the analogues that have completed testing, it is clear that these compounds are rapidly absorbed (T_{max} ≤1). Unfortunately the exposure in the plasma for LT-02-50 (C_{max} = 995ng/mL) and LT-02-86 (C_{max} = 664ng/mL), this could be consequence of extensive CYP metabolism. The bioavailability of LT-02-50 and LT-02-86 was lower than that of LT-01-25. Based on microsomal data, it is likely that LT-02-53 and RKA-018 will exhibit similar PK profiles.

As with LT-01-26 and LT-01-89, the analgesic effect of these analogues is likely be fast acting but short-lived. In addition these analogues are extremely potent, so the initial pharmacological response could be higher than LT-01-25, but high clearance will mean the effect is brief. To be certain how efficacy and metabolism impact analgesia, these analogues must be tested in the same animal model of neuropathic pain.

3.4.3 Testing in the Chung Lesion Model of Neuropathic Pain

The analogues of LT-01-25 were sent to King's College London to be tested in the Chung lesion model of neuropathic pain. Testing was carried using fasted, male Sprague-Dawley rats following the same protocol used in previous Chung lesion experiments. As before the rats were dosed orally at three concentrations (3, 10 and 30mg/Kg) formulated in 10% DMSO, 10% solutol and 80% saline. Gabapentin and lamotrigine (30mg/Kg P.O) were used as controls. The data is presented as a percentage reversal of the pre-dose baseline, representing a neuropathic pain state. Mechanical allodynia was measured via paw withdrawal thresholds in response to mechanical pressure and cold hyperalgesia was measured as paw withdrawal latencies from a cold stimulus (10°C). The results of LT-02-50 can be seen below in Figure 3.27.

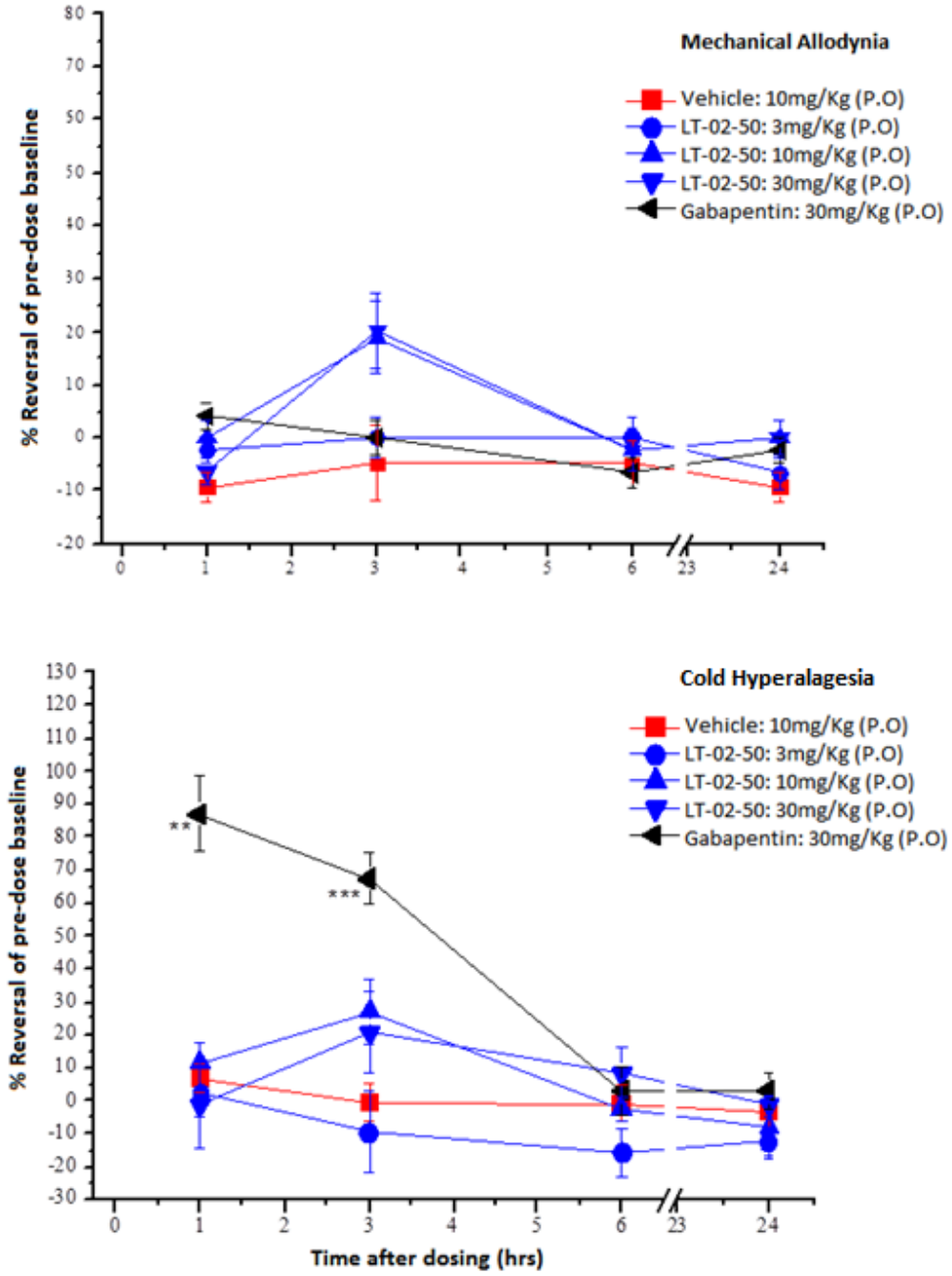

Figure 3.27. The effect of LT-02-50 on mechanical allodynia (*top*) and cold hyperalgesia (*bottom*) in the Chung lesion neuropathic pain model: Fasted, male, Sprague-Dawley rats were treated with LT-02-50 at 3, 10 and 30mg/Kg (Vehicle = 10% DMSO, 10% solutol, 80% saline). Gabapentin (30mg/Kg) was used as a control analgesic. Mechanical allodynia is measured as paw withdrawal threshold from application of von Frey hairs and cold hyperalgesia is measured as paw withdrawal latency from a source of noxious cold (10°C). Data is presented as mean ± SEM (n=6) percentage reversal of the pre-dose baseline. Statistical analysis between LT-02-50 and gabapentin was carried out using one-way ANOVA, comparison and Turkey's HSD test for time-matched vehicle group (* = P ≤ 0.05, ** = P ≤ 0.01, *** = P 0.001).

**Data from King's College London.*

While, LT-02-50, was able to outperform gabapentin at 3 hours with a 20% reversal of mechanical allodynia (10 and 30mg/Kg), the compound was considerably less effective than LT-01-25, which produced 90% reversal at the same dose and time. LT-02-50 appeared to have little effect on cold hyperalgesia. The analogue was not able to achieve greater reversal than gabapentin; the maximum reversal of gabapentin was 85% at 1 hour. At the same dose (30mg/Kg), LT-02-50 produced 25% reversal (maximum) at 3 hours. The analgesic effect in a living organism is not reflective of the outstanding potency exhibited in electrophysiology testing at recombinant GlyRα1 (EC_{50} =1.2pM). This is most likely the result of low bioavailability (38.8%). LT-02-50 was extensively metabolised in rat liver microsomes, with a short half-life (70 minutes) and high clearance (9.9mL/min/mg protein). The maximum concentration seen in the plasma of rats was 995ng/mL. Despite being highly selective for the target, the availability of free drug is low, this could possibly be the result of high phase I metabolism. This is illustrated in the lower analgesic response seen in the neuropathic pain model.

It should also be noted, that the control gabapentin had little effect on mechanical allodynia. This was also case in the experiments carried out on LT-01-26. During testing with LT-01-25 and LT-01-89, lamotrigine was used as a control. Lamotrigine was much more effective in treating mechanical allodynia than gabapentin. There was little difference between the two control drugs in cold hyperalgesia. It was decided that LT-02-39 (Figure 3.28*a*-*b*) would be tested against lamotrigine, as it is appeared to be stronger analgesic in this particular pain model.

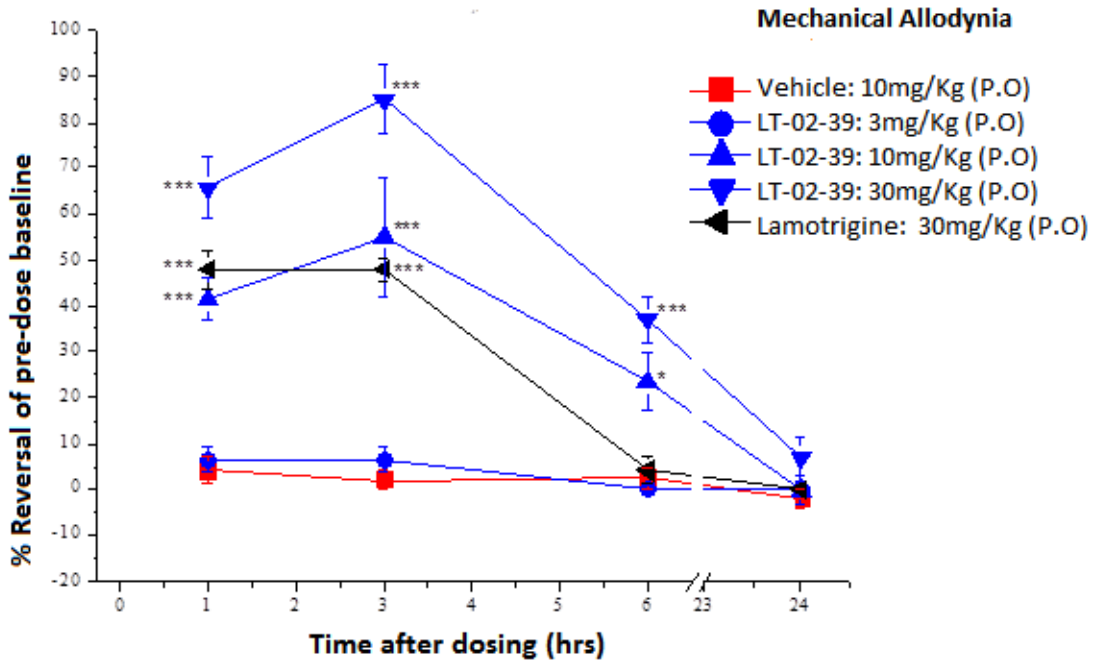

Figure 3.28*a*. The effect of LT-02-39 on mechanical allodynia in the Chung lesion model of neuropathic pain model: Fasted, male, Sprague-Dawley rats were treated with LT-02-39 at 3, 10 and 30mg/Kg (Vehicle = 10% DMSO, 10% solutol, 80% saline). The positive control was lamotrigine (30mg/Kg). Mechanical allodynia is measured as paw withdrawal threshold from application of von Frey hairs. Data is presented as mean ± SEM (n=6) percentage reversal of the pre-dose baseline. Statistical analysis between LT-02-39 and lamotrigine was carried out using one-way ANOVA, comparison and Turkey's HSD test for time-matched vehicle group (* = P ≤ 0.05, ** = P ≤ 0.01, *** = P 0.001).
**Data provided by King's College London.*

LT-02-39 responded much better than LT-02-50. In mechanical allodynia the maximum reversal (85%) was seen at 3 hours following a 30mg/Kg dose. Under the same conditions, lamotrigine achieved 50% reversal. The analgesic effect of LT-02-39 was very close to that of LT-01-25 (90% maximum reversal, 3 hours, 30mg/Kg).

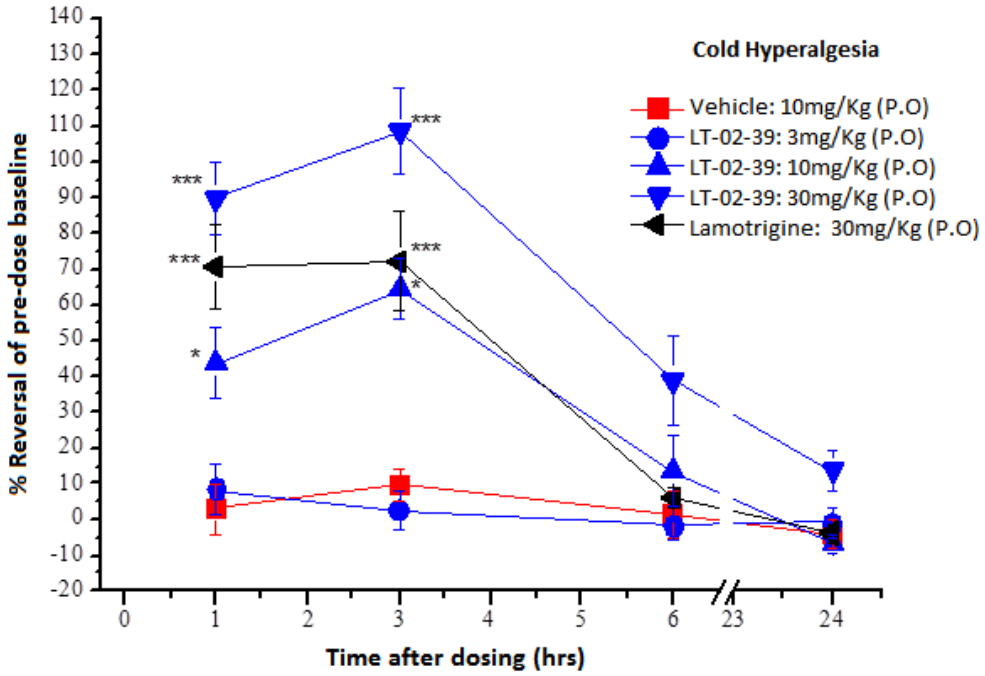

Figure 3.28*b*. The effect of LT-02-39 on cold hyperalgesia in the Chung lesion neuropathic pain model: Fasted, male, Sprague-Dawley rats were treated with LT-02-39 at 3, 10 and 30mg/Kg (Vehicle = 10% DMSO, 10% solutol, 80% saline). The positive control was lamotrigine (30mg/Kg). Cold hyperalgesia is measured as paw withdrawal latency from a source of noxious cold (10°C). Data is presented as mean ± SEM (n=6) percentage reversal of the pre-dose baseline. Statistical analysis between LT-02-39 and lamotrigine was carried out using one-way ANOVA, comparison and Turkey's HSD test for time-matched vehicle group (* = P ≤ 0.05, ** = P ≤ 0.01, *** = P 0.001).
**Data provided by King's College London.*

Interestingly, LT-02-39 out-performed both the control and LT-01-25 in cold hyperalgesia. At 3 hours, LT-02-39 reversed paw withdrawal latency by 110% (30mg/Kg). In comparison, lamotrigine reached 70% reversal. LT-01-25 and LT-02-39 both demonstrated 90% reversal at 1 hour, however the effect produced by LT-01-25 gradually diminished over time, whereas LT-02-39 peaked at 3 hours before falling sharply. Although the maximum reversal generated by LT-02-39 was much higher than LT-01-25, the same effect could not be maintained at lower

doses. Whilst, LT-01-25 showed some analgesia at 3mg/Kg (maximum reversal = 15% at 3 hours), LT-02-39 did not have any effect on mechanical allodynia or cold hyperalgesia. The powerful, yet short-lived effect of LT-02-39 makes the compound an unreliable analgesic as the effect is dependent on high dose, resulting in good exposure at the target. LT-02-53 has good efficacy at GlyRα1 (EC_{50} = 60pM) and is efficiently absorbed (C_{max} = 3723ng/mL, T_{max}=40 minutes) however the compound has at least 50% metabolic breakdown by CYPs and has high intrinsic clearance in rats (Cl_{int}= 9mL/min/Kg), close to that of propofol. The maximum percentage reversal of allodynia and hyperalgesia for LT-02-39 and LT-02-50 is summarised in Table 3.21.

Table 3.21. Maximum percentage reversal of mechanical allodynia (*top*) and cold hyperalgesia (*bottom*) in the Chung lesion model of neuropathic pain: LT-02-39 and LT-02-50 were tested at three concentrations in the Chung lesion pain model. Data is presented as a percentage reversal of the pre-dose baseline in mechanical allodynia behavioural tests. The highest reversal values are highlighted.

Compound/Dose (mg/Kg)	Max % Reversal	Time (hr)
LT-02-39 (3 mg/Kg)	5%	3 hrs
LT-02-39 (10 mg/Kg)	55%	3 hrs
LT-02-39 (30 mg/Kg)	**85%**	**3 hrs**
LT-02-50 (3 mg/Kg)	0%	3 hrs
LT-02-50 (10 mg/Kg)	20%	3 hrs
LT-02-50 (30 mg/Kg)	**20%**	**3 hrs**

Compound/Dose (mg/Kg)	Max % Reversal	Time (hr)
LT-02-39 (3 mg/Kg)	0%	3 hrs
LT-02-39 (10 mg/Kg)	65%	3 hrs
LT-02-39 (30 mg/Kg)	**110%**	**3 hrs**
LT-02-50 (3 mg/Kg)	5%	3 hrs
LT-02-50 (10 mg/Kg)	**25%**	**3 hrs**
LT-02-50 (30 mg/Kg)	20%	3 hrs

The data for LT-02-53, LT-02-86 and RKA-018 is not currently available as these studies are on-going. Based on the metabolic profiles of these compounds it is possible that any analgesic effect will be short-lived, although there is a chance that increase potency will lead to greater maximum reversal that LT-01-25. Alongside, testing in the Chung lesion model of neuropathic pain, these compounds were undergoing other methods of testing, including the investigation into the inhibition of CYP isoforms.

3.4.4 Cytochrome P450 Inhibition Screening

Identifying compounds that may inhibit CYPs is a significant part of understanding drug safety. Previously tested analogues did not produce more than 40% inhibition at 10µM when incubated with five major CYP isoforms; CYP1A2, CYP2C9, CYP2C19, CYP2D6 and CYP3A4. As part of the analogue design, functional groups that are commonly associated with protein adduct formation and enzyme inhibition, for example quinones, have been avoided. It is unlikely that these compounds will be strong CYP inhibitors based on their structure and previous testing results of the amide analogues. CYP inhibition is measured as fluorescence released following successful metabolic reaction. The data for CYP1A2 is presented below (Figure 3.29) as the level of fluorescence taken at the experimental end-point of 60 minutes. Only the values for the highest testing concentration (10µM) are shown, however the test compounds were also tested at 1µM and 0.1µM.

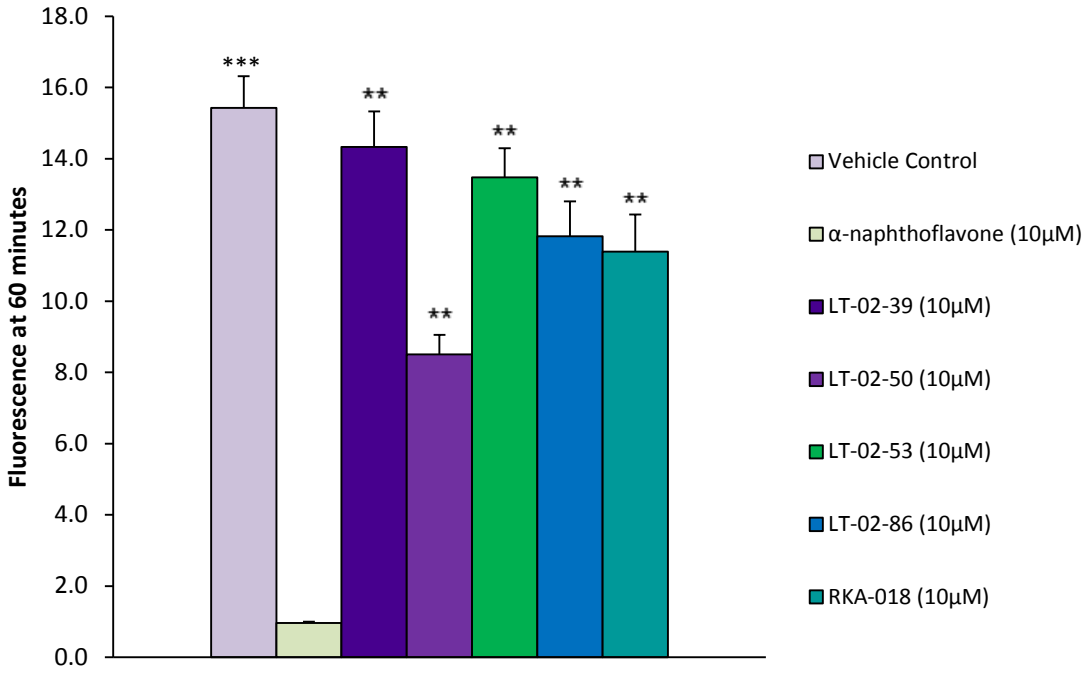

Figure 3.29 Inhibition of CYP1A2 by analogues of LT-01-25: CYP1A2 baculosomes incubated with test compounds; LT-02-39, LT-02-50, LT-02-53, LT-02-86 and RKA-018 (10µM) for 60 mins in a fluorescent plate reader (37.1°C). Inhibition was measured by the maximum fluorescence at 60 mins. A vehicle control (1.25% DMSO) and positive control (α-Naphthoflavone, 10µM) were also tested as a comparison for inhibition. Data is presented as mean ±SEM (n=3). Statistical analysis was carried out between the positive control and test compounds using one-tailed T-Test (* = P ≤ 0.05, ** = P ≤ 0.01, *** = P ≤ 0.001).

Comparisons made to the vehicle control (no inhibition) were calculated as a percentage difference, while statistical comparisons were made between the test compounds and the positive controls (high inhibition). The difference between the positive control, α-Naphthoflavone (94% ±0.03 inhibition) and all of the analogues tested was highly statistically significant (P≤0.01). None of the analogues caused 50% inhibition and therefore would be considered weak CYP inhibitors (IC_{50} > 10µM)[56]. LT-02-50, showed the highest level of inhibition (45% ±0.58). Fluorine substitutions are not usually associated with negative CYP-

drug interactions[57]. LT-02-50 was rapidly metabolised by CYP in microsomal incubations, as such there may be a relation between extensive metabolism and low levels of fluorescence. The least inhibitory analogue was LT-02-39, demonstrating only 7% (±0.99) inhibition. RKA-018 also had a relatively minor inhibitory effect (13% ±1.04), while both LT-02-39 and LT-02-53 produced roughly 26% inhibition compared to the vehicle control.

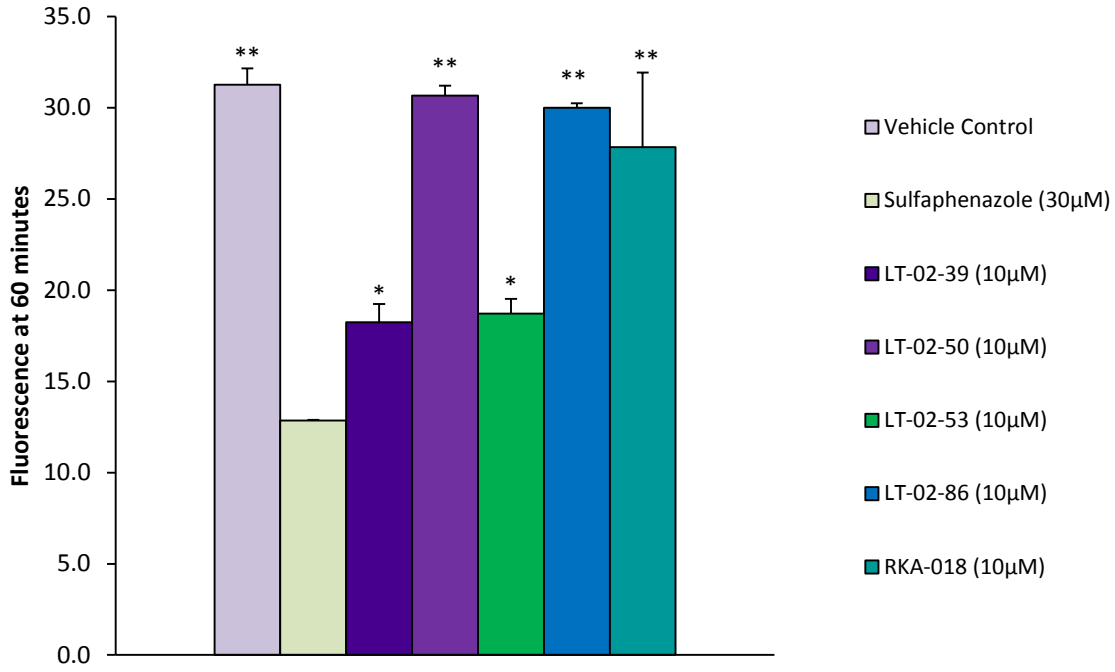

Figure 3.30 Inhibition of CYP2C9 by analogues of LT-01-25: CYP2C9 baculosomes incubated with test compounds; LT-02-39, LT-02-50, LT-02-53, LT-02-86 and RKA-018 (10µM) for 60 mins in a fluorescent plate reader (37.1°C). Inhibition was measured by the maximum fluorescence at 60 mins. A vehicle control (1.25% DMSO) and positive control (Sulfaphenazole, 30µM) were also tested as a comparison for inhibition. Data is presented as mean ±SEM (n=3). Statistical analysis was carried out between the positive control and test compounds using one-tailed T-Test (* = P ≤ 0.05, ** = P ≤ 0.01, *** = P ≤ 0.001).

LT-02-50 had little to no effect on CYP2C9, causing only 2% (± 4.58) inhibition (Figure 3.30), this is a complete contrast to the level of inhibition seen with CYP1A2. This might suggest that CYP2C9 is not a major metabolising enzyme of LT-02-50. By the same token, LT-02-39 inhibited CYP2C9 by 40% (±4.62), whereas it was the least inhibitory analogue of CYP1A2. LT-02-86 also had a very minor effect on CYP2C9 (4% ±1.08), as did RKA-018 (11% ±4.08). LT-02-53 had a moderate impact (40% ±4.77) but would still be considered a weak CYP inhibitor.

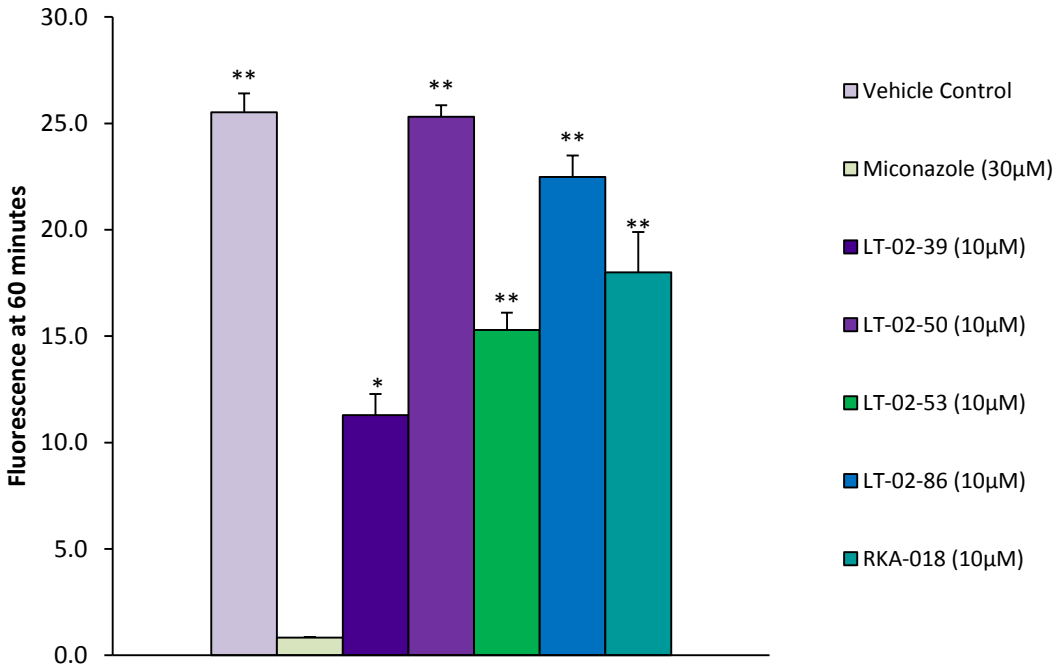

Figure 3.31 Inhibition of CYP2C19 by analogues of LT-01-25: CYP2C19 baculosomes incubated with test compounds; LT-02-39, LT-02-50, LT-02-53, LT-02-86 and RKA-018 (10µM) for 60 mins in a fluorescent plate reader (37.1°C). Inhibition was measured by the maximum fluorescence at 60 mins. A vehicle control (1.25% DMSO) and positive control (Miconazole, 30µM) were also tested as a comparison for inhibition. Data is presented as mean ±SEM (n=3). Statistical analysis was carried out between the positive control and test compounds using one-tailed T-Test (* = $P \leq 0.05$, ** = $P \leq 0.01$, *** = $P \leq 0.001$).

The results for CYP2C19 are shown in Figure 3.31. In this case, one analogue, LT-02-39 did produce over 50% inhibition (52% ±0.04). The IC_{50} was calculated as 9.4µM using a percentage inhibition-concentration plot. While this is not ideal, the IC_{50} value is very close to the upper range for a moderate inhibitor (IC_{50} = 1-10µM)[55]. The structure of LT-02-39 contains no functional groups that would suggest CYP inhibition, so this result is unusual. As with CYP2C9, LT-02-50 caused almost no inhibition (2% ±1.17). The second strongest inhibitor was LT-02-53 (43% ±1.54), followed by RKA-018 (33% ±1.89). LT-02-86 showed some mild inhibitory activity (17% ±5.85), which is in keeping with the results from CYP1A2 and CY2C19.

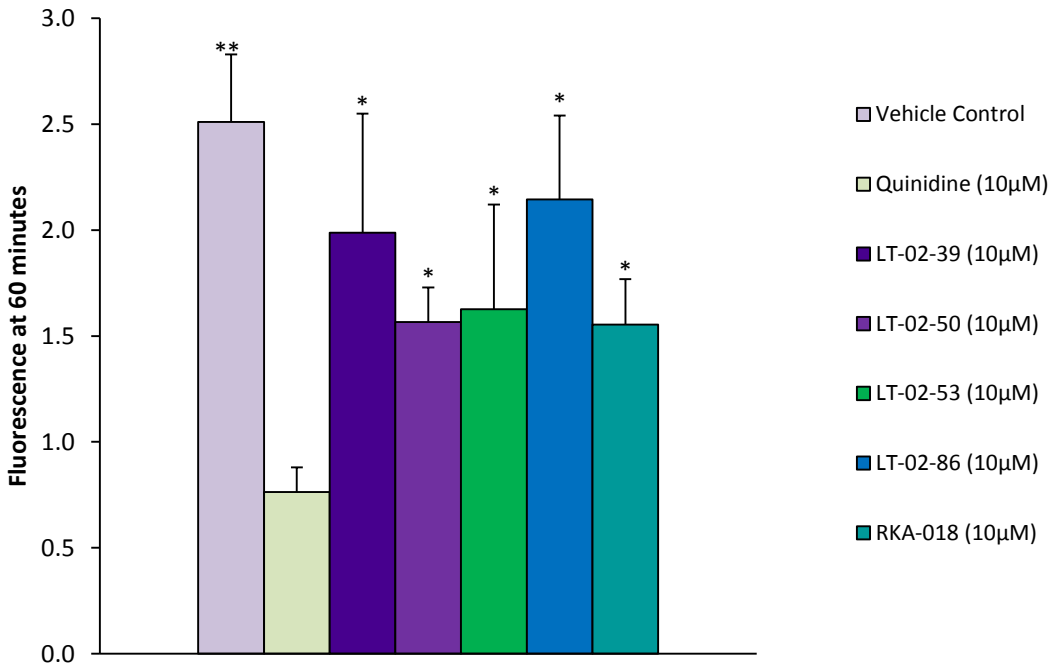

Figure 3.32 Inhibition of CYP2D6 by analogues of LT-01-25: CYP2D6 baculosomes incubated with test compounds; LT-02-39, LT-02-50, LT-02-53, LT-02-86 and RKA-018 (10µM) for 60 mins in a fluorescent plate reader (37.1°C). Inhibition was measured by the maximum fluorescence at 60 mins. A vehicle control (1.25% DMSO) and positive control (Quinidine, 10µM) were also tested as a comparison for inhibition. Data is presented as mean ±SEM (n=3). Statistical analysis was carried out between the positive control and test compounds using one-tailed T-Test (* = P ≤ 0.05, ** = P ≤ 0.01, *** = P ≤ 0.001).

LT-02-86 had the smallest effect on CYP2D6, causing only 15% (±0.37) inhibition. The monomethyl analogue, LT-02-39, produced 21% (±0.56) inhibition of CYP2D6. The other analogues, LT-02-50, LT-02-53 and RKA-018 caused marginal inhibition. LT-02-50 inhibited CYP2D6 by 28% (±0.16), as did RKA-018 (38% ±0.21). LT-02-53 demonstrated slightly less inhibition at 35% (±0.39). All of these values were significantly different to the positive control quinidine, which caused 60% (±0.11) inhibition at the same concentration.

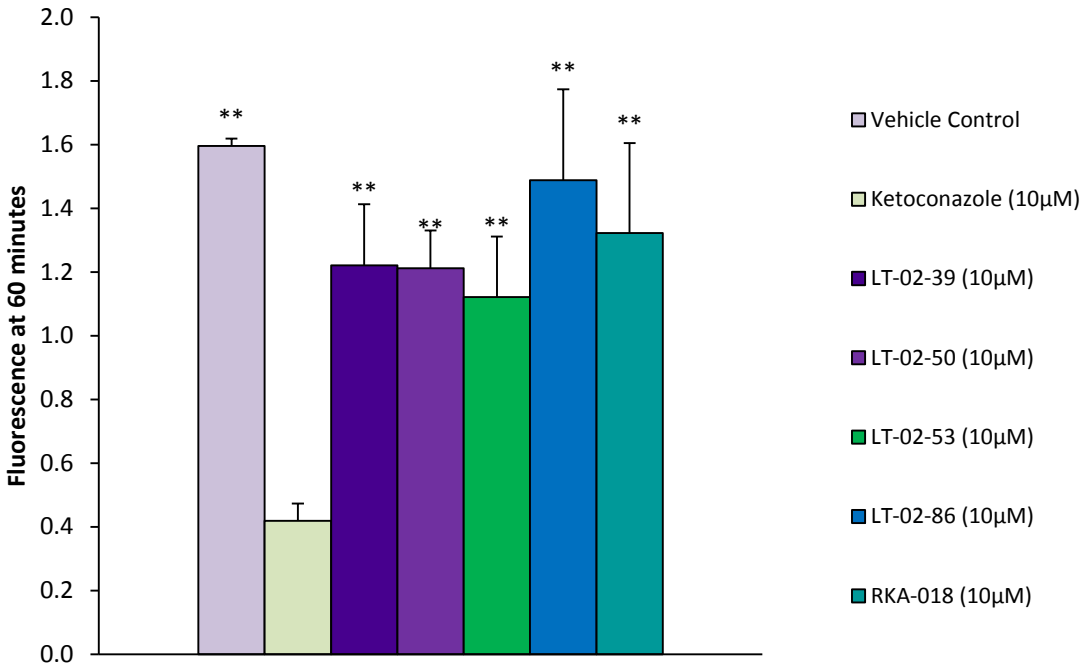

Figure 3.33 Inhibition of CYP3A4 by analogues of LT-01-25: CYP3A4 baculosomes incubated with test compounds; LT-02-39, LT-02-50, LT-02-53, LT-02-86 and RKA-018 (10µM) for 60 mins in a fluorescent plate reader (37.1°C). Inhibition was measured by the maximum fluorescence at 60 mins. A vehicle control (1.25% DMSO) and positive control (Ketoconazole, 10µM) were also tested as a comparison for inhibition. Data is presented as mean ±SEM (n=3). Statistical analysis was carried out between the positive control and test compounds using one-tailed T-Test (* = P ≤ 0.05, ** = P ≤ 0.01, *** = P ≤ 0.001).

As with CYP2D6, LT-02-86 was the least inhibitory analogue of CYP3A4, resulting in 7% (±0.29) inhibition. RKA-018 inhibited CYP3A4 by 17% (±0.28), making the bioisostere analogue the second weakest inhibitor of this isoform. LT-02-39 and LT-02-50 both results in roughly 24% inhibition. The strongest CYP3A4 inhibitor was the spirocyclic analogue, LT-02-53 (30%± 0.19).

With the exception of LT-02-39 causing moderate inhibition of CYP2C19 (IC_{50}=9.4μM), all of the analogues can be considered weak enzyme inhibitors of five chief CYP isoforms. These analogues, along with LT-01-26, are currently undergoing more intensive drug safety testing, such as the Ames test and hERG toxicity.

3.4.5 Summary

A series of propofol analogues were synthesised as positive allosteric modulators of SSGRs. For drugs acting in the CNS, ensuring a high probability of BBB penetration is one of the most vital aspects of drug design. Using a mutliparameter algorithm created by Pzifer, the likelihood of drugs successfully entering the CNS can be assessed (CNS MPO ≥ 4). The MPO scoring system was used to determine which analogue would be taken into further testing.

After various different structural scaffolds, including bi-phenyls and amino-alkyls, a group of analogues based around the inclusion of an amide morpholine ring produced a desire MPO score. In addition, three of these analogues, LT-01-25, LT-01-26 and LT-01-89 had high efficacy at the target receptor (GlyRα1). These compounds were incubated with microsomes to assess

phase I metabolic breakdown. LT-01-25, was particular stable, whereas its sister compound, LT-01-26 was almost completely metabolised. The analogues were also tested in rats to determine the *in vivo* pharmacokinetic. Initial experiments were carried out using LT-01-25 in both fasted and non-fasted rats. The effect of different formulations was also investigated. LT-01-25 had the strongest pharmacokinetic profile, demonstrating the best absorption, lowest clearance and highest bioavailability. The analogues were also screened for negative CYP interactions. None of the analogues caused more than 40% inhibition at 10μM, making them weak inhibitors of CYP enzymes.

LT-01-25, LT-01-26 and LT-01-89 were then tested against gabapentin and lamotrigine, two drugs currently used to treat chronic pain, in the Chung lesion model of neuropathic pain. Gabapentin is typically dosed following a regime starting at 300mg per day, increasing the frequency of the dose to 3 times per day. In some cases, dosing can reach as high as 3600mg per day for sufficient pain relief[58]. In comparison, lamotrigine is recommended to be taken once a day at 200mg-400mg[59]. All three compounds outperformed to the two control analgesics at a low dose of 30mg/Kg. Out the analogues, LT-01-25, once again produced the most promising results. This compound was able to reverse neuropathic pain behaviours, allodynia and hyperalgesia, to a greater extent than the other analogues. LT-01-26 was also fairly effective; however LT-01-89 fell short of expectations. At this point it was decided that only LT-01-25 and LT-01-26 would be taken into further testing.

While LT-01-26 is currently undergoing additional pharmacological testing, such as CSF exposure and hepatic cytotoxicity, the results for LT-01-25 have been presented above. At present, LT-01-25 has met every desired criteria laid out for upcoming drugs, with the

exception of pKa, which is considered too high for successful CNS penetration. In order to reduce to pKa, whilst retaining positive testing results a number of LT-01-25 were produced. The design of these analogues was driven by literature research into the replacement of morpholines and phenols within drug optimisation. Five analogues, LT-02-39, LT-02-50, LT-02-53, LT-02-86 and RKA-018, were remarkably potent at GlyRα1. Only two of these compounds, LT-02-50 (MPO=4.0) and LT-02-86 (MPO=4.4) achieved a desirable MPO score. The compounds were tested in rat and human liver microsomes. Most of the compound shared similar stability with LT-01-25 and LT-01-89. However, LT-02-50 and LT-02-39 both had half-lives below 100 minutes, shorter than the value for all the other analogues. LT-02-50 showed particular poor microsomal metabolism, even having higher clearance than propofol. LT-02-50 also demonstrated poor absorption and bioavailability in rats. LT-02-86 had far better bioavailability, although not as high as LT-01-25. In the Chung lesion model, LT-02-39 outperformed both the control analgesic and LT-01-25, but this effect was short-lived and only occurred at the highest testing concentration. In comparison, LT-02-50 was unable to attenuate allodynia and hyperalgesia. This compound was far less effective than LT-01-25, despite showing greater efficacy at GlyRα1; extensive metabolism is most likely to blame. The structural optimisation of LT-01-25 lead to both positive and negative pharmacological changes. To fully understand which analogue would make the most suitable drug candidate, the testing results for all analogues should be reviewed together.

3.5 References

1. Wager, T. T., Hou, X., Verhoest, P. R. & Villalobos, A. (2010). Moving beyond rules: the development of a central nervous system multiparameter optimization (CNS MPO) approach to enable alignment of druglike properties. *ACS Chem Neurosci* **1**, 435-49.
2. Segall, M. D. (2012). Multi-parameter optimization: Identifying high quality compounds with a balance of properties. *Current Pharmaceutical Design* **18**, 1292-1310.
3. Mahar Doan, K. M., Humphreys, J. E., Webster, L. O., Wring, S. A., Shampine, L. J., Serabjit-Singh, C. J., Adkison, K. K. & Polli, J. W. (2002). Passive permeability and P-glycoprotein-mediated efflux differentiate central nervous system (CNS) and non-CNS marketed drugs. *J Pharmacol Exp Ther* **303**, 1029-37.
4. Pajouhesh, H. & Lenz, G. R. (2005). Medicinal Chemical Properties of Successful Central Nervous System Drugs. *NeuroRx* **2**, 541-553.
5. Alavijeh, M. S., Chishty, M., Qaiser, M. Z. & Palmer, A. M. (2005). Drug Metabolism and Pharmacokinetics, the Blood-Brain Barrier, and Central Nervous System Drug Discovery. *NeuroRx* **2**, 554-571.
6. Pangalos, M. N., Schechter, L. E. & Hurko, O. (2007). Drug development for CNS disorders: strategies for balancing risk and reducing attrition. *Nat Rev Drug Discov* **6**, 521-32.
7. Pardridge, W. M. (2005). The Blood-Brain Barrier: Bottleneck in Brain Drug Development. *NeuroRx* **2**, 3-14.
8. Abbott, N. J., Patabendige, A. A. K., Dolman, D. E. M., Yusof, S. R. & Begley, D. J. (2010). Structure and function of the blood–brain barrier. *Neurobiology of Disease* **37**, 13-25.
9. Pardridge, W. M. (2012). Drug transport across the blood-brain barrier. *J Cereb Blood Flow Metab* **32**, 1959-1972.
10. Wager, T. T., Chandrasekaran, R. Y., Hou, X., Troutman, M. D., Verhoest, P. R., Villalobos, A. & Will, Y. (2010). Defining Desirable Central Nervous System Drug Space through the Alignment of Molecular Properties, in Vitro ADME, and Safety Attributes. *ACS Chemical Neuroscience* **1**, 420-434.
11. Li, Y. T. & Yu, J. Y. (2010). *40th International Conference on Computers and Industrial Engineering: Soft Computing Techniques for Advanced Manufacturing and Service Systems, CIE40 2010*.
12. Nicolaou, K. C. (2014). Advancing the drug discovery and development process. *Angewandte Chemie - International Edition* **53**, 9128-9140.
13. Milardi, D. & Pappalardo, M. (2015). Molecular dynamics: New advances in drug discovery. *European Journal of Medicinal Chemistry* **91**, 1-3.
14. Kola, I. & Landis, J. (2004). Can the pharmaceutical industry reduce attrition rates? *Nature reviews Drug discovery* **3**, 711-716.
15. Wang, J. & Urban, L. (2004). The impact of early ADME profiling on drug discovery and development strategy. *DDW DRUG DISCOVERY WORLD* **5**, 73-86.
16. Gallo, J. M. (2010). Pharmacokinetic/Pharmacodynamic‐Driven Drug Development. *Mount Sinai Journal of Medicine: A Journal of Translational and Personalized Medicine* **77**, 381-388.

17. Hughes, J. P., Rees, S. S., Kalindjian, S. B. & Philpott, K. L. (2011). Principles of early drug discovery. *British Journal of Pharmacology* **162**, 1239-1249.
18. Castellino, S., O'Mara, M., Koch, K., Borts, D. J., Bowers, G. D. & MacLauchlin, C. (2012). Human metabolism of lapatinib, a dual kinase inhibitor: Implications for hepatotoxicity. *Drug Metabolism and Disposition* **40**, 139-150.
19. Kim, K. J., Yoon, Y. W. & Chung, J. M. (1997). Comparison of three rodent neuropathic pain models. *Experimental Brain Research* **113**, 200-206.
20. Chung, J. M., Kim, H. K. & Chung, K. (2004). Segmental spinal nerve ligation model of neuropathic pain. *Methods in molecular medicine* **99**, 35-45.
21. Kim, S. H. & Chung, J. M. (1992). An experimental model for peripheral neuropathy produced by segmental spinal nerve ligation in the rat. *Pain* **50**, 355-363.
22. Leung, S. C., Gibbons, P., Amewu, R., Nixon, G. L., Pidathala, C., Hong, W. D., Pacorel, B., Berry, N. G., Sharma, R., Stocks, P. A., Srivastava, A., Shone, A. E., Charoensutthivarakul, S., Taylor, L., Berger, O., Mbekeani, A., Hill, A., Fisher, N. E., Warman, A. J., Biagini, G. A., Ward, S. A. & O'Neill, P. M. (2012). Identification, Design and Biological Evaluation of Heterocyclic Quinolones Targeting Plasmodium falciparum Type II NADH:Quinone Oxidoreductase (PfNDH2). *Journal of Medicinal Chemistry* **55**, 1844-1857.
23. Cooke, A., Anderson, A., Buchanan, K., Byford, A., Gemmell, D., Hamilton, N., McPhail, P., Miller, S., Sundaram, H. & Vijn, P. (2001). Water-soluble propofol analogues with intravenous anaesthetic activity. *Bioorganic and Medicinal Chemistry Letters* **11**, 927-930.
24. Ahrens, J., Haeseler, G., Leuwer, M., Mohammadi, B., Krampfl, K., Dengler, R. & Bufler, J. (2004). 2,6 di-tert-butylphenol, a nonanesthetic propofol analog, modulates alpha1beta glycine receptor function in a manner distinct from propofol. *Anesth Analg* **99**, 91-6.
25. Ahrens, J., Leuwer, M., de la Roche, J., Foadi, N., Krampfl, K. & Haeseler, G. (2009). The non-anaesthetic propofol analogue 2,6-di-tert-butylphenol fails to modulate GABA(A) receptor function. *Pharmacology* **83**, 95-8.
26. Cernak, T., Dykstra, K., Levorse, D., Verras, A., Balkovec, J., Nargund, R. & DeVita, R. (2011). Synthesis of oxaspiropiperidines as a strategy for lowering logD. *Tetrahedron Letters* **52**, 6457-6459.
27. Roberts, M. S., Magnusson, B. M., Burczynski, F. J. & Weiss, M. (2002). Enterohepatic circulation: physiological, pharmacokinetic and clinical implications. *Clin Pharmacokinet* **41**, 751-90.
28. Pestel, S., Martin, H. J., Maier, G. M. & Guth, B. (2006). Effect of commonly used vehicles on gastrointestinal, renal, and liver function in rats. *Journal of Pharmacological and Toxicological Methods* **54**, 200-214.
29. Jacob, S. W. & Herschler, R. (1986). Pharmacology of DMSO. *Cryobiology* **23**, 14-27.
30. Willson, J. E., Brown, D. E. & Timmens, E. K. (1965). A toxicologic study of dimethyl sulfoxide. *Toxicology and Applied Pharmacology* **7**, 104-112.
31. Hartung, T. (2013). Food for Thought Look Back in Anger – What Clinical Studies Tell Us About Preclinical Work. *ALTEX* **30**, 275-291.

32. Li, A. P. (2009). Overview: Evaluation of metabolism-based drug toxicity in drug development. *Chemico-Biological Interactions* **179**, 1-3.
33. Stephens, C., Andrade, R. J. & Lucena, M. I. (2014). Mechanisms of drug-induced liver injury. *Current Opinion in Allergy and Clinical Immunology* **14**, 286-292.
34. Regev, A. (2014). Drug-induced liver injury and drug development: industry perspective. *Semin Liver Dis* **34**, 227-39.
35. Choi, J. M., Oh, S. J., Lee, J. Y., Jeon, J. S., Ryu, C. S., Kim, Y. M., Lee, K. & Kim, S. K. (2015). Prediction of Drug-Induced Liver Injury in HepG2 Cells Cultured with Human Liver Microsomes. *Chem Res Toxicol* **28**, 872-85.
36. Ju, C. & Reilly, T. (2012). Role of immune reactions in drug-induced liver injury (DILI). *Drug Metab Rev* **44**, 107-15.
37. Williams, C. D. & Jaeschke, H. (2012). Role of innate and adaptive immunity during drug-induced liver injury. *Toxicology Research* **1**, 161-170.
38. Lavandera, J. V., Parera, V. E., Batlle, A. & Buzaleh, A. M. (2006). CYP2D6 Polymorphisms in Patients with Porphyrias. *Molecular Medicine* **12**, 259-263.
39. Cohen, L. H., Remley, M. J., Raunig, D. & Vaz, A. D. N. (2003). In vitro drug interactions of cytochrome p450: An evaluation of fluorogenic to conventional substrates. *Drug Metabolism and Disposition* **31**, 1005-1015.
40. Nayadu, S., Behera, D., Sharma, M., Kaur, G. & Gudi, G. (2013). Fluorescent probe based CYP inhibition assay: A high throughput tool for early drug discovery screening. *International Journal of Pharmacy and Pharmaceutical Sciences* **5**, 303-307.
41. Gad, S. C. *Preclinical Development Handbook: ADME and Biopharmaceutical Properties. [electronic book]*. Online access via Linkfinder: EBSCO eBook Clinical Collection (EBSCOhost), John Wiley & Sons Incorporated.
42. Nassar, A. F., Hollenberg, P. F. & Scatina, J. (2009). *Drug metabolism handbook. [electronic book] : concepts and applications*. Online access with purchase: Wiley-Blackwell online books, Hoboken, New Jersey : Wiley-Blackwell, 2009.
43. Wodarski, R., Clark, A. K., Grist, J., Marchand, F. & Malcangio, M. (2009). Gabapentin reverses microglial activation in the spinal cord of streptozotocin-induced diabetic rats. *Eur J Pain* **13**, 807-11.
44. Huang, X.-P., Mangano, T., Hufeisen, S., Setola, V. & Roth, B. L. (2010). Identification of Human Ether-à-go-go Related Gene Modulators by Three Screening Platforms in an Academic Drug-Discovery Setting. *Assay and Drug Development Technologies* **8**, 727-742.
45. Vieweg, W. V. & Wood, M. A. (2004). Tricyclic antidepressants, QT interval prolongation, and torsade de pointes. *Psychosomatics* **45**, 371-7.
46. Mortelmans, K. & Zeiger, E. (2000). The Ames Salmonella/microsome mutagenicity assay. *Mutat Res* **455**, 29-60.
47. Wager, T. T., Hou, X., Verhoest, P. R. & Villalobos, A. (2010). Moving beyond rules: The development of a central nervous system multiparameter optimization (CNS MPO) approach to enable alignment of druglike properties. *ACS Chemical Neuroscience* **1**, 435-449.

48. Schönherr, H. & Cernak, T. (2013). Profound Methyl Effects in Drug Discovery and a Call for New C□H Methylation Reactions. *Angewandte Chemie International Edition* **52**, 12256-12267.
49. Deyrup, J. A. (2008). Aziridines. In *Chemistry of Heterocyclic Compounds*, pp. 1-214. John Wiley & Sons, Inc.
50. Park, B. K., Kitteringham, N. R. & O'Neill, P. M. (2001). Metabolism of fluorine-containing drugs. In *Annual Review of Pharmacology and Toxicology*, Vol. 41, pp. 443-470.
51. Burkhard, J. A., Wuitschik, G., Rogers-Evans, M., Müller, K. & Carreira, E. M. (2010). Oxetanes as versatile elements in drug discovery and synthesis. *Angewandte Chemie - International Edition* **49**, 9052-9067.
52. Burkhard, J. A., Wagner, B., Fischer, H., Schuler, F., Müller, K. & Carreira, E. M. (2010). Synthesis of azaspirocycles and their evaluation in drug discovery. *Angewandte Chemie - International Edition* **49**, 3524-3527.
53. Wright, J. L., Gregory, T. F., Kesten, S. R., Boxer, P. A., Serpa, K. A., Meltzer, L. T., Wise, L. D., Espitia, S. A., Konkoy, C. S., Whittemore, E. R. & Woodward, R. M. (2000). Subtype-selective N-methyl-D-aspartate receptor antagonists: Synthesis and biological evaluation of 1-(heteroarylalkynyl)-4-benzylpiperidines. *Journal of Medicinal Chemistry* **43**, 3408-3419.
54. Wilkening, R. R., Ratcliffe, R. W., Fried, A. K., Meng, D., Sun, W., Colwell, L., Lambert, S., Greenlee, M., Nilsson, S., Thorsell, A., Mojena, M., Tudela, C., Frisch, K., Chan, W., Birzin, E. T., Rohrer, S. P. & Hammond, M. L. (2006). Estrogen receptor β-subtype selective tetrahydrofluorenones: Use of a fused pyrazole as a phenol bioisostere. *Bioorganic and Medicinal Chemistry Letters* **16**, 3896-3901.
55. http://www.cyprotex.com/admepk/in-vitro-metabolism/microsomal-stability.
56. http://www.cyprotex.com/admepk/in-vitro-metabolism/cytochrome-p450-inhibition.
57. Fuhr, U., Strobl, G., Manaut, F., Anders, E. M., Sorgel, F., Lopez-de-Brinas, E., Chu, D. T., Pernet, A. G., Mahr, G., Sanz, F. & et al. (1993). Quinolone antibacterial agents: relationship between structure and in vitro inhibition of the human cytochrome P450 isoform CYP1A2. Mol Pharmacol 43, 191-9.
58. Backonja, M. & Glanzman, R. L. (2003). Gabapentin dosing for neuropathic pain: Evidence from randomized, placebo-controlled clinical trials. Clinical Therapeutics 25, 81-104.
59. Wiffen, P. J., Derry, S. & Moore, R. A. (2011). Lamotrigine for acute and chronic pain. Cochrane Database Syst Rev 16.

Chapter 4

Conclusions

Table of Contents

4.1 Conclusions

4.1.1 Summary of Lead Optimisation

This project was focussed on the lead optimisation of positive allosteric modulators of SSGRs. These compounds are being developed with the aim to produce a new therapeutic for the treatment of chronic pain. Chronic pain is a condition that is thought to affect roughly about 20% of adults in Europe[1]. It is a disease that can develop as part of old age, as a by-product of degenerative diseases or aa the result of external factors, such a surgical nerve injury or chemotherapy[2]. Any pain that persists for more than six months or occurs without a clear stimulus can be classified as chronic pain. The three main characteristics of chronic pain are allodynia, hyperalgesia and spontaneous activity. According to recent surveys, only one third of chronic pain sufferers in the UK seek therapy and more than half of these patients will discontinue their treatments due to insufficient pain relief and adverse-effects[1]. Many of these issues may arise because the drugs prescribed were intended to treat chronic pain and have merely been adapted to this purpose. There is a great need for new treatments that are specifically designed to target the underlying mechanisms of chronic pain.

SSGRs containing the α3 subunit are known to be down-regulated in animal models of neuropathic pain. It is also known that drugs can produce analgesia by potentiating glycine currents[3]. Positive allosteric modulators acting on GlyRα1 may able to compensate for the inhibitory glycinergic activity that is reduced in chronic pain. Potential modulators were developed from the anaesthetic propofol, which is able to activate glycine receptors at high concentrations. Propofol normally causes sedation through the modulation of inhibitory

$GABA_A$Rs, which are co-localised with GlyRs within the spinal cord. Research has shown than activation of GlyRs over $GABA_A$Rs can produce analgesia without sedation[4]. It has also been reported that halogenated analogues of propofol show a greater degree of selectivity for GlyRs over $GABA_A$Rs[5; 6]. Upon this rationale, a series of propofol analogues was synthesised and tested at recombinant GlyRs containing the α1 subunit.

Throughout lead optimisation, seven analogues stood out as the most promising drug candidates. The structures of the lead compound, LT-01-25 and six back-up compounds are shown in Figure 4.1. Although LT-01-25 was not the most potent analogue nor did it have the highest MPO score, overall it proved to be the most effective compound in attenuating allodynia and hyperalgesia in models of neuropathic pain.

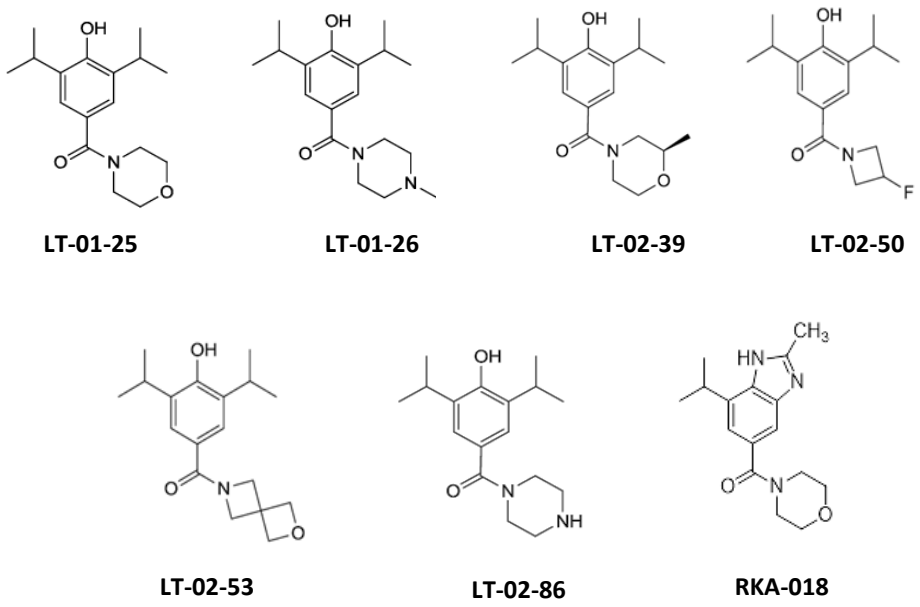

Figure 4.1. Structures of propofol analogues with the most promising candidate profiles.

Many of the analogues created within the project exhibited higher efficacy at GlyRα1 than propofol. Unfortunately many of these compounds also displayed high ClogP, ClogD and pKa. Following the 'rule of five', these analogues would be considered to have poor drug-like properties[7]. It is recommended that drugs acting in the CNS have physiochemical properties within a particular range. The MPO algorithm created by Pzifer can be used to assess to the likelihood of CNS penetration[8]. Lead candidates should have an MPO score above 4 and must elicit the desired response at the target receptor (GlyRα1 EC_{50} = 1μM). The seven analogues that had the best MPO assessment profiles are shown in Table 4.1.

Table 4.1. The physiochemical properties and MPO scores for positive allosteric modulators of GlyRs: Propofol analogues designed as positive allosteric modulators of GlyRs. The analogues are ranked by CNS MPO score. The individual parameters are coloured coded in accordance with the recommended values for dugs acting in the CNS[8].
**Physiochemical parameters and MPO scores were provided by the Department of Chemistry*.

Parameter	LT-02-86	RKA-018	LT-01-26	LT-01-25	LT-02-50	LT-02-53	LT-02-39
ClogP	3.10	2.21	3.54	3.10	3.30	3.30	3.60
ClogD	1.92	2.50	2.50	2.80	3.57	3.93	3.90
TPSA (Å)	52.27	53.93	43.78	49.8	40.54	49.77	49.77
MW (Da)	290.40	287.36	304.43	291.1	279.35	303.34	305.41
HBD	1.00	1.00	1.00	1.00	1.00	1.00	1.00
PKa	10.14	13.10	10.10	10.14	9.77	10.10	10.08
MPO Score	4.8	4.6	4.4	4.3	4.0	3.7	3.6

Through the use of MPO evaluation, five analogues in the project were able to meet the desired MPO score (≥4). Two additional analogues, LT-02-53 and LT-02-39, did not have a desirable MPO score but were including in optimising because of their extreme potency at GlyRα1. The first two analogues to produce successful MPO profiles were the amide

analogues, LT-01-25 and LT-01-26. The amide analogues, particularly LT-01-25, generated very promising results in other aspects of optimisation.

The pKa of these analogues was considered too high for successful penetration of the BBB however the compounds tested in the Chung model were able to attenuate neuropathic pain and LT-01-25 demonstrated good exposure within the CSF. MPO evaluation revealed that despite high pKa the compounds can still access the CNS. Table 4.1 shows that the analogues with the highest pKa values, LT-02-86 and RKA-018 had the best MPO scores as a result of low ClogP and ClogD. This emphasises the usefulness of MPO evaluation in the assessment of new analogues.

Good potency at the GlyRα1 was one of the first and most significant measures carried out during the optimisation of these GlyR modulators. Target efficacy was measured through the use of electrophysiology. The test compounds were exposed to recombinant GlyRα1 in the presence of glycine (10μM) and the current response was recorded. In order to continue optimisation the analogues must have an EC_{50} value below 1μM. To ensure good selectivity, the analogues were also tested at $GABA_AR$; none of the analogues were able to activate GAB_AR below 30μM. While many compounds showed sufficient activity at GlyRα1, only the testing results for the seven analogues shown in Table 4.1 are presented below (Table 4.2).

Table 4.2. Ranked GlyRα1 EC_{50} values of propofol analogues: The propofol analogues that displayed the highest efficacy at the target receptor.
**GlyRα1 data was collected at the University of Tübingen.*

Analogue	GlyRα1 EC_{50}
LT-02-86	137aM
LT-01-26	1.2pM
LT-02-50	1.2pM
LT-02-53	1.6pM
LT-02-39	60pM
LT-01-25	350pM
RKA-018	4.2nM

All the analogues with a MPO score above 4, were successfully able to potentiate glycine currents to a greater extent than propofol (EC_{50} = 4.8μM[9]). The most potent compound was the piperazine analogue, LT-02-86, which was able to activate GlyRs at attomolar (10^{-18}M) concentration; LT-02-86 also produced the best MPO profile. On this basis, LT-02-86 would make a more suitable lead compound than LT-01-25, which was the second least potent compound and had less favourable physiochemical properties.

MPO assessment and GlyRα1 efficacy testing are extremely useful tools to determine which compounds are best suited to be taken into further testing. The aim of lead optimisation is to generate a drug candidate that will eventually be used by patients; therefore it is important to keep in mind the numerous external and internal factors that may have an effect of success of a drug. As such, extraordinary potency at the isolated drug target may not translate to an effective therapeutic in humans. Drug metabolism and

pharmacokinetics play a huge role in how a drug acts within in a living organism. The first step in studying pharmacokinetics as part of lead optimisation is to determine phase I metabolism by CYPs.

Propofol analogues were incubated with both rat and human liver microsomes. The goal of these experiments was to test the extent by which the analogues are broken-down by CYPs. These analogues are designed to be administered orally, and so they must be absorbed from the GI tract, but first they must pass through the liver where they will come into contact with CYPs. Compounds that are microsomally stable will be absorbed into the blood rather than being broken-down, meaning there is more free drug available to move into the CNS. From the data collected in microsomal incubations, the half-life, clearance by CYPs and intrinsic clearance values were calculated. The microsomal parameters for the seven lead candidate analogues are shown in Table 4.3 and Table 4.4

Table 4.3. Microsomal parameters of lead analogues in rat liver microsomes: The analogues are ranked from most to least metabolically stable. A long half-life and low clearance indicates a low level of CYP mediated metabolism.

RLM	$T_{1/2}$ (min)	Cl_{CYP} (µL/min/mg)	Cl_{int} (mL/min/kg)
LT-01-25	770	0.9	1.6
RKA-018	135	5.1	9.1
LT-02-53	106	6.5	11.7
LT-02-86	103	6.7	12
LT-02-39	86	8	14
LT-02-50	70	9.9	17.7
LT-01-26	46	15	26.88

LT-01-25 was by far the most stable compound when incubated with rat liver microsomes. The amide morpholine analogue had an extremely long half-life and underwent very little microsomal break-down. RKA-018, the least potent analogue also demonstrated good rat microsomal stability. LT-02-86, which had the best MPO and EC_{50} values, experienced some CYP mediated metabolism. The analogue with the highest incidence of break-down in rat microsomes was LT-01-26. This analogue was almost completely metabolised in rats and had a very short half-life. LT-01-26 produced the second best response at the GlyRα1 and had one of the highest MPO scores; however poor metabolic stability would make it an unsuitable lead candidate. Interestingly, this analogue demonstrated much better stability in human liver microsomes.

Table 4.4. Microsomal parameters of lead analogues in human liver microsomes: The analogues are ranked from most to least metabolically stable. A long half-life and low clearance indicates a low level of CYP mediated metabolism.

HLM	$T_{1/2}$ (min)	Cl_{CYP} (µL/min/mg)	Cl_{int} (mL/min/kg)
LT-01-25	533	1.3	1.75
LT-02-53	407	1.7	2.1
RKA-018	330	2.1	2.6
LT-01-26	126	5.8	6.9
LT-02-39	96	7.2	9
LT-02-86	95	7.3	9
LT-02-50	47	14.7	18.5

Differences in microsomal stability between rat and human liver microsomes are most likely caused by variations in CYP isoform expression for each species[10]. In human

microsomes, LT-01-25 was still the most stable, although the differences in the stability between the analogues were much smaller. The least stable compound was LT-02-50, a spirocyclic analogue with a low MPO score. LT-02-50 had a much higher clearance value than propofol, the analogue was also extensively metabolised in rat microsomes. This analogue would be considered a highly metabolic compound[11]. LT-01-26 did not undergo the same level of breakdown in human microsomes. In fact, this analogue was fairly metabolically stable. The most potent analogue, LT-02-86 was significantly metabolised in humans. This means that LT-02-86 is likely to have much lower exposure in the CNS.

Based on the data from CYP phase I metabolism testing, LT-01-25 has the most potential as a lead candidate. However, hydroxylation by CYPs is just one of two main routes of propofol metabolism; the other major metabolic pathway is glucuronidation of the phenol group. The most effective way to test for alternate routes of metabolism is through *in vivo* metabolism. Measuring metabolism in a living system not only allows conjugative biotransformation to be investigated but also how external factors such as diet and formulation, along with numerous internal factors may affect ADME as a whole.

The amide analogues, LT-01-25 and LT-01-26 were administered orally (10mg/Kg) to male, Wistar rats. Pilot experiments carried out using LT-01-25, explored the effect of fasting on metabolism; LT-01-25 appeared to undergo enterohepatic circulation, resulting in slow absorption. In the original vehicle (10% DMSO, 10% solutol and 80% saline), fasting prior to dosing had a huge effect on absorption. The calculated C_{max} and T_{max} were much higher in fasted rats, indicating that food does slow absorption. The original vehicle contained DMSO, which can have an effect on absorption and is thought to have mild inflammatory properties.

An alternate SSV was chosen (0.5% sodium carboxymethylcellulose, 0.5% benzyl alcohol, 0.4 Tween 80 and 98.6% saline). Fasting appeared to have less of an impact when the SSV was used. The new vehicle seemed to slow absorption slightly; though the overall exposure in the plasma was higher than seen in the DMSO containing vehicle. The SSV is considered to be more innocuous than DMSO and the effect on metabolism, however small, was positive. It was decided that LT-01-26 would be formulated in the SSV rather than the original vehicle. In addition, extensive hepatic re-circulation was not seen in experiments using SSV, so LT-01-26 was not tested in fasted rats. The pharmacokinetic parameters for LT-01-25 and LT-01-26 are shown in Table 4.5.

Table 4.5. Pharmacokinetic parameters of amide propofol analogues: LT-01-25 and LT-01-26 were administered orally to non-fasted, male, Wistar rats (10mg/Kg, SSV). Pharmacokinetic parameters calculated using PK Solutions, in an one-compartmental analysis.

Parameters	LT-01-25	LT-01-26
AUC (min*µg/mL)	1140	273
C_{max} (µg/mL)	2.1	0.5
T_{max} (min)	15	18
$t_{1/2}$ (min)	217	72
CL (mL/hr/kg)	0.5	2.2
V_d (L/Kg)	2.7	3.7

LT-01-26 was absorbed a little slower than LT-01-25; however the maximum exposure in the plasma is almost 4x less. This could possibly be due to large amounts of CYP mediated metabolism reducing the amount of free drug available for absorption. The pharmacokinetic

parameters for LT-01-26 tie in with the microsomal parameters. As seen with microsomal incubations the half-life of LT-01-25 was much higher than that of LT-01-26. The clearance and distribution for both compounds are within the desired range. Low exposure in plasma would suggest low exposure within the CNS, while LT-01-26 is more potent and more drug-like, it may be not be as effective in a living organism.

For the remaining analogues, *in vivo* metabolism was carried out by ChemPartners' DMPK group. In these studies, fasted, male, Wistar rats were dosed orally at 10 mg/Kg. The original DMSO based vehicle was used. These studies are currently being conducted; as such a complete data set for each analogue is not available. The pharmacokinetic parameters that have been provided by ChemPartners, at present, are shown in Table 4.6, LT-01-25 was also tested to give a comparison under the same experimental conditions.

Table 4.6. Pharmacokinetic parameters provided by ChemPartners: Fasted, male, Wistar rats were dosed at 10mg/Kg (P.O. 10% DMSO, 10% solutol, 80% saline). Data collection and analysis was carried out by ChemPartners.

	LT-01-25	**LT-02-39**	**LT-02-50**	**LT-02-86**
T_{max} (min)	30	40	30	60
C_{max} (ng/mL)	4.6	3.7	0.9	0.6
$T_{1/2}$ (min)	2.5	154.2	154.8	184.8
CL (L/hr/kg)	0.43	--	1.64	2.11
F (%)	85.9	--	38.8	74

The *in vivo* metabolic studies carried out by ChemPartners show that LT-01-25 has the highest bioavailability of all the compounds. This value is also close to the bioavailability calculated from in house metabolism experiments (81.9%). LT-02-86, the most potent compound at the target, had a high bioavailability as well; however the exposure in plasma was far lower than that of LT-01-25. This analogue also took twice as long to reach maximum plasma concentration, suggesting slow absorption; poor absorption could be the result of CYP break-down. LT-02-50, a compound that underwent almost complete microsomal breakdown, also demonstrated low plasma concentration levels. The compound was absorbed as quickly as LT-01-25, suggesting that poor exposure in this case is due to the rapid metabolism by CYPs.

One compound that did demonstrate high plasma exposure was the monomethyl analogue, LT-02-39. This compound was highly metabolised by CYPs, due to the vulnerable methyl group, so it is interesting that the plasma concentration level is so high. It is possible that LT-02-39 is a highly permeable compound. This analogue was not absorbed as efficiently as LT-01-25, but it was much better than LT-02-50 and LT-02-86. A complete data-set is not yet available for LT-02-39, as such the bioavailability and potential exposure at the target cannot be commented on. LT-02-53 and RKA-018 are waiting testing, so no data is available for these analogues. These compounds were stable in rat liver microsomes, beaten by only LT-01-25, so it is probable that they will have similar *in vivo* pharmacokinetic profiles.

Along with pharmacokinetics, establishing safety pharmacological profiles is becoming a significant part of early drug development. Toxicity is one of the major causes of failure at both pre-clinical and clinical stages. Metabolism related toxicity plays a substantial role in drug candidate failure. This type of toxicity can be caused by the build-up of toxic drugs or by the formation of enzyme adducts. The inhibition of CYPs can be indicated in both of these processes; CYPs are responsible for more than 70% of marketed drugs. If these vital enzymes are inhibited then, there could be a build-up leading to overdose. Drug and their metabolites may also inhibit an enzyme through conjugation; this could trigger the necrotic pathways that lead to the death of healthy hepatocytes. Investigating CYP inhibition is something that can be carried out during lead optimisation and will help refine the safety profiles of drug candidates.

The seven candidate analogues were testing using fluorescence based CYP inhibition kit developed by Life Technologies. In this kit, a substrate tagged with dye is incubated with different CYP isoforms and the test compound. Successful metabolism causes the dye to emit fluorescence; the level of fluorescence is used as a measure of metabolism. A vehicle control and positive control are used for comparison. The vehicle control is taken as no inhibition, while the positive control (a known CYP inhibitor) is taken as high inhibition. The data presented in Table 4.7, is the percentage inhibition from the vehicle control. The five isoforms tested are thought be responsible for most CYP related toxicity.

Table 4.7. Inhibition of five major CYP isoforms by propofol analogues: Five major CYP isoforms associated with negative enzyme-drug interactions were incubated with analogues of propofol. A recommended inhibitor of each isoform was used a positive control. The data is expressed as percentage inhibition from the vehicle control (interpreted as no inhibition) at the highest testing concentration (10μM). Drugs that produced more than 50% inhibition are highlighted.

Compound	CYP1A2	CYP2C9	CYP2C19	CYP2D6	CYP3A4
Positive Control	**94%**	**59%**	**97%**	**70%**	**74%**
LT-01-25	7%	2%	32%	30%	30%
LT-01-26	16%	15%	29%	3%	6%
LT-02-39	7%	42%	**63%**	21%	24%
LT-02-50	45%	2%	2%	38%	24%
LT-02-53	13%	40%	43%	35%	30%
LT-02-86	26%	40%	43%	15%	7%
RKA-018	26%	11%	33%	38%	17%

Weak CYP inhibitors are classed as drugs with an IC_{50} above 10μM[12]. None of the analogues were able to produce more than 50% inhibition across all CYP isoforms, with the exception of LT-02-39. LT-02-39 inhibited CYP2C19 by 63% at 10μM. Using an inhibition-concentration plot the IC_{50} was calculated to be 9.4μM. This means that LT-02-39 is considered a moderate inhibitor on CYP2C19, however the value is extremely close to the recommended $IC_{50} \geq 10\mu M$[12]. LT-02-39 underwent substantial CYP metabolism, which may be contributing to high inhibition percentage by occupying the catalytic sites, thus reducing the amount of enzymes free to metabolise the tagged substrate.

There was no obvious pattern to the mild inhibition produced by the other analogues. Some isoforms were barely affected, whilst others experienced some inhibition. LT-01-25 and LT-01-26 appeared to have the least inhibitory effect across all analogues. LT-01-26 only resulted in more than 20% inhibition in one isoform, CY2C19. While, the highest level of inhibition caused by LT-01-25 was 32% in the same isoform. LT-02-53 and RKA-018 caused at least 10% across all analogues, making them the most inhibitory analogues on average. LT-02-53 was only able to achieve less than 10% in CYP1A2. The same was true for LT-02-86 acting on CYP3A4. While most of the analogues would be considered weak inhibitors, LT-01-25 and LT-01-26 proved to be the lowest inhibition overall. The data suggests that these analogues will not trigger DILI through the formation of protein adducts nor will they cause negative drug-drug interactions through the inhibition of phase I metabolism. Additional safety testing is still ongoing, notably the genotoxicity Ames test, hepatoxicity and hERG cardiotoxicity. At present only LT-01-25 has a complete safety profile.

The next key aspect of the lead optimisation process is to prove effectiveness in an animal model of the target disease. The end-goal of any lead optimisation process is to produce a compound that will eventually be used as a drug in the treatment of a particular disease. Everything from potency at the isolated receptor to pharmacokinetics can ultimately affect how a drug acts within the body. The usefulness and safety of a drug within man cannot be entirely predicted through the use of individual pharmacological testing. These tests are beneficial for selecting the most promising candidates, to ensure that animals are not used needlessly. However it is essential that a drug be tested against the target disease in a living organism.

Chronic pain can develop as a result of numerous diseases and injuries. Spinal nerve damage is one of the main contributing factors, as it can be caused by both injury and degenerative disease[13]. Ligation or axotomy of a nerve leads to the rapid development of neuropathic pain; an aspect of chronic pain that is extremely difficult to treat[14]. It was decided that a chronic pain model based on nerve ligation would be the most suitable proof of concept model. The Chung lesion model of nerve injury was used to develop a state of neuropathic pain. Response to an innocuous stimulus was measured as mechanical allodynia, while hyperalgesia was measured as response to a noxious cold. Behavioural baselines were taken pre-surgery and pre-dose to ensure that the rats had developed neuropathic pain. Rats were tested with the test analogue at three concentrations. The positive controls were either gabapentin or lamotrigine, drugs commonly used to treat chronic pain. Analgesia was measured as percentage reversal from the pre-dose baseline. The maximum reversal of mechanical allodynia and the time taken to achieve it, for the analogues tested so far can be seen in Table 4.8.

Table 4.8. Maximum percentage reversal of mechanical allodynia in the Chung lesion model of neuropathic pain: LT-01-25, LT-01-26, LT-02-39 and LT-02-50 were tested at three concentrations in the Chung lesion pain model. Data is presented as a percentage reversal of the pre-dose baseline in mechanical allodynia behavioural tests. The highest reversal values are highlighted.

Compound/Dose (mg/Kg)	Max % Reversal	Time (hr)
LT-01-25 (3 mg/Kg)	65%	3 hrs
LT-01-25 (10 mg/Kg)	90%	3 hrs
LT-01-25 (30 mg/Kg)	**90%**	**3 hrs**
LT-01-26 (3 mg/Kg)	20%	3 hrs
LT-01-26 (10 mg/Kg)	70%	3 hrs
LT-01-26 (30 mg/Kg)	**75%**	**3 hrs**
LT-02-39 (3 mg/Kg)	5%	3 hrs
LT-02-39 (10 mg/Kg)	55%	3 hrs
LT-02-39 (30 mg/Kg)	**85%**	**3 hrs**
LT-02-50 (3 mg/Kg)	0%	3 hrs
LT-02-50 (10 mg/Kg)	20%	3 hrs
LT-02-50 (30 mg/Kg)	**20%**	**3 hrs**

At this time, testing for LT-02-53, LT-02-86 and RKA-018 is still being undertaken. From the data available it can be seen that LT-01-25 is able to produce the highest level of analgesia at every testing concentration, and did outperform the control analgesic lamotrigine (data not shown). Out of the analogues tested in Chung lesion model, LT-01-25 produced lowest response at isolated recombinant GlyR, but had the strongest pharmacokinetic profile. It is possible that strong metabolic resistance it contributing to high exposure within the CNS, allowing LT-01-25 to exert a greater response. LT-02-50 the least metabolically stable

compound was one of the most potent compounds at GlyRα1. This effect was not reflected in the Chung lesion testing results. Not only was LT-02-50 the least effective compound but it was not able to outperform the control analgesic. LT-01-26 and LT-02-39 both performed amenably, although the effect was not maintained at lower doses, suggesting low exposure at the target. The effect on cold hyperalgesia was also tested and the results are displayed in Table 4.9.

Table 4.9. Maximum percentage reversal of cold hyperalgesia in the Chung lesion model of neuropathic pain: LT-01-25, LT-01-26, LT-02-39 and LT-02-50 were tested at three concentrations in the Chung lesion pain model. Data is presented as maximum percentage reversal of the pre-dose baseline in cold hyperalgesia behavioural tests. The highest reversal values are highlighted.

Compound/Dose (mg/Kg)	Max % Reversal	Time (hr)
LT-01-25 (3 mg/Kg)	55%	1 hrs
LT-01-25 (10 mg/Kg)	88%	1 hrs
LT-01-25 (30 mg/Kg)	**95%**	**1 hrs**
LT-01-26 (3 mg/Kg)	20%	1 hrs
LT-01-26 (10 mg/Kg)	90%	3 hrs
LT-01-26 (30 mg/Kg)	**105%**	**3 hrs**
LT-02-39 (3 mg/Kg)	0%	3 hrs
LT-02-39 (10 mg/Kg)	65%	3 hrs
LT-02-39 (30 mg/Kg)	**110%**	**3 hrs**
LT-02-50 (3 mg/Kg)	5%	3 hrs
LT-02-50 (10 mg/Kg)	**25%**	**3 hrs**
LT-02-50 (30 mg/Kg)	20%	3 hrs

Overall, the analogues were more effective at attenuating hyperalgesia than allodynia; this suggests that the glycine receptor may play a more significant role in the malfunction of nociceptive neurons rather than non-nociceptive neurons. LT-01-26 and LT-02-39 were both able to outperform LT-01-25 in cold hyperalgesia behavioural tests. Although maximum reversal was achieved much slower; taking 3 hours as opposed to the 1 hour taken by LT-01-25. This may be suggestive of slow absorption of LT-01-26 and LT-02-39. The effect was not maintained at lower concentrations, where LT-01-25 produced at least 50% reversal at the lowest testing concentration. High metabolic stability of LT-01-25 is likely to result in higher exposure even at low concentrations, whereas LT-01-26 and LT-02-39 underwent extensive metabolism. Therefore, at lower concentrations, metabolic breakdown has considerably more impact of the amount of free drug remaining. As with mechanical allodynia, LT-02-50 had a minor impact on cold hyperalgesia, once again this analogue was unable to outperform the control analgesic. On a whole, LT-01-25 produced the most consistent level of analgesia despite not being particularly potent at GlyRα1 compared to the other analogues.

The lead optimisation process was driven by criteria set out in the drug target profile (Table 4.10). The target values in the profile are commonly used in early drug development[11; 15]. The analogues discussed above are still undergoing many of these tests. Only, LT-01-25 has been completely tested to these criteria and the analogue has met every desired value, except pKa. The concerns about high pKa are directly related to CNS penetration, however testing in a neuropathic pain model showed that even at a low dose (3 mg/Kg) was able to attenuate pain by at least 50%. This indicates that LT-01-25 is able to successful cross the BBB regardless of its high pKa.

Table 4.10. Target testing profile for lead optimisation

Parameter	Target
Physiochemical	
Aq. Sol (mg/mL)	0.01- 0.5mg/mL (pH7.4)
LogP	≤4
LogD	1-3
MW (Da)	≤450
TPSA (Å)	40-90
HBD	≤3
pKa	3-9
MPO	4≥
Selectivity	
GlyRα1 EC_{50}	≤1μM
$GABA_AR$ EC_{50}	≥ 100x GlyRα1 EC_{50}
Pharmacokinetics	
Oral Bioavailability (%)	≥20
$T_{1/2}$ (Rat Liver Microsomes)	≥60 min
$T_{1/2}$ (Human Hepatocytes)	≥30 min
Brain CSF	3x GlyRα1 EC_{50} (at 2/3 hrs, 1-3mg/Kg)
Protein Binding	≤99.5%
Toxicity	
hERG toxicity	IC_{50} ≥ 10μM
HepG2 toxicity	No tox at 50x GlyRα1 EC_{50}
AMES genotoxicity	negative
CYP Inhibition	IC_{50} ≥ 10μM

From the data available, all the analogues were able to achieve desired selectivity for GlyRα1 over $GABA_AR$. Two analogues, LT-01-26 and LT-02-50, failed to achieve a desired MPO

due to high ClogD and pKa. High pKa is a problem that persists across all the analogues, however many of them still achieved MPO over 4 and were able to have some effect in the Chung lesion model. LT-01-26 had a lower $T_{1/2}$ in rat liver microsomes that desired and was not able to meet the benchmark value. It should be noted that LT-02-50 was just able to beat the desired value by 10 minutes. The monomethyl analogue, LT-02-39 was the only analogue to have a toxicity alert via inhibition of CYP2C19. Although the IC_{50} (9.4μM) was very close to the desired value. Overall the analogues have produced very favourable testing profiles.

Complete testing has not been completed for the other analogues; as such a true comparison cannot be made. However, out of the data available, LT-01-25 would appear to be the most promising compound. This analogue produced the best pharmacokinetic profile and was the most effective and reliable analgesic in the Chung lesion model. While it neither was the most potent nor had the highest MPO, it did meet the desired values. There is a possibility that compounds like LT-02-86, (highest MPO and GlyRα1 EC_{50}) will achieve a greater level of analgesia and have a good safety profile. At present, however, LT-01-25 remains the leading analogue, primarily because of its strong pharmacokinetic profile and high metabolic stability. It is important to note that lead optimisation is not restricted to testing criteria set out in Table 4.9. There are many additional tests that can be incorporated into early drug development.

4.1.2 Further Development

While the other analogues are undergoing testing to develop a full target profile, LT-01-25 was carried into further development, namely effectiveness in an alternate animal model, dose-dependent toxicity and response in an *ex vivo* neuronal network. The neuronal electrophysiology studies will focus on wide dynamic range neurons (WDR). WDR neurons can exist as both interneurons and projection neurons[16]. These neurons are typically located in laminae V, much deeper than nociceptive primary afferents, however these neurons respond to inputs from Aβ, Aδ and C-fibres[17]. WDR neurons feature a 'wind-up' ability, which produces a greater response via repetitive stimulus[16]. These neurons are known to interact with inhibitory interneurons and are highly likely to express glycine receptors[17]. Such experiments will allow LT-01-25 to be tested under '*in vivo* like' conditions, in a way that is more mechanism specific than a whole animal pain model[18].

LT-01-25 is also being prepared for testing in an alternate chronic pain model, more specifically a diabetic pain model. Many diseases associated with chronic pain result in some form of nerve injury, a major contributor to neuropathic pain. Even so, it is highly important to remember that other aspects of disease may affect the development of pain and how a drug produces analgesia. Therefore it is extremely useful to test LT-01-25 in various different pain models. The diabetic model is a good choice as diabetes effects almost 4 million people in the UK and at least one quarter of diabetics experience some degree of chronic pain[19]. The diabetic pain model also includes changes in metabolism that may be seen in diabetic patients[20].

LT-01-25 is also undergoing *in vivo* dose-dependent toxicity studies. Assessment of safety pharmacology through the use of cell-based assays is useful to identifying highly toxic compounds; however the testing concentrations are very low in comparison to 'real-life' therapeutic doses. In addition, hypothetically a drug may not be completely metabolised before the next dose, causing build-up beyond the therapeutic dose. As such, toxicity up to and beyond therapeutic doses must be observed in a living organism. LT-01-25 will be tested in a dose dependant manner up to an extremely high dose, to measure the potential acute toxicity. This study, along with the ones mentioned previously, is just some of the aspects that make up the lead optimisation process.

This project is part of the early drug development of positive allosteric modulators of SSGRs. The work in this thesis has focussed on drug metabolism and pharmacokinetics as a part of the lead optimisation process. A strong pharmacokinetic profile can have a huge impact on the effectiveness of a drug, as demonstrated by LT-01-25. The development of LT-01-25 and other propofol analogues, is still on-going, however based on previous testing results, the prospects are highly promising.

4.2 References

1. Breivik, H., Collett, B., Ventafridda, V., Cohen, R. & Gallacher, D. (2006). Survey of chronic pain in Europe: Prevalence, impact on daily life, and treatment. *European Journal of Pain* **10**, 287-333.
2. Stemkowski, P. L., Biggs, J. E., Chen, Y., Bukhanova, N., Kumar, N. & Smith, P. A. (2013). Understanding and treating neuropathic pain. *Neurophysiology* **45**, 67-78.

3. Xiong, W., Cui, T., Cheng, K., Yang, F., Chen, S. R., Willenbring, D., Guan, Y., Pan, H. L., Ren, K., Xu, Y. & Zhang, L. (2012). Cannabinoids suppress inflammatory and neuropathic pain by targeting alpha3 glycine receptors. *J Exp Med* **209**, 1121-34.
4. Chen, Y., Dai, T. J. & Zeng, Y. M. (2007). Strychnine-sensitive glycine receptors mediate the analgesic but not hypnotic effects of emulsified volatile anesthetics. *Pharmacology* **80**, 151-157.
5. Ahrens, J., Leuwer, M., De La Roche, J., Foadi, N., Krampfl, K. & Haeseler, G. (2009). The non-anaesthetic propofol analogue 2,6-di-tert-butylphenol fails to modulate GABAA receptor function. *Pharmacology* **83**, 95-98.
6. de la Roche, J., Leuwer, M., Krampfl, K., Haeseler, G., Dengler, R., Buchholz, V. & Ahrens, J. (2012). 4-Chloropropofol enhances chloride currents in human hyperekplexic and artificial mutated glycine receptors. *BMC Neurology* **12**.
7. Wager, T. T., Chandrasekaran, R. Y., Hou, X., Troutman, M. D., Verhoest, P. R., Villalobos, A. & Will, Y. (2010). Defining Desirable Central Nervous System Drug Space through the Alignment of Molecular Properties, in Vitro ADME, and Safety Attributes. *ACS Chemical Neuroscience* **1**, 420-434.
8. Wager, T. T., Hou, X., Verhoest, P. R. & Villalobos, A. (2010). Moving beyond rules: The development of a central nervous system multiparameter optimization (CNS MPO) approach to enable alignment of druglike properties. *ACS Chemical Neuroscience* **1**, 435-449.
9. Haeseler, G., Ahrens, J., Krampfl, K., Bufler, J., Dengler, R., Hecker, H., Aronson, J. K. & Leuwer, M. (2005). Structural features of phenol derivatives determining potency for activation of chloride currents via α(1) homomeric and α(1)β heteromeric glycine receptors. *British Journal of Pharmacology* **145**, 916-925.
10. Cohen, L. H., Remley, M. J., Raunig, D. & Vaz, A. D. N. (2003). In vitro drug interactions of cytochrome p450: An evaluation of fluorogenic to conventional substrates. *Drug Metabolism and Disposition* **31**, 1005-1015.
11. Hughes, J. P., Rees, S. S., Kalindjian, S. B. & Philpott, K. L. (2011). Principles of early drug discovery. *British Journal of Pharmacology* **162**, 1239-1249.
12. http://www.cyprotex.com/admepk/in-vitro-metabolism/cytochrome-p450-inhibition.
13. Jay, G. W. & Barkin, R. L. (2014). Neuropathic pain: Etiology, pathophysiology, mechanisms, and evaluations. *Disease-a-Month* **60**, 6-47.
14. Jefferies, K. (2010). Treatment of neuropathic pain. *Seminars in Neurology* **30**, 425-432.
15. Segall, M. D. (2012). Multi-parameter optimization: Identifying high quality compounds with a balance of properties. *Current Pharmaceutical Design* **18**, 1292-1310.
16. Hanai, F. (1998). C fiber responses of wide dynamic range neurons in the spinal dorsal horn. *Clin Orthop Relat Res* **349**, 256-67.
17. D'Mello, R. & Dickenson, A. H. (2008). Spinal cord mechanisms of pain. *Br J Anaesth* **101**, 8-16.
18. Okamoto, K., Ishikawa, T., Abe, R., Ishikawa, D., Kobayashi, C., Mizunuma, M., Norimoto, H., Matsuki, N. & Ikegaya, Y. (2014). Ex vivo cultured neuronal networks emit in vivo-like spontaneous activity. *J Physiol Sci* **64**, 421-31.

19. https://www.diabetes.org.uk/Documents/Position%20statements/Facts%20and%20stats%20June%202015.pdf.
20. Morrow, T. J. (2004). Animal models of painful diabetic neuropathy: the STZ rat model. *Curr Protoc Neurosci* **9**.

Chapter 5

Experimental

Table of Contents

5.1 Microsomal Stability

5.1.1 Reagents and Solutions

Analogues of propofol were synthesised in University of Liverpool, Department of Chemistry (Liverpool, UK). High-Performance Liquid-Chromatography (HPLC) grade solvents, H_2O, MeOH, EtOAc and ACN, were purchased from Thermo Fisher Scientific (Loughborough, UK). $MgCl_2$, dimethyl sulfoxide (DMSO), reduced nicotinamide adenine dinucleotide phosphate (NADPH) and formic acid and were purchased from Sigma-Aldrich (Poole, UK). Rat and human liver microsomes, pooled from a group of 20 subjects (1mg protein/mL) and phosphate buffered saline (PBS - pH 7.4) were purchased from BD Biosciences (Oxford, UK). Test compound solutions and microsomes were stored at -80°C. All other reagents and solutions were stored at room temperature. Pre-prepared solutions required for the incubation assay were made as stated in Table 5.1.

Table 5.1: Pre-prepared solutions for incubation assay: Test compound and NAPDH solutions were made at 10x final concentration, MgCl2 solution was made at 25 x final concentration. PB = Phosphate buffer.

Phosphate Buffer (PB) (0.1M)	**10mL - PBS**	**40mL - H_2O**
$MgCl_2$ Solution (50mM)	**5.08mg - $MgCl_2$**	**500µL - PB**
Test Compound (20µM)	**50µL - 400µM dilution (From 10mM Stock in DMSO)**	**950µl - PB**
NADPH Solution (1mM)	**8.33mg - NADPH**	**1mL - PB**

5.1.2 Incubation assay

The reaction mixture consisted of 760µL phosphate buffer (final concentration = 0.1M), 40µL $MgCl_2$ solution (final concentration = 2mM), 50µL compound (final concentration = 1µM) and 50µL microsomes (1mg protein/mL) in a 1.5mL eppendorf. The reaction mix was incubated in a shaking incubator (37°C, 250 rpm) for 15 minutes. The reaction was started by the addition of 100µL NADPH (final concentration = 1mM) to make the final volume 1mL. The reaction was incubated for a further 60 minutes. Aliquots of 150µL were removed at time points 0, 10, 30 and 60 minutes. Samples were added to 150µL ice cold stop solution containing MeOH:ACN (1:1) and internal standard (IS) (LT-01-89 (26.6ng/mL) or LT-01-25 (133ng/mL)). LT-01-89 was the main IS, used in the analysis of all the analogues. For LT-01-89 experimental testing LT-01-25 was used as the IS. Samples were stored at -20°C for a minimum of 2 hours. Control reactions lacking NADPH were also carried out. Each reaction was carried out in duplicate.

5.1.3 Extraction and Analysis

When ready for extraction the samples were thawed at room temperature and centrifuged at 13,000 rpm for 10 minutes (4°C). 200µL of the supernatant was removed and added to 200µL of H_2O. 500µL of EtOAc was added and the samples were vortexed then centrifuged at 10,000 rpm for 1 minute. 400µL of the organic layer was removed and placed in a new 1.5mL eppendorf. A further 500µL of EtOAc was added and the process was repeated. The organic layer was dried at room temperature using nitrogen gas. The dried samples were stored at -

20°C until ready for analysis. For analysis by LC-MS the samples were reconstituted with 200µL MeOH/H_2O (1:1). Analysis was carried out using both LC-MS systems; the *Accela System* and *Agilent Infinity System.* The quantity of a compound was measured by the area under the curve (AUC) ratio of the analyte peak and IS peak. Microsomal stability was measured as a percentage of t=0. Mean (± standard deviation, SD) values were calculated (n=3).

Pharmacokinetic parameters, half-life ($t_{1/2}$), clearance per mg microsomal protein (Cl_{CYP}) and intrinsic Clearance (Cl_{int}) were calculated from the mean (±SD). The parameters were calculated using microsomal stability-time plots to determine the gradient, K and applying the following formulas[1]:

$$T_{1/2} = 0.693/K$$

$$Cl_{CYP} = [(final\ volume/microsomal\ protein\ concentration) * 0.693]/T_{1/2}$$

$$Clint = (0.693/T_{1/2}) * (1/microsomal\ protein\ concentration) * Scaling\ Factor\ ^{(Table\ 5.2)}$$

Table 5.2: Scaling factors used to calculate an approximate intrinsic clearance per Kg: Scaling factor was calculated as (microsomal protein per gram of liver) * (liver weight per kilogram of body weight)[1].

Species	Microsomal Protein (per g of Liver)	Liver Weight (per Kg of Body Weight)	Scaling Factor
Rat	44.8	40	1792
Human	48.8	25.7	1254.2

5.2 Cytochrome P450 Inhibition Assay

5.2.1 VIVID Cytochrome P450 Inhibition Screening Kit

Vivid® CYP450 Screening kits[2] contained Vivid® CYP450 reaction buffer (50mL, pH 8.0), CYP Baculosomes® plus P450 proteins (0.5mL, 0.5nM), Vivid® regeneration system (0.5mL 100x), Vivid® substrate (0.1mg) and $NADP^+$ (0.5mL, 10mM). The reaction buffer used was either buffer I (200mM) or buffer II (100mM). The appropriate buffer for each screening kit is shown in Table 5.3. The baculosomes consisted of recombinant CYP isoform, cytochrome p450 reductase and human cytochrome b_5. The regeneration system was made using 333mM glucose-6-phosphate and 30 units/mL glucose-6-phosphate dehydrogenase in 100mM phosphate buffer (pH 8.0). The $NADP^+$ was made up in 100mM phosphate buffer (pH8.0). Lyophilized Vivid® substrates were reconstituted with ACN as outlined in Table 5.4. Baculosomes, regeneration system and $NADP^+$ were stored at -80°C. The substrate was light-protected and stored at -20°C.

Table 5.3: Vivid® CYP450 Kit requirements: Adapted from Vivid® CYP450 Screening Kits User Guide[2].

Vivid® CYP450 Kit	Reaction Buffer	Vivid® Substrate	Positive Control (µM) (Final concentration)
Vivid® CYP1A2 Blue	I	Vivid® EOMCC Substrate	α-napthoflavone (10 µM)
Vivid® CYP2C9 Green	II	Vivid® BOMF Substrate	Sulfaphenazole (30 µM)
Vivid® CYP2C19 Blue	II	Vivid® EOMCC Substrate	Miconazole (30 µM)
Vivid® CYP2D6 Blue	I	Vivid® EOMCC Substrate	Quinidine (10 µM)
Vivid® CYP3A4 Red	I	Vivid® BOMR Substrate	Ketoconazole (10 µM)

Table 5.4: Vivid® Substrate requirements: Adapted from Vivid® CYP450 Screening Kits User Guide[2].

Vivid® Substrate	Volume of acetonitrile added (µL)	Varioskan™ Flash Multimode Reader	
		SkanIt™ Programme	Excitation/Emission (nm)
Vivid® EOMCC Substrate	205	CYP2D6BLUE	415/460
Vivid® BOMF Substrate	110	CYP2C9GREEN	490/520
Vivid® BOMR Substrate	150	CYP3A2RED	550/590

5.2.2 Materials and Solutions

VIVID Cytochrome P450 Inhibition Screening Kit was supplied by Life Technologies (Paisley, UK). Positive controls were purchased from Sigma-Aldrich. Black, untreated, clear-bottomed 96-well plates were purchased from Appleton Woods (Birmingham, UK). Test compound were made at 2.5 x final concentration (10 µM, 1 µM, 0.1 µM) in 1.25% DMSO/Reaction Buffer and stored at -80°C. The appropriate reaction buffer (Table 5.3) was prepared with H_2O (1:1) and was stored at room temperature. Dilution and reconstitution information was taken from the Vivid® CYP450 Screening Kits User Guide provided by the manufacturer[2].

5.2.3 Inhibition Screening Assay

In a 96-well plate, 40µL of test compound (0.1µM, 1µM, 10µM) was added to individual wells in triplicate. 40µL of vehicle control (1.25% DMSO) and positive control (Table 5.3) was

also added in triplicate. A master pre-mixed containing, 4850µL buffer, 50µL desired Baculosomes® and 100µL regeneration system was made and 50µL was added to each well. The plate was incubated at room temperature for 10 minutes. A mixture containing 885µL buffer, 100µL of NADP+ and 15µL of Vivid™ Substrate was prepared. The reaction was started by addition of 10µL of substrate mixture to each well, making a final volume of 100µL. The plate was incubated in a Varioskan™ Flash Multimode Reader (Thermo Scientific) at 37.1°C for 60 minutes. Data was collected using SkanIt™ Software (Thermo Scientific) set to kinetic mode and fluorescent readings were recorded using the appropriate programme (Table 5.3).

5.3 *in vivo* Rat Metabolism

5.3.1 Materials and Animals

Sodium carboxymethylcellulose, benzyl alcohol, tween 80, DMSO, Kolliphor® HS 15, NaOH and lyophilized rat pooled plasma (containing anticoagulant, 3.8% trisodium citrate) were purchased from Sigma-Aldrich, UK. Saline solution (0.9%) was made with 0.9g NaOH in 100mL d.H_2O. Heparin and isoflurane anaesthetic were supplied by the University of Liverpool. HPLC grade solvents, H_2O, MeOH and ACN, were purchased from Thermo Fisher Scientific. Male Wistar rats (250g-500g) were supplied and housed by University of Liverpool, Biomedical Science Unit. Under normal testing conditions rats were given free access to food and water. Fasted rats were denied access to food 12 hours prior to dose.

5.3.2 Formulations

The test compounds were formulated in three vehicles. The amount of vehicle was prepared as 5mL/Kg per rat. The first vehicle (vehicle 1) consisted of 10% DMSO, 10% solutol (Kolliphor® HS 15) and 80% Saline (0.9%). Vehicle 1 was made by heating solutol until it become a liquid and then adding DMSO. The mixture was sonicated for 10 minutes. When sufficiently mixed saline was added to reach the desired final volume and the solution was sonicated for 5 minutes. Vehicle 1 was freshly prepared before each experiment. The second vehicle, Vehicle 2, was a standard Suspension Vehicle (SSV) (vehicle 2) made up using 0.5% sodium carboxymethylcellulose, 0.5% benzyl alcohol and 0.4 Tween 80 in 98.6% saline. All components were combined and sonicated for 15 minutes. Vehicle 2 was made up prior to testing and stored at -4°C for 1 month. The final vehicle (Vehicle 3) was made using 10% DMSO and 20% solutol through the same method as vehicle 1. The desired volume was achieved by adding H_2O. Vehicle 3 was also freshly prepared before each experiment.

5.3.3 Sample Collection and Preparation

Fasted and non-fasted rats were given a 10mg/kg oral dose of the test compound in two formulations (Vehicle 1 and Vehicle 2). Blood was collected under anaesthetic from the tail vein. Blood (300µL) samples were collected 0.25, 0.5, 1, 3, 5, 7 and 24 hours after dosing in pre-heparinised 1.5mL eppendorfs. Throughout the experiment blood samples were stored on ice.

A 5mg/kg intravenous dose was given to rats via the tail vein under anaesthetic in a single formulation (Vehicle 3). Blood (300µL) was taken from the tail vein at 0.08, 0.25, 0.5, 1, 3 and 6 hours post dose and collected in heparinised eppendorfs. Blood samples were kept on ice for the duration of sample collection and stored at -80^{o}C overnight.

All blood samples were centrifuged at 13,000 rpm for 15 minutes to separate the plasma. 100µL of the supernatant (plasma) was removed and added to 300µL of the MeOH:ACN stop solution containing IS (LT-01-25 or LT-01-89). The samples were spun for an additional 15 minutes at 13,000 rpm. For analysis by LC-MS 200µL of the supernatant was taken and placed in LC-MS vials. All samples were stored at -80^{o}C. LC-MS analysis was carried out using the *Accela System*. For each analytical run a standard curve in blank plasma was included.

5.3.4 Standard Curves

LC-MS instrument methods were tested with calibration curves. The curves were produced in LCQuan™ Quantitative Software (Thermo Scientific). Validation of the curves was determined by predicted concentration accuracy below 20%. The test compounds were made into a 1mg/mL stock solution in MeOH. A series of serial dilutions in blank plasma were carried out to obtain a number of concentrations; 10ng/mL, 100ng/mL, 500ng/mL, 1000ng/mL, 2000ng/mL and 4000ng/mL. For analysis of *in vivo* PK samples, standard curves were used to extrapolate plasma-concentration levels.

5.3.5 Pharmacokinetic Analysis

Test compound plasma concentration levels were calculated using the standard curve via LCQUAN™. Plasma concentration levels and dosing information was then applied to PK Solutions software (SummitPK™) to generate PK parameters: The area under the plasma concentration–time curve from 0 h to the last sampling time (AUC_{0-t}), the area under the plasma concentration–time curve from 0h to infinity (AUC_{0-1}), elimination half-life ($T_{1/2}$), apparent volume of distribution (V_d), maximum concentration reached in plasma(C_{max}), the time required to reach Cmax (T_{max}) and oral clearance (Cl). PK parameters for each individual animal were generated and the mean (± standard deviation) was calculated. Oral bioavailability (*F*) was determined using mean values:

$$F = (AUC_{oral}/AUC_{i.v.})\times 100\%$$

5.4 Liquid-Chromatography Mass-Spectrometry

5.4.1 Accela System

Two liquid-chromatography mass-spectrometry (LC-MS) systems were used to analyse samples from microsomal stability and *in vivo* rat metabolism studies. The LC consisted of a variable loop Accela auto-sampler (200 vial capacity (4°C) and Accela LC pump interfaced with a TSQ Quantum MS detector. The MS detector was fitted with atmospheric pressure ionization (API) ion source and two E2M30 rotary vacuum pumps and a NG1 nitrogen generator (Peak Scientific, Scotland, UK) supplying nitrogen and argon. A HyPurity C18 column (10cm x 2.1mm, 5µM diameter) was used. All system parts and column were from Thermo

Scientific, UK. The mobile phase consisted of ACN and 0.1% FA (H_2O) running on a gradient (Table 5.5). HPLC grade ACN was purchased from Thermo Fisher Scientific and FA was from Sigma Aldrich. The flow rate was set to 300µL/min and the injection volume was 10µL. Data was obtained and analysed using Xcalibur™ and LCQuan™ set to positive mode. The instrument was tuned to each compound using TSQ Tune™ (Thermo Scientific).

Table 5.5: Mobile phase gradient using ACN and FA (0.1%) for Accela System.

Time (min)	ACN	FA (0.1%)
0.00	40%	60%
2.00	75%	25%
3.50	90%	10%
5.00	90%	10%
5.10	40%	60%
6.00	40%	60%
7.00	40%	60%

5.4.2 Agilent Infinity System

The second system consisted of the following set-up: an Agilent Infinity 1260 auto sampler with a 108 vial capacity (RT) and an Agilent Infinity 1260 Quaternary VL. The LC system was connected to a hybrid triple quadruple/LIT (linear ion trap) 4000 QTRAP® MS detector with a Turbo V™ ion source. Nitrogen and argon gas was supplied by an API Systems gas generator from Peak Scientific. The same HyPurity C18 column (10cm x 2.1mm, 5µM diameter) was used in both systems. Auto-sampler and pump were provided by Agilent Technologies (Stockport,

UK). The mass spectrometer detector was supplied by SCIEX (Warrington, UK). The mobile phase consisted of ACN and 0.1% FA running on a gradient (Table 5.6). The flow rate was set to 300µL/min and the injection volume was 20µL. Data was obtained and analysed with Analyst® Software (SCIEX) set in positive mode.

Table 5.6: Mobile phase gradient using ACN and FA (0.1%) for Agilent Infinity System.

Time (min)	ACN	FA (0.1%)
0.00	40%	60%
2.00	75%	25%
3.50	90%	10%
5.00	95%	5%
5.10	40%	60%
6.10	40%	60%
9.00	40%	60%

5.4.3 Transition States

The *Accela System* was used to detect and optimise the parent and product ions for each compound. The instrument methods were integrated into the *Agilent Infinity System* (Table 5.7). In the *Accela System* the following parameters underwent auto optimisation using TSQ Tune™: Spray voltage (V), vaporiser temperature (°C), sheath gas pressure, ion sweep pressure, aux gas pressure, capillary temperature (°C), tube lens offset (V) and collision energy (V).

Table 5.7: Parent and product ions (m/z) used to detect the compounds.

Compound	MW (g/Mol)	Parent Ion (m/z)	Product Ions (m/z)	
LT-01-25	291	292.2	205.1	163.1
LT-01-26	304	305.2	214.2	208.5
LT-01-45	323	324.2	303.9	283.0
LT-01-88	317	318.1	262.0	233.0
LT-01-89	319	320.2	233.2	204.2
LT-02-50	279	280.1	238.1	205.1
LT-02-53	303	304.2	163.1	126.1
LT-02-86	290	291.1	205.1	135.0
LT-02-39	305	306.3	205.2	149.2
RKA-018	287	286.2	270.3	172.1

5.5 References

1. Lubei Mao, J. H., Changxia Li. (2013). To evaluate metabolic stability of test compound in incubation with rat liver microsomes. In *Metabolic stability* (Co, S. C., ed.).
2. https://tools.thermofisher.com/content/sfs/manuals/Vivid_CYP450_Screening_Kits_man.pdf.

Appendix

Table of Contents

Appendix I

Physiochemical Properties and MPO evaluation

Aqueous solubility was determined by ChemPartners (n=2). An eight-point (0.02, 0.1, 0.2 (1:1). The test compound was prepared from a stock solution to a final concentration of 100µM in 0.1% DMSO (100 mM phosphate buffer). The sample was shaken at 1000 rpm for 1 hour at room temperature. The sample was then centrifuged for 10 mins at 12000 rpm precipitate un-dissolved particles. The supernatant was transferred to a new tube at different dilutions (undiluted, 1:10 diluted, 1:100 diluted). 5 µL of supernatants was added to 95 µL ACN containing IS. The samples were analysed by LC-MS-MS against the calibration curve. Propranolol, ketoconazole and tamoxifen were also tested for solubility comparison.

The six physiochemical properties used in MPO assessment were calculated at the University of Liverpool, Chemistry Department. ChemDraw software from PerkinElmer (Massachusetts, USA) was used to calculate the ClogP, MW and TPSA. The HBD groups were determined by the number of hydrogens attached to an electronegative atom (e.g. N or O) within the structure. The pKa and ClogD were calculated using ACD/ChemSketch software from ACD/Labs (Ontario, Canada).

The physiochemical parameters were then used to calculate the MPO score. MPO evaluation was carried out using the MPO excel worksheet shown below (Figure 1)[1]. The physiochemical parameters can be inserted into the worksheet to calculate the MPO score.

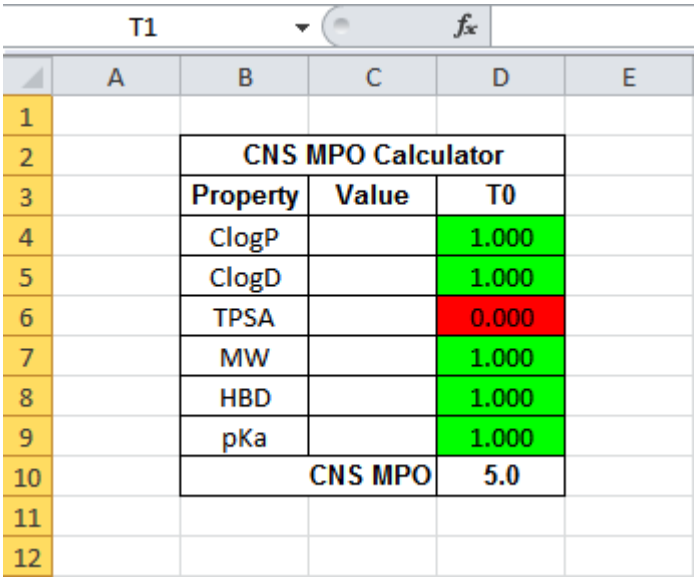

T1

	A	B	C	D	E
1					
2		CNS MPO Calculator			
3		Property	Value	T0	
4		ClogP		1.000	
5		ClogD		1.000	
6		TPSA		0.000	
7		MW		1.000	
8		HBD		1.000	
9		pKa		1.000	
10			CNS MPO	5.0	
11					
12					

Figure 1. MPO Calculator for Microsoft Excel™

Appendix II

GyRα1 Selectivity Electrophysiology Assay

Claw frog (*Xenopus laevis)* oocytes were surgically removed under anaesthetic (0.3% tricaine in water). The cells were dissected and stored in sterile-filtered ND96+ medium (96mM NaCl, 2mM KCl, 1mM CaCl, 1mM MgCl, 5mM HEPES, pH 7.4) containing gentamycin (50µg/mL). The oocytes were isolated as described in Grudzinska *et al*., 2005[2]. Cells were injected with 5ng of cRNA, at a volume of 0.05µL, and incubated in the ND96+ medium for 24 hours (18°C) prior to electrophysiology experiments. Whole-cell recordings were carried out in solution (115mM NaCl, 1mM KCl, 1.8mM CaCl, 10mM HEPES, pH 7.4). A resting potential of -70mV was maintained during the experiment. To ensure current quality and 20 % maximal activation (EC_{20}), effected currents were measured in response to increasing glycine concentration. The test compound was applied in the presence of glycine (EC_{20}). The cells were perfused with test compound for 30s before addition of glycine. Over the course the experiment, individual oocytes response to glycine (EC_{20}) varied in peak amplitude 8 ± 2 %. All experiments were performed at room temperature.

Currents were measured with Clampfit 9.2 software (Molecular Devices, California USA). The data was analysed using KaleidaGraph program (Synergy Software, Pennsylvania, USA) and GraphPad Prism (GraphPad Software Inc., California, USA). Current response was plotted against drug concentration to establish EC_{50} parameters. These experiments were carried out by Michael Kilb under the supervision of Prof. Bodo Laube at the University of Tübingen. The protocol above was provided by Michael Kilb.

Appendix III

Chung Lesion Model of Neuropathic Pain

Male Wisar rats (125-149g) were used in proof of concept studies. Neuropathic pain was induced by partial ligation of the left sciatic nerve. The rats were anaesthetised (isoflurane/O_2 inhalation). The left sciatic nerve exposed at mid-thigh level through a small incision. The nerve was tightly ligated with 7.0 silk. The wound was closed with skin clips. Testing occurred 12-15 days following surgery to ensure the development of neuropathic pain. Treatment groups were randomised and blinded (n=6). A pre-dose behavioural baseline was taken by 14 days following nerve ligation before drug treatment. Following drug administration, behavioural testing was carried out at 1, 3, 6 and 24 hours post-dose. The drug was tested at 3, 10 and 30mg/Kg (P.O). A 10mg/Kg vehicle control (10% DMSO, 10% solutol and 80% saline) and 30mg/Kg positive control (gabapentin or lamotrigine) was included for comparison.

Mechanical allodynia was examined in a model of neuropathic pain by measuring paw withdrawal thresholds (PWT) to increasing mechanical force applied to the dorsal surface of the rat paw using an Analgesymeter (Ugo-Basile, Milan) equipped with a wedge-shaped probe (area 1.75 mm^2). The maximum force applied was 250 g and the end-point was taken as withdrawal of the ipsilateral hind paw. The withdrawal latency (s) and threshold (g) were recorded. The contralateral paw was also tested, however the data is not shown in this thesis.

Cold hyperalgesia was measured as paw withdrawal latencies (s) were from a cold-plate set at 10°C (Ugo Basile, Milan). Prior to testing, the cold plate was calibrated for 5 minutes at the

set temperature. The animals were carefully restrained and each hind paw was placed onto the cold-plate. The end point was taken as the withdrawal of the paw and recorded as the withdrawal latency for both the ipsilateral and contralateral paw. A maximum cut-off of 30s was used for each paw. The experiments were carried out at King's College London by Clive Gentry under the supervision of Prof. Steve McMahon. The protocol described above was supplied by Clive Gentry.

Appendix IV

$GABA_A$ α1β2γ3 Receptor Profiling

Whole-cell recordings were carried on out cells expressing $GABA_A$ α1β2γ3 using a PatchXpress automated patch clamp system (Molecular Devices). Cell lines were validated via direct application of GABA at an increasing dose. The cells were maintained it a holding potential -60mV. The internal solution was 90mM KCl, 50mM KF, 11mM EGTA, 10mM HEPES, 1mM $MgCl_2$ and 2mM Mg-ATP. The external solution used was 137mM NaCl, 4mM KCl, 10mM HEPES, 1.8mM $CaCl_2$, 1 mM $MgCl_2$ and 10 mM glucose.

The test compound was applied at six concentrations (0.12, 0.37, 1.11, 3.33, 10 and 30μM) with and without GABA (2μM) (n=3). The vehicle used was 0.3% DMSO. The cells were treated with GABA (30μM) and vehicle to ensure activity of GABAA α1β2γ3 receptors and determine the EC_{20} for GABA. The cells where then washed for 2 mins. Vehicle and GABA (2μM) where applied and the cells where washed again for 2 mins. This process was repeated. The cells were pre-treated for 1 min with the test compound, and then GABA (2μM) was applied along with the testing compound to record the effect on current. The cells were again washed for 2 mins. Finally propofol (30μM) and GABA (2μM) was applied as a positive control (Figure 2). This method was adapted from the data report provided by BioFocus.

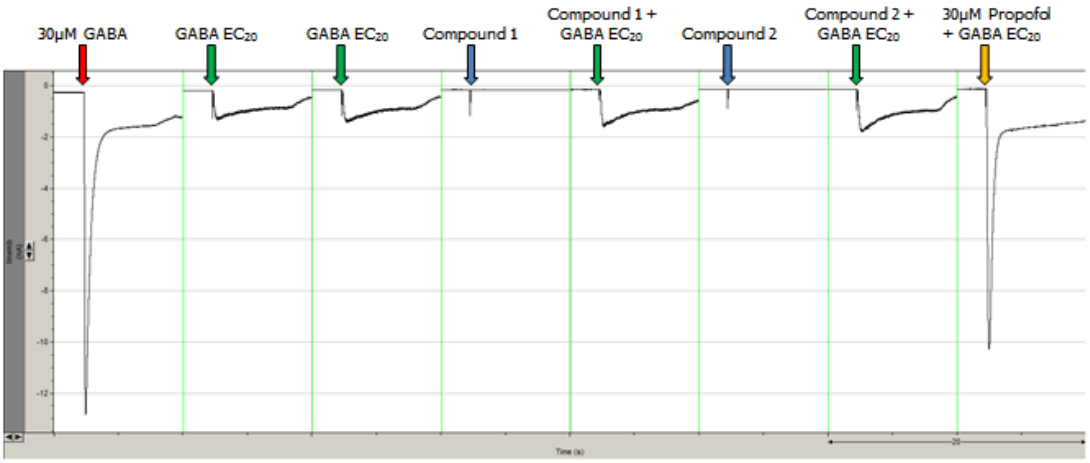

Figure 2. Example of Compound Testing Regime

Appendix V

Hepatocyte Stability

Cryopreserved rat and human hepatocytes were taken from liquid nitrogen storage and thawed in a shaking water bath for 2 mins (37°C). The cells were transferred to 50mL of the thawing medium (see Table 1 below). The cell pellet was resuspended by the addition of Krebs-Henseleit buffer (pre-warmed) buffer containing 5.6g/L HEPES. The mixture was centrifuged for 3 minutes (500 rpm). Cell viability and yield was confirmed. If needed the cells were diluted to a density of $2x10^6$ cells/mL.

Table 1. Preparation of Thawing Medium from ChemPartner's Protocol

Reagent	Initial Concentration	Final Concentration	Quantities of reagents to add based on volume needed
			50 mL
Williams E Medium	-	-	35 mL
Isotonic Percoll (90% Percoll/10% DPBS)	-	30%	15 mL
DPBS 10 ×			
Glutamax	200 mM/100 ×	2 mM	500 µL
HEPES	1 M	15 mM	750 µL
Fetal Bovine Serum	-	5%	2.5 mL
Human Recombinant Insulin	4 mg/mL	4 µg/mL	50 µL
10 mM Dexamethasone (dissolved in DMSO)	10 mM	1 µM	5 µL

The test compound (final concentration = 1µM) was prepared as a dosing solution containing 990µL of Krebs-Henseleit buffer and 10µL spiking solution (200µM). The spiking solution was made-up with 20µL of test compound stock solution (10mM) and 980µL DMSO.

The dosing solution (50µL) was added to a 96-well plate. The wells were organised into time points (0, 15, 60, 120 and 240 mins, n=2). The pre-warmed hepatocyte solution was also added to each well (50µL, $2x10^6$ cells/mL). The plate was incubated at 37°C.

At designated time points, 100µL of ACN containing IS (Osalmid) was added to the corresponding wells. The wells were sealed and the plate was returned to the incubator. This was repeated for each time-point. At the final time point the plate was removed from the incubator and centrifuged for 15 minutes (4000 rpm, 4°C). The supernatants were removed and diluted with ultrapure H_2O (2-fold). The samples were analysed by LC-MS. This study was conducted by ChemPartners. The protocol is adapted from the data-sheet provided.

Appendix VI

CSF and Plasma Exposure

Male Sprague-dawley rats (260-290g) were fasted overnight (n=9). Free access to food and water was given 4 hours post dose. An oral 3mg/Kg dose of the test compound was administered. The testing compound was formulated in 10% DMSO, 10% solutol and 80% saline. Blood was collected via cardiac punctures at 2, 3 and 4 hours post dose following termination by raising CO_2 The blood samples (150µL) were stored into EDTA-2K tubes and centrifuged to obtain plasma (2000 G,4°C , 10 min). The CSF samples were collected via direct puncture into the cisterna magna using a butterfly needle attached to a syringe. White paper was used as a background to monitor colour change during collection. Following a colour change, the tubing was quickly clamped and cut just above the clamped site. The clear sample was collected into the syringe. All samples were stored at -80°C.

For LC-MS analysis, a 30µL aliquot of the plasma samples were added to 150µL ACN containing IS (Dexamethasone, 500ng/mL). The mixture was vortexed for 5 mins and centrifuged at 14000 rpm for a further 5 mins. For the CSF samples, a 15 µL aliquot of the sample was added to 15µL MeOH:H_2O (1:1). Then 100µL of the ACN/IS solution was added. The mixture was vortexed for 5 mins, then centrifuged at 14000 rpm for 5 mins. These experiments were carried out by ChemPartners; the protocol was adapted from the data sheet.

Appendix VII

Plasma Protein Binding Assay

Plasma protein binding was tested via equilibrium dialysis (Figure 3)[3; 4]. Rat plasma and 0.5 M sodium phosphate buffer were applied to a 96-well plate (380µL). The test compound and positive controls were added to the plate (20µL). The test compound (1µM) and positive controls (Warfarin and Quinidine, 1µM) were formulated in 0.2% DMSO (in buffer). For dialysis sample loading, 100µL of blank dialysis buffer was added to the receiver side of dialysis chamber. Then, 100µL of the plasma and testing compounds were applied to the donor side of the dialysis chamber.

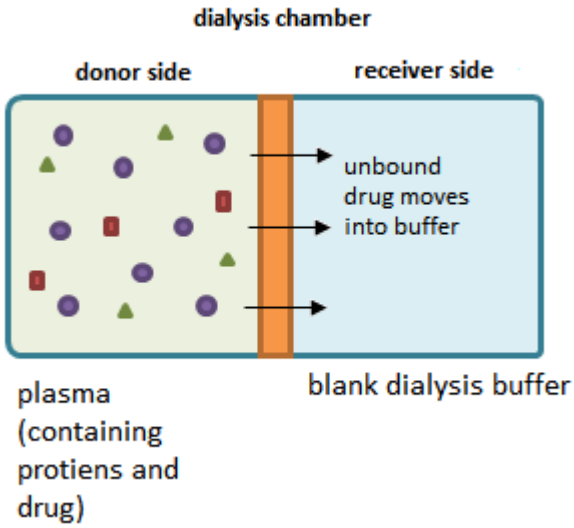

Figure 3. Simplified Schematic of Equilibrium Dialysis[3].

The dialysis block was covered and was incubated in a shaking incubator (60 rpm, 37°C) for 5 hours. After incubation 25µL aliquots were taken from both dialysis chambers and placed in

a clean 96-well plate (n=2). The relevant matrix (buffer or plasma, 100µL) was also applied to the plate. The samples were quenched with 200µL of ice-cold ACN containing IS (Osalmid) and vortexed for 10 mins at 600 rpm. The samples were then centrifuged for a further 15 mins (6000 G). 50µL of the supernatant was transferred to a new plates and mixed with 50µL Mili-Q H_2O. The plate was covered stored at -20°C until analysis by LC-MS.

A second plate was prepared to measure protein binding at t=0. Aliquots (25µL) of plasma and testing compound were taken from the original 96-well plate. The same volume of buffer was added to each well and the samples were immediately quenched with 200µL of the ACN/IS solution. The plate was covered stored at -20°C until analysis by LC-MS. The above protocol was adapted from the data sheet provided by ChemPartners.

Appendix VIII

hERG Cardiotoxicity Assay

CHO-K1 cells were transfected with hERG cDNA to express hERG channels. The cells were cultured in CO_2 incubator using a medium containing Ham's F12, 10% heated fetal bovine serum, hygromycin B (100 μg/ml) and geneticin (100 μg/ml). To ensure culture quality only colonies with 95% viability and a density of 3-8 × 106 cells/mL were used. During recording cells were stored in serum-free HEPES medium for up to four hours. The internal solution was 120mM KCl, 5mM EGTA, 10mM HEPES, 1.75mM $MgCl_2$, 5.3mM $CaCl_2$ and 4mM Na-ATP. The external solution used was 145mM NaCl, 4mM KCl, 10mM HEPES, 2mM $CaCl_2$, 1 mM $MgCl_2$ and 10 mM glucose.

Whole-cell recordings were performed using QPatch automated clamp system (Sophion, Sweden). The cells were voltage clamped at resting potential (-80 mV). The hERG current was activated by depolarizing at +20 mV for 5 sec. The current was then taken back to -50 mV for 5 sec to observe the deactivating tail current. The maximum tail current size was used to determine hERG current amplitude. The cells were recorded for 120 sec to assess current stability. Only stable cells with recording parameters above threshold were selected for the drug testing assay.

The test compound was tested at six concentrations (0.1, 0.3, 1, 3, 10 and 30μM). The vehicle used was 0.1% DMSO (except for 30 μM which was formulated in 0.3% DMSO). The positive control was cisapride (0.1, 0.3, 1, and 3μM). The cells were exposed to the vehicle solution to establish the baseline. After allowing the current to stabilize for 3 minutes, the test

compound was applied. The cells were kept in the test solution until the effect on current reached a steady state for 4 mins. For dose response assay, compound was applied to the cells from low to high concentration. The cells were washed with vehicle solution after testing. The positive control cisapride was applied to the same cell batch. The data was analysed using Assay Software (Sophion) and Graphpad Prism. This protocol was taken from the data report provided by ChemPartners.

Appendix IX

HepG2 MTT Cytotoxicity Assay

Hepatoxicity was measure by the effect on MTT metabolism to formazan[5]. HepG2 cells were applied to a 96-well clear-bottom plate (100µL per well). The plate was incubated at 37°C for 24 hours. The cells were then dosed the test compound (0.04, 0.1, 0.4, 1.0, 4.0, 10, 40, 100µM), a positive control (chlorpromazine) and a vehicle control (0.5% DMSO) in triplicate. The plate was incubated for a further 72 hours. One hour before the end of the incubation period, MTT was added to each well and the plate was dried. The formazan precipitate was then re-solubilised using DMSO.

The plates are then scanned at 570 nm in a Sunrise™ microplate absorbance reader (TECAN Group Ltd, Männedorf, Switzerland). Cell death was indicated by lack of formazan formation. Effect of the compounds is measured as a ratio of the vehicle control. HepG2 MTT cytotoxicity was performed by Cyprotex (Macclesfield, UK). The above protocol was taken from the data report provided by Cyprotex.

Appendix X

AMES Assay

Two *S. typhimurium* strains, TA98 (hisD3052, rfa, uvrB/pKM101) and TA100 (hisG45, rfa, uvrB/pKM101) (see Table 2) were exposed to a vehicle control, two positive controls (2-nitrofluorine/4-nitroquinoline n-oxide and aminoanthracene) and the test compound, LT-01-25 (8, 16, 31, 62, 125 and 250µg/mL) for 90 minutes in a low histidine medium. The cultures were then diluted into a histidine free medium and allotted in to 48 wells of a 348-well plate. The plate was incubated at 37°C for 48 hours. Colony growth was indicated by a colour change. A visual comparison was made between the vehicle control and test compound. Positive response (mutation) was indicated by a minimum 2-fold increase in colony growth from the vehicle control (mean ± SEM).

Statistical analysis was carried out using an unpaired, one-sided Student's T-test. Experiments were carried out with and without 4.5% S9 (S9 fraction taken from the liver of Aroclor-1254 treated rats) to measure the effect of metabolism. A NADPH-regeneration system was added in experiments including S9. AMES assay was carried out by Apredica (Cyprotex US) in Watertown, MA, USA. The above protocol was taken from the data report provided by Apredica.

Table 2. Breakdown of *S. typhimurium* Testing Strains[6].

uvrB	DNA repair mutation makes strains more vulnerable to DNA damage from UV light
hisD3052	Mutated allele resulting in a frameshift mutation
hisG45	Mutated allele resulting in a base-pair substitution
rfa	Mutation that increases cell permeability
pkM101	Ampicillin resistant plasmid that is highly responsive to mutagens

References

1. Wager, T. T., Hou, X., Verhoest, P. R. & Villalobos, A. (2010). Moving beyond Rules: The Development of a Central Nervous System Multiparameter Optimization (CNS MPO) Approach To Enable Alignment of Druglike Properties. *ACS Chemical Neuroscience* **1**, 435-449.
2. Grudzinska, J., Schemm, R., Haeger, S., Nicke, A., Schmalzing, G., Betz, H. & Laube, B. (2005). The β Subunit Determines the Ligand Binding Properties of Synaptic Glycine Receptors. *Neuron* **45**, 727-739.
3. Banker, M. J., Clark, T. H. & Williams, J. A. (2003). Development and validation of a 96‐well equilibrium dialysis apparatus for measuring plasma protein binding. *Journal of pharmaceutical sciences* **92**, 967-974.
4. Di, L., Umland, J. P., Trapa, P. E. & Maurer, T. S. (2012). Impact of recovery on fraction unbound using equilibrium dialysis. *Journal of pharmaceutical sciences* **101**, 1327-1335.
5. Schiller, C. D., Kainz, A., Mynett, K. & Gescher, A. (1992). Assessment of viability of hepatocytes in suspension using the MTT assay. *Toxicol In Vitro* **6**, 575-8.
6. Tejs, S. (2008). The Ames test: a methodological short review. *Environmental Biotechnology* **4**, 7-14.